The role of magnetic resonance imaging in the development of novel transcatheter cardiovascular interventions

Rogers, Toby

Awarding institution:
King's College London

The role of magnetic resonance imaging in the development of novel transcatheter cardiovascular interventions

Dr Toby Rogers, MA, BM BCh, MRCP

King's College London

A thesis submitted for the degree of Doctor of Philosophy

ABSTRACT

Transcatheter cardiovascular interventions are an increasingly attractive alternative to open-chest surgery. Fluoroscopy, historically the cornerstone of imaging guidance for transcatheter procedures, has fundamental limitations when operating in three-dimensions and cannot visualise soft tissue. Structural heart and electrophysiology interventions require precise device localisation in space and direct visualization of anatomic structures. Cardiovascular magnetic resonance imaging (CMR) offers a number of tools that may be ideally suited to these advanced applications: excellent soft tissue visualization in unlimited imaging planes, real-time procedural guidance, three-dimensional imaging, quantification of blood flow and tissue characterization techniques.

In this thesis we describe four original interventions and explore the role of CMR at each stage of the development process: defining the clinical problem, designing potential solutions, building and testing prototypes, and evaluating device performance in pre-clinical experiments. The first structural heart intervention, transatrial intrapericardial tricuspid annuloplasty, is a percutaneous therapy for functional tricuspid regurgitation. CMR was used to determine device configuration and evaluate device-imparted geometric change to the heart. The second structural heart intervention, intentional right atrial exit and pericardial CO2 insufflation, facilitates easy and safe subxiphoid access to the naïve pericardial space. CMR was used to quantify pericardial effusion volume over time, a key parameter that is impossible to measure with fluoroscopy or echocardiography. The third structural heart intervention, fully percutaneous transthoracic left atrial entry and closure, is a potential access route to deliver large transcatheter prostheses to the mitral valve. Transthoracic trajectories to the left atrium were planned and the procedure was performed using real time CMR guidance and active visualization devices. The fourth electrophysiology intervention, transcatheter myocardial needle chemoablation was also performed under CMR guidance, enabling arrhythmic substrate and ablation lesion visualization in real time. The purpose of this thesis is to explore the role of CMR in the development of each of these novel transcatheter interventions.

STATEMENT OF ORIGINALITY

I declare that the work presented in this thesis has been primarily carried out by me. I performed all pre-clinical experiments, including creation of porcine models of disease. I personally designed prototype devices for pre-clinical feasibility experiments. I participated as an operator in first-in-man testing of intentional right atrial exit. I prepared the included manuscripts and personally consulted all the quoted references.

This thesis is submitted as a 'thesis incorporating publication' in accordance with the King's College guidelines. Permission to include reproductions of published manuscripts was granted by the publishers. I declare that this thesis has not been submitted elsewhere for a higher degree.

ACKNOWLEDGEMENTS

I am fortunate to have wonderful academic and clinical mentors. Dr Robert Lederman provided a fertile research environment, encouraging me to innovate and grow as a physician and scientist. His enthusiasm, knowledge and vision have been truly inspirational. I thank Dr Jonathan Hill for inspiring me to pursue a career in interventional cardiology. I thank Dr Valentina Puntmann and Prof Eike Nagel for introducing me to clinical CMR, encouraging me to pursue CMR research and supporting me throughout my studies. I thank the Division of Imaging Sciences and Biomedical Engineering at King's College London, in particular Dr Steve Keevil and Prof Reza Razavi, for allowing me the opportunity to undertake research at the NIH. I thank the exceptional multidisciplinary team of the Cardiovascular Intervention Program at NIH. Finally, I thank the patients who took part in this research and the structural heart team at Henry Ford Hospital in Detroit, Michigan.

CONTENTS

LIST OF FIGURES

LIST OF TABLES

ABBREVIATIONS

CMR	Cardiovascular magnetic resonance
iCMR	Interventional cardiovascular magnetic resonance
LA	Left atrium
LGE	Late gadolinium enhancement
LV	Left ventricle
MRI	Magnetic resonance imaging
RAA	Right atrial appendage
TRAIPTA	Transatrial intrapericardial tricuspid annuloplasty
VT	Ventricular tachycardia

PUBLICATIONS

1. **Rogers T**, Mahapatra S, Kim S, Eckhaus M, Schenke W, Mazal J, Campbell-Washburn A, Sonmez M, Faranesh A, Ratnayaka K, Lederman R. Transcatheter Myocardial Needle Chemoablation During Real-Time Magnetic Resonance Imaging: A New Approach to Ablation Therapy for Rhythm Disorders. *Circulation: Arrhythmia and Electrophysiology*. 2016; 9(4): e003926.

2. **Rogers T**, Ratnayaka K, Schenke W, Sonmez M, Kocaturk O, Mazal J, Flugelman M, Chen M, Troendle, J, Faranesh A, Lederman R. Fully percutaneous left atrial transthoracic entry and closure as a potential access route for transcatheter mitral valve interventions. *Circulation Cardiovascular Interventions*, 2015; 8(6):e002538.

3. Ratnayaka K, **Rogers T**, Schenke W, Mazal J, Hansen M, Kocaturk O, Faranesh A, Lederman R. Magnetic Resonance Imaging-Guided Transcatheter Cavopulmonary Shunt. *Journal of the American College of Cardiology: Cardiovascular Interventions*. 2016; 9(9):959-70.

4. Greenbaum A*, **Rogers T***, Paone G, Flynn S, Borgi J, Guerrero M, O'Neill W, Lederman R. Intentional right atrial exit and CO2 insufflation allows safe subxiphoid needle entry into the empty pericardial space: first human experience. *Journal of the American College of Cardiology: Clinical Electrophysiology*. 2015; 1(5):434-441. ***Authors contributed equally.**

5. **Rogers T**, Lederman RJ. Interventional CMR: Clinical Applications and Future Directions. *Current Cardiology Reports.* 2015; 17(5):580.

6. **Rogers T**, Ratnayaka K, Sonmez M, Franson DN, Schenke WH, Mazal JR, Kocaturk O, Chen MY, Faranesh AZ, Lederman RJ, Trans-Atrial Intra-Pericardial Tricuspid Annuloplasty. *Journal of the American College of Cardiology: Cardiovascular Interventions*. 2015; 8(3):483-91.

7. **Rogers T**, Ratnayaka K, Schenke W, Faranesh A, Mazal J, O'Neill W, Greenbaum A, Lederman R. Intentional right atrial exit for microcatheter infusion of pericardial carbon dioxide or iodinated contrast to facilitate sub-xiphoid access for structural heart and electrophysiological interventions. *Catheterization and Cardiovascular Interventions*. 2014; 86(2):E111-8..

8. Lederman R, Chen M, **Rogers T**, Wang D, Paone G, Guerrero M, O'Neill W, Greenbaum A. Planning transcaval access using CT for large transcatheter implants. *Journal of the American College of Cardiology: Cardiovascular Imaging*. 2014; 11:1167-1171.

9. Campbell-Washburn A, **Rogers T**, Xue H, Hansen M, Lederman R, Faranesh A. Dual echo positive contrast bSSFP for real-time visualization of passive devices during MRI-guided cardiovascular catheterization. *Journal of Cardiovascular Magnetic Resonance.* 2014; 16:88.

10. **Rogers T**, Ratnayaka K, Lederman R. MRI catheterization in cardiopulmonary disease. *Chest*. 2014; 145(1):30-36.

BOOK CHAPTERS

1. **Rogers T**, Lederman R. Interventional Cardiovascular MRI. In: Cardiovascular Magnetic Resonance Imaging, 2nd Edition, Kwong R, Heydari B, Jerosch-Herold M. *Humana Press*. 2015.

2. **Rogers T**, Greenbaum A, Lederman R. Transcaval access for larger caliber transcatheter aortic implants. In: Catheter Based Valve and Aortic Surgery, Ailawadi G, Kron I. *Springer*. 2016.

ABSTRACTS PRESENTED AT SCIENTIFIC MEETINGS

1. **Rogers T**, Ratnayaka K, Schenke W, Sonmez M, Kocaturk O, Mazal J, Hansen M, Faranesh A, Lederman R. Fully percutaneous transthoracic left atrial entry and closure to deliver large caliber transcatheter mitral valve implants. ***PICS-AICS 2015.***

2. **Rogers T**, Ratnayaka K, Schenke W, Faranesh A, Mazal J, O'Neill W, Greenbaum A, Lederman R. Intentional right atrial exit for microcatheter infusion of pericardial carbon dioxide or iodinated contrast to facilitate sub-xiphoid access. *Journal of the American College of Cardiology: Cardiovascular Interventions* 2015; 8(2)(Suppl):S53. ***CRT 2015.***

3. **Rogers T**, Ratnayaka K, Schenke WH, Faranesh AZ, Sonmez M, Franson DN, Lederman RJ. Transcatheter extra-cardiac tricuspid annuloplasty. *Journal of the American College of Cardiology: Cardiovascular Interventions* 2015; 8(2)(Suppl):S55. ***CRT 2015.***

4. **Rogers T**, Ratnayaka K, Schenke W, Sonmez M, Kocaturk O, Mazal J, Flugelman M, Chen M, Faranesh A, Lederman R. Fully percutaneous transthoracic left atrial access to deliver large interventional devices. *Journal of the American College of Cardiology: Cardiovascular Interventions* 2015; 8(2)(Suppl): S54-5. ***CRT 2015.***

5. **Rogers T**, Ratnayaka K, Stine A, Grant L, Schenke W, Mazal J, Hansen M, Faranesh A, Lederman R. MR guided right heart catheterization – the NIH experience. *Journal of Cardiovascular Magnetic Resonance* 2014; 17(Suppl 1): O20. ***SCMR 2015.***

6. **Rogers T**, Schenke W, Mazal J, Sonmez M, Kocaturk O, Ratnayaka K, Hansen M, Faranesh A, Lederman R. Percutaneous MR guided direct left atrial access to deliver large interventional devices. *Journal of Cardiovascular Magnetic Resonance* 2014; 17(Suppl 1): O19. ***SCMR 2015.***

7. Campbell-Washburn A, **Rogers T**, Basar B, Sonmez M, Kocaturk O, Lederman R, Hansen M, Faranesh A. Two channel passive visualization of a nitinol guidewire with iron markers. *Journal of Cardiovascular Magnetic Resonance* 2014; 17(Suppl 1): P236. ***SCMR 2015.***

8. Campbell-Washburn A, **Rogers T**, Basar B, Sonmez M, Kocaturk O, Lederman R, Hansen M, Faranesh A. Positive contrast spiral imaging of a nitinol guidewire. *Journal of Cardiovascular Magnetic Resonance* 2014; 17(Suppl 1): Q15. ***SCMR 2015.***

9. **Rogers T**, Karmarkar P, Kocaturk O, Ratnayaka K, Hansen M, Faranesh A, Lederman R. Realtime MR guided endomyocardial biopsy with an active visualization bioptome. *Journal of Cardiovascular Magnetic Resonance* 2014; 17(Suppl 1): P235. ***SCMR 2015.***

10. Ratnayaka K, **Rogers T**, Schenke W, Mazal J, Chen M, Hansen M, Kocaturk O, Faranesh A, Lederman R. Transcatheter bidirectional Glenn shunt guided by real-time MRI. *Journal of Cardiovascular Magnetic Resonance* 2014; 17(Suppl 1): O23. ***SCMR 2015.***

11. Basar B, Campbell-Washburn A, **Rogers T**, Sonmez M, Faranesh A, Ratnayaka K, Lederman R, Kocaturk O. Stiffness-matched segmented metallic guidewire for interventional cardiovascular MRI. *Journal of Cardiovascular Magnetic Resonance* 2014; 17(Suppl 1): P414. ***SCMR 2015.***

12. **Rogers T**, Ratnayaka K, Schenke WH, Faranesh AZ, Sonmez M, Franson DN, Lederman RJ. Trans-Atrial Extra-Cardiac Tricuspid Annuloplasty. *Eurointervention*. 2014; 10(5)(Suppl);OP028. ***PCR London Valves 2014.***

13. **Rogers T**, Ratnayaka K, Mazal J, Schenke W, Grant L, Stine A, Kellman P, Faranesh A, Lederman R. Provocative MRI catheterization. *Journal of Cardiovascular Magnetic Resonance* 2014; 16(Suppl 1):P143. ***SCMR 2014.***

14. Campbell-Washburn A, **Rogers T**, Hansen M, Lederman R, Faranesh A. Dual echo bSSFP for real-time positive contrast of passive nitinol guidewires in MRI-guided cardiovascular interventions. *Journal of Cardiovascular Magnetic Resonance* 2014; 16(Suppl 1):O79. ***SCMR 2014.***

15. Faranesh A, Hansen M, **Rogers T**, Lederman R. Interactive Black Blood Preparation for Interventional Cardiovascular MRI. *Journal of Cardiovascular Magnetic Resonance* 2014; 16(Suppl 1):P32. ***SCMR 2014.***

16. Mazal J, **Rogers T**, Faranesh A, Kellman P, Schenke W, Stine A, Grant L, Ratnayaka K, Lederman R. An efficient, free-breathing protocol for MR right heart catheterization. *Journal of Cardiovascular Magnetic Resonance* 2014; 16(Suppl 1):T5. ***SCMR 2014.***

17. **Rogers T**, Ratnayaka K, Schenke WH, Faranesh AZ, Sonmez M, Franson DN, Lederman RJ. Trans-Auricular Intra-Pericardial Tricuspid Annuloplasty (TRAIPTA). *Journal of the American College of Cardiology*. 2013; 62(18 Suppl 1):B41. ***TCT 2013.***

Chapter 1. Summary

1.1 Background

Multimodality imaging has enabled procedures that were historically performed through open chest surgery to be accomplished using transcatheter techniques. Fluoroscopy and echocardiography are the most commonly used modalities in catheterization laboratories today, but increasingly complex interventions require more advanced capabilities. The development of new cardiovascular interventions requires at a minimum (1) understanding of normal and abnormal anatomy in order to design novel devices; (2) real-time three-dimensional imaging for procedural guidance; and (3) post-procedural evaluation of the results of therapy. CMR offers a number of unique capabilities that could facilitate novel cardiovascular interventions, including 3D, flow, real-time and late gadolinium enhancement CMR. Feasibility of real-time CMR to guide diagnostic cardiac catheterization, electrophysiology studies and simple structural interventions has been demonstrated in the last decade. Innovative real-time CMR pulse sequences and active and passive visualization MRI-conditional devices should enable more complex interventions. Even if fluoroscopy remains the preferred modality for procedural guidance, CMR can offer additional information to plan interventions and evaluate the results.

In this thesis, the role of CMR is explored in the development of four different novel transcatheter cardiovascular interventions. These four interventions address clinical problems for which there is currently no or unsatisfactory transcatheter solutions: (1) the treatment of tricuspid regurgitation; (2) access to the naïve pericardium for structural or electrophysiology procedures; (3) wide-bore access to the left atrium to deliver large mitral prostheses; and (4) ablation in the thick ventricular myocardium for rhythm disorders.

It is important to recognise the limitations of interventional CMR, in terms of feasibility of clinical translation of these novel interventions. While CMR may offer advantages during the design, testing and refinement process, the limited availability of interventional CMR cath labs and lack of commercially available MRI-conditional guidewires and catheters remains a serious obstacle. Therefore it is important to distinguish the benefit of CMR during the development process and the reality of clinical translation using widely available imaging modalities such as echocardiography and X-ray fluoroscopy.

1.2 Overview of thesis and chapter description

This thesis is submitted as a 'thesis incorporating publication' in accordance with the King's College guidelines.

Clinical roll out of real-time MRI guidance for interventional cardiovascular procedures remains limited by availability of guidewires, catheters and other interventional devices. Nonetheless, CMR may offer unique capabilities in the development process even if CMR is not the imaging modality of choice for eventual clinical translation, particularly for more complex interventions that disrupt traditional vascular boundaries. To explore the role of CMR in this process, we selected three novel cardiovascular interventions that require the operator to intentionally exit the heart to access the pericardium, navigate within the pericardium to encircle the heart, and traverse the thorax to access the left atrium. Finally we selected a procedure that simply could not be performed safely and effectively using X-ray fluoroscopy or echocardiography guidance to highlight how CMR could be a truly disruptive technology in the future.

Chapter 2 comprises an overview and literature review of interventional CMR. This is word for word the chapter to be published in the forthcoming 2nd edition of 'Cardiovascular Magnetic Resonance Imaging' (*Humana Press*, New York) edited by Dr Kwong, Dr Heydari and Dr Jerosch-Herold due for publication in 2016.

Chapter 3 describes a transcatheter device and methods to treat functional tricuspid regurgitation. The original research manuscript is presented as published in the '*Journal of the American College of Cardiology: Cardiovascular Interventions*' in 2015. Two related patent applications covering devices and methods for tricuspid annuloplasty can be found in the appendices. CMR played a critical role in understanding the anatomy of the atrioventricular valves, quantitatively assessing device tensioning, and measuring the treatment effect in naïve and porcine animal models. Most procedure steps were performed using X-ray fluoroscopy guidance and for clinical translation, we expect tensioning could be performed using echocardiography guidance, titrating tension to the degree of tricuspid regurgitation.

Chapter 4 describes a technique for facilitating sub-xiphoid access to the naïve pericardial space that involves right atrial appendage exit with a microcatheter and insufflation of the pericardial space with CO_2 to separate pericardial layers. The original pre-clinical research manuscript is presented as published in '*Catheterization and Cardiovascular Interventions*' in

2014. Our report of the first human experience of this technique is presented as published in the '*Journal of the American College of Cardiology: Clinical Electrophysiology'* in 2015. In order to assure safety of the technique before clinical translation, we needed to confirm in pre-clinical experiments that pericardial bleeding was negligible. This required serial non-invasive accurate measurements of pericardial fluid volume. CMR is an ideal imaging modality for this application. Once safety was assured, such measurements were no longer required for clinical translation, as a pericardial drain was left in place after each procedure.

Chapter 5 describes an alternative wide-bore access route to the mitral valve to deliver large transcatheter prostheses using real-time MRI guidance. The original research manuscript is presented as published in '*Circulation: Cardiovascular Interventions*' in 2015. The procedure was developed using real-time CMR, because it permits imaging in unlimited planes and full visualization of all soft tissue structures. However, once optimal trajectories were established and procedure steps refined, we were able to replicate the procedure using X-ray fluoroscopy augmented with rotational angiography, which should enable easier clinical implementation.

Chapter 6 described a completely new approach to myocardial ablation to treat ventricular arrhythmias by chemoablation using acetic acid rather than radiofrequency energy. The procedure is performed under real-time MRI guidance enabling instantaneous depiction of irreversible necrosis and overcomes the major limitations of contemporary VT ablation. This procedure exploits the unique tissue characterization capability of CMR and cannot be replicated using X-ray or echocardiography for guidance.

Chapter 2. Interventional cardiovascular magnetic resonance

2.1 Introduction

Interventional cardiovascular MRI (or "iCMR") is potentially revolutionary because of the exquisite tissue and blood imaging afforded to guide therapeutic procedures. By making small compromises in spatial or temporal resolution, and with little or no modifications to commercial high performance MRI systems, images can be acquired and displayed almost instantaneously to operators. This may be useful simply to avoid ionizing radiation during conventional catheter-based procedures, especially in children. Perhaps more important, iCMR promises to enable more advanced procedures not otherwise possible without open surgical exposure.

X-Ray fluoroscopy is widely available and is used to drive a wealth of catheter-based and minimally invasive cardiovascular and non-cardiovascular interventions. Other procedures are guided by external or invasive ultrasound (*i.e.* transesophageal or intravascular), or electromagnetic position mapping (*Carto, Biosense Webster; Ensite NavX, St Jude Medical*), alone or in tandem with X-Ray. To change the primary image guidance modality away from X-Ray would require a more favourable risk-benefit profile or would require applications not otherwise possible with X-Ray. For certain applications, iCMR is likely to meet these requirements.

iCMR does not expose patients or operators to ionizing radiation. Children with congenital cardiovascular disease suffer excess risk of late malignancy after exposure to ionizing radiation [1]. They also are prone to multiple catheter-based treatments, subjecting them to higher cumulative radiation exposure. Cumulative exposure is also a risk to operators and staff [2]. Lead aprons worn during X-Ray procedures are associated with career-threatening musculoskeletal injuries.

iCMR, by virtue of imaging soft tissue, blood spaces, and catheter devices simultaneously, may enable novel procedures. In preclinical experiments, iCMR has been shown to guide and track targeted cell delivery into or around myocardial infarctions, to guide atrial septal puncture, to drain pericardial effusions, and to obtain direct transthoracic access to the heart. iCMR is being developed in preclinical systems to guide cardiac valve repair and replacement, and extra-anatomic bypass, procedures that in the past would have required surgical exposure. In some settings, iCMR may provide a safety advantage over conventional

image guidance, by revealing complications such as vascular perforation or rupture more rapidly, and enabling more rapid treatment.

In recent years, iCMR in humans has become a clinical reality. Several institutions now perform MR-guided diagnostic right heart catheterization, and first-in-man MR-guided arrhythmia ablation and structural cardiac interventions have performed recently. In this chapter, we discuss the technical challenges of iCMR and evaluate the potential solutions, describe how to equip an iCMR suite for clinical applications, and review the published pre-clinical and clinical experience to date.

2.2 Technical issues

2.2.1 Pulse sequence and image reconstruction

iCMR is possible because of the same technical advances that enable MRI of moving cardiac structures. Newer hardware with homogeneous magnetic fields and with rapidly switching magnetic gradients permit repetition times (TR) shorter than 3ms. The most widely used pulse sequences are steady-state free precession (SSFP, also known as balanced fast field echo, trueFISP, and FIESTA), because of the relatively high signal-to-noise ratio (SNR) generated with short TRs. Gradient echo techniques, used especially to enhance magnetic susceptibility artefacts, can be equally fast but usually have inferior SNR.

During “interventional” MRI, pulse sequences are often adjusted interactively to change image contrast and to adjust the compromise between temporal and spatial resolution in favour of speed [3]. Compared with X-Ray imaging, which typically uses 1024x1024 pixel images at 15 frames per second, a typical iCMR image will be 192x160 pixels at 10 frames per second. Because of enhanced tissue imaging, the relative information content in these small-matrix iCMR images is comparable to larger-matrix X-Ray images.

We define “real-time” imaging as acquisition-to-display latency (or delay) of 250ms or less, which is at the border of perceptibility by catheter operators, and at a frame rate sufficient for the specific application, generally 5–15 frames/second. Imaging speed is adjusted through a combination of acquisition and post-processing techniques.

Under-sampling refers to image creation with less-than-complete data sets. iCMR acquisitions can be under-sampled further to increase temporal resolution, often combining multiple methods including interleaving echos (analogous to alternating even and odd lines on older television sets), incomplete phase sampling of frequency space (“k-space”), and

sampling of incomplete echoes. Alternative frequency-space sampling trajectories also can employ under-sampling. For example, frequency space can be sampled radially so that each echo intersects the centre frequency [4], which are attractive because they intrinsically over-sample the centre of frequency space and under-sample the outer frequencies. Others advocate "spiral" sampling of frequency space to combine advantages both of conventional rectilinear and radial sampling.

Parallel imaging techniques exploit the fact that differently located receiver coils each have different "perspectives." This is analogous to the enhanced imaging afforded by binoculars compared with monocular telescopes. Such techniques, bearing monikers such as SENSE and GRAPPA, require multiple hardware receiver channel systems, special receiver coils with reduced crosstalk, and increased computational horsepower. In practice they readily increase frame rate 2–4-fold or more at an acceptable cost of image noise.

2.2.2 MRI features especially useful for iCMR

Most commercial MRI systems provide rtMRI functionality using SSFP with interactive graphics slice prescription during continuous scanning. Additional functionality may be available using external computer workstations to control the scanner during iCMR procedures and display rtMRI images.

Our labs have found several additional features to be valuable in preclinical and clinical iCMR. Perhaps most important is the ability independently to process signals from individual receiver channels, especially those attached to intravascular devices (see next section). Specifically, this permits signals from device channels, such as intravascular guidewires or endocardial injection needles, to be displayed in colour (Figure 2-1). This simple modification provides high user confidence in device location during rtMRI procedures. It has proven helpful also to be able to alter gain settings for each channel interactively, much as operators adjust gain on intravascular or transthoracic ultrasound devices.

Other features we have found useful include the ability to alter slice thickness, or toggle on and off saturation pre-pulse to enhance the appearance of gadolinium-filled balloons and to highlight areas of gadolinium-enhanced myocardium. Image-acceleration, such as with GRAPPA, is also toggled interactively. The interaction also can be automated. For example, investigators at Case Western Reserve University automatically reduces the field of view or increases temporal resolution during rapid device motion; the pictures may be fast-but-blurry during coarse device movements but slow-and-sharp during fine device positioning [5].

Similarly the field of view may be large during rapid movement, or small during fine positioning.

Multiple slices acquired and displayed in rapid succession guide our investigational interventional procedures. Updates of individual slices can be paused or reactivated to speed the frame rate of other slices. This type of display also can be enhanced by interactive user point-marking to identify important anatomic features or targets, the ability to make measurements on-line, and the ability to combine with prior roadmap images to make rapid before and after comparisons (Figure 2-1).

iCMR operators have two general imaging strategies. For some applications, rtMRI is directed at target pathology, while devices are manipulated in or out of the desired target slice. Alternatively, the rtMRI slice can automatically track catheter movements and alter the slice prescription so as always to keep the desired catheter-device in view, while changing the view of the neighbouring anatomy. Ideally, both imaging techniques should be available to the operator. We have found a “projection-mode” feature useful during catheter manipulations within target slices. When parts of catheter devices move outside these selected slices, they appear “lost.” By toggling projection-mode (which switches to thick-slice or slice-less imaging akin to X-ray fluoroscopic projections), the catheter can be “found” and manipulated back into the target slice (Figure 2-1).

2.3 Logistics and safety: Assembling a clinical interventional MRI suite

Constructing a clinical laboratory suitable for iCMR procedures is straightforward but requires a degree of customization [6, 7]. Once configured, the laboratory resembles conventional X-Ray fluoroscopy suites (Figure 2-2).

2.3.1 Infrastructure requirements

All major systems manufacturers provide turnkey installation of combined X-Ray/MRI (XMR) systems consisting of single- or biplane X-Ray fluoroscopy system, clinical 1.5-3T MRI system, the capacity to transport patients rapidly and safely between the modalities, and X-Ray and radiofrequency shielded doors that permit the two imaging systems to be used independently when they are not being used together. We believe XMR installations are both useful and cost-effective in providing adjunctive and bailout treatment environments. Moreover, the incremental cost over two separate labs is fairly low, consisting only of the barrier doors and the inter-modality patient transport system. As more experience is gained

and the safety of iCMR is established, we anticipate that in the future an adjacent X-ray room will no longer be required.

For transfemoral arterial or transjugular venous access, the length of conventional 1.5T MRI bores (approximately 150cm) does not significantly interfere with catheter manipulations in adults. Shorter-bore (120cm) 1.5T MRI systems are commercially available and may reduce these obstacles but are certainly not a requirement. Shorter-bore MRI systems also may reduce patient anxiety and claustrophobia and may ease intra-procedural nursing care and observation.

One noteworthy logistical point: at present transfemoral or transjugular access may best be obtained using X-ray or ultrasound guidance for backup. In a combined XMR system, arterial access is obtained under X-Ray and the patient is then transferred rapidly into the MRI system for further procedure conduct.

2.3.2 Communications

Real time MRI is loud. Even in newer "acoustically-shielded" systems, the acoustic noise is sufficiently loud that unassisted verbal communication is impossible, and protective headsets are necessary to avoid occupational injury. Several commercial systems are now available, combining noise-suppression headsets, multiple channels, and wireless connectivity to facilitate movement around the MRI room (*Optoacoustics, Innovere*). Unless patients will always be under general anaesthesia, multiple communication channels are valuable, as well as the ability for staff to switch between channels to address each other and/or the patient separately.

2.3.3 Video display

At NIH, we customize a commercial rtMRI workstation, but similar systems are available (*Interventional Front End, Siemens; RTHawk, HeartVista*; *Cleartrace, MRI Intervention; iSuite, Philips*). We use multiple video displays: one for instantaneous hemodynamics, one mirroring the host computer for scanner control, and one for rtMRI display. Available display options include in-lab shielded LCD displays, either floor- or ceiling-mounted. Commercial LCD projectors can be shielded (*Gaven Industries*) against radiofrequency noise emissions, can be positioned inside the lab, and can project onto inexpensive aluminium-framed projector screens. Digital signals are transmitted into the MRI room through fibre-optic transmission lines passed through waveguides (large conductive cylinders installed across the radiofrequency shield that allow nonconductive materials to pass freely). Alternatively,

projectors can project from outside the lab through waveguides onto the screen in the MRI room.

2.3.4 Sterility

Sterile procedure during iCMR is similar to other procedures. In our laboratories, before transfer from X-Ray to MRI systems, we cover the sterile patient access site (usually groin or neck area) with large sterile drapes, especially to protect that site while surface MRI coils are placed. We enclose surface coils in sterile plastic bags, and interventional coil connectors in sterile plastic sheaths marketed to enclose intravascular ultrasound connectors. Finally, we line the MRI bore and controls with adhesive clear plastic sterile drapes.

2.3.5 Safety, patient monitoring and emergency evacuation

iCMR procedures require standard operating procedures that are an extension of those applied for standard non-invasive MRI procedures.

Suites need to be designed to minimize trips by “circulating” staff members across the RF barrier to gather devices. Opening the door, interrupting the RF barrier, usually interferes with the iCMR procedure by introducing excessive noise into images. This requires both circulating staff and disposable devices to be positioned inside the iCMR room.

Contingency plans must exist to avoid introducing ferrous “missiles” into the iCMR suite. As with standard non-invasive MRI, the risk is highest during emergencies. Defibrillator consoles or oxygen cylinders become missiles if inadvertently brought into the MRI room by emergency team members. As during standard MRI, contingency plans should be in place rapidly to evacuate the patient outside the field during emergencies. At NIH, we drill evacuations regularly and are able to move a patient out of the scanner, transfer to the adjacent X-ray suite and defibrillate in under 1min. We expect MR-conditional defibrillators to become available in the near future, enabling ‘in-bore’ therapy.

A great deal of biomechanical patient care equipment is commercially available for operation in the MRI suite, including patient monitoring equipment, intravenous fluid pumps, and mechanical ventilators. Such equipment still should be tested and *marked* as being safe for operation inside the high magnetic field. All other ferrous materials that are deemed essential must be tethered outside the high field line if they must remain inside the scanning room. Nitric oxide administration systems can be modified with extended plastic tubing that is passed through the waveguide.

MR-safe hemodynamic monitoring systems are available commercially (*Invivo, GE, Medrad*) and are sufficient for basic monitoring. However, there are currently no high-fidelity hemodynamic recording systems sold commercially. Custom systems have been built for research purposes using filters to correct for interference from the scanner and fibre optic cables or wireless systems to transmit signals out of the room, and using research acquisition hardware (*National Instruments*, *ADInstruments, Biopac*). A commercial system, which should integrate into conventional catheterization laboratory hemodynamic analysis systems (e.g. *Siemens Sensis, GE Mac-Lab*) is currently under development (*Pinmed*).

A surprisingly large number of lines are connected to the patient, and their management should be planned in advance. They are enumerated here for effect: (1) oxygen and other gases; (2) mechanical ventilation; (3) oximetric detector; (4) microphone; (5) headset; (6) multiple intravenous lines; (7) intra-arterial pressure transducer connectors; (8) interventional fluid manifold including contrast, flush, and waste lines; (9) urinary catheters; (10) electrocardiography leads for MRI and for bailout X-ray; (11) surface MRI coil connectors; (12) intravascular MRI coil connectors. These should be arranged so that no inadvertent loops are formed of conductive materials, and so that conductive materials are kept away from the wall of the MRI bore, both of which can contribute to heating. The lines also should be organized so that the patient can be evacuated rapidly without disrupting and disconnecting them.

2.4 Catheter devices

X-Ray fluoroscopic interventional devices are conspicuous because they attenuate X-Ray photons. Most off-the-shelf devices are intrinsically conspicuous under X-Ray; others incorporate heavy metals like barium or platinum. Catheter devices usually incorporate ferrous materials (such as wire braiding) to make them rigid and torque-resistant. By contrast, under MRI, structures are conspicuous because they contain or adjoin excited proton spins. Off-the-shelf catheter devices, designed for X-Ray, usually distort the MR image because the ferrous materials destroy the local magnetic field. Devices rendered "MR-compatible" by having ferrous materials removed are also rendered invisible because they still don't contain water protons. Attempts to coat or fill catheter devices with gadolinium-type contrast agents have for the most part been unsuccessful, because not enough excited proton spins are able to interact with the gadolinium-type "relaxation" agent. Moreover, "MR-compatible" guidewire materials such as nitinol are electrically conductive and, when long enough to be clinically useful, they are vulnerable to rapid

heating from the MRI radio energy excitation, much as they would be inside a microwave oven. Table 2-1 and Figure 2-3 provide an overview of general approaches to making catheter devices visible under MRI.

2.4.1 Passive device visualization

"Passive" catheter devices are the simplest, and are visualized based on their intrinsic materials properties. Most passive devices are visible because they do not contain water protons and therefore appear black using most MRI pulse sequences. Tracking dark devices can be challenging using MRI, because the darkness can be difficult to spot when it is diluted (or "volume-averaged") in a larger imaging slice. The dark spots can be enhanced by adding small amounts of metal to create "blooming" or magnetic susceptibility artefacts (Figure 2-3). These artefacts can make the passive device appear larger than the actual size, and can even obscure surrounding tissue detail. Guidewires and catheters [8-10] have been made out of non-metallic polymers (Figure 2-3), and clinical procedures have been conducted using polymer guidewires [11], passive CO_2-filled [12-14] or dilute gadolinium-filled balloon catheters [15].

2.4.2 Active device visualization

We prefer to use MRI catheter devices that are modified to incorporate MRI receiver coils, or antennae. These so-called "active" catheter devices become highly visible when they are attached to the MRI scanner hardware because they accentuate nearby excited water protons. Early designs were intended for high-resolution tissue imaging or spectroscopy [16-22] of nearby tissue. In their simplest designs, the entire length or "profile" of active catheters are made conspicuous [23-29]. In addition, these profile-design active catheters can help visualize the devices even if they move outside the selected scanning plane (Figure 2-1). Profile-design active catheters generally are imaged along with target tissue, and require no modification of imaging pulse sequences. Active catheter coils can be attached to separate receiver channels in the MRI system, analogous to separate audio channels in a stereo audio system, and images deriving from catheters can be assigned colours that help to distinguish them from surrounding structures in 2D or 3D space [30] (Figure 2-3)**.** When active guidewires are combined with passive catheters or balloons filled with dilute gadolinium MRI contrast, the pair becomes readily visible.

Another type of active catheter design, embedding tracking-microcoils, is used to track individual points on the catheter during MRI [21, 31-33]. Tracking-microcoil catheters require a slight modification of the MRI pulse sequences, a small number of intermittent non-selective

excitations to localize the microcoils in space and calculate their position on the image. The microcoil location usually is depicted as a cross hair overlaid on the image (Figure 2-3). These tracking-microcoil systems are simple and effective, but unfortunately cannot depict the full length of catheter devices unless the catheter contains dozens of them.

Active catheter designs require conductive connections to the MRI scanner. These tend to heat if longer than 10–15cm. MRI pulse sequence techniques can reduce the energy deposited per image and therefore heating [34], at an acceptable penalty in image quality. These include radial sampling, spiral sampling and echo planar imaging which use fewer excitation pulses and longer repetition times, variable flip angle sequences [35] and parallel imaging. Methods being developed to reduce specific absorption rate (SAR) at high fields, such as adaptive parallel transmission, may also prove helpful at lower fields to reduce heating during MRI-guided interventions [36].

Several teams have developed circuitry for detuning or decoupling conductive transmission lines [37-41], or have developed alternative transmission lines such as fibre optics [42-45]. Using loopless antennae, existing interventional devices such as nitinol occluder delivery cables can be modified and tuned to indicate device deployment state (for example, open versus closed) [46]. One profile-design, loopless active decoupled and detuned guidewire, the SurgiVision 0.030” x 100cm guidewire, briefly obtained US FDA marketing clearance for invasive intravascular MRI in humans [6, 47, 48]. The limitation of this device was that the receiver sensitivity fell to zero at the distal tip, which was difficult to visualize and insufficient to navigate vasculature under rtMRI. Improved designs have not yet been commercialized [28].

MR-conditional guidewires would facilitate numerous interventions using otherwise intrinsically MR-safe devices (e.g. angioplasty balloons or non-braided catheters). To date polymeric guidewires do not afford the requisite mechanical properties (i.e. stiffness and torquability) but metallic (non-ferromagnetic) guidewires risk heating. Our lab designed an alternative strategy to address the issue of device heating by embedding a fibre optic temperature probe into a 0.035” active guidewire with similar mechanical properties to commercial X-ray guidewires [29]. Heating was monitored continuously during in vivo use and was negligible under normal operating conditions. Importantly, the whole shaft is active and the tip has a distinct signal which is critical when navigating the vasculature [49]. We plan to test this guidewire in human subjects once US FDA approval is granted (Figure 2-4).

Several teams have reported “wireless” active catheters or stents [50-53], which are inductively

coupled with the MRI system (Figure 2-3). Theoretically these can be exploited to enhance later non-invasive imaging, for example, of restenosis or of captured thromboemboli.

Of note, multiple approaches to enhance device visibility can be combined. For example an interventional MRI system could include an active-profiling guidewire that incorporates tracking-microcoils near the tip to enhance distal visibility; a passive balloon incorporating passive platinum marker bands when deflated and filled with dilute gadolinium when inflated; used together to deliver an inductively-coupled stent-graft device.

The main barrier to further clinical translation of iCMR remains the limited commercial availability of clinical-grade active and devices. Nevertheless, a wide range of prototype applications has been demonstrated in animals.

2.5 iCMR applications

Certain applications lend themselves to iCMR development. Target anatomic structures that are relatively immobile or slow moving (such as peripheral arteries) are attractive because MR images can be updated slowly and therefore can have higher SNR or spatial resolution. Large or thick-walled structures (such as heart or aorta) are attractive because they contain many proton spins, can be imaged with high SNR, and contrast mechanisms might be available readily to distinguish them from neighbouring structures. Structures that can be contained within a single imaging plane (such as straight segments of iliac arteries) can be imaged rapidly, compared with tortuous smaller structures such as coronary arteries, which are difficult to image in real-time.

The myocardium is an attractive target despite its high degree of cardiac and respiratory motion because it is a large, thick-walled structure that is readily depicted (using SSFP MRI) in high contrast compared with the blood space. Even thin-walled structures, such as the myocardial atria, are visible with current rtMRI.

2.5.1 Coronary artery disease

The SNR of proton MRI is too low to provide temporal resolution (33–66 ms) at anywhere near the spatial resolution (200 µm) currently enjoyed by X-Ray fluoroscopy operators conducting complex coronary interventions in heavily diseased, even occluded, coronary arteries using 0.014” (0.35mm) guidewires. Barring unforeseen technical breakthroughs, meaningful coronary artery interventions are not likely to be conducted using MRI.

That said, Speuntrup et al [54] demonstrated navigation and delivery of passively-visualized stainless steel stents in the coronary arteries of healthy swine. The devices and target proximal coronary arteries were readily visible using SSFP at 1.5T despite cardiac motion and the small size of these structures. Nonetheless, we do not believe that coronary artery intervention is suited for iCMR, because the imaging is inferior and there is no clear benefit compared with X-ray fluoroscopy.

2.5.2 Peripheral vascular disease

The most straightforward iCMR applications, transluminal angioplasty [55-59] and stent deployment [60-65], have been conducted in numerous animal models. Similarly, investigators have reported placement of vena cava filters [66-68] and even transcatheter visceral embolization of, for example, renal or hepatic parenchyma [69-71]. These are important proofs of concept toward clinical development. Indeed a few human examples of peripheral artery angioplasty and stenting have been reported. For the most part, these represent straightforward axial displacement of devices requiring little interactive image guidance.

iCMR also offers the convenience of using a single imaging modality to determine reference vessel size, whereas X-ray guided angioplasty requires adjunctive intravascular ultrasound to determine arterial wall characteristics (including media-to-media diameter). However, even in simple angioplasty and stenting, iCMR offers a potential safety advantage over conventional X-Ray. Raval *et al* [65] conducted iCMR-guided stenting of aortic coarctation in a pig model. Continuous imaging both of target pathology and devices immediately revealed catastrophic aortic rupture when deliberately oversized devices were employed. Early recognition offers the only opportunity effectively to treat this life-threatening complication.

Perhaps more compelling are applications that exploit the ability of MRI to visualize vascular spaces not conspicuous using X-ray. In a pig model of chronic total occlusion of peripheral arteries, Raval *et al* [72], used iCMR to navigate a recanalizing guidewire. These trajectories cannot be determined using X-ray because the occluded lumen cannot fill with contrast. iCMR permitted the operators to traverse complex occlusions while remaining within the walls of the target operator. This can be especially important in recanalization of tortuous peripheral artery occlusions, such as those found in the pelvis.

Aortic aneurysm disease often entails complex tortuous three-dimensional structures that are difficult to visualize using projection X-ray. iCMR might provide a single-modality solution to procedure planning, device deployment, and anatomic and hemodynamic

assessment of catheter-based (endograft) treatment of aortic aneurysm. In a simple pig model, Raman *et al* [73] demonstrated all of the above steps using custom "active" stent graft devices. Endograft treatment under MRI restored a normal lumen contour and restored laminar flow. Moreover, MRI demonstrated device apposition to the target aortic wall and allowed interrogation for endoleak.

The team at University Hospital Essen has elegantly applied iCMR to guide the placement of stent grafts in an animal model of thoracic aortic dissection [74]. They used unmodified, passive stent graft devices. MRI clearly revealed the true and false lumens of the dissected aorta, guided stent-graft deployment, and demonstrated stent-graft obliteration of the false lumen. This was another excellent example of the intrinsic value of simultaneous tissue and device imaging using real-time MRI (Figure 2-7).

2.5.3 Cardiac catheterization and structural heart interventions

The UCSF group [75] reported a comprehensive diagnostic cardiac catheterization procedure in a porcine model of atrial septal defect using iCMR. They used catheters containing catheters containing tracking microcoils embedded near the tip. They were easily able to accomplish left and right heart catheterization including continuous intra-cavitary pressure monitoring and blood sampling. They also incorporated phase-contrast MRI into their procedures for the determination of shunt ratios. Other groups have reported rtMRI catheter manipulation using selective arteriography using, for example, tracking-microcoil-based catheters for selective carotid artery catheterization [76], passive catheters over active guidewires for selective coronary arteriography [77], or active catheters for selective visceral artery catheterization [78] in swine.

Several groups have deployed passively-visualized nitinol occluder devices to treat porcine models of atrial septal defect [79] and thereafter to assess hemodynamics using phase-contrast MRI [80, 81].

Kuehne *et al* [82] have reported preliminary experience deploying a passively-visualized nitinol-based aortic valve prosthesis from a transfemoral approach in healthy swine. Theirs is a good demonstration of the value of combined tissue and device imaging for the precise placement of critical prosthetic devices.

Our lab [83, 84] and others [85-88] have used iCMR to deliver cells and other materials into specified targets in normal and infarcted animal hearts. We have found it particularly useful to interleave multiple slices during iCMR, and to render them in 3D to represent their true

geometric relationship. This technology provides “exposure” of the inside of the beating heart even better than does open-chest surgery. Targeting can be based on wall motion, late gadolinium enhancement (infarction), perfusion defects, strain maps, or any other contrast mechanism selected. When the injectate includes a contrast agent, real-time MRI can interactively depict the intramyocardial dispersion of the injected materials. This can be valuable for confirming successful delivery, for assuring confluence of treated volumes, and for avoiding inadvertently overlapping injections.

2.5.4 Cardiac electrophysiology

Cardiac electrophysiology procedures are currently conducted using catheter techniques without compelling image guidance. Endocardial surface maps are generated using electromagnetic mapping techniques, but these provide only “roadmaps” that do not account for respiratory and other dynamic changes. Most catheter-based ablation procedures are ultimately guided by multichannel intracardiac electrograms. Alternatively, ablation is conducted under direct surgical exposure [89]. iCMR might provide similar “exposure” for image-guided transcatheter ablation of cardiac arrhythmia and visualization of ablation lesions.

Several groups have performed pre-clinical catheter tracking experiments using active catheters that acquire filtered local intracardiac electrograms [90] and have characterized ablated myocardium over time [91]. The team at Massachusetts General Hospital positioned electrophysiology catheters in an MRI system and overlaid these positions onto high-resolution cardiac images [92]. More recently, they performed left ventricular mapping in a porcine model of chronic infarction [93]. Others have used similar systems to ablate the cavotricuspid isthmus or pulmonary veins [94-96].

2.5.5 Extra-anatomic communications

iCMR may even enable interventions outside normal lumen spaces. Arepally et al [97] conducted image-guided puncture of the cardiac interatrial septum, a procedure usually conducted primarily using tactile feedback under X-ray. Our lab conducted similar septal puncture followed by balloon septostomy and MRI assessment of the resulting small intracardiac shunts [98]. While similarly guidance is afforded by intracardiac or transesophageal ultrasound, these are important preclinical steps toward more elaborate procedures guided by MRI.

With the advent of trans-catheter valvular interventions, alternative access routes to deliver

large devices to the heart are required. iCMR facilitates development of novel approaches that are not feasible under X-ray guidance, for example direct transthoracic access to the left ventricle through the cardiac apex [99] or right ventricle [100]. Ratnayaka *et al* [101] demonstrated that a direct transthoracic approach could be used to close ventricular septal defects in an animal model (Figure 2-5). An added advantage is the ability to monitor for and manage complications early, for example pericardial effusion [102].

Using a unique double-doughnut MRI configuration containing an integrated flat-panel X-Ray fluoroscopy system, Kee *et al* have conducted preclinical [103] and clinical [104] transjugular intrahepatic porto-systemic shunt (TIPS) procedures. Even in this proof-of-concept experiment, MRI reduced the number of trans-hepatic needle punctures compared with historical controls. Arepally *et al* conducted even more adventurous preclinical experiments in creating a catheter-based mesocaval shunt outside the liver capsule [105]. Ratnayaka *et al* recently created percutaneous bidirectional Glenn shunts in swine, connecting the superior vena cava and right pulmonary artery, using rtMRI guidance and an "active" needle (Figure 2-6). This sort of extra-anatomic bypass, once made available to non-surgeons, has the potential to revolutionize mechanical revascularization.

2.6 Human iCMR procedures

2.6.1 Diagnostic cardiac catheterization

Razavi *et al* [13] at Kings College in London conducted the first diagnostic cardiac catheterization in children using a combined XMR environment. The same group conducted X-ray Fused with MRI (XFM) procedures, in which prior MRI datasets were combined with real-time XRF to conduct therapeutic procedures. Kuehne *et al* also conducted diagnostic cardiac catheterization procedures using passive catheter devices under rtMRI [14]. Three groups have reported invasive imaging of peripheral artery atheromata using profile-design active guidewire receiver coils [6, 47, 48]. In the report by Dick *et al* [6], we concluded this guidewire design adds little to surface coils for diagnostic MRI of atherosclerosis, but might have value in delivering interventional devices using iCMR. A team in Regensburg, Germany, conducted high quality selective intra-arterial MR angiography [106] and reported preliminary revascularization procedures using passive devices in the iliac [107] and femoral [108] arteries. The Stanford team conducted iCMR-assisted TIPS procedures in patients [104].

At NIH [15] we perform MR-guided right heart catheterization using MR-safe catheters with gadolinium-filled balloons (Figure 2-10). The procedure has been re-classified as a standard

medical procedure in our hospital and to date we have performed over 80 clinical cases in adults with a wide range of diseases, including pulmonary hypertension, heart failure, and intra-cardiac shunt. We have also opened an interventional MRI suite at Children's National Medical Center in Washington DC to provide 'radiation-free' catheterization to paediatric and adult patients with congenital heart disease.

Importantly, MR-guided catheterization promises to provide hemodynamic and functional information that X-ray fluoroscopy cannot [109]. Cardiac chamber volumes and function, and large vessel dimensions can be assessed using cine imaging. In many diseases, for example pulmonary hypertension or advanced heart failure, right ventricular mass, volume and function have independent prognostic value [110, 111]. Phase contrast MRI permits measurement of flow through major vessels (e.g. pulmonary arteries and aorta) and calculation of Qp and Qs. Muthurangu elegantly demonstrated that important hemodynamic parameters such as pulmonary vascular resistance [112] or pulmonary artery compliance [113] were more accurately assessed by combining MR phase contrast-derived cardiac output and invasive pressure measurements, compared with traditional cath lab techniques (e.g. Fick or thermodilution), particularly during pulmonary vasoreactivity testing with high flow oxygen and inhaled nitric oxide.

By adding sequences such as lung perfusion to screen for chronic pulmonary thromboemboli, T1 mapping or delayed contrast enhancement to screen for diffuse of regional myocardial fibrosis, a comprehensive 'one-stop' cardiopulmonary assessment can be obtained [114, 115]. By repeating imaging and invasive hemodynamic measurements under different physiological provocations, for example with exercise, saline challenge or inhaled nitric oxide, iCMR catheterization could help unmask latent symptoms and pathology not apparent at rest and provide useful prognostic information [109, 116-118]. We now routinely perform functional imaging, phase contrast to measure cardiac output and invasive hemodynamic measurements at baseline and repeated with up to two physiological provocations in all patients, all within less than two hours. We have also streamlined scanning protocols to eliminate the need for patient breath holding, using investigational realtime sequences and free-breathing phase contrast with averaging [119, 120]. This is critical because many patients with advanced disease struggle to breath hold, particularly if they receive sedation for the catheterization procedure.

2.6.2 Structural heart interventions

Some structural iCMR procedures have already been performed in humans, including aortic

coarctation angioplasty [121], femoral and popliteal artery angioplasty [108] and pulmonary valvuloplasty [11]. But widespread clinical adoption has been delayed by the unavailability of commercial MR-safe guidewires, catheters and devices that meet the mechanical standards expected of conventional catheters and devices used in X-ray.

2.6.3 Cardiac electrophysiology

Several manufacturers (*Imricor, MRI-Interventions*) have developed MR-conditional electrophysiology ablation systems and catheters, using passive or active tracking to navigate the cardiac chambers (Figure 2-9). Using these systems, ablation of simple atrial arrhythmias has been reported in early human studies [122, 123] (Figure 2-8). Extensive work is on going to optimize ablation lesions visualization, which has the potential to improve arrhythmia termination rates by enabling the operator to verify adequate ablation depth and continuity of ablation lines in realtime [124-129]. There is evidence that procedural success defined by rates of arrhythmia recurrence after ablation correlates with the extent of late gadolinium enhancement [130].

2.7 Conclusion

Advocates promote the development of iCMR for the sake of reduction of radiation exposure to patients, especially young patients who are anticipated to require a large cumulative radiation exposure during diagnostic and therapeutic procedures; reduction of radiation exposure to operators and staff, who endure a large cumulative radiation exposure during their careers; reduction of patient exposure to nephrotoxic iodinated contrast, which is important in patients with moderate-severe renal disease; and to eliminate the requirement that staff wear heavy protective lead garments, which are associated with a high incidence of chronic musculoskeletal injury. Detractors argue that iCMR represents a costly and cumbersome alternative to procedures that otherwise are conducted rapidly and efficiently under X-ray guidance and occasionally enhanced with adjunctive ultrasound. Detractors also argue that despite any potential benefit, the large capital outlays and expected higher marginal cost of disposable (catheter) equipment are simply unjustifiable. These arguments are less tenable. Existing XMR facilities are constructed to permit each imaging system to be used independently of the other. The only incremental expense over separate angiography and MRI systems is the cost of the inter-modality transfer table and the barrier doors connecting the systems.

As described above, the chief obstacle to further development of iCMR is the limited

availability of clinical grade catheters and devices suitable for use in the MR environment. This in turn discourages wider deployment of XMR or iCMR systems. That said, clinical iCMR for simple diagnostic cardiac catheterization is feasible using existing technology and off-the-shelf catheters, and is in routine clinical use in institutions in the US and Europe. iCMR electrophysiology is expected to be an area of particular interest and technical development, now that MR-conditional electrophysiology mapping and ablation systems are available and first-in-man arrhythmia ablation has been demonstrated.

However, iCMR may prove superior because using a single modality, 3D anatomy, composition, function, and hemodynamics can be combined. iCMR can provide surgical-grade exposure to guide non-surgical minimally-invasive procedures and could enable completely new procedures to be developed. This has the potential to revolutionize the conduct of minimally invasive image-guided treatments.

2.8 Figures

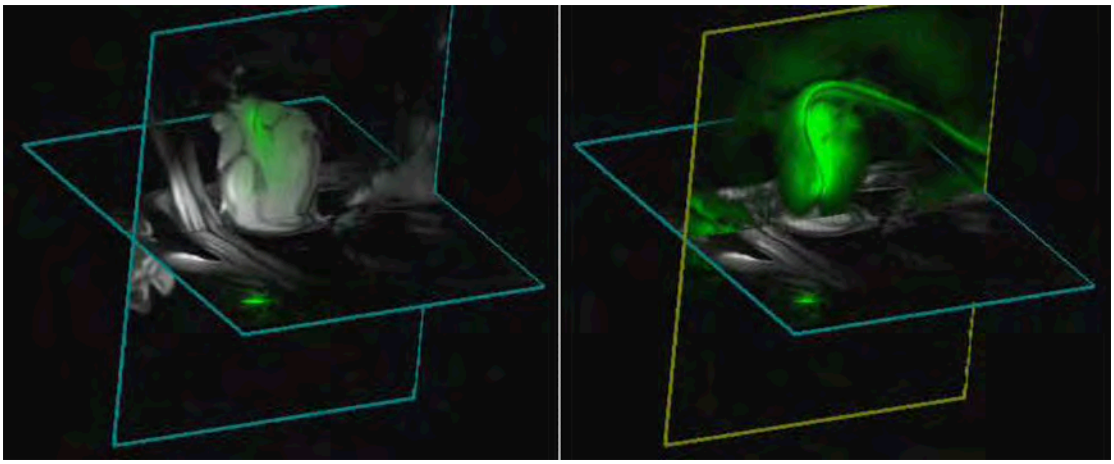

Figure 2-1: Demonstration of multi-slice imaging

Two slices are acquired together and displayed in their true 3-dimensional relationship. This also demonstrates the problem of out-of-plane catheters. On the left, the heart is visualized in multiple concurrent imaging planes while a transaortic myocardial injection needle is manipulated. The guiding catheter is coloured green. The distal end of the catheter is outside the selected imaging plane, and is therefore not visible. On the right, 'projection mode' is activated in the coronal view so that the entire length of the guiding catheter can be visualized. This functionality is possible with catheters incorporated 'active' receiver coils.

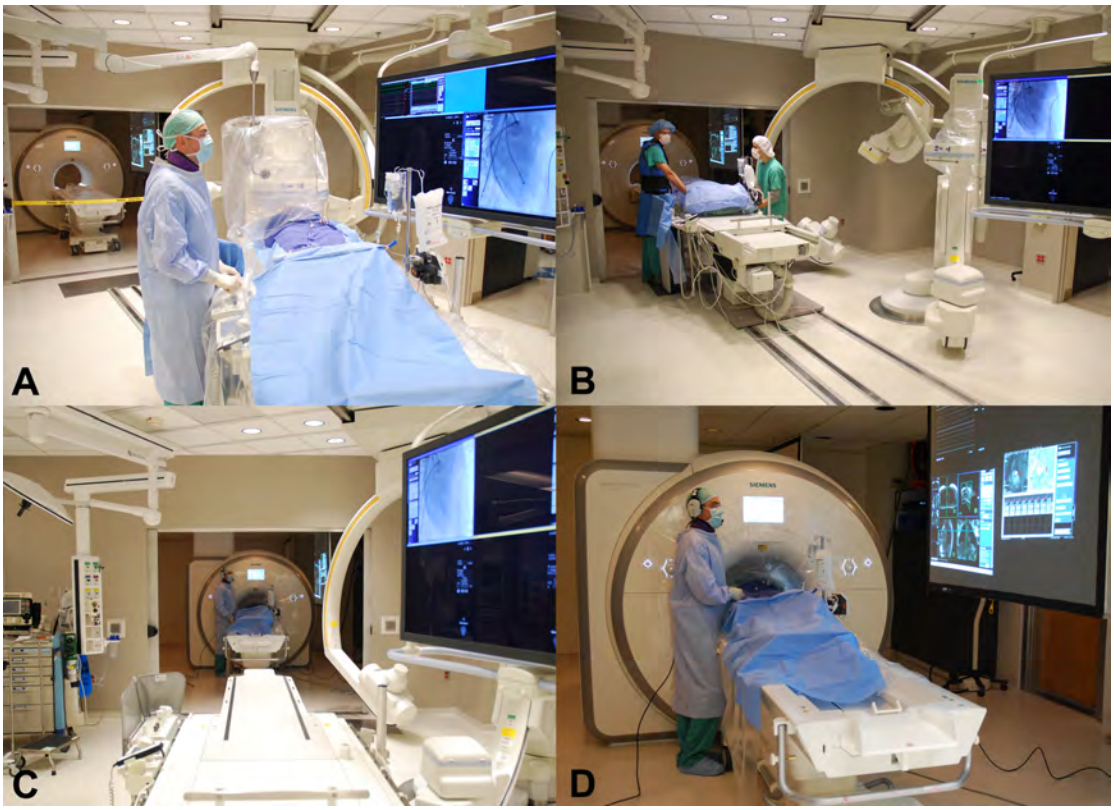

Figure 2-2: iCMR suite

A view of the NIH XMR suite during a procedure – (A) Conventional X-ray fluoroscopy is used for coronary artery catheterization. (B-C) The patient is transferred to MRI on the transfer table. (D) Diagnostic right heart catheterization is performed using realtime MR-guidance. The operators wear fibre optic noise-suppression headsets with microphones, and watch realtime MR images and hemodynamics projected from shielded projectors.

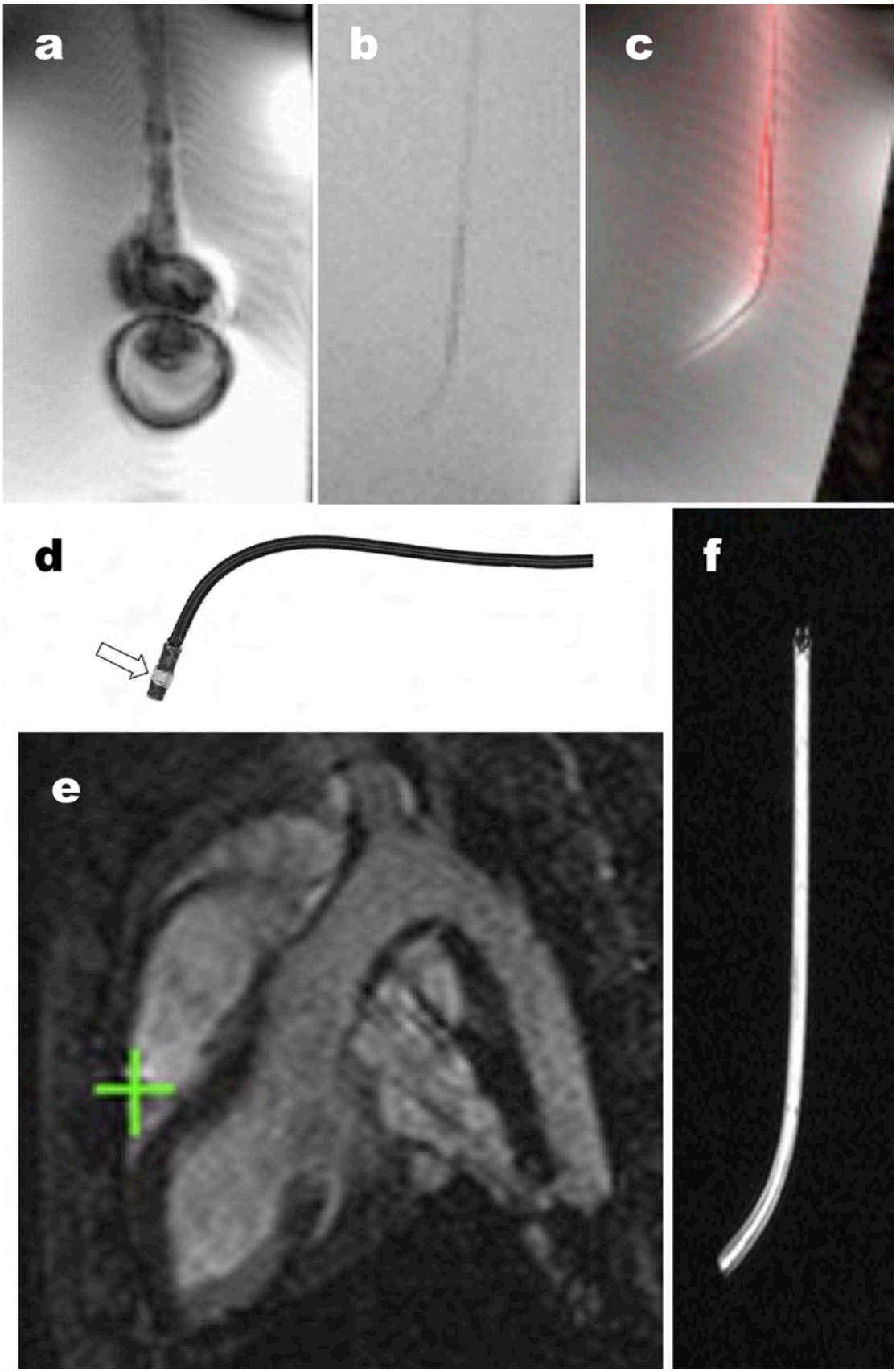

Figure 2-3: A comparison of representative catheter designs for iCMR

(A) Shows a traditional X-ray catheter, which incorporates stainless steel braid for strength.

The steel distorts the MR image and has the potential to heat, as it would in a microwave oven. (B) Shows the same passive catheter without steel braids, rendering it nearly invisible even *in vitro*. (C) Shows the same catheter shape in an 'active-profile' design, incorporating an MRI receiver coil to make it visible. (D) Shows a tracking-microcoil-design catheter incorporating a microcoil near the tip. The 3D position of the microcoil can be tracked rapidly and indicated using computer-synthesized cross-hairs (green) as it is moved into the right ventricle of the animal shown in (E), Courtesy of Michael. Bock, *DKFZ Heidelberg, Germany*). The rest of the catheter is not visible under MRI. (F) Shows a catheter incorporating a 'wireless' inductively-coupled receiver coil (Courtesy of Harald H. Quick, *University Essen, Germany*) that can be visualized as a bright signal using MRI[131].

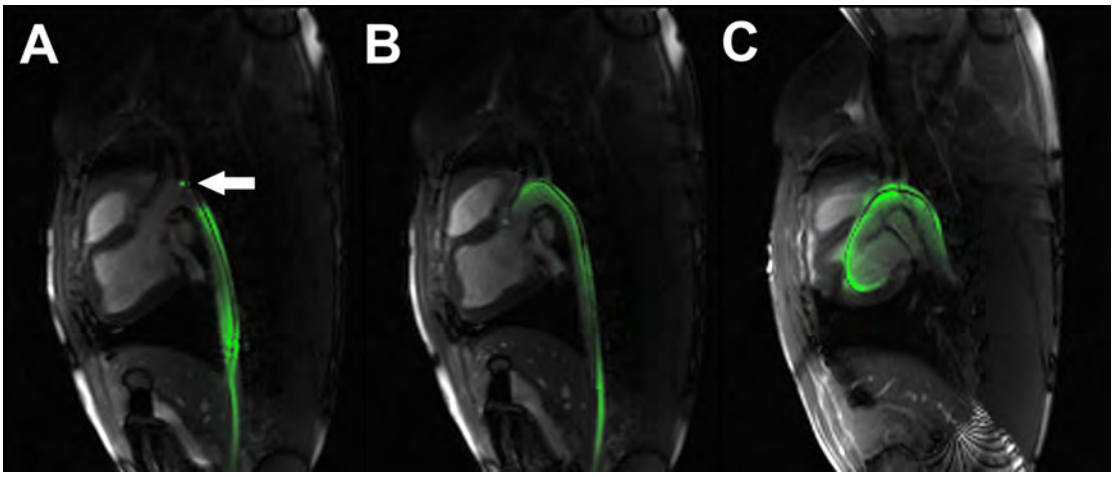

Figure 2-4: Left heart catheterization in a pig using the NHLBI active iCMR guidewire

The whole shaft of the guidewire is active and the tip has a separate and distinct signal (arrow). The guidewire is navigated to the (A) aortic arch, (B) aortic valve and (C) through the aortic valve into the left ventricle under realtime MR-guidance.

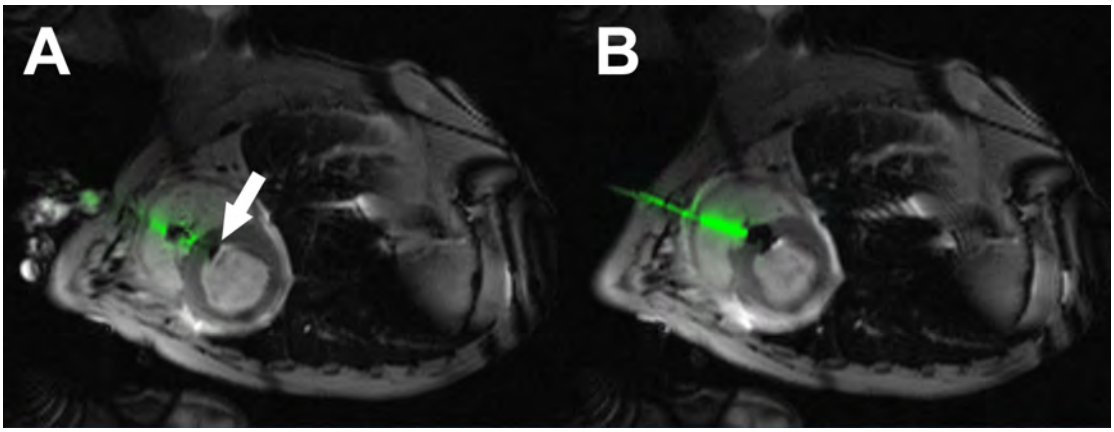

Figure 2-5: iCMR direct transthoracic ventricular septal defect closure

The right ventricle is accessed directly through the chest wall using an MR 'active' needle under realtime MR-guidance. The ventricular septal defect (VSD) is crossed anterogradely and then closed using an Amplatz muscular VSD occluder. The delivery cable for the closure device is also active. (A) The left ventricular disk (arrow) is deployed and pulled back against the septum. The right ventricular disk is then deployed and pushed forward against the septum to close the defect. The right ventricle free wall puncture is closed using an off-the-shelf vascular closure plug.

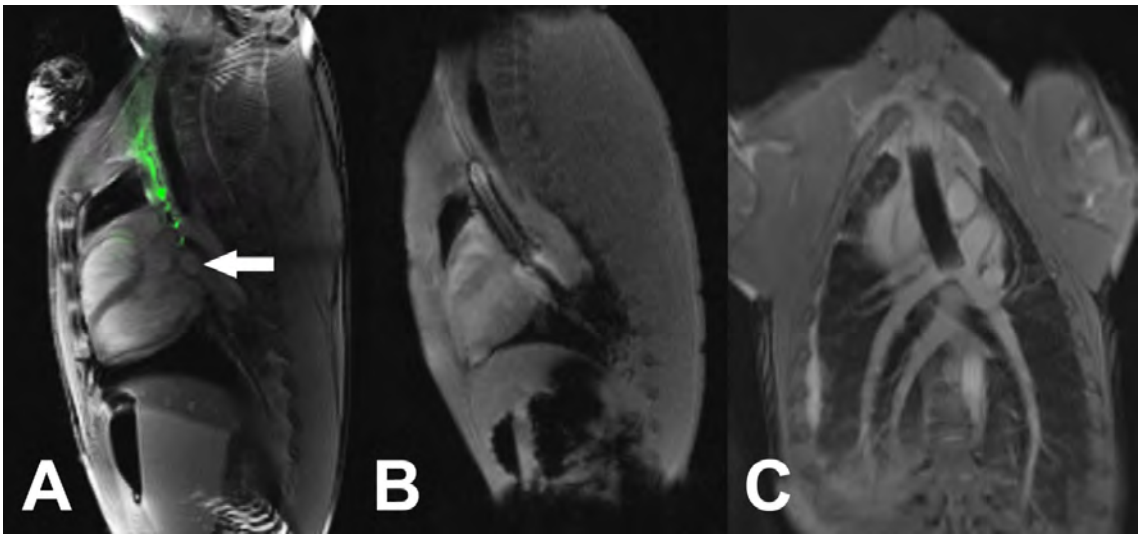

Figure 2-6: iCMR percutaneous bi-directional Glenn shunt

Central venous access is obtained via the right internal jugular vein. (A) An active needle is used to puncture from the superior vena cava in to the right pulmonary artery under realtime MR-guidance (arrow). A guidewire is then positioned into the distal left pulmonary artery. (B) A covered stent is then deployed from the SVC into the right pulmonary artery. The stent balloon is filled with gadolinium. (C) The SVC and right pulmonary artery are now connected with a conduit (i.e. 'Glenn' shunt).

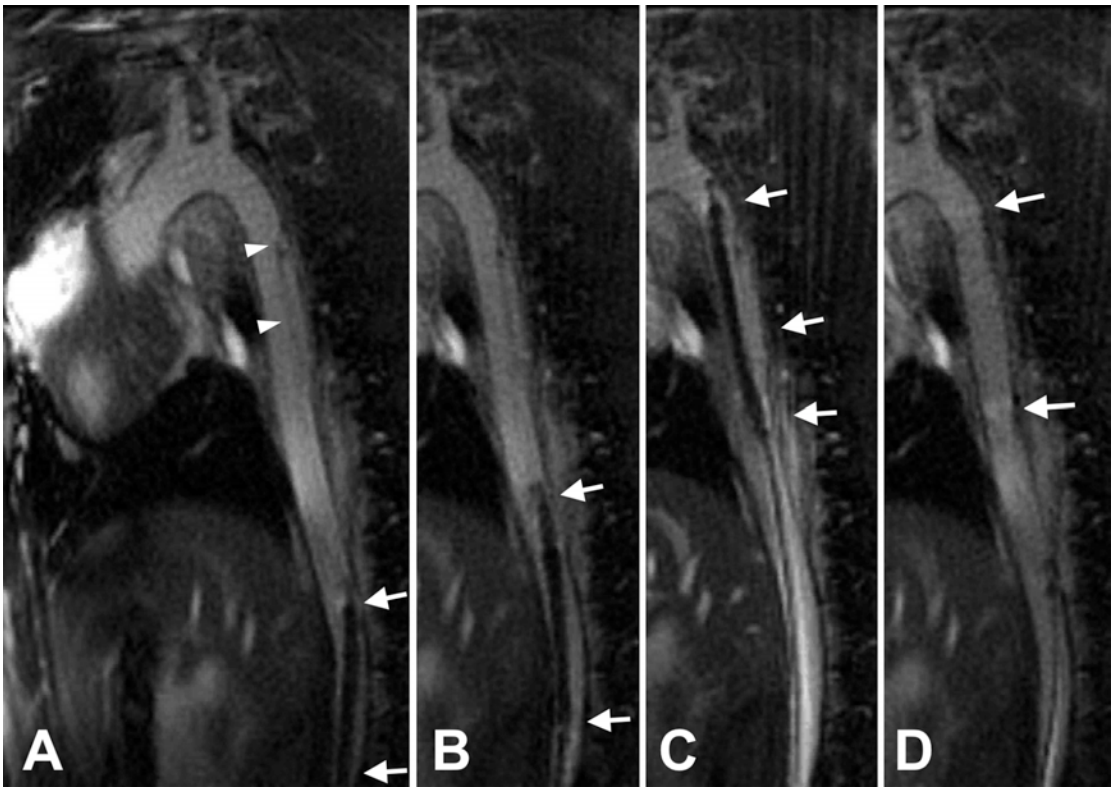

Figure 2-7: Endograft treatment of thoracic aortic dissection in a pig model, using a commercially available passive device

(A) Baseline aortic dissection. The dissection is depicted with arrowheads. (B) The endograft is advanced retrograde from the iliac artery. The tip of the endograft (arrows) approaches the inferior aspect of the dissection, inside the true lumen. (C) The endograft is in final position before deployment. (D) Most of the false lumen is obliterated after endograft delivery. (Courtesy of Holger Eggebrecht, MD and Harald H. Quick, PhD, *University Hospital Essen, Germany*).

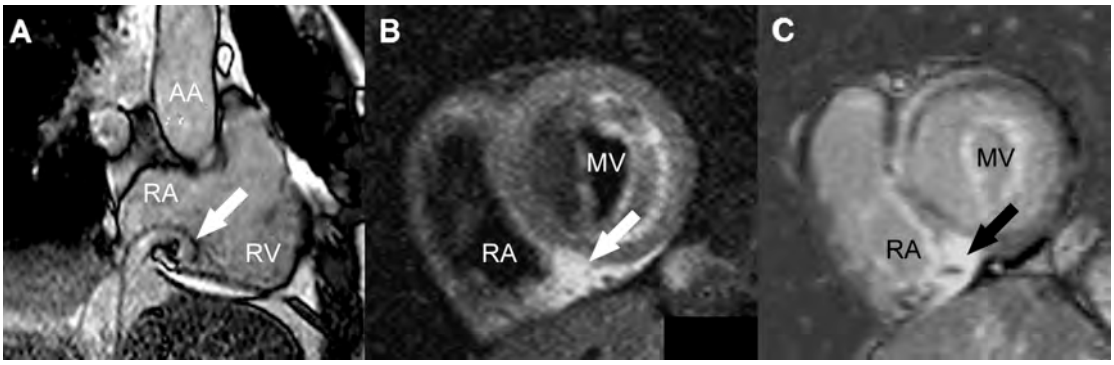

Figure 2-8: Cavo-tricuspid isthmus ablation in a human subject

(A) The passively tracked tip of the ablation catheter is positioned above the cavo-tricuspid isthmus (arrow). Post-ablation T2 weighted (B) and late gadolinium enhancement (C) images of the cavo-tricuspid isthmus show the newly created ablation lesion (arrows). AA: ascending aorta; MV: mitral valve; RA: right atrium; RV: right ventricle. (Courtesy of M. Gutberlet, M. Grothoff and G. Hindricks, *University of Leipzig, Germany*).

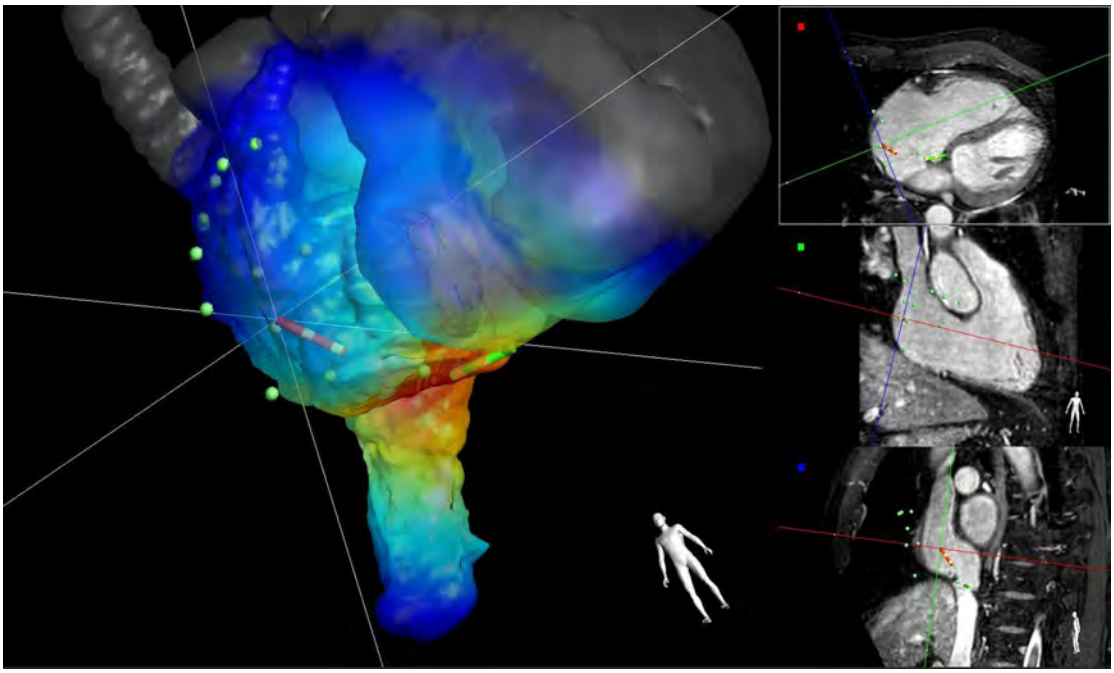

Figure 2-9: Catheter ablation of typical right atrial flutter under MR guidance

The intracardiac electrogram is acquired at several locations with a first actively tracked catheter (red, Imricor Vision MR-EP catheter) while pacing with a second actively tracked catheter (green) located in the coronary sinus. The Interventional MR iSuite (Philips Research Hamburg) uses the position tracking data of the green catheter and corresponding activation time data to update a color-coded activation time map for each new mapped point. The colours represent the interpolation of previously acquired activation times on the right atrial endocardial shell. Red indicates early and blue late activation. The shell has been derived from the segmentation of a 3d cardiac scan acquired immediately before the intervention (Courtesy of R. Rezavi, M. O'Neill and T. Schaeffter, *King's College London, UK*; S. Weiss and S. Krueger, *Philips Research, Hamburg, Germany*; S. Wedan, G. Stenzel, T. Lloyd and D. Sunnarborg, *Imricor, Minnesota, US*).

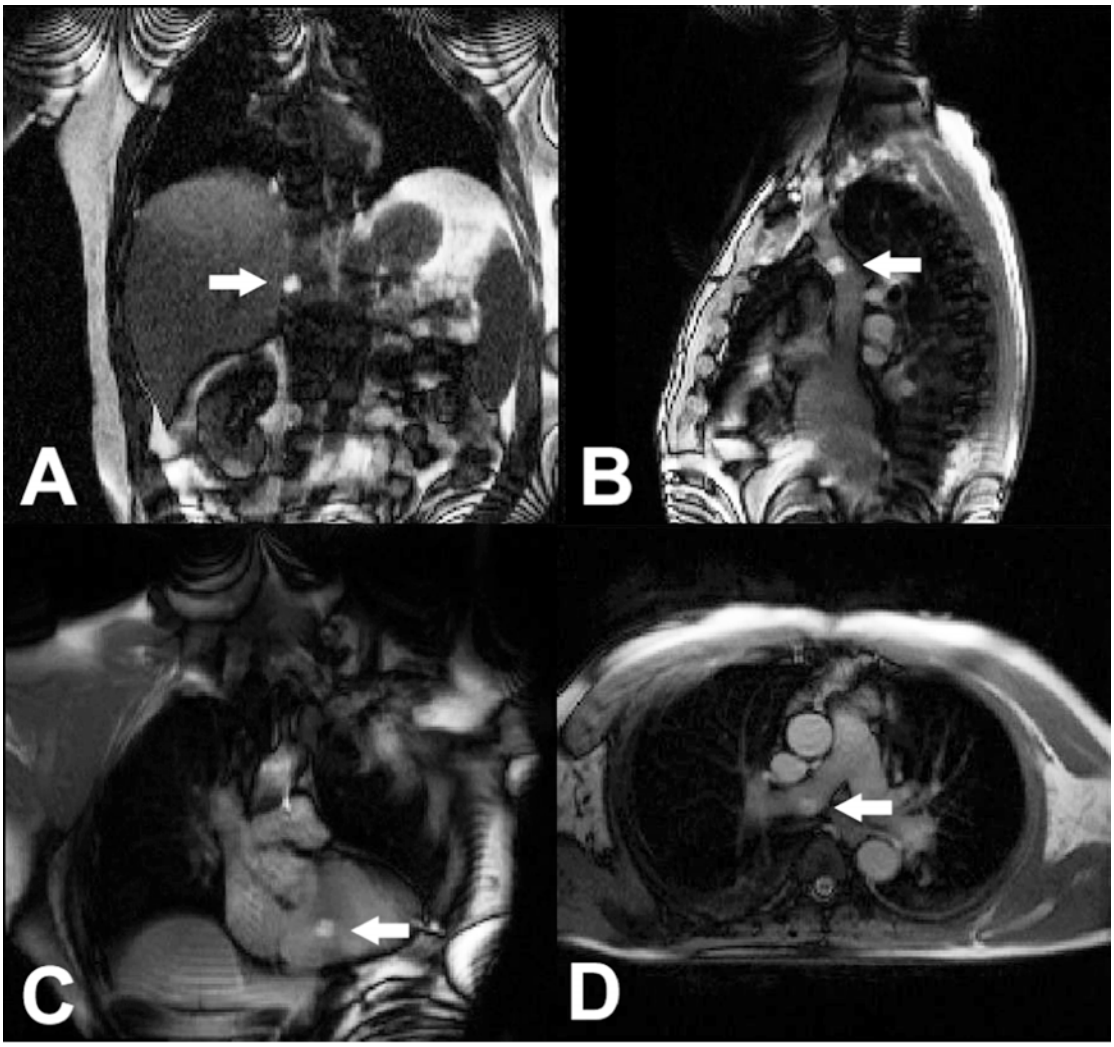

Figure 2-10: MRI guided right heart catheterization

The gadolinium-filled balloon wedge end hole catheter is navigated through the right heart using realtime MR-guidance. The balloon appears as a white ball on the images (arrows). Catheter tip positioned in (A) Inferior vena cava, (B) superior vena cava, (C) right ventricle, and (D) right pulmonary artery. At key positions, for example main pulmonary artery, simultaneous invasive pressures and MR phase contrast flow measurements are acquired.

2.9 Table

Approach	Advantages	Disadvantages	Solutions	Examples
Passive devices: Catheter materials directly influences MR image	Simple and inexpensive View device by imaging device in tissue context Reduced technical and regulatory requirements	Visibility is reduced Susceptibility markers (steel, dysprosium) destroy nearby signal Conductive lines, if present, can heat	Can work in combination with active-devices (*e.g.* passive balloon over active guidewire)	Gd-filled balloon [15, 58, 59, 65, 108, 132] CO2-filled balloon [12-14]. Nitinol stent [60, 62, 63, 65, 103, 107] *Imricor* EP mapping and ablation system [96]
Active "profile" devices: Catheter incorporates an MRI receiver coil ("antenna") along much of its length and is imaged along with target tissue	View device by imaging device in tissue context Can use special MRI features: colour-highlighting, projection mode, plane-tracking	Potential heating Less visible at tip than at shaft ("loopless" designs) "Profile" of devices is blurry compared with sharp profile of devices under X-Ray or sharp "points" using active tracking devices	De-tuning and de-coupling can prevent heating Coils can enhance tip visibility	SurgiVision *Intercept* 0.030" guidewire coil [6, 47, 48]. NIH active 0.035" guidewire with embedded temperature probe [29, 49].
Active "tracking-coil" devices: Catheter incorporates small MRI receiver coils that can be tracked with simple pulse sequences alternating with MRI pulse sequences	Points on device can be visualized rapidly and accurately Points can be tracked without imaging, to increase speed or reduce absorbed RF Useful in automatic scan control (plane-tracking, etc.)	"Synthesized" points might deviate from "true" location on image Number of points is usually limited Requires "special" MRI pulse sequences, a minor modification	Can be combined with other approaches	MGH/GE EP mapping system [92, 93]. *MRI Interventions* EP mapping and ablation system [95]

Table 2-1: General approaches to make catheter devices conspicuous under MRI

Chapter 3. Transatrial intrapericardial tricuspid annuloplasty (*publication*)

3.1 Introduction

The tricuspid valve is often referred to as the 'forgotten valve'. Surgery for lone tricuspid regurgitation is rarely performed due to high mortality and morbidity. Persistent tricuspid regurgitation after aortic or mitral valve surgery is associated with poor prognosis. As more and more patients undergo transcatheter treatment for aortic and mitral valve disease, a transcatheter solution for the tricuspid valve is needed. While transcatheter solutions to treat aortic, mitral and pulmonary valve disease are now commercially available, there are none for the tricuspid valve.

Most tricuspid regurgitation is 'functional' or 'secondary', i.e. the leaflets are normal but the annulus is dilated, usually due to dilation of the right ventricle. Surgical treatment almost always involves implantation of an annuloplasty ring to correct the geometry of the annulus. Transatrial intrapericardial tricuspid annuloplasty is a fully percutaneous alternative that effects geometric change to the lateral tricuspid annulus from a circumferential extra-cardiac device positioned along the atrioventricular groove in the pericardial space.

3.2 The role of CMR

Understanding the complex geometry of the atrioventricular plane and the morphology of the tricuspid annulus in health and in disease requires a truly three-dimensional imaging modality with excellent soft tissue visualization. Three-dimensional echocardiography is limited by field of view and was therefore not ideal for this application. CMR is better suited to this application because it affords unlimited imaging planes and excellent soft tissue characterization. During this project, CMR was used to determine anatomical parameters for device design during the prototyping phase, to assess the effect of the device on dynamic cardiac geometry in vivo post-implantation and at different tension levels, to monitor for acute complications (specifically tricuspid valve obstruction and pericardial effusion), and to assess for short-term results in survival experiments. Evaluating the differential effect of tensioning on the tricuspid and mitral annuli was particularly important in order to determine the optimal geometry of the permanent implant.

The actual device implantation procedure was performed using X-ray fluoroscopy guidance

and CMR is unlikely to be needed for clinical translation. Tensioning would be performed under echocardiography guidance focussed on the tricuspid annulus and titrated to reduce tricuspid regurgitation. The TRAIPTA device would ideally be constructed from MRI-conditional materials so that patients could undergo CMR to assess position and device interaction with other structures (e.g. mitral annulus, right ventricular outflow tract) throughout the cardiac cycle, although dynamic cardiac CT would also be feasible.

3.3 Candidate's contribution

I performed all of the pre-clinical TRAIPTA experiments, including creation of the animal model. I worked with our in-house engineering team to develop and build the TRAIPTA implant. I analysed the MRI images, collected the haemodynamic data and performed the statistical analysis. I drafted the manuscript and prepared the figures, tables and supplementary materials.

3.4 Creation of a porcine model of tricuspid regurgitation

There are several published animal models of functional tricuspid regurgitation. None use percutaneous techniques; rather all are invasive surgical procedures. Otaki first described a surgical model in which multiple small incisions were made around the circumference of the tricuspid annulus on cardiopulmonary bypass[133]. Walter described a similar technique performed off-pump with a video-assisted endoscope through a thoracotomy[134]. Bai reported a percutaneous technique of tearing the chordae tendineae, but this is a model of organic and not functional regurgitation[135].

We hypothesized that serial insults to the right heart could cause accelerated right ventricle and tricuspid annular dilation resulting in secondary (or 'functional') tricuspid regurgitation. We tested a combination of the following approaches in swine: (1) right ventricle myocardial injury through right ventricle marginal artery infarction; (2) right heart volume overload through atrial septal defect creation (atrial septostomy); (3) right ventricle pressure overload through pulmonary artery micro-particle embolization; (4) right ventricle volume overload through pulmonary valve disruption inducing free-flowing pulmonary regurgitation; and (5) targeted ethanol needle injection into the right ventricular papillary muscle. Importantly, all are transcatheter techniques rather than open surgery.

3.4.1 **Right ventricular free wall infarction**

Animals were pre-medicated with oral Amiodarone 400mg daily for 5 days prior to and after

the procedure and a further 300mg intravenous bolus was given at the time of procedure. The animals were anticoagulated with 150IU/kg of unfractionated Heparin. A biphasic cardiac defibrillator was connected. A temporary pacing wire was positioned in the right ventricular apex and set to pace at 60bpm on demand. The right coronary artery was engaged with an 8Fr multipurpose catheter and angiograms were taken in multiple projections. If the right coronary artery was dominant and the posterior descending artery diameter was >2mm then a 190cm hi-torque balance middleweight universal 0.014" guidewire (*Abbott Vascular*, Santa Clara, CA) was positioned in the posterior descending artery. A short (8-12mm) monorail compliant balloon, sized to occlude the vessel, was positioned as a distal protection device in the right coronary artery just proximal to the crux. A second 300cm hi-torque balance middleweight universal 0.014" guidewire was positioned in the mid right coronary artery and a short (8-12mm) over-the-wire balloon, sized to occlude the proximal right coronary artery. If the vessel was non—dominant or the posterior descending artery diameter was ≤2mm then the distal protection balloon was not used. Intravenous fluid bolus of 500mL was given. The distal balloon was inflated first and an angiogram was taken to confirm occlusion of the distal vessel. The proximal balloon was then inflated and an angiogram was taken to confirm occlusion of the proximal vessel. The proximal balloon guidewire was withdrawn and 1mL of Ethanol 100% doped with iodinated contrast was injected slowly through the over-the-wire balloon guidewire lumen into the space between the two inflated balloons. Both balloons were kept inflated for at least 5min and 12-lead electrocardiogram was monitored to confirm ischemic ST segment changes. The proximal balloon was deflated first to allow antegrade flow to flush any remaining Ethanol down the right coronary artery. After 30sec the distal balloon was deflated. In 4 animals, reperfusion was complicated by ventricular fibrillation requiring DC cardioversion and catecholamines. 4 animals developed severe right heart failure and/or intractable ventricular fibrillation and were euthanized. Final angiograms in the 4 surviving animals confirmed slow or absent flow in the acute marginal branches of the right coronary artery but normal flow in the posterior descending artery. Follow up imaging with magnetic resonance late gadolinium enhancement imaging confirmed subendocardial scar in the right ventricular free wall. There was no evidence of scar in the inferior wall of the left ventricle. This finding confirms that safeguarding the posterior descending artery with a distal protection balloon effectively limits the delivery of ethanol to right ventricular myocardium. However, the high mortality from right ventricle infarction was not acceptable and so this technique is not ideal.

3.4.2 Atrial septostomy

A 5Fr multipurpose catheter was positioned in the right atrium. Probing of the inter-atrial septum for a patent foramen ovale was performed with a 260cm 0.035" hydrophilic-coated guidewire (*Terumo*, Somerset, NJ). If the wire was able to cross into the left atrium then the catheter was advanced through the foramen ovale into the left atrium. If resistance was met then the catheter was exchanged for a 5Fr hydrophilic-coated catheter (*Terumo*). If no PFO was found then trans-septal puncture was performed under intra-cardiac echocardiographic guidance (*AcuNav, Siemens*) using a Brockenbrough trans-septal needle and Mullins sheath (*Medtronic*, Minneapolis, MN). An exchange-length 0.035" Rosen guidewire was positioned in the left upper pulmonary vein and the catheter/sheath was then removed. An 18-22mm diameter (length 4cm) balloon was then advanced over the guidewire and positioned across the inter-atrial septum. The balloon was inflated, first at low pressure to confirm a waist at the level of the septum and then up to the rated pressure (usually 2-3atm) until the waist disappeared. The balloon was then deflated and re-inflated twice. Flow across the inter-atrial septum, was confirmed with intracardiac echocardiography and/or angiography. No significant hemodynamic compromise and no peri-procedural complications were observed in any animal. However, right ventricle dilation was very slow to develop and therefore this technique is not ideal.

3.4.3 Pulmonary arterial microsphere embolization

A 7Fr balloon-tip Berman catheter (*Arrow*, Reading, PA) was positioned in the main pulmonary monitoring of pulmonary arterial pressure. Pulmonary hypertension was induced by infusion of non-bioresorbable 600-1200µm diameter microspheres (*Embospheres, Merit Medical*, South Jordan, UT) into the left and then right pulmonary arteries sequentially in 2mL aliquots every 15 minutes. After each administration, pulmonary and systemic arterial pressures were measured. Microspheres were administered until target pulmonary pressure was reached (defined as ≥30% increase from baseline) without systemic pressure compromise (<10% reduction from baseline). The average volume of microspheres administered was 8mL split equally between left and right pulmonary arteries. Infusion of microspheres was well tolerated with no hemodynamic compromise and no peri-procedural complications. Right ventricle dilation occurred rapidly and without complication, therefore this approach appears to be a good option to induce functional tricuspid regurgitation.

3.4.4 Pulmonary valve disruption

Disruption of the pulmonary valve results in free pulmonary regurgitation, which in turn results in volume overload of the right ventricle. Pulmonary valve disruption was achieved by deploying a large custom-built self-expandable Nitinol stent within the valve, pinning the leaflets open. Stent implantation was well tolerated although positioning large sheath in the right ventricular outflow tract to deliver the stent was very arrhythmogenic in swine. Right ventricle dilation occurred rapidly; therefore this approach appears to be a good option to induce functional tricuspid regurgitation. One animal developed a pericardial effusion, which upon necropsy was caused by erosion of a sharp end of the stent braid through the right ventricular outflow tract. Stents with smooth, atraumatic ends should prevent this complication.

3.4.5 Right ventricular papillary muscle ethanol injection

Under intracardiac echocardiography guidance, a Brockenbrough needle was advanced into the right ventricle and into the base of the right ventricular papillary muscle. A small amount of 100% ethanol was injected (approximately 0.5-1mL) and the needle withdrawn. Although visible using intracardiac echocardiography, the right ventricular papillary muscle was small in swine and therefore was difficult to target accurately. In addition, this technique causes tricuspid regurgitation through restriction of the papillary muscle and chords, which is a primary rather than secondary mechanism of regurgitation. For this reason, this technique was not considered useful and was abandoned.

3.4.6 Combination of techniques

For the purposes of the TRAIPTA experiments, we used animals with tricuspid regurgitation caused through a number of different combinations of the above techniques (as detailed in the Section 3.5). For future experiments, in order to minimize complications and mortality, the preferred technique would be to create functional tricuspid regurgitation via simultaneous pressure and volume overload of the right ventricle, by pulmonary artery microsphere embolization and stenting open the pulmonary valve. We expect mortality and morbidity from these two procedures to be low. Right ventricular dilation appears to occur rapidly (within approximately 2 weeks) resulting in tricuspid annular dilation and development of tricuspid regurgitation.

3.5 Transatrial intrapericardial tricuspid annuloplasty

An original research manuscript published in the '*Journal of the American College of Cardiology: Cardiovascular Interventions'* in 2015.

JACC: CARDIOVASCULAR INTERVENTIONS
VOL. 8, NO. 3, 2015

ISSN 1936-8798/$36.00
PUBLISHED BY ELSEVIER INC.
http://dx.doi.org/10.1016/j.jcin.2014.10.013

TRANSLATIONAL

Transatrial Intrapericardial Tricuspid Annuloplasty

Toby Rogers, BM, BCH,* Kanishka Ratnayaka, MD,*† Merdim Sonmez, PHD,* Dominique N. Franson, BS,* William H. Schenke, BA,* Jonathan R. Mazal, MS,* Ozgur Kocaturk, PHD,*‡ Marcus Y. Chen, MD,* Anthony Z. Faranesh, PHD,* Robert J. Lederman, MD*

ABSTRACT

OBJECTIVES This study sought to demonstrate transcatheter deployment of a circumferential device within the pericardial space to modify tricuspid annular dimensions interactively and to reduce functional tricuspid regurgitation (TR) in swine.

BACKGROUND Functional TR is common and is associated with increased morbidity and mortality. There are no reported transcatheter tricuspid valve repairs. We describe a transcatheter extracardiac tricuspid annuloplasty device positioned in the pericardial space and delivered by puncture through the right atrial appendage. We demonstrate acute and chronic feasibility in swine.

METHODS Transatrial intrapericardial tricuspid annuloplasty (TRAIPTA) was performed in 16 Yorkshire swine, including 4 with functional TR. Invasive hemodynamics and cardiac magnetic resonance imaging (MRI) were performed at baseline, immediately after annuloplasty and at follow-up.

RESULTS Pericardial access via a right atrial appendage puncture was uncomplicated. In 9 naïve animals, tricuspid septal-lateral and anteroposterior dimensions, the annular area and perimeter, were reduced by 49%, 31%, 59%, and 24% ($p < 0.001$), respectively. Tricuspid leaflet coaptation length was increased by 53% ($p < 0.001$). Tricuspid geometric changes were maintained after 9.7 days (range, 7 to 14 days). Small effusions (mean, 46 ml) were observed immediately post-procedure but resolved completely at follow-up. In 4 animals with functional TR, severity of regurgitation by intracardiac echocardiography was reduced.

CONCLUSIONS Transatrial intrapericardial tricuspid annuloplasty is a transcatheter extracardiac tricuspid valve repair performed by exiting the heart from within via a transatrial puncture. The geometry of the tricuspid annulus can interactively be modified to reduce severity of functional TR in an animal model. (J Am Coll Cardiol Intv 2015;8:483-91)

Tricuspid regurgitation (TR) is a predictor of mortality, increasing with regurgitation severity and independent of age, biventricular function or dimensions, or pulmonary artery pressure (1). In patients with mitral regurgitation (2) or undergoing left-sided valve surgery (3), TR is associated with heart failure and worse outcome. Persistent TR after left-sided valve surgery predicts poor

From the *Cardiovascular and Pulmonary Branch, Division of Intramural Research, National Heart, Lung, and Blood Institute, National Institutes of Health, Bethesda, Maryland; †Department of Cardiology, Children's National Medical Center, Washington, DC; and the ‡Institute of Biomedical Engineering, Bogazici University, Istanbul, Turkey. This work was supported by the Division of Intramural Research, NHLBI, NIH (Z01-HL006040). Dr. Rogers, Dr. Ratnayaka, Dr. Sonmez, Ms. Franson, Dr. Kocaturk, and Dr. Lederman are coinventors on patents, assigned to NIH, for TRAIPTA devices. All other authors have reported that they have no relationships relevant to the contents of this paper to disclose.

Manuscript received June 10, 2014; revised manuscript received September 8, 2014, accepted October 8, 2014.

ABBREVIATIONS AND ACRONYMS

CT = computed tomography

MRI = magnetic resonance imaging

RAA = right atrial appendage

RV = right ventricular

TR = tricuspid regurgitation

TRAIPTA = transatrial intrapericardial tricuspid annuloplasty

outcome (4). Isolated tricuspid valve surgery is associated with high mortality (5,6) and, therefore, is seldom justifiable.

Most clinical TR is "functional" and is caused by dilation of the right ventricle and tricuspid annulus (7), resulting from volume or pressure overload. Less commonly, dilation results from primary right ventricular (RV) pathology such as RV infarction or cardiomyopathy. The severity of TR corresponds to tricuspid annulus dimension (8) and is dependent on individual patient preload and afterload conditions, which vary with time.

Surgical annuloplasty restores annular geometry and improves leaflet coaptation (9). Replacement tricuspid valves are more susceptible to thrombosis compared with prostheses in the mitral or aortic positions. Transcatheter repairs have been developed for functional mitral regurgitation (10–12) but not functional TR.

SEE PAGE 492

Transatrial intrapericardial tricuspid annuloplasty (TRAIPTA) is a novel transcatheter tricuspid valve repair, guided by x-ray fluoroscopy. The pericardium is accessed via a puncture of the right atrial appendage (RAA) from within. A circumferential implant, which exerts compressive force over the tricuspid annulus, is delivered along the atrioventricular groove within the pericardial space. Tension on the implant is adjusted interactively to modify tricuspid annular geometry and reduce TR. The RAA puncture is sealed using off-the-shelf nitinol closure devices.

In this study, we tested pre-clinical feasibility of transcatheter extracardiac tricuspid annuloplasty in swine and showed that substantial modification of tricuspid annular geometry is achieved and sustained for at least 7 days. In animals with induced functional TR, we showed that TRAIPTA effectively reduces the severity of tricuspid regurgitation. We also explored the feasibility of clinical translation through human cardiac computed tomography (CT) analysis.

METHODS

Procedures were approved by the institutional animal care and use committee. TRAIPTA was performed in 16 Yorkshire swine (mean 48 ± 14 kg) under general anesthesia and mechanical ventilation. Of these, 9 naïve animals were survived for 7 to 14 days, 4 with functional TR were survived for up to 48 days and 3 underwent nonsurvival characterization of TRAIPTA tension and coronary artery protection elements. Hemodynamics and geometry were characterized at each time point by angiography, magnetic resonance imaging (MRI) at mid-systole at 1.5-T, and/or 320-detector row CT. Selective coronary angiography was performed before and after TRAIPTA.

TRAIPTA SYSTEM CONFIGURATION. We designed and built a catheter system comprising a delivery device and a permanent implant (**Figure 1**). The delivery device is formed from an interrupted 0.035-inch nitinol wire, pre-shaped into a self-expanding loop to open inside the pericardium and encircle the heart. The TRAIPTA implant comprises a 2.5-mm diameter hollow tube of braided 0.005-inch nitinol wire. The braided design allows the implant to shorten longitudinally by more than 50%. A braided polyester suture (Ti-Cron size 2, Covidien, Waltham, Massachusetts) runs within the hollow implant with a pre-tied sliding Roeder knot that allows interactive tightening after deployment and that ensures continuous myocardial apposition. The implant is pre-mounted on the delivery device loop and is pre-loaded into a 12-F braided sheath (Cook Medical, Bloomington, Indiana) for deployment.

TRANSATRIAL PERICARDIAL ACCESS. The RAA was engaged from the femoral vein with a 4-French multipurpose catheter (**Figure 2**) and punctured using the back end of a 0.035-inch guidewire. The catheter was exchanged for a 14-F sheath (Cook Medical); 10 ml of 50% iopamidol/saline was injected into the pericardial sheath to visualize epicardial structures (Online Appendix, Online Figure 1).

DELIVERY AND TIGHTENING OF TRAIPTA IMPLANT. The nitinol loop of the TRAIPTA system opened inside the pericardium to encircle the heart along the atrioventricular groove (**Figure 1**). The delivery device was then withdrawn, leaving the TRAIPTA implant in place. The suture was tightened interactively during real-time 1.5-T MRI (Aera, Siemens, Erlangen, Germany) to achieve the desired tension.

In animals with functional TR, implant tension was adjusted during intracardiac echocardiography. In 2 naïve animals, we assessed the tension-geometry relationship by applying progressive tension measured with a force meter, 3 times in each animal, during real-time MRI.

CLOSURE OF THE RAA PUNCTURE. After TRAIPTA deployment, pericardial contrast was washed out and 2 mg/kg triamcinolone was infused to impede pericardial adhesions (13). Alongside a 0.014-inch "buddy" guidewire (Ironman, Abbott Vascular, Santa Clara, California) for emergency bailout, a 5- or 6-mm nitinol atrial septal occluder (Amplatzer, St. Jude

Medical, St. Paul, Minnesota or Lepu Medical, Bejing, China) closed the appendage puncture site. A final RAA angiogram confirmed hemostasis before all wires and sheaths were withdrawn.

ANIMAL MODEL OF FUNCTIONAL TR. Ten naïve Yorkshire swine underwent procedures to cause right ventricular (RV) volume and/or pressure overload or tricuspid papillary restriction. This included combinations of (1) isolated RV infarction by ethanol infusion into the right coronary artery during balloon protection of the posterior descending artery (n = 8); (2) interatrial septostomy with a 20-mm balloon (n = 4); (3) pulmonary artery infusion of 8 ml of 300- to 700-μm polyvinyl-alcohol spheres to induce pulmonary hypertension (n = 5); (4) ethanol needle injection directly into the RV papillary muscles (n = 1); and (5) stenting open the pulmonary valve to cause severe regurgitation (n = 1). Of these 10 animals, 4 were euthanized for intractable ventricular fibrillation or severe right heart failure after RV infarction. The remaining 6 developed a dilated right ventricle, but only 4 of these developed moderate-severe TR after a mean of 117 days. These 4 animals underwent TRAIPTA with intracardiac echocardiography and were survived for up to 48 days.

HUMAN IMAGING FOR SUITABILITY. We studied human cardiac CT angiograms of patients with RV enlargement in the anonymized and delinked National Heart, Lung, and Blood Institute database. This does not constitute human subjects research under US45CFR§46.102(f). Suitability criteria for transatrial access were the presence of a discrete lobe from which to puncture and anterior orientation. Patients were evaluated for the presence of a clearly demarcated atrioventricular groove suitable for TRAIPTA. Epicardial coronary arteries at risk of compression were identified.

STATISTICAL ANALYSIS. Data were analyzed using SPSS 19.0 (IBM, Armonk, New York) and reported as mean ± SD. Differences were examined by 1-way repeated-measures analysis of variance, with Bonferroni post-hoc tests as appropriate. A $p \leq 0.05$ was considered significant.

RESULTS

TRAIPTA was performed in a total of 16 animals (9 naïve survived for 7 to 14 days, 4 with functional TR survived up to 48 days, and 3 were not survived to characterize tension-geometry and coronary protection elements). Transatrial pericardial access was successful in a single pass, and the TRAIPTA device was consistently delivered to the atrioventricular groove in 16 of 16 animals. These 2 stages required <10 min to perform (Online Video 1).

FIGURE 1 TRAIPTA System and Procedural Steps

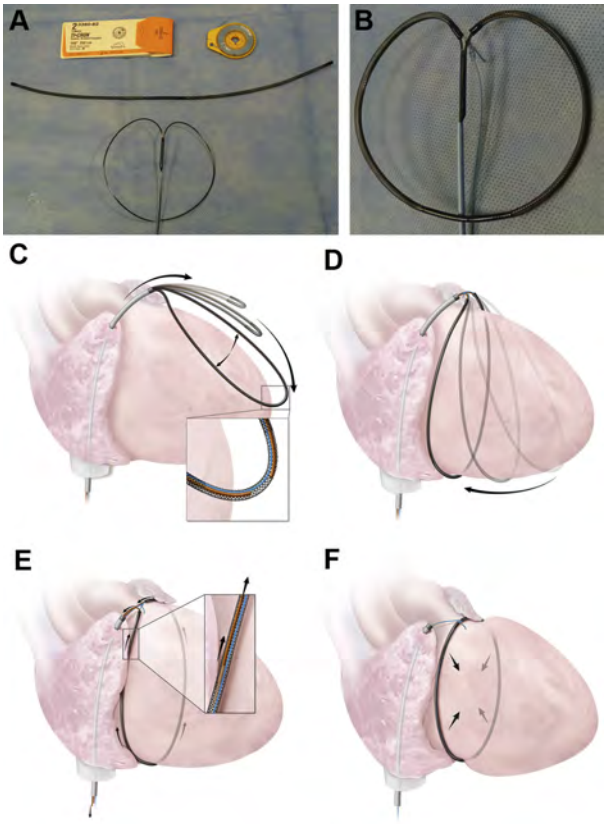

(A) Braided suture (packaging and spool), transatrial intrapericardial tricuspid annuloplasty (TRAIPTA) implant and delivery device. **(B)** TRAIPTA implant loaded onto delivery device. The suture is housed within the hollow TRAIPTA implant with a pre-tied Roeder sliding knot. **(C)** The system is advanced into the pericardium through the right atrial appendage. **(D)** The nitinol delivery device ensures that the system opens into a loop inside the pericardium and reaches the atrioventricular groove. **(E)** The delivery device is withdrawn. **(F)** The implant is tightened. See Online Video 1 for demonstration of TRAIPTA procedure. TRAIPTA = transatrial intrapericardial tricuspid annuloplasty.

SURVIVAL EXPERIMENTS IN 9 NAÏVE ANIMALS. Significant tricuspid annular geometric reduction was achieved by tightening the TRAIPTA implant (Table 1, Figures 3 and 4), with 49% ($p < 0.001$) reduction in the septal-lateral dimension and 31% ($p < 0.001$) in the anteroposterior dimension. The tricuspid annular area and perimeter were reduced by 59% ($p < 0.001$) and 24% ($p < 0.001$), respectively.

JACC: CARDIOVASCULAR INTERVENTIONS VOL. 8, NO. 3, 2015
MARCH 2015:483–91

FIGURE 2 TRAIPTA Procedure In Vivo

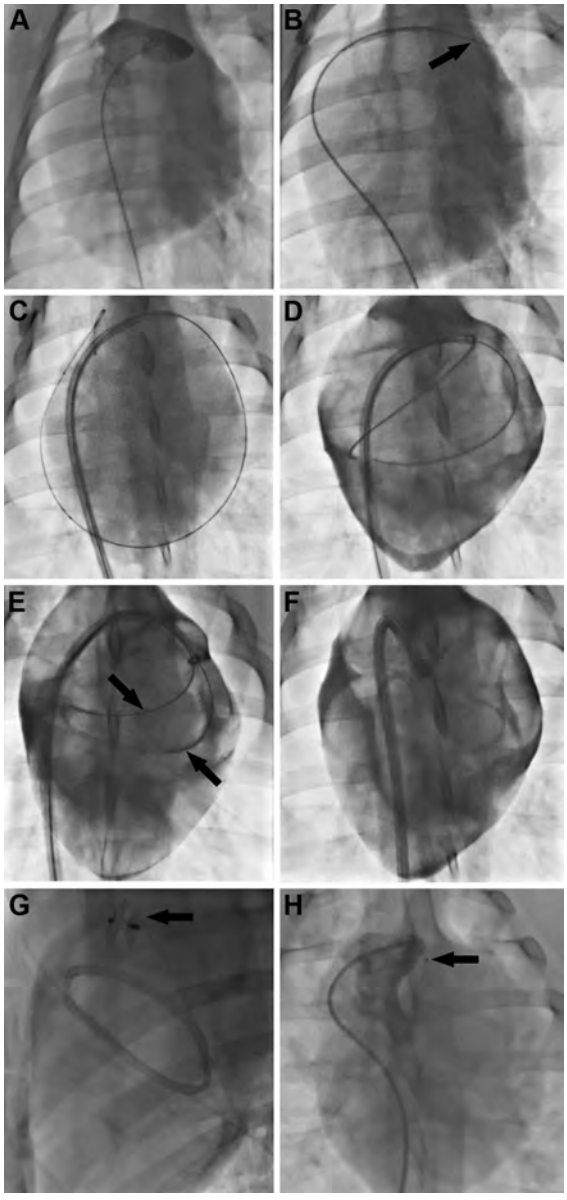

(A) Right atrial appendage (RAA) angiogram. **(B)** RAA puncture with 0.035-inch guidewire. **(C)** A 14-French sheath introduced into the pericardium. **(D)** The transatrial intrapericardial tricuspid annuloplasty (TRAIPTA) implant is deployed around the heart within the contrast-filled pericardial space. **(E)** Delivery system **(arrows)** withdrawal leaving the TRAIPTA implant in the atrioventricular groove. **(F)** The TRAIPTA implant is tightened by a sliding Roeder knot. **(G)** Closure of the RAA puncture with a nitinol closure device **(arrow)**. **(H)** RAA angiogram 7 days later (**arrow** indicates the closure device).

Tricuspid leaflet coaptation length (Figure 4) was significantly increased by 53% ($p < 0.001$). Lesser mitral annular geometric change was observed with a mean reduction in the septal-lateral and antero-posterior dimensions of 15% ($p < 0.05$) and 15% ($p < 0.05$), respectively. No significant hemodynamic changes and no sustained arrhythmias were observed (Online Table 1). Coronary artery compression was not seen in any animal (Online Figure 2).

The RAA puncture was consistently closed using a nitinol closure device in all 9 animals. Post-procedure MRI demonstrated small pericardial effusions (mean, 46 ± 44 ml), but there was no evidence of tamponade (Online Table 1). No animal required pericardial drainage. At follow-up (mean, 9.7 days; range, 7 to 14 days), the TRAIPTA implant remained in place without migration, and pericardial effusions had resolved. On necropsy (Figure 5), the implant was encased in fibrous tissue and fused to the myocardium along its entire course. There were no adhesions between the visceral and parietal pericardial layers.

SURVIVAL EXPERIMENTS IN 4 ANIMALS WITH FUNCTIONAL TR. TRAIPTA successfully reduced the severity of TR by intracardiac echocardiography (Figure 4). This was maintained up to 48 days of follow-up. After euthanasia, the TRAIPTA implant remained intact in the correct anatomic position on necropsy and was completely endothelialized and fused to the myocardium (Figure 5).

NONSURVIVAL EXPERIMENTS IN 3 NAÏVE ANIMALS. Implant tension correlated with changes in annular geometry (Figure 3), and the feasibility of coronary artery protection was demonstrated (Online Figure 2), although, in fact, no coronary compression was observed in any of these experiments.

ANATOMIC SUITABILITY IN HUMANS. We reviewed 14 cardiac CT angiograms for anatomic suitability from patients with an intracardiac shunt and a dilated right heart. RAA morphology and anatomic position were consistent across subjects. All 14 met both suitability criteria for transatrial pericardial access. Thirteen of 14 patients (93%) had a clearly defined atrioventricular groove. Of those, all had at least 1 epicardial coronary artery that crossed the projected course of the TRAIPTA implant.

DISCUSSION

To our knowledge, this is the first description of a transcatheter tricuspid valve repair and the first

mechanical intervention accomplished via a right atrial exit to the pericardium. In contrast with the mitral valve, where primary leaflet or subvalvular apparatus pathology often contributes to regurgitation, most symptomatic TR is caused by annular dilation with intact valvular apparatus. For this reason, annuloplasty is the preferred surgical repair. We showed a dose-response relationship between TRAIPTA tension and tricuspid geometry and leaflet coaptation; we showed that TRAIPTA treats functional TR in a clinically relevant animal model, that the right atrial exit port is reliably closed, that the procedure is rapid and reproducible, and that eligible humans appear to have suitable anatomy.

TRANSATRIAL PERICARDIAL ACCESS. Transatrial pericardial access was first described by Verrier et al. (14) to sample pericardial fluid, drain effusions, and deliver drugs. A number of interventional (15) and electrophysiology procedures require pericardial access, which is usually obtained through a "dry" subxiphoid puncture and which risks hemopericardium from right ventricular or coronary artery laceration.

TRAIPTA is the first mechanical intervention performed by exiting the heart from within via a transatrial puncture. This approach provides direct access to the base of the heart in the plane of the atrioventricular groove. The puncture was sealed with off-the-shelf nitinol closure devices, and hemostasis was consistently achieved in all animals. However, right atrial pressures were low in these animals, and the risk of bleeding could be higher in patients with severe TR or coagulopathy. Small post-procedural pericardial effusions were observed but without tamponade, whereas in patients, a temporary pericardial drain would likely be placed. Complete resolution of these effusions was observed in all animals at follow-up, even with the permanent TRAIPTA implant in situ. Our current technique requires inversion of the appendage to ensure proper nitinol closure device positioning. We believe that the device redistributes force adequately to protect against appendage injury.

INTRAPERICARDIAL TRICUSPID ANNULOPLASTY. Aortic and mitral valve disease commonly coexist with tricuspid valve disease. Despite the adoption of transcatheter aortic and mitral valve interventions, there remains an unmet need for transcatheter tricuspid valve repair (16), particularly because untreated TR after aortic or mitral surgery confers a poor outcome. Percutaneous orthotopic (17,18) or heterotopic (19,20) prosthetic tricuspid valve replacement has been described, but these risk thrombosis without anticoagulation. TRAIPTA would not require anticoagulation because the implant is extravascular, although some patients may have other indications (e.g., atrial fibrillation). Transcatheter tricuspid replacement valves are contraindicated in the presence of transvenous pacing or defibrillator leads, but TRAIPTA is possible because it is extravascular. Transatrial exit is possible in the presence of right atrial pacing leads because the puncture can be performed distant to the lead insertion point. TRIAPTA may also be a treatment strategy for pediatric and adult congenital systemic single right ventricle patients with TR.

In this study, we correlated implant tension with reduction in tricuspid annular dimensions, especially in the septal-lateral dimension, which is the main axis of annular dilation (7) and the principal target for surgical annuloplasty. The magnitude of geometric modification easily exceeded ranges reported for surgical annuloplasty (21). We observed lesser geometric modification of the mitral annulus, likely reflecting the higher pressures and increased myocardial thickness of the left heart. Nevertheless,

TABLE 1 MRI Findings (N = 9)

	Baseline	Post-TRAIPTA	Follow-Up (Mean 9.7 days)
Cardiac chambers			
RA area, cm^2	11.8 ± 1.6	12.0 ± 1.2	11.4 ± 2.1
RV end-diastolic volume, ml	84.5 ± 12.3	65.6 ± 20.9	73.9 ± 20.4
RV end-systolic volume, ml	42.5 ± 14.8	35.8 ± 16.9	36.8 ± 17.8
RV stroke volume, ml	42.0 ± 7.5	29.9 ± 5.9*	37.1 ± 6.5
RV ejection fraction, %	50.8 ± 11.6	47.6 ± 10.3	52.1 ± 10.4
LA area, cm^2	12.3 ± 2.6	11.1 ± 1.1	12.1 ± 1.9
LV end-diastolic volume, ml	93.3 ± 14.7	66.9 ± 13.3*	79.2 ± 8.7
LV end-systolic volume, ml	51.5 ± 13.9	36.6 ± 11.3*	41.9 ± 5.6
LV stroke volume, ml	41.8 ± 8.8	30.3 ± 5.6*	37.3 ± 8.0
LV ejection fraction, %	45.3 ± 9.6	46.1 ± 8.3	46.8 ± 6.5
TV annulus‡			
TV septal-lateral, mm	24.4 ± 2.1	12.6 ± 2.8†	13.9 ± 3.1†
TV anteroposterior, mm	32.8 ± 2.4	22.6 ± 4.0†	22.6 ± 3.6†
TV area, cm^2	11.8 ± 1.9	5.3 ± 1.8†	4.4 ± 1.5†
TV annular perimeter, cm	13.2 ± 1.1	9.6 ± 2.4†	9.8 ± 1.2†
TV leaflet coaptation length, mm	3.1 ± 0.9	6.8 ± 0.8†	6.1 ± 0.8†
MV annulus‡			
MV septal-lateral, mm	29.2 ± 3.7	24.8 ± 3.8*	25.2 ± 2.4
MV anteroposterior, mm	31.1 ± 2.5	26.3 ± 2.4*	26.1 ± 3.3*
MV area, cm^2	9.3 ± 2.0	6.0 ± 1.3†	5.6 ± 1.2†
MV annular perimeter, cm	11.9 ± 1.1	9.3 ± 1.2†	9.1 ± 0.9†
Pericardium			
Pericardial effusion, ml	0.0 ± 0.0	45.8 ± 43.7†	0.0 ± 0.0

Values are mean ± SD. *p < 0.05. †p < 0.001 compared with baseline. ‡Annular measurements were performed in mid-systole.

LA = left atrium; LV = left ventricle; MRI = magnetic resonance imaging; MV = mitral valve; RA = right atrium; RV = right ventricle; TRAIPTA = transatrial intrapericardial tricuspid annuloplasty; TV = tricuspid valve.

JACC: CARDIOVASCULAR INTERVENTIONS VOL. 8, NO. 3, 2015
MARCH 2015:483–91

FIGURE 3 Geometric Change Resulting From Annuloplasty

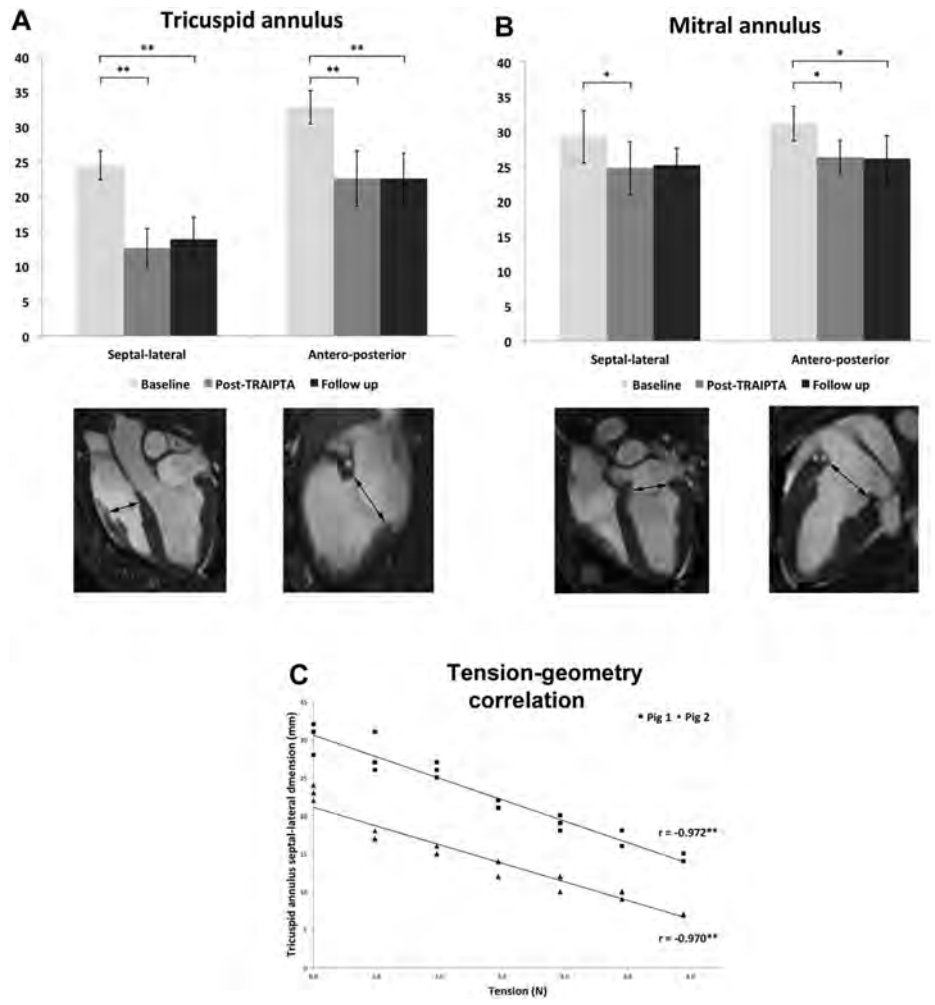

(A) Mean tricuspid valve annular dimensions in 5- and 2-chamber MRI views. **(B)** Mean mitral valve annular dimensions in 4- and 2-chamber magnetic resonance imaging views. **Arrows** denote measured annular dimensions **(A and B)**. **(C)** The transatrial intrapericardial tricuspid annuloplasty (TRAIPTA) implant was tensioned using a force meter attached to the suture. *p < 0.05; **p < 0.001.

this technique could potentially be adapted to treat both atrioventricular valves. Unlike surgery, TRAIPTA can be performed in the beating heart and titrated in real time under varying loading conditions imposed by hemodynamic provocations such as exercise and volume. Importantly, we found geometric change was maintained over the follow-up period.

ANIMAL MODEL. TR has been induced in animals by surgical annular disruption (22,23), but there are no transcatheter large animal models of functional TR. In this study, we found that to create TR required multiple insults, including volume and pressure overload, as well as considerable time to allow the right ventricle to remodel.

STUDY LIMITATIONS AND POTENTIAL FAILURE MODES. TRAIPTA requires the pericardial space to be free of adhesions, which could impede implant delivery. This likely precludes TRAIPTA in

FIGURE 4 Imaging of Tricuspid Valve and Annulus Before and After Annuloplasty

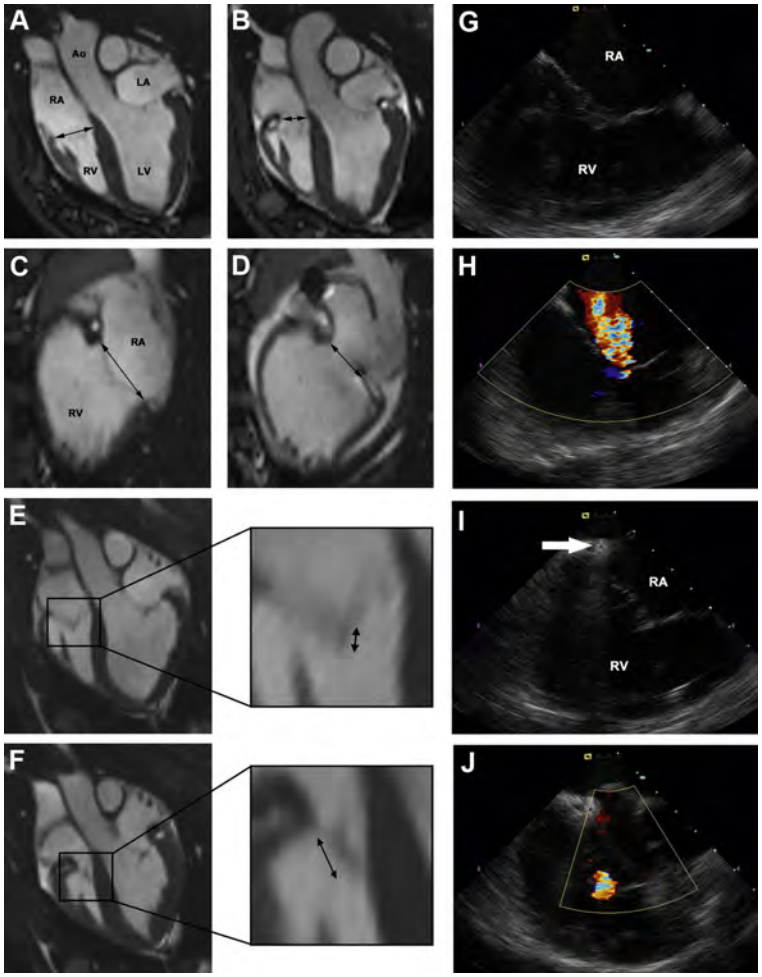

(A) Magnetic resonance imaging 5-chamber view at baseline. **Arrow** denotes tricuspid annulus. **(B)** A 5-chamber view after transatrial intrapericardial tricuspid annuloplasty (TRAIPTA). **(C)** A 2-chamber view at baseline. **(D)** A 2-chamber view after TRAIPTA. **(E)** Tricuspid leaflet coaptation at baseline. **Arrow** denotes coaptation length. **(F)** Tricuspid leaflet coaptation after TRAIPTA. **Arrow** denotes coaptation length. **(G)** Intracardiac echocardiography of the tricuspid valve before deployment of the TRAIPTA implant. **(H)** Color Doppler shows a central jet of moderate-severe tricuspid regurgitation (peak velocity 1.8 m/s). **(I)** Tensioned TRAIPTA implant at the level of the tricuspid annulus **(arrow)**. **(J)** Color Doppler showing significant reduction in tricuspid regurgitation severity after TRAIPTA. Ao = aorta; LA = left atrium; LV = left ventricle; RA = right atrium; RV = right ventricle.

patients with previous pericardiotomy or pericarditis. However, the technique might be useful in conjunction with transcatheter aortic valve replacement and/or mitral valve repair. Because of its circumferential position around the heart, 1 potential complication is coronary artery and coronary sinus compression. At the level of tension exerted to achieve 40% reduction in the tricuspid septal-lateral dimension, we did not observe any coronary artery or sinus compression (Online Figure 2), albeit in animals without severe RV hypertension. To address this potential complication, we demonstrated that a protection element could be incorporated into the TRAIPTA implant (Online Figure 2) and that its

FIGURE 5 Necropsy

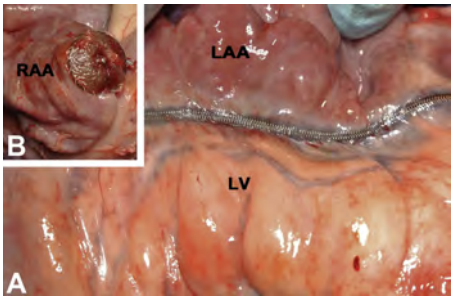

(A) Transatrial intrapericardial tricuspid annuloplasty (TRAIPTA) implant at 48 days of follow-up endothelialized and fused to the myocardium along the atrioventricular groove. **(B)** Right atrial appendage (RAA) puncture site at 7 days of follow-up, sealed with nitinol closure device. LAA = left atrial appendage; LV = left ventricle.

position along the TRAIPTA implant was adjustable interactively in situ. This bridgelike element, originally developed in our lab for mitral cerclage annuloplasty (12), directs compressive force away from an entrapped coronary artery or sinus. Finally, in common with all permanent implants, potential failure modes are implant migration and tissue erosion. We did not observe any implant migration, and on necropsy, the TRAIPTA device was fully adhered to the myocardium with no macroscopic evidence of tissue erosion (**Figure 5A**). Similar macroscopic findings were observed for the nitinol closure device at the right atrial puncture site. No pericarditis or pericardial adhesions were observed, perhaps because we administered intrapericardial glucocorticoids after deployment. These finding suggests a very low likelihood of late device migration or tissue erosion, but this will be evaluated in a future long-term animal study.

CLINICAL TRANSLATION AND SUITABILITY OF HUMAN ANATOMY. RAA morphology was suitable for transatrial pericardial access in all patients, and most had a clearly defined atrioventricular groove suitable for TRAIPTA. Most patients also had epicardial coronary arteries crossing the projected course of the TRAIPTA implant, and we therefore anticipate that protection elements would be required in human implementation (Online Figure 2).

CONCLUSIONS

We report a novel transcatheter tricuspid annuloplasty technique using transatrial pericardial access and pericardial deployment of a permanent implant. We demonstrate interactive adjustment of tricuspid annular and leaflet geometry in naïve swine, comparable to that achieved with surgical annuloplasty. In animals with functional tricuspid regurgitation, this geometric adjustment reduces the severity of regurgitation.

ACKNOWLEDGMENTS The authors thank Katherine Lucas and Joni Taylor for animal experiments and Irena Cich for help with device prototyping.

REPRINT REQUESTS AND CORRESPONDENCE: Dr. Robert J. Lederman, National Heart, Lung, and Blood Institute, National Institutes of Health, Building 10, Room 2c713, Bethesda, Maryland 20892-1538. E-mail: lederman@nih.gov.

REFERENCES

1. Nath J, Foster E, Heidenreich PA. Impact of tricuspid regurgitation on long-term survival. J Am Coll Cardiol 2004;43:405-9.

2. Agricola E, Stella S, Gullace M, et al. Impact of functional tricuspid regurgitation on heart failure and death in patients with functional mitral regurgitation and left ventricular dysfunction. Eur J Heart Fail 2012;14:902-8.

3. Turina J, Stark T, Seifert B, Turina M. Predictors of the long-term outcome after combined aortic and mitral valve surgery. Circulation 1999;100:II48-53.

4. Ruel M, Rubens FD, Masters RG, Pipe AL, Bedard P, Mesana TG. Late incidence and predictors of persistent or recurrent heart failure in patients with mitral prosthetic valves. J Thorac Cardiovasc Surg 2004;128:278-83.

5. Mangoni AA, DiSalvo TG, Vlahakes GJ, Polanczyk CA, Fifer MA. Outcome following isolated tricuspid valve replacement. Eur J Cardiothorac Surg 2001;19:68-73.

6. Kwon DA, Park JS, Chang HJ, et al. Prediction of outcome in patients undergoing surgery for severe tricuspid regurgitation following mitral valve surgery and role of tricuspid annular systolic velocity. Am J Cardiol 2006;98:659-61.

7. Ton-Nu TT, Levine RA, Handschumacher MD, et al. Geometric determinants of functional tricuspid regurgitation: insights from 3-dimensional echocardiography. Circulation 2006;114:143-9.

8. Sugimoto T, Okada M, Ozaki N, Hatakeyama T, Kawahira T. Long-term evaluation of treatment for functional tricuspid regurgitation with regurgitant volume: characteristic differences based on primary cardiac lesion. J Thorac Cardiovasc Surg 1999;117:463-71.

9. Shinn SH, Schaff HV. Evidence-based surgical management of acquired tricuspid valve disease. Nat Rev Cardiol 2013;10:190-203.

10. Siminiak T, Wu JC, Haude M, et al. Treatment of functional mitral regurgitation by percutaneous annuloplasty: results of the TITAN Trial. Eur J Heart Fail 2012;14:931-8.

11. Whitlow PL, Feldman T, Pedersen WR, et al. Acute and 12-month results with catheter-based mitral valve leaflet repair: the EVEREST II (Endovascular Valve Edge-to-Edge Repair) High Risk Study. J Am Coll Cardiol 2012;59:130-9.

12. Kim JH, Kocaturk O, Ozturk C, et al. Mitral cerclage annuloplasty, a novel transcatheter treatment for secondary mitral valve regurgitation: initial results in swine. J Am Coll Cardiol 2009;54:638-51.

13. Maisch B, Ristic AD, Pankuweit S. Intrapericardial treatment of autoreactive pericardial effusion with triamcinolone; the way to avoid side effects of systemic corticosteroid therapy. Eur Heart J 2002;23:1503–8.

14. Verrier RL, Waxman S, Lovett EG, Moreno R. Transatrial access to the normal pericardial space: a novel approach for diagnostic sampling, pericardiocentesis, and therapeutic interventions. Circulation 1998;98:2331–3.

15. Bartus K, Bednarek J, Myc J, et al. Feasibility of closed-chest ligation of the left atrial appendage in humans. Heart Rhythm 2011;8:188–93.

16. Agarwal S, Tuzcu EM, Rodriguez ER, Tan CD, Rodriguez LL, Kapadia SR. Interventional cardiology perspective of functional tricuspid regurgitation. Circ Cardiovasc Interv 2009;2:565–73.

17. Pott D, Malasa M, Urban U, et al. A novel approach to an anatomical adapted stent design for the percutaneous therapy of tricuspid valve diseases: preliminary experiences from an engineering point of view. ASAIO J 2012;58:568–73.

18. Boudjemline Y, Agnoletti G, Bonnet D, et al. Steps toward the percutaneous replacement of atrioventricular valves an experimental study. J Am Coll Cardiol 2005;46:360–5.

19. Lauten A, Ferrari M, Hekmat K, et al. Heterotopic transcatheter tricuspid valve implantation: first-in-man application of a novel approach to tricuspid regurgitation. Eur Heart J 2011;32:1207–13.

20. Laule M, Stangl V, Sanad W, Lembcke A, Baumann G, Stangl K. Percutaneous transfemoral management of severe secondary tricuspid regurgitation with Edwards Sapien XT bioprosthesis: first-in-man experience. J Am Coll Cardiol 2013;61:1929–31.

21. Min SY, Song JM, Kim JH, et al. Geometric changes after tricuspid annuloplasty and predictors of residual tricuspid regurgitation: a real-time three-dimensional echocardiography study. Eur Heart J 2010;31:2871–80.

22. Otaki M, Lust RM. Modification of De Vega's tricuspid annuloplasty for experimental tricuspid regurgitation. J Cardiac Surg 1994;9:399–404.

23. Walter EMD, Delmo Walter E, Vasilyev N, et al. Creation of a tricuspid valve regurgitation model from tricuspid annular dilatation using the cardioport video-assisted imaging system. J Heart Valve Dis 2011;20:184–8.

KEY WORDS annuloplasty, structural heart interventions, transcatheter repair, tricuspid regurgitation

APPENDIX For supplemental material and a video, please see the online version of this article.

3.6 Supplemental figures

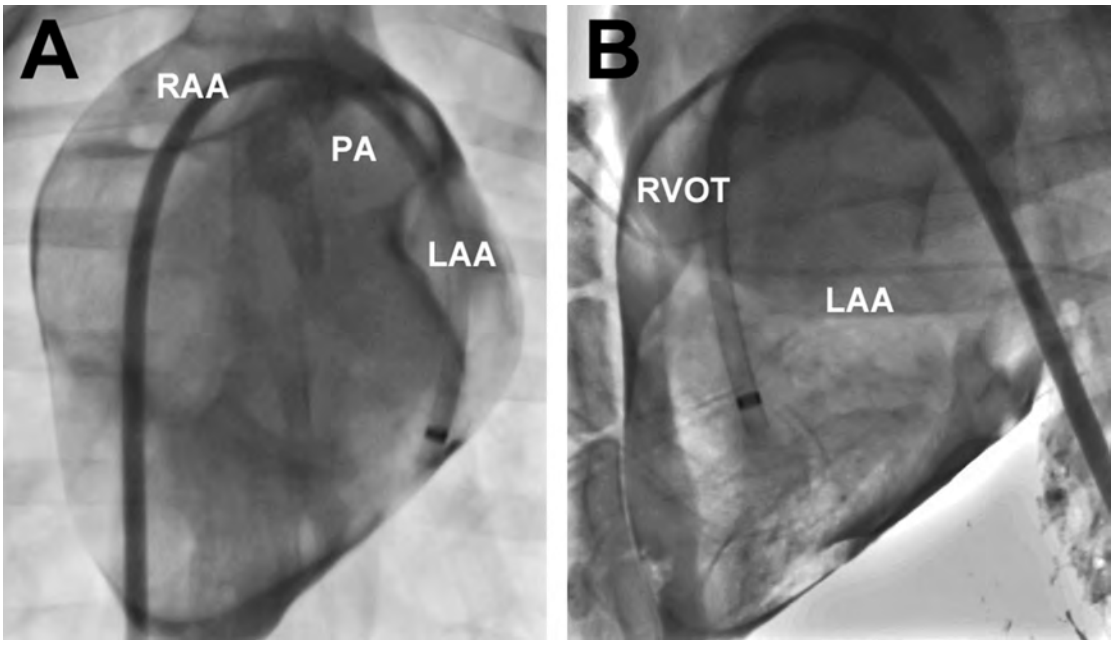

Figure 3-6: Epicardial anatomy revealed with intrapericardial iodinated contrast

(A) Antero-posterior projection. (B) Lateral projection. The sheath has been introduced into the pericardium via trans-auricular puncture. RAA: right atrial appendage; LAA: left atrial appendage; RVOT: right ventricular outflow tract.

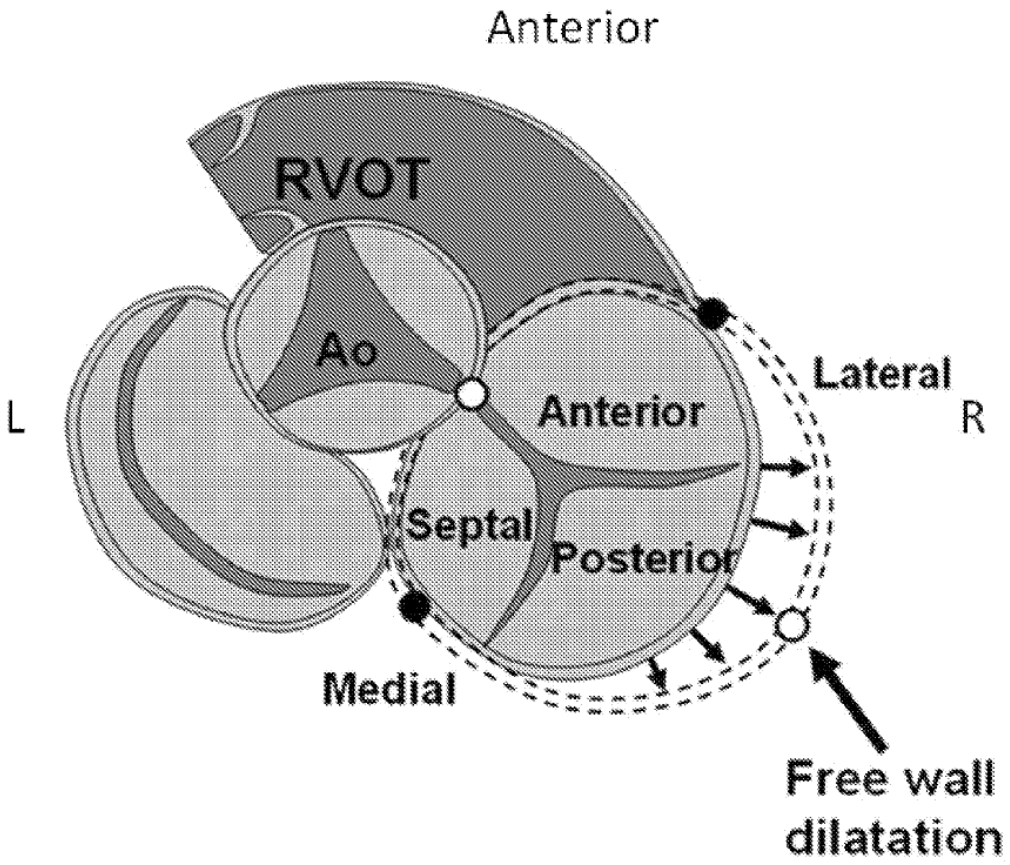

Figure 3-7: Atrioventricular plane anatomy and mechanism of functional tricuspid regurgitation

'Secondary' or 'functional' tricuspid regurgitation is caused by progressive dilation of the tricuspid valve annulus. This is usually a result of progressive right ventricular dilation. The tricuspid annulus dilates towards the free wall. The goal of surgical tricuspid annuloplasty is to bring the free wall component of the tricuspid annulus back towards the septum and improve leaflet coaptation.

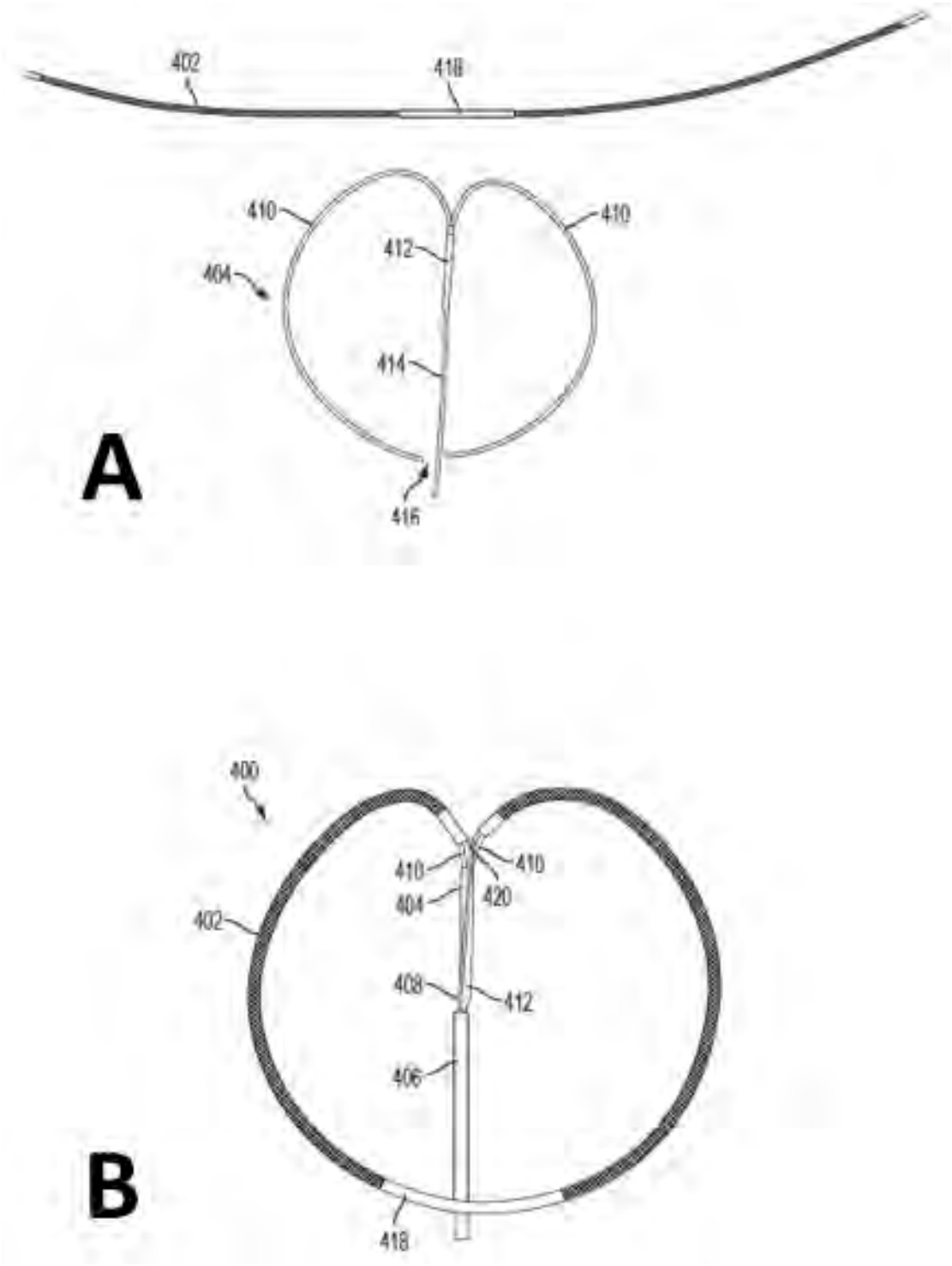

Figure 3-8: TRAIPTA implant

The TRAIPTA implant is formed of braided nitinol to enable it to shorten during tensioning. It is pre-mounted on a shaped delivery catheter to facilitate positioning around the heart in the atrioventricular groove.

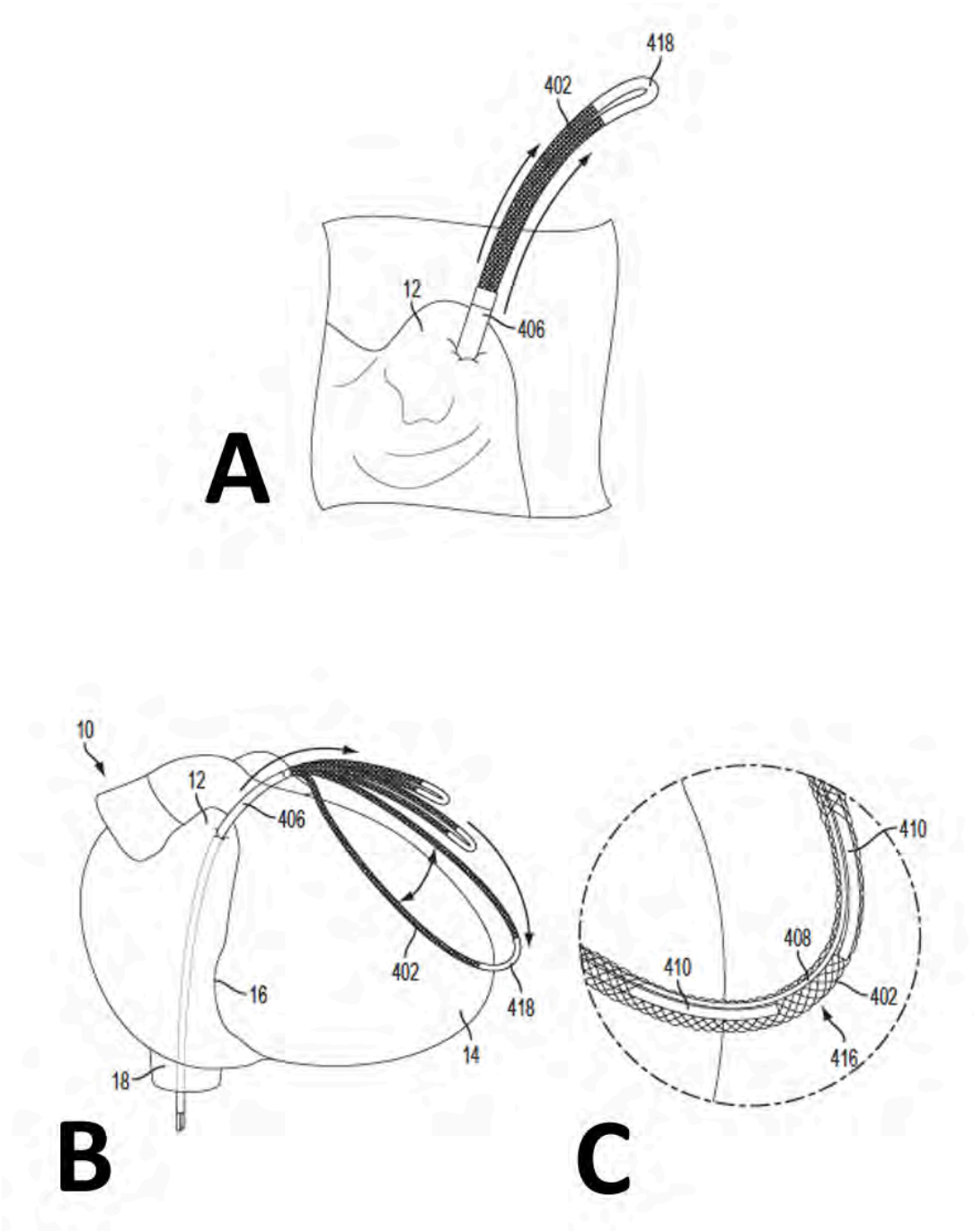

Figure 3-9: TRAIPTA procedure steps (part 1)

(A) The TRAIPTA implant is advanced through the right atrial appendage sheath into the pericardium. (B) The shaped delivery catheter opens up within the pericardium to form a lasso. (C) The limbs of the delivery catheter are separated at the distal portion so that they can be withdrawn once the TRAIPTA implant is in the correct position.

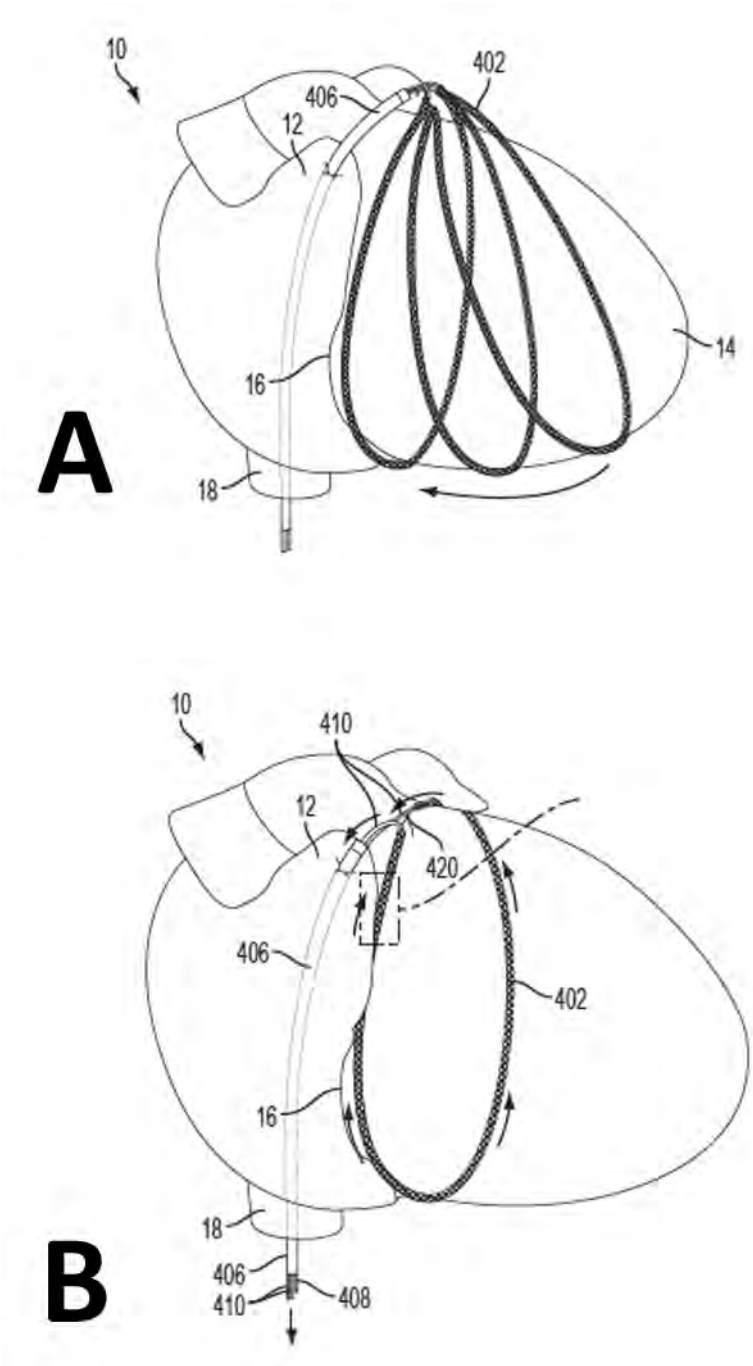

Figure 3-10: TRAIPTA procedure steps (part 2)

(A) The TRAIPTA implant is navigated within the pericardium to reach the desired position around the heart in the atrioventricular groove. (B) The limbs of the delivery catheter are withdrawn, leaving the TRAIPTA implant in place.

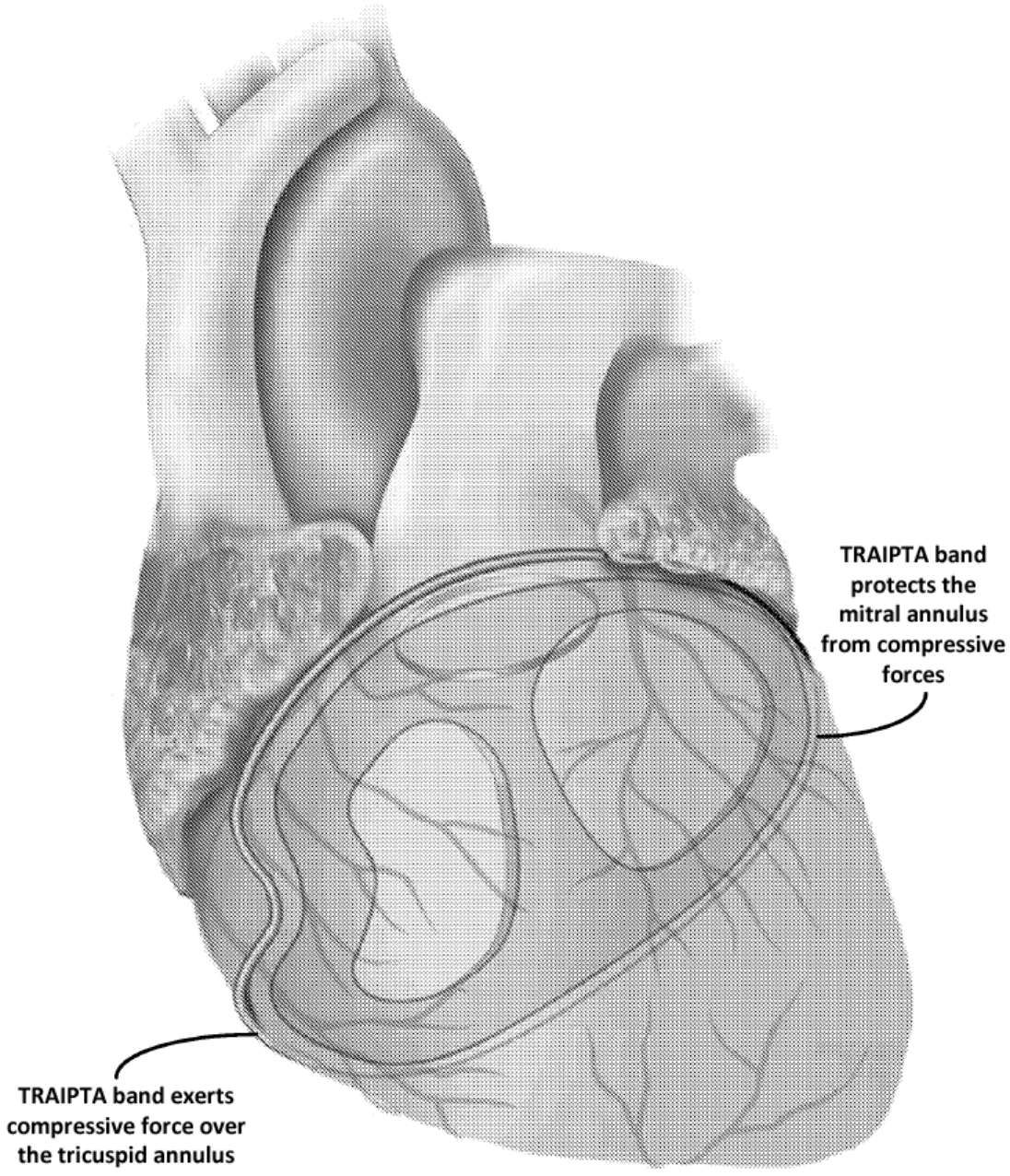

Figure 3-11: Differential compression of tricuspid and mitral annuli by the TRAIPTA implant band

By imparting different shapes to different portions of the TRAIPTA implant, it is possible to direct compressive force to the tricuspid annulus, while protecting the mitral annulus.

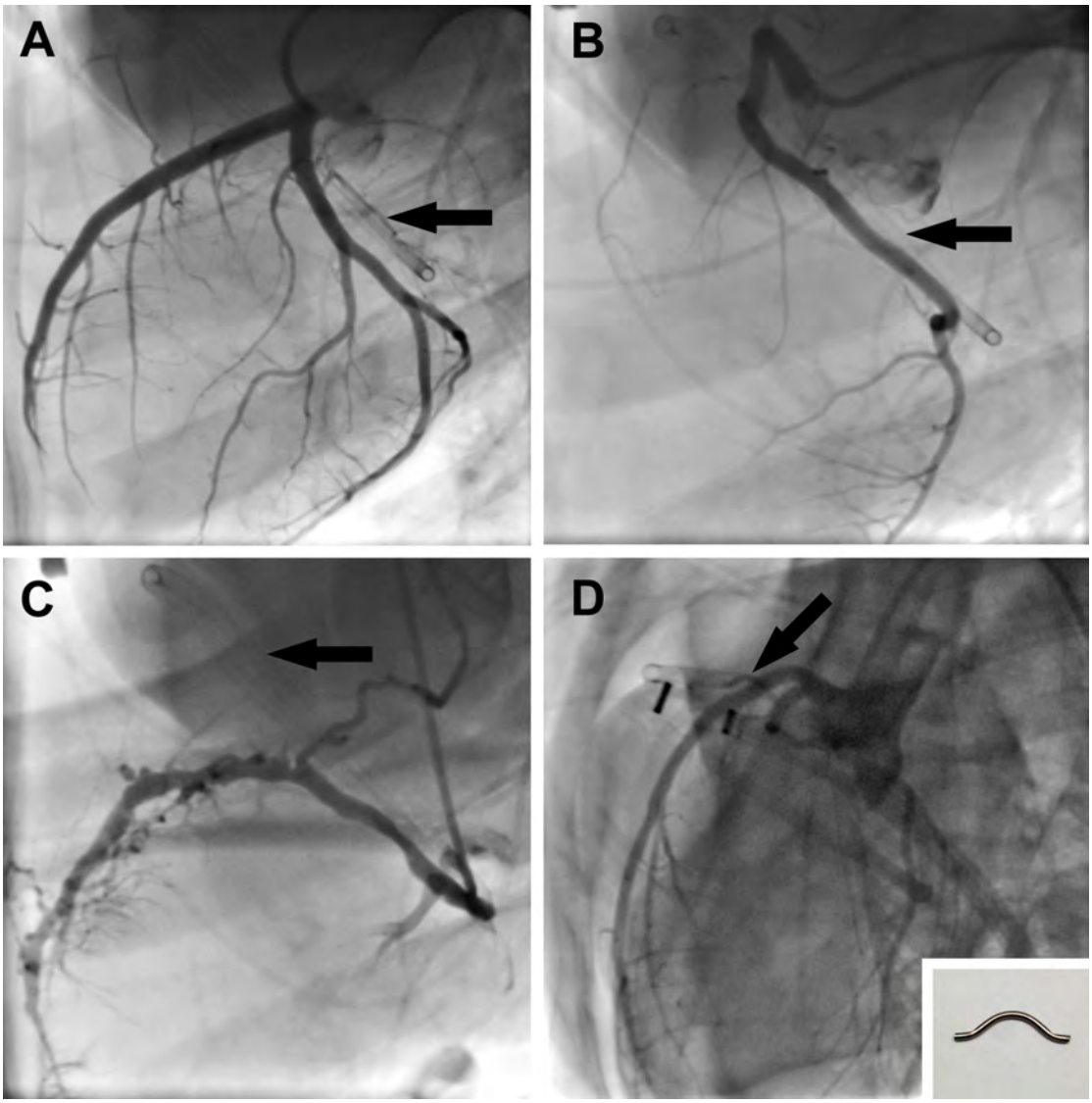

Figure 3-12: Coronary arteries and coronary sinus angiography following annuloplasty

(A) Left coronary artery angiogram with tensioned TRAIPTA implant (arrow). (B) Right coronary artery angiogram with tensioned TRAIPTA implant (arrow). (C) Coronary sinus angiogram with tensioned TRAIPTA implant (arrow). (D) Left coronary angiogram with a rigid protection element (insert) mounted within the TRAIPTA implant (arrow) to demonstrate feasibility of left anterior descending coronary artery protection. Coronary artery or sinus compression was not observed in any animal.

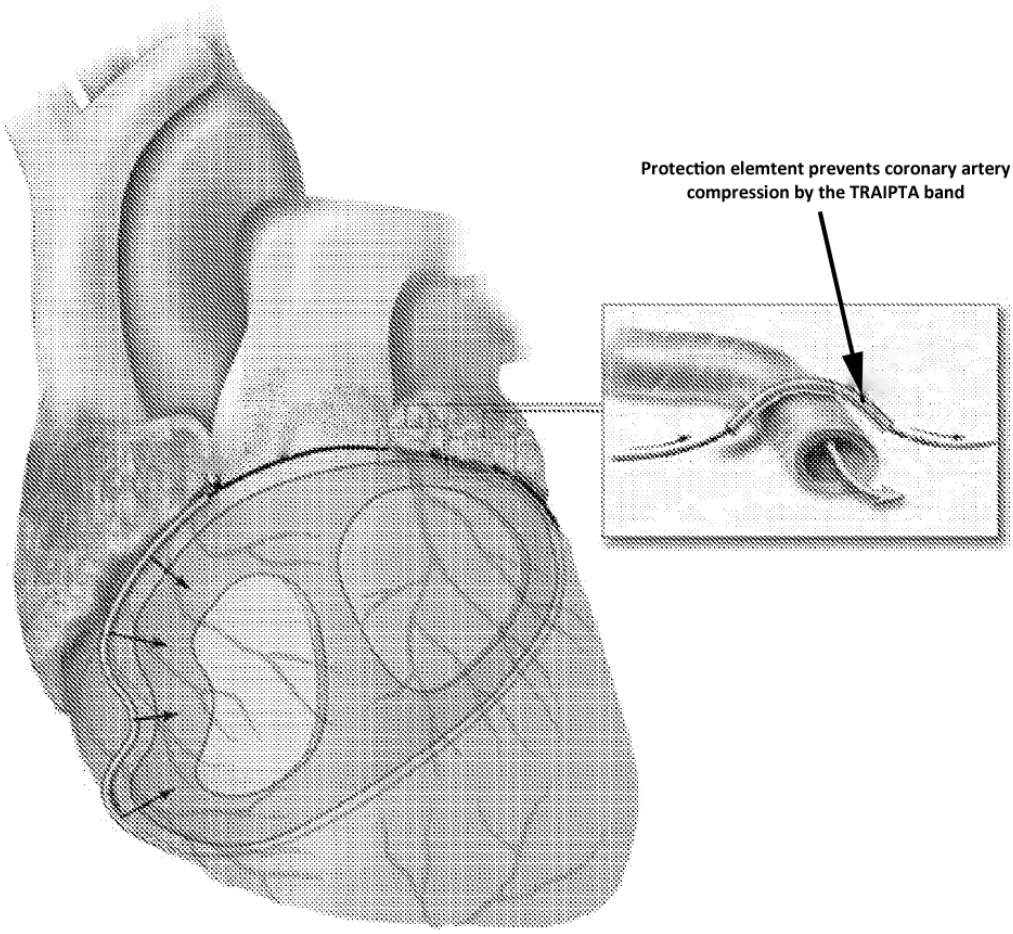

Figure 3-13: Coronary artery protection

The coronary artery protection element is positioned over a coronary artery to deflect compression away from the artery and preserve myocardial perfusion.

3.7 Supplemental table

n=9	Baseline	Post-TRAIPTA	Follow-up
Heart rate (bpm)	95±15	106±11	101±15
Ao systolic (mmHg)	83±9	72±7	75±10
Ao diastolic (mmHg)	50±7	48±5	48±7
IVC (mmHg)	1±2	2±1	2±1
SVC (mmHg)	1±2	2±1	2±2
RA (mmHg)	1±2	2±1	2±2
RV systolic (mmHg)	16±5	16±5	16±2
RV diastolic (mmHg)	1±1	0±0	1±1
PA systolic (mmHg)	16±5	13±3	14±3
PA diastolic (mmHg)	5±4	4±2	5±2
PA mean (mmHg)	10±4	8±2	9±2
PA wedge pressure (mmHg)	2±2	2±2	3±2

Table 3-2: Haemodynamic findings

No statistically significant differences. Ao: aorta; IVC: inferior vena cava; PA: pulmonary valve; RA: right atrium; SVC: superior vena cava.

Chapter 4. Intentional right atrial exit and CO2 insufflation to facilitate subxiphoid access to the naïve pericardial space (*two publications*)

4.1 Introduction

Access to the naïve or 'dry' pericardium is required for a number of electrophysiology and structural heart interventions. However, serious complications remain high despite technical refinements (e.g. the use of micropuncture needles). Having demonstrated that accessing the pericardium through the right atrial appendage appears safe for transatrial intrapericardial tricuspid annuloplasty, we explored whether this approach could be used to access the pericardium using much smaller transatrial catheters and by infusing contrast into the pericardial space to separate visceral from parietal pericardial layers and create a space for safe and easy access sub-xiphoid access.

4.2 The role of CMR

The main risk of intentionally puncturing the right atrial appendage is bleeding into the pericardium and tamponade. To assure safety of the technique before clinical translation, it was therefore critical to be able to monitor for and accurately measure the volume of accumulating pericardial fluid at multiple time points. Introducing a second pericardial catheter to monitor pericardial fluid accumulation could have confounded the results by causing additional bleeding and therefore we preferred a non-invasive measurement. Intercostal and subcostal windows limit echocardiography of the pericardium. Because CMR can clearly differentiate between tissue and fluid, and because CMR is not constrained by imaging windows and is therefore an ideal imaging modality for this application. For clinical translation, serial non-invasive measurements of pericardial fluid are not required and so this procedure can be performed using X-ray fluoroscopy in a conventional cath lab.

4.3 Candidate's contribution

I performed all the pre-clinical experiments, collected the hemodynamic data, analysed the MRI images and performed the statistical analysis. I drafted the manuscript and prepared the figures, tables and supplementary materials.

4.4 Intentional right atrial exit for microcatheter infusion of pericardial carbon dioxide or iodinated contrast to facilitate subxiphoid access

An original research manuscript published in the journal '*Catheterization and Cardiovascular Interventions'* in 2014.

Basic Science

Intentional Right Atrial Exit for Microcatheter Infusion of Pericardial Carbon Dioxide or Iodinated Contrast to Facilitate Sub-Xiphoid Access

Toby Rogers,[1] BM, BCh, MRCP, Kanishka Ratnayaka,[1,2] MD, William H. Schenke,[1] BA, Anthony Z. Faranesh,[1] PhD, Jonathan R. Mazal,[1] MS, William W. O'Neill,[3] MD, Adam B. Greenbaum,[3] MD, and Robert J. Lederman,[1*] MD

Objectives: We test the safety of transatrial pericardial access using small catheters, infusion of carbon dioxide (CO_2) or iodinated contrast to facilitate sub-xiphoid access, and catheter withdrawal under full anticoagulation. Background: Sub-xiphoid pericardial access is required for electrophysiological and structural heart interventions. If present, an effusion protects the heart from needle injury by separating the myocardium from the pericardium. However, if the pericardium is 'dry' then there is a significant risk of right ventricle or coronary artery laceration caused by the heart beating against the needle tip. Intentional right atrial exit is an alternative pericardial access route, through which contrast media could be infused to separate pericardial layers. Methods: Transatrial pericardial access was obtained in a total of 30 Yorkshire swine using 4Fr or 2.8Fr catheters. In 16 animals, transatrial catheters were withdrawn under anticoagulation and MRI was performed to monitor for pericardial hemorrhage. In 14 animals, iodinated contrast or CO_2 was infused before sub-xiphoid access was obtained. Results: Small effusions (mean 18.5 ml) were observed after 4Fr (1.3 mm outer-diameter) but not after 2.8Fr (0.9 mm outer-diameter) transatrial catheter withdrawal despite full anticoagulation (mean activated clotting time 383 sec), with no hemodynamic compromise. Pericardial CO_2 resorbed spontaneously within 15 min. Conclusions: Intentional transatrial exit into the pericardium using small catheters is safe and permits infusion of CO_2 or iodinated contrast to separate pericardial layers and facilitate sub-xiphoid access. This reduces the risk of right ventricular or coronary artery laceration. 2.8Fr transatrial catheter withdrawal does not cause any pericardial hemorrhage, even under full anticoagulation. © 2014 Wiley Periodicals, Inc.

Key words: pericardial access; epicardial intervention; transatrial puncture; structural heart intervention; electrophysiology

INTRODUCTION

Access to the naïve or 'dry' pericardial space in the absence of effusion is required for interventional procedures, for example epicardial mapping and radiofrequency ablation for ventricular tachycardia and for left

Additional Supporting Information may be found in the online version of this article.

Contract grant sponsor: Division of Intramural Research, National Heart Lung and Blood Institute, National Institutes of Health; Contract grant number: Z01-HL006040-01, Z01-HL005062..

[1]Cardiovascular and Pulmonary Branch, Division of Intramural Research, National Heart Lung and Blood Institute, National Institutes of Health, Bethesda, Maryland
[2]Department of Cardiology, Children's National Medical Center, Washington DC
[3]Institute for Structural Heart Disease, Division of Cardiology, Henry Ford Health System, Detroit, Michigan

Conflict of Interest: Nothing to report

*Correspondence to: Robert J. Lederman, National Heart Lung and Blood Institute, National Institutes of Health, Building 10, Room 2c713, Bethesda, MD 20892-1538. E-mail: lederman@nih.gov

Received 15 September 2014; Revision accepted 11 October 2014

DOI: 10.1002/ccd.25698
Published online 00 Month 2014 in Wiley Online Library (wileyonlinelibrary.com)

atrial appendage suture ligation [1–3]. Sub-xiphoid access is usually obtained under fluoroscopic guidance. A needle is advanced slowly towards the heart and aliquots of iodinated contrast are injected until the tip is confirmed inside the pericardial space. A soft-tipped wire is then introduced through the needle, over which larger sheaths can be exchanged. Even though 18-gauge (1.3 mm outer diameter) needle entry into the right ventricle is considered benign [4], there is a risk of laceration to the right ventricle or epicardial coronary arteries. Torsional cardiac and translational respiratory motion exacerbate the risk of more serious injury by laceration as the heart beats against the sharp needle tip. Bleeding complication rates of 4–7% have been reported in single and multicenter studies [5–7] but real world complication rates may be higher [8–10].

An alternative transatrial approach for pericardial access, by intentionally puncturing through the right atrial appendage (RAA), was first proposed for diagnostic sampling and delivery of drugs [11]. A catheter is navigated to the tip of the RAA from the inferior vena cava. Next a needle or guidewire is used to puncture through the RAA wall into the pericardial space. Animal experiments have demonstrated that pericardial effusions did not develop after needle withdrawal and the puncture site healed rapidly [12]. Importantly, this approach appeared technically easy and safe with no evidence of injury to epicardial vessels or to the thin-walled right ventricle. Other groups have proposed this approach for epicardial pacing wire implantation [13] or epicardial mapping and ablation [14]. We have advocated transatrial access to the pericardium to achieve other therapeutic procedures, such as intraperiardial tricuspid annuloplasty [15].

We hypothesized that despite aggressive anticoagulation, atrial tissue recoil would avoid significant pericardial hemorrhage or effusion after transatrial access used to introduce a small catheter into the 'dry' pericardium. Second, contrast media could then be infused through this catheter to separate visceral and parietal pericardial layers and enhance the safety of sub-xiphoid access with larger sheaths for electrophysiological or heart interventions. Third, we compared pericardial infusion of carbon dioxide versus iodinated contrast, reasoning that gas would separate the pericardial walls preferentially at the anterior site of supine sub-xiphoid access, and further that gas might spontaneously resorb as a margin of safety.

METHODS

Procedures were approved by the institutional animal care and use committee. Yorkshire swine were anesthetized with ketamine (25 mg/kg), midazolam (15 mg/kg), and glycopyrrolate (0.01 mg/kg), and maintained on sevoflurane (1–4%) with mechanical ventilation, and femoral arteries, and veins were accessed. Experiments took advantage of a combined interventional cardiovascular magnetic resonance imaging (MRI) and biplane X-ray fluoroscopy suite (1.5T Aera and Artis Zee, Siemens, Erlangen, Germany) for characterization of pericardial effusion. Pericardial access via RAA puncture was obtained in a total of 30 Yorkshire swine with mean weight 48 kg (range 27–66 kg). To test safety of transatrial pericardial access, 8 animals (4Fr Puncture group) underwent RAA puncture with a 4Fr (1.3 mm outer diameter) diagnostic multipurpose catheter and the back end of a 0.035 inches guidewire and 8 animals (2.8Fr Puncture group) underwent RAA puncture with a 2.8Fr (0.9 mm outer diameter) microcatheter (Excelsior, Boston Scientific) and the back end of a 0.018 inches guidewire (V18, Boston Scientific).

To test CO_2 insufflation of the pericardial space to facilitate sub-xiphoid access, 7 animals (2.8Fr + CO_2 group) underwent RAA puncture with a 2.8Fr microcatheter and the back end of a 0.018 inches guidewire. The pericardium was then insufflated with CO_2 and sub-xiphoid pericardial access was obtained. To test iodinated contrast-facilitated sub-xiphoid access, iopamidol (Isovue 300, Bracco) diluted to 25% in normal saline was infused through a 2.8Fr transatrial microcatheter using a power injector in 7 animals (2.8Fr + Contrast group). Figure 1 summarizes the experimental design.

In all animals, a 6Fr diagnostic multipurpose or angled-tip balloon wedge end-hole catheter was navigated to the RAA from the inferior vena cava using fluoroscopic guidance (Fig. 2). Position at the tip of the RAA was confirmed with contrast angiography. The back end of a guidewire (either 0.035 or 0.018 inches) was used to puncture through the wall of the RAA into the pericardial space. A catheter (4Fr multipurpose or 2.8Fr microcatheter) was then advanced over the wire into the pericardium. To exaggerate the risk of bleeding, unfractionated heparin (150–200 IU/kg bodyweight) was administered to the first 16 animals to achieve a mean activated clotting time [16] of 383 sec (range 263–517 sec), before withdrawal of the transatrial catheter back into the right atrium.

In the 2.8Fr + CO_2 group, 100–150 ml of CO_2 (~2–3 ml/kg bodyweight) was delivered into the pericardial space through the transatrial microcatheter to separate the visceral and parietal layers (target separation 10 mm). Selective coronary angiography was performed before and after CO_2 insufflation to monitor for coronary artery compression or spasm. Quantitative

Catheterization and Cardiovascular Interventions DOI 10.1002/ccd.
Published on behalf of The Society for Cardiovascular Angiography and Interventions (SCAI).

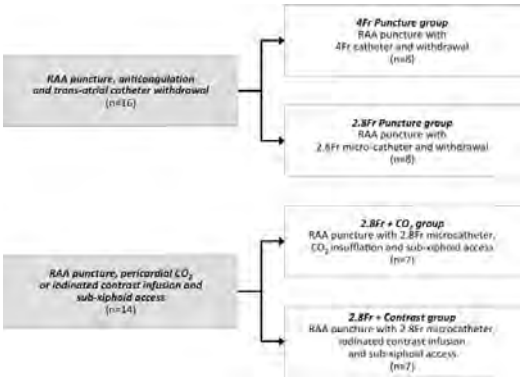

Fig. 1. Experimental design—4Fr Puncture group: RAA puncture with 4Fr (1.3 mm) catheter then withdrawal after heparinization; 2.8Fr Puncture group: RAA puncture with 2.8Fr (0.9 mm) microcatheter then withdrawal after heparinization; 2.8Fr + CO_2 group: RAA puncture with 2.8Fr microcatheter, insufflation with CO_2, sub-xiphoid access and RAA microcatheter withdrawal. 2.8Fr + Contrast group: RAA puncture with 2.8Fr microcatheter, infusion of iodinated contrast, sub-xiphoid access and RAA microcatheter withdrawal. RAA: right atrial appendage.

coronary angiography analysis was performed in the mid left anterior descending artery (LAD) and mid left circumflex artery (LCx) using *Syngo* QCA software (Siemens). Sub-xiphoid access was then obtained using a 20-gauge micro-puncture needle (0.8 mm outer diameter) and 0.018 inches guidewire using biplane fluoroscopic guidance. After sub-xiphoid access was obtained, the transatrial microcatheter was withdrawn back into the right atrium.

In the 2.8Fr + Contrast group, 2–3 ml/kg bodyweight of iodinated contrast diluted to 25% in normal saline was infused into the pericardial space through a transatrial microcatheter using a power injector at a rate of 1 ml/sec to minimize microcatheter tip whip. Sub-xiphoid access was obtained using a 20-gauge micro-puncture needle and 0.018 inches guidewire.

All animals underwent serial MRI to monitor for pericardial effusion and/or tamponade after transatrial catheter withdrawal. We prefer MRI for this purpose because transthoracic echocardiography is suboptimal in swine. Contiguous true axial slices were acquired using a steady-state free precession (SSFP) sequence with breath hold and ECG gating. Slices were prescribed to include cardiac anatomy from base to apex to ensure coverage of the entirety of the pericardial space. Acquisition parameters were: repetition time (TR)/echo time (TE), 2.96/1.25 msec; number of averages 2; acceleration factor (GRAPPA) 2; flip angle 80°; bandwidth 1157 Hz/pixel; field of view 300 × 300 mm^2; matrix 240 × 128 pixels; slice thickness 6 mm; and slice distance 0 mm. Pericardial and cardiac contours were drawn manually on each slice and the pericardial effusion volume was calculated by subtracting the total cardiac volume from the total pericardial volume using *Syngo* MR analysis software (Siemens).

Data were analyzed using SPSS (v19.0, IBM) and reported as mean ± standard deviation unless otherwise described. Mean differences were examined by *t*-test or one-way repeated measures ANOVA. A *P*-value ≤ 0.05 was considered significant. To estimate the probability of an adverse event, the binomial confidence interval was calculated using a one-tailed adjusted Wald interval, and a point estimate using the LaPlace method. The 95% confidence interval was calculated using an online tool (http://www.measuringusability.com/wald.htm). This same method was used to calculate the number of trials needed to achieve 95% confidence that the true event rate would be less than 1% and 0.1%, based on the observed event rate.

RESULTS

Pericardial access via RAA puncture was successfully obtained in all animals. Once the catheter position was confirmed in the RAA with angiography, exit into the pericardium took a few seconds only. The guidewire tracked along—but did not puncture—the parietal pericardium in all animals. In the 4Fr Puncture group (1.33 mm puncture with 4Fr catheter) small pericardial effusions were observed in 5/8 anticoagulated animals with mean volume 18.5 ml (range 7–76 mL) 15 min after transatrial catheter withdrawal. Effusions did not enlarge over the following 2 h. There was an insignificant decline in systolic and diastolic blood pressures (Fig. 3). There was no change in right atrial pressure. The largest effusion (76 ml) was observed in one animal with the highest ACT of 498 sec before transatrial catheter withdrawal. Otherwise there was no correlation between ACT and effusion volume. In the 2.8Fr Puncture group, no effusions were observed despite full anticoagulation.

In the 2.8Fr + CO_2 group, pericardial CO_2 insufflation effectively separated visceral and parietal layers anteriorly to the target separation of 10 mm in all 7 animals. This separation was highly visible on lateral plane fluoroscopy (Fig. 4). A mild transient reduction in systolic blood pressure and increase in heart rate was observed during insufflation, but these did not reach statistical significance (Fig. 3). Selective coronary angiography did not show any significant coronary artery compression or vasospasm up to 15 min post-CO_2 insufflation (Fig. 2). Minimum lumen diameters at baseline versus with pericardial CO_2 insufflation were 2.8 versus 2.7 mm in the

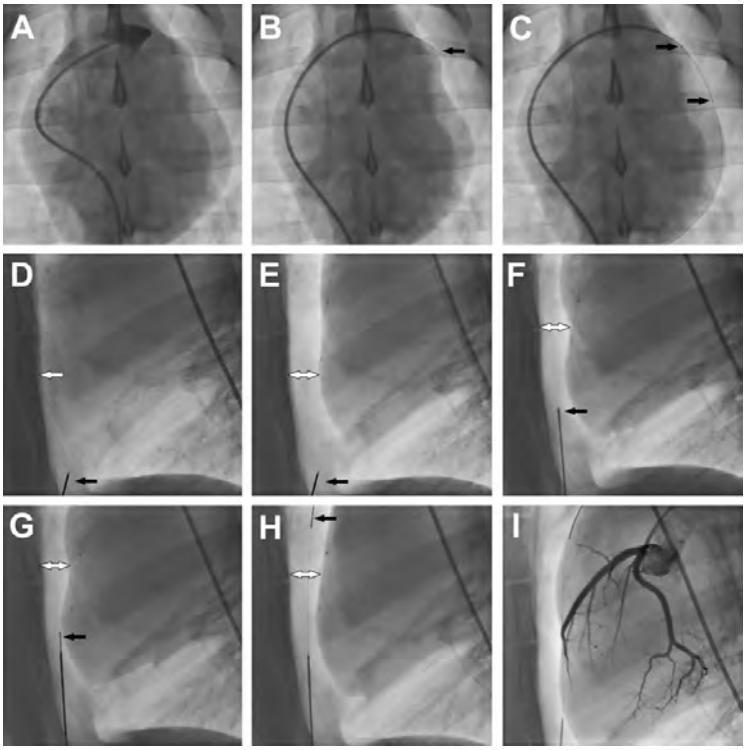

Fig. 2. Procedural steps—(A) Right atrial appendage angiogram. (B) Transatrial puncture with the back end of a 0.018 inches guidewire. (C) 2.8Fr microcatheter advanced over the 0.018 inches guidewire into the pericardial space. Black arrows show radiopaque markers on the microcatheter. (D) Lateral plane fluoroscopy showing close apposition of anterior surface of the myocardium and the sternum (white arrow). Black arrow shows the sub-xiphoid needle. (E) Pericardial insufflation with CO_2. Black arrow shows the sub-xiphoid needle. White arrow shows separation of pericardial layers. (F) Sub-xiphoid needle positioned to enter the pericardial space. Black arrow marks the tenting of the pericardium. (G) 0.018 inches guidewire (black arrow) introduced through the sub-xiphoid needle into the pericardium. (H) 0.018 inches guidewire (black arrow) tracked along anterior pericardial surface. (I) Coronary angiogram to assess for coronary artery compression or spasm.

mid LAD and 2.7 versus 2.5 mm in the mid LCx. Subxiphoid access with a micro-puncture needle aiming for the space created by the CO_2 was technically easy, took under a minute and was successful in all 7 animals without complication (Fig. 2 and Online Video Supporting Information). The separation of pericardial layers enabled the needle to avoid contact with the myocardium altogether. Serial fluoroscopy after insufflation with CO_2 showed pericardial CO_2 spontaneously and completely resorbed within 15 min in all animals. No pericardial effusions were observed on MRI after withdrawal of the transatrial microcatheter.

On the basis of observing 0 effusions out of 15 transatrial access attempts with the 2.8Fr microcatheter (2.8Fr Puncture and 2.8Fr + CO_2 groups), the binomial confidence interval and best point estimate were calculated to be 0–18% (95% CI) and 6%, respectively. To achieve 95% confidence that the true incidence of effusion is less than 1% and 0.1%, we would need to perform 325 and 3150 observations each without any effusion, respectively.

In the 2.8Fr + Contrast group, infusion of dilute iodinated contrast effectively separated visceral and parietal pericardial layers posteriorly in all 7 animals. This separation was highly visible on lateral plane fluoroscopy (Fig. 4), and created a target for easy and uncomplicated subxiphoid posterior pericardial access using a micro-puncture needle. However, it did not separate the heart from the sternum for anterior pericardial access.

Catheterization and Cardiovascular Interventions DOI 10.1002/ccd.
Published on behalf of The Society for Cardiovascular Angiography and Interventions (SCAI).

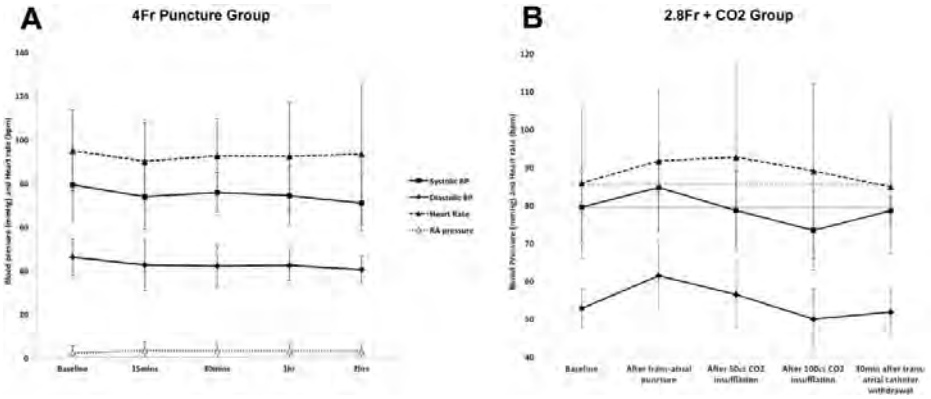

Fig. 3. Hemodynamic parameters—(A) Hemodynamic parameters do not change significantly before transatrial pericardial access with 4Fr catheter, and 15, 30, 60, and 120 min after transatrial catheter withdrawal. (B) Hemodynamic parameters before transatrial pericardial access with 2.8Fr microcatheter, after pericardial CO_2 insufflation, and 30 min after sub-xiphoid access and transatrial catheter withdrawal. Gray horizontal solid and dashed lines indicate baseline systolic blood pressure and heart rate respectively. BP: blood pressure.

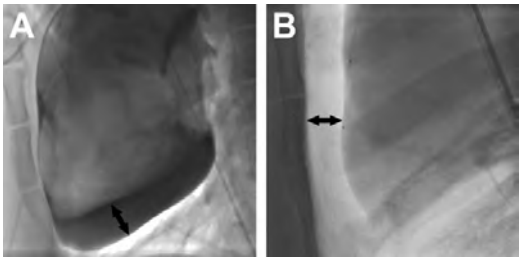

Fig. 4. Pericardial iodinated contrast versus carbon dioxide. Lateral plane fluoroscopy in a supine animal of (A) iodinated contrast and (B) CO_2 in the pericardium, both introduced through a transatrial microcatheter. Black arrows show the separation of the inferior surface of the heart from the pericardium in (A) and of the anterior surface of the heart from the sternum in (B).

DISCUSSION

Sub-Xiphoid 'Dry' Pericardial Access

The commonest complication to arise from sub-xiphoid 'dry' pericardial access is bleeding from right ventricle (RV) or coronary artery injury [5–7]. This can lead to tamponade and require surgical intervention. Unusual complications such as RV pseudoaneurysm or hepatic puncture with hematoma or abdominal bleeding have also been described [17]. Studies have not suggested an operator learning curve, as the complication rate does not appear to fall with time—even in expert hands. Strategies to improve the technique have been proposed and are elegantly summarized in a recent review article by Lim et al. [10]. These strategies include suspending ventilation during pericardial puncture to prevent the heart from impaling itself on the needle, using micro-puncture or blunt scalloped-tip Tuohy epidural needles to reduce the risk of serious RV or coronary artery injury, integrating the needle with an electroanatomic mapping system for better tip navigation [18], or using live spectral analysis of the pressure waveform from the sub-xiphoid needle to detect the higher-frequency phasic signal characteristic of pericardial entry [19]. Importantly, none of these strategies specifically separate the heart from the potentially injurious needle.

The same studies also reported rates of failure to obtain access of 3–10%, usually because of pericardial adhesions after prior open chest cardiac surgery or epicardial ablation. It is likely that the risk of RV injury is higher in these patients because the myocardium is tethered to the parietal pericardium. Adhesions do not necessarily preclude access because adhesion disruption with guidewires or catheters is possible [20].

Interestingly, the rate of RV puncture without bleeding in these studies was high (5–17%) suggesting that puncturing the myocardium with a needle can be safe. Another single center study reported inadvertent RV puncture with an 18-gauge needle in fully anticoagulated patients but no bleeding was observed [4]. These observations support our hypothesis that puncturing the substantially lower pressure right atrium with a small microcatheter is safe and should also be safe in patients with elevated right atrial pressures. It is

important to recognize that many of the serious bleeding complications caused by sub-xiphoid 'dry' pericardial access are due to lacerations caused by the heart beating against the sharp needle tip, rather than from a direct needle puncture.

Transatrial 'Dry' Pericardial Access

In this article, we describe a novel use of intentional transatrial pericardial access. Our study confirmed the finding of prior preclinical experiments: that accessing the pericardium by deliberately exiting through the RAA with small catheters is easy and safe [11,12]. We found that a multipurpose diagnostic catheter enabled navigation to the tip of the RAA in most animals. In animals with prominent RAA trabeculation, an angled-tip balloon wedge end-hole catheter was preferred because the balloon prevented the catheter tip from becoming entangled in the trabeculae. Puncturing the RAA wall with the blunt back end of a guidewire (either 0.035 or 0.018 inches) was simple. Advancing a small catheter into the pericardial space over the wire did not meet with resistance.

Even in the presence of full anticoagulation and the larger 4Fr transatrial catheter, we observed only small pericardial effusions with no evidence of tamponade physiology after catheter withdrawal. Spontaneous closure of small RAA punctures has been described previously, with small thrombi at the puncture site, focal inflammatory infiltrates and increased collagen deposition seen on histology [12]. We therefore tested whether using a microcatheter could eliminate effusions altogether. With the smaller 2.8Fr microcatheter, we did not observe any effusions after transatrial microcatheter withdrawal in any of the 15 animals (2.8Fr Puncture and 2.8Fr + CO_2 groups).

We consider these findings, of zero effusions after 15 transatrial access attempts with CO_2 insufflation, to be compelling. However, these data provide 95% confidence only that the true incidence of effusion is 18% or less. To achieve similar confidence that the true incidence of effusion is less than 1% would require 325 observations of 0 effusions, and if less than 0.1% would require 3150 such observations. Both are unattainable. Moreover, we believe even a small pericardial effusion may be considered clinically acceptable in order to avoid more serious complications. On the basis of these observations, we have commenced enrollment in a clinical trial to test intentional right atrial exit to facilitate subxiphoid access to the anterior pericardial space in patients undergoing left atrial appendage suture ligation.

Pericardial Contrast Media

Pericardial iodinated contrast has been shown to facilitate navigation within the pericardial space [21]. Important structures such as atrial appendages, right ventricular outflow tract or atrioventricular groove can be delineated. However, contrast is heavier than water and so preferentially collects behind the heart when the patient is supine. This separates the layers of pericardium inferiorly and posteriorly and provides a target for the sub-xiphoid needle for access to the posterior pericardial space (Fig. 4). However, because of its viscosity it is difficult to aspirate iodinated contrast—even diluted in normal saline—through the transatrial microcatheter. Contrast would need to be aspirated through a larger sheath after sub-xiphoid access is established.

CO_2 is much lighter than water so collects anteriorly between the sternum and the heart when the patient is supine (Fig. 4). It affords excellent visualization of the heart contour and provides a space to aim for with the sub-xiphoid needle. This space enables anterior pericardial access without contacting the anterior surface of the heart. Anterior access is a prerequisite for certain interventions such as percutaneous left atrial appendage suture ligation. The space created by the CO_2 reduces the risk of lacerating the RV free wall or a coronary artery, usually caused by the heart beating against the sharp needle tip. An additional advantage of CO_2 is that if, for any reason, sub-xiphoid access cannot be obtained, then the CO_2 introduced does not need to be aspirated, but instead will resorb spontaneously.

Insufflating body cavities with CO_2 is safe. Because CO_2 solubility in blood is high, the reported incidence of significant CO_2 gas embolism from pneumoperitoneum during laparoscopy is less than 0.002% [22]. Flooding the surgical field with CO_2 while coming off cardiopulmonary bypass has been shown to reduce the incidence of air embolism [23]. Some studies of laparoscopic abdominal surgery have documented hypercarbia, thought to be due to CO_2 absorption from the peritoneal cavity and tissues [24]. However, much of this effect is likely attributable to hypoventilation caused by diaphragmatic splinting, which is unlikely to occur with pericardial CO_2 insufflation. In this study, pericardial CO_2 insufflation was very well tolerated. A transient reduction in systolic blood pressure was seen (mean decrease from baseline 6 mmHg or 7.7%) but this was reversible with spontaneous absorption of the pericardial CO_2. We did not observe any evidence of cardiac tamponade in any animal. Fluid or gas in the pericardial space can interfere with epicardial interventions, for example by elevating defibrillation thresholds during electrophysiological interventions [25]. However, this concern is not relevant to the present technique because pericardial iodinated contrast or CO_2 can be easily aspirated through the sub-xiphoid access port and moreover, CO_2 will resorb rapidly and spontaneously.

CONCLUSION

Intentional right atrial exit to access the 'dry' pericardium with small catheters was technically easy and safe in this preclinical study. Iodinated contrast or CO_2 infused through a transatrial catheter created a target that enhanced the safety of sub-xiphoid access so large sheaths could be introduced for electrophysiological or structural heart interventions. Iodinated contrast collected posteriorly, facilitating sub-xiphoid access to the posterior pericardium, whereas CO_2 separated the RV free wall from the sternum facilitating sub-xiphoid access to the anterior pericardium. This separation should reduce the risk of RV or coronary artery laceration. Transatrial microcatheters, which are smaller than 18-gauge needles, were withdrawn uneventfully despite full anticoagulation. On the basis of these preclinical findings, we commenced enrollment in a clinical trial to test this new technique in patients undergoing left atrial appendage suture ligation.

ACKNOWLEDGMENTS

The authors would thank Katherine Lucas and Joni Taylor for their help with animal experiments.

REFERENCES

1. Bartus K, Bednarek J, Myc J, Kapelak B, Sadowski J, Lelakowski J, Yakubov SJ, Lee RJ. Feasibility of closed-chest ligation of the left atrial appendage in humans. Heart Rhythm 2011;8:188–193.
2. Sosa E, Scanavacca M, d'Avila A, Pilleggi F. A new technique to perform epicardial mapping in the electrophysiology laboratory. J Cardiovasc Electrophysiol 1996;7:531–536.
3. Sosa E, Scanavacca M, D'Avila A, Piccioni J, Sanchez O, Velarde JL, Silva M, Reolao B. Endocardial and epicardial ablation guided by nonsurgical transthoracic epicardial mapping to treat recurrent ventricular tachycardia. J Cardiovasc Electrophysiol 1998;9:229–239.
4. Page SP, Duncan ER, Thomas G, Ginks MR, Earley MJ, Sporton SC, Dhinoja M, Schilling RJ. Epicardial catheter ablation for ventricular tachycardia in heparinized patients. Europace 2013;15:284–289.
5. Della Bella P, Brugada J, Zeppenfeld K, Merino J, Neuzil P, Maury P, Maccabelli G, Vergara P, Baratto F, Berruezo A, Wijnmaalen AP. Epicardial ablation for ventricular tachycardia: A European multicenter study. Circ Arrhythm Electrophysiol 2011;4:653–659.
6. Sacher F, Roberts-Thomson K, Maury P, Tedrow U, Nault I, Steven D, Hocini M, Koplan B, Leroux L, Derval N, Seiler J, Wright MJ, Epstein L, Haissaguerre M, Jais P, Stevenson WG. Epicardial ventricular tachycardia ablation a multicenter safety study. J Am Coll Cardiol 2010;55:2366–2372.
7. Tung R, Michowitz Y, Yu R, Mathuria N, Vaseghi M, Buch E, Bradfield J, Fujimura O, Gima J, Discepolo W, Mandapati R, Shivkumar K. Epicardial ablation of ventricular tachycardia: An institutional experience of safety and efficacy. Heart Rhythm 2013;10:490–498.
8. Price MJ, Gibson DN, Yakubov SJ, Schultz JC, Di Biase L, Natale A, Burkhardt JD, Pershad A, Byrne TJ, Gidney B, Aragon JR, Goldstein J, Moulton K, Patel T, Knight B, Lin AC, Valderrábano M. Early safety and efficacy of percutaneous left atrial appendage suture ligation: Results from the U.S. transcatheter LAA ligation consortium. J Am Coll Cardiol 2014;64:565–572.
9. Miller MA, Gangireddy SR, Doshi SK, Aryana A, Koruth JS, Sennhauser S, d'Avila A, Dukkipati SR, Neuzil P, Reddy VY. Multicenter study on acute and long-term safety and efficacy of percutaneous left atrial appendage closure using an epicardial suture snaring device. Heart Rhythm 2014 Jul 25 doi: 10.1016/j.hrthm.2014.07.032. [Epub ahead of print]
10. Lim HS, Sacher F, Cochet H, Berte B, Yamashita S, Mahida S, Zellerhoff S, Komatsu Y, Denis A, Derval N, Hocini M, Haissaguerre M, Jais P. Safety and prevention of complications during percutaneous epicardial access for the ablation of cardiac arrhythmias. Heart Rhythm 2014;11:1658–1665.
11. Verrier RL, Waxman S, Lovett EG, Moreno R. Transatrial access to the normal pericardial space: a novel approach for diagnostic sampling, pericardiocentesis, and therapeutic interventions. Circulation 1998;98:2331–2333.
12. Waxman S, Pulerwitz TC, Rowe KA, Quist WC, Verrier RL. Preclinical safety testing of percutaneous transatrial access to the normal pericardial space for local cardiac drug delivery and diagnostic sampling. Catheter Cardiovasc Interv 2000;49:472–477.
13. Mickelsen SR, Ashikaga H, DeSilva R, Raval AN, McVeigh E, Kusumoto F. Transvenous access to the pericardial space: An approach to epicardial lead implantation for cardiac resynchronization therapy. Pacing Clin Electrophysiol 2005;28:1018–1024.
14. Scanavacca MI, Venancio AC, Pisani CF, Lara S, Hachul D, Darrieux F, Hardy C, Paola E, Aiello VD, Mahapatra S, Sosa E. Percutaneous transatrial access to the pericardial space for epicardial mapping and ablation. Circ Arrhythm Electrophysiol 2011;4:331–336.
15. Rogers T, Ratnayaka K, Sonmez M, Franson DN, Schenke WH, Mazal JR, Kocaturk O, Chen MY, Faranesh AZ, Lederman RJ. Trans-atrial intra-pericardial tricuspid annuloplasty. J Am Coll Cardiol Interventions 2014 (in press).
16. The Task Force on the management of stable coronary artery disease of the European Society of Cardiology, 2013 ESC guidelines on the management of stable coronary artery disease. Eur Heart J, 2013;34:2949–3003
17. Koruth JS, Aryana A, Dukkipati SR, Pak HN, Kim YH, Sosa EA, Scanavacca M, Mahapatra S, Ailawadi G, Reddy VY, d'Avila A. Unusual complications of percutaneous epicardial access and epicardial mapping and ablation of cardiac arrhythmias. Circ Arrhythm Electrophysiol 2011;4:882–888.
18. Bradfield JS, Tung R, Boyle NG, Buch E, Shivkumar K. Our approach to minimize risk of epicardial access: standard techniques with the addition of electroanatomic mapping guidance. J Cardiovasc Electrophysiol 2013;24:723–727.
19. Mahapatra S, Tucker-Schwartz J, Wiggins D, Gillies GT, Mason PK, McDaniel G, Lapar DJ, Stemland C, Sosa E, Ferguson JD, Bunch TJ, Ailawadi G, Scanavacca M. Pressure frequency characteristics of the pericardial space and thorax during subxiphoid access for epicardial ventricular tachycardia ablation. Heart Rhythm 2010;7:604–609.
20. Tschabrunn CM, Haqqani HM, Zado ES, Marchlinski FE. Repeat percutaneous epicardial mapping and ablation of ventricular tachycardia: safety and outcome. J Cardiovasc Electrophysiol 2012;23:744–749.
21. Cohn WE, Winkler JA, Tuzun E, Hjelle A, Bassett K, Ahmad A, Frazier OH. Contrast pericardiography facilitates

intrapericardial navigation under fluoroscopy. Ann Thorac Surg 2010;90:1537–1540.
22. Cueto-Garcia J, Jacobs M, Gagner M. Laparoscopic Surgery. New York: McGraw-Hill; 2003.
23. Ng WS, Rosen M. Carbon dioxide in the prevention of air embolism during open-heart surgery. Thorax 1968;23:194–196.
24. Hirvonen EA, Nuutinen LS, Kauko M. Ventilatory effects, blood gas changes, and oxygen consumption during laparoscopic hysterectomy. Anesth Analg 1995;80:961–966.
25. Yamada T, McElderry HT, Platonov M, Doppalapudi H, Kay GN. Aspirated air in the pericardial space during epicardial catheterization may elevate the defibrillation threshold. Int J Cardiol 2009;135:e34–e35.

Catheterization and Cardiovascular Interventions DOI 10.1002/ccd.
Published on behalf of The Society for Cardiovascular Angiography and Interventions (SCAI).

4.5 Intentional right atrial exit and CO2 insufflation to facilitate subxiphoid needle entry into the empty pericardial space: first human experience

An original research manuscript accepted for publication in the '*Journal of the American College of Cardiology: Clinical Electrophysiology'* in 2015.

4.5.1 Background

Subxiphoid access to the normal or "empty" pericardial space is required for therapeutic procedures including epicardial suture ligation of the left atrial appendage[136, 137] and epicardial ablation of ventricular tachycardia[138]. "Dry" subxiphoid needle access is variably described as straightforward or perilous[139-142]. Inadvertent needle entry into the atria or ventricles is seldom clinically important, however myocardial and coronary artery laceration usually causes intractable haemopericardium requiring surgical repair. These complications continue despite small-diameter needles, oblique-endhole needles, and temporary suspension of respiration, because of the small distance between visceral and parietal pericardial walls and because of continuous cardiac motion[143]. In many cases, myocardium lacerates as the heart moves across the subxiphoid needle sharp tip.

Transatrial entry to the pericardial space was initially described in animals to facilitate homogeneous epicardial drug delivery [144] or chamber visualization [145]. We refined transatrial pericardial entry and contrast infusion using 2.4-2.8Fr (0.80 to 0.93mm outer diameter) microcatheters in animals as a method to facilitate subxiphoid needle access to the anterior or posterior pericardial spaces[146]. Despite high-intensity anticoagulation, we observed no important haemopericardium using careful MRI examination after simple withdrawal of these microcatheters from across the wall of the right atrial appendage.

We hypothesized that in patients the right atrial appendage can safely be crossed with a microcatheter and that the microcatheter can be withdrawn without causing clinically important pericardial haemorrhage. We further hypothesize that transatrial CO_2 insufflation can reduce the risk of subxiphoid pericardial needle entry in patients undergoing epicardial suture ligation of the left atrial appendage, by separating the visceral and parietal pericardial walls to keep the subxiphoid needle away from the heart. We describe the first human experience with intentional transcatheter right atrial exit and pericardial CO_2 insufflation.

4.5.2 Methods

Subjects: The Henry Ford Health System Institutional Review Board approved this protocol. From June 2014 through May 2015, consecutive candidates were invited to participate who were undergoing intrapericardial suture ligation of the left atrial appendage (*Lariat*, Sentreheart, Redwood City, CA) for high risk of thromboembolism and intolerance of anticoagulation for atrial fibrillation. All subjects consented in writing.

Technique of transatrial pericardial exit: Intentional exit of the right atrial appendage was performed via the femoral vein. A pulmonary artery catheter was placed via a separate vein to record hemodynamics solely for this protocol. The right atrial appendage was engaged with a catheter (7Fr Sones in the first subject and 7Fr balloon wedge endhole catheter the others, inside a transseptal introducer sheath) using a sweeping ascending clockwise motion from the lateral right atrial wall. Right atrial appendage angiography was performed using a hand injection of 2-5mL iodinated contrast. Through the guidewire lumen, a 2.4Fr braided microcatheter (*Renegade STC*-18 150cm, Boston Scientific) was positioned at the tip of the catheter and the back end of a guidewire (initially 0.014" Balance Middleweight, Abbott and later 0.018" V-18, Boston Scientific) advanced into the pericardial space. Next the microcatheter was advanced into the apical pericardial space and the guidewire was withdrawn. Out of caution, the larger transfemoral catheter was retracted to prevent inadvertent rail-advancement over the microcatheter into the pericardium, which might enlarge the hole. The technique was further refined as described in the results.

After refinement, we used SL2 or SL3 curve introducer sheaths (St Jude Medical) to direct a curved balloon wedge endhole catheter (Medtronic Pulmonary Artery Balloon or *Double-Lumen Hi-Shore Catheter T-Tip*, Edwards) to direct the back-end of a guidewire shaft known to be polymer coated (0.014" Runthrough, Terumo).

Transatrial pericardial CO_2 insufflation and subxiphoid needle access: The subxiphoid needle trajectory was planned according to the usual technique, aiming towards the left atrial appendage shadow on an antero-posterior projection. A coaxial long 21G x12 cm needle (Stiffen Bariatric, Galt, Harland, TX or Mak NV 216, Merit Medical, Chester, VA) was inserted alone or coaxially inside an 18G x 9cm spinal needle (Havel, Cincinnati, OH) under the skin but not yet abutting the cardiac shadow.

For CO_2 insufflation, a closed bag with one-way valve and manifold (Figure 4-5) was filled and purged in three cycles using filtered pure CO_2 as taught by Kyung Cho [147]. The system

stopcock was connected to the hub of the pericardial microcatheter and serous pericardial fluid was aspirated in all patients to assure an air-free connection and proper positioning. Carbon dioxide was injected by hand through this closed system until adequate (approximately 5-10mm) anterior fluoroscopic pericardial separation was obtained. The initial gas clearance of the microcatheter was slow to avoid a high pressure "jet effect" that might injure soft tissue. Subxiphoid needle access to the anterior pericardium was obtained in the lateral projection, without using a finder syringe or contrast injections, and instead with the guidewire 0.018" guidewire (Steelcore, Abbott) pre-positioned inside the needle to ease advancement into the pericardium immediately upon needle entry.

The transatrial pericardial microcatheter was withdrawn over a guidewire immediately after the subxiphoid Lariat SoftTip sheath was advanced into the pericardial space. Next transseptal access was obtained under transesophageal echocardiography guidance and unfractionated heparin administered immediately to achieve an activated clotting time > 300s. Next Lariat suture ligation of the left atrial appendage was performed according to usual methods, and a subxiphoid pericardial drain left in overnight.

Data analysis: Data were collected using REDCap (www.project-redcap.org)[148], and analysed using Excel (v2010, Microsoft). Data were described as mean ± standard deviation if they were normally distributed, otherwise as median (first quartile, third quartile). Continuous data were compared using an unpaired *t*-test. A $p<0.05$ was considered significant.

4.5.3 Results

All consecutive patients undergoing *Lariat* suture closure during the study period consented to participate. Of the 13 subjects enrolled in the study, the mean age was 75±8, 46% were women, 46% had prior TIA or stroke, all were intolerant of anticoagulation, 92% used aspirin at the time of the procedure, 0% used a P2Y12 blocker, 85% had prior haemorrhage, the average $CHADS_2$ score was 2.8±1.4, the average CHA_2DS_2-VASc score was 4.6±1.6, and the average HAS-BLED score was 3.2±1.2. Baseline hemodynamics under general anaesthesia were heart rate, 70±16 bpm, right atrial pressure 7±3 mmHg, mean pulmonary artery 23±6, mean aortic 72±17. Left ventricular ejection fraction was 0.58±0.10, and 31% had moderate tricuspid regurgitation.

Right atrial exit was successful in 11 of 13 cases, and required 2.2±1.7guidewire passes. Figure 4-6 shows a representative sequence of right atrial angiography, transatrial guidewire exit, and transatrial microcatheter advancement into the pericardial space.

After pericardial insufflation, subxiphoid needle pericardial entry was consistently rapid and straightforward in all cases because the pericardial layers clearly separated. Figure 4-7 shows a representative sequence of CO_2 insufflation, subxiphoid needle, and subxiphoid guidewire delivery. These steps were associated with no change in heart rate, central aortic blood pressure, or pulmonary artery pressure. The mean time from right atrial angiography to right atrial exit was 1:44±1:16 minutes, and from right atrial exit to subxiphoid needle entry was 7:49±2:31 minutes.

The right atrial exit angle relative to horizontal, in the antero-posterior projection, appeared to differ between successful and unsuccessful exits. The horizontal exit angle was 23±12^{o} when successful compared with 45±14^{o} for unsuccessful exits, p=0.01. An average of 96±22mL of CO_2 achieved 12±4mm anterior pericardial separation

Microcatheters were withdrawn from the right atrial appendage 11:27±5:44 minutes before heparin was administered (during which time transseptal access was obtained) to raise the activated clotting time from 170±53 to 313±14s.

The equipment selected for right atrial exit evolved during the protocol. At first we applied standalone multi-purpose-type catheters (Sones, multipurpose guiding catheters, balloon-wedge endhole catheters). Then we used standalone three-dimensional curved catheters (heat-gun shaped sheaths and MP guiding catheters. Ultimately we settled upon three-dimensional curve introducer sheaths intended for atrial transseptal access (SL1 or SL2 or SL3, Daig, St Jude Medical) selected according to RA size, and used these to direct balloon-wedge endhole catheters to the right atrial appendage. We found the combination achieved a helical trajectory from the IVC along the lateral and then anterior right atrial and appendage wall that allowed backup support for the transatrial guidewire exiting horizontally from the right atrial appendage.

One patient (#8) had a serious complication of left atrial suture ligation despite, and unrelated to, successful transatrial access. She required sternotomy for repair of visually confirmed left ventricular myocardial abrasion most likely attributable to introducing the Sentreheart *SoftTip* subxiphoid sheath. In this patient, the right atrial appendage exit site was inspected directly and was found haemostatic and with surrounding plethora, as expected (Figure 4-8). The pericardium was evacuated and she recovered uneventfully for discharge on day 5.

One patient had mild pericardial bleeding after withdrawal of the transatrial microcatheter,

evident on angiography of the right atrial appendage, amounting to 125 mL total drainage. This was treated conservatively with close echocardiographic surveillance. The subject was discharged uneventfully on day 2.

After CO_2 insufflation, no patient suffered right ventricular or coronary artery laceration by the subxiphoid needle, or even inadvertent right ventricular entry.

4.5.4 Discussion

To our knowledge this is the first human experience intentionally exiting the right atrium to enter the pericardial space. We found that a catheter can intentionally traverse the right atrial appendage wall into the pericardium and be withdrawn without important sequelae as part of a therapeutic procedure that requires brief intensive anticoagulation. We infer the small 0.8mm hole recoils immediately. This should come as no surprise, since transcameral needle perforation is common using 0.6-0.9mm outer diameter needles (for example, 18-21G pericardial access and transseptal needles) and usually is not clinically significant. Indeed intraoperative cardiac pressures are often recorded from plunge needles that are withdrawn despite anticoagulation. Transatrial CO_2 insufflation separated the anterior pericardial walls sufficiently to keep a subxiphoid needle far from the epicardial surface throughout the cardiac and respiratory cycles, allowing safe and rapid subxiphoid needle access, and without changing hemodynamics.

The main shortcoming of our approach was failure to exit the right atrial appendage in two of twelve subjects (fourth and seventh in sequence). We attribute this to inexperience, to misalignment of the right atrial catheter with the right atrial appendage and intended empty pericardial space, and also to the subjectively greater advancement force required to perforate the appendage in humans compared with swine [146]. We believe that with experience our success rate is likely to improve, especially now that we recognize the importance of good backup support through a helical geometry of the coaxial atrial catheter system (see below). We were unable to obtain meaningful measurements of thickness of the right atrial appendage wall at the resolution of the available CT scans to determine if thickness was a contributing factor. Fortunately, all transatrial exit failures were clinically uneventful, and were addressed by switching to conventional “dry” subxiphoid pericardial access.

We refined our catheter technique during the protocol. First, we imparted a three-dimensional curve on the right atrial appendage catheter system, extending from the cava to

the supero-anterior wall of the right atrial appendage. This afforded better backup support and aligned the catheter system with the crest of the appendage and the pericardial space. Second, we switched to a balloon wedge endhole catheter, which in a cautious inflation-deflation manoeuvre acted to separate the anterior and posterior walls of the right atrial appendage and allowed the catheter tip to advance to the leftmost tip of the appendage despite trabeculations. The inflated balloon tip catheter may also protect against inadvertent advancement of the support catheter across the right atrial appendage wall along the microcatheter. We warn that incautious inflation-deflation may be hazardous in the right atrial appendage. Third, we began to orient our crossing system more horizontally leftward, reasoning that more vertical upward oriented crossing may contribute to failure because of constraint from cephalad pericardial reflections as depicted in Figure 4-9. We took care to select transatrial exit sites near the cephalad extent of the right atrial appendage, which was consistently far from the right coronary artery on CT.

Important limitations warrant mention. First, pericardial fluid infusion has been shown to increase defibrillation thresholds in animals[149], and we speculate nonconductive CO_2 may increase defibrillation thresholds by surrounding the heart with an insulator. We found the typical pericardial insufflation of 100 mL (1-1.5mL/kg) CO_2 accumulated anteriorly over less than 10% of the antero-posterior dimension of the heart, and defibrillation is likely attainable using laterally positioned electrodes. CO_2 need only be insufflated a few seconds before the subxiphoid needle is advanced in the lateral fluoroscopic projection. In our preclinical experience, much larger volumes (3-5mL/kg) of CO_2 gas spontaneously absorb in 5-10 minutes. Overall the risk of ventricular fibrillation during subxiphoid access is low. Second, transatrial access requires an extra step and extra equipment beyond simple subxiphoid access. This is offset by the more simple and perhaps more safe subxiphoid needle access with the pericardial walls separated. Third, transatrial separation of the pericardial walls does not address all the risks of the Lariat suture ligation procedure, including sheath injury (which required surgical bailout in one patient in our series), perforation of the LAA by the docking magnet wires, and avulsion of the LAA by the suture delivery apparatus. Fourth, our series included only patients with relatively preserved myocardial function and relatively normal right atrial pressure, so our findings should not be extended to patients with more severe cardiomyopathy until after further investigation. Fifth, a larger clinical experience obtained from more than one medical centre will be required more convincingly to prove the safety of this technique beyond the data presented here.

Transatrial pericardial insufflation may have value in other applications. These include conventional applications requiring subxiphoid access to the pericardium, such as epicardial mapping and ablation of ventricular tachycardia. Right atrial appendage exit alone also may have value in more novel applications, such as transatrial intrapericardial tricuspid annuloplasty [150] and emergency anterior pericardial access in acute low-volume tamponade when conventional access fails. Transatrial instillation of iodinated radiocontrast accumulates in the posterior pericardium and may enhance the safety of subxiphoid posterior pericardial access[146] if desired, although this was not tested in this protocol.

4.5.5 Conclusions

We report the first human intentional transatrial exit procedure. Transatrial access to the pericardium can be achieved safely. Pericardial insufflation with CO_2 makes subxiphoid access to the empty anterior pericardium rapid and safe. With further experience this technique might prevent life-threatening complications of "dry" subxiphoid pericardial access.

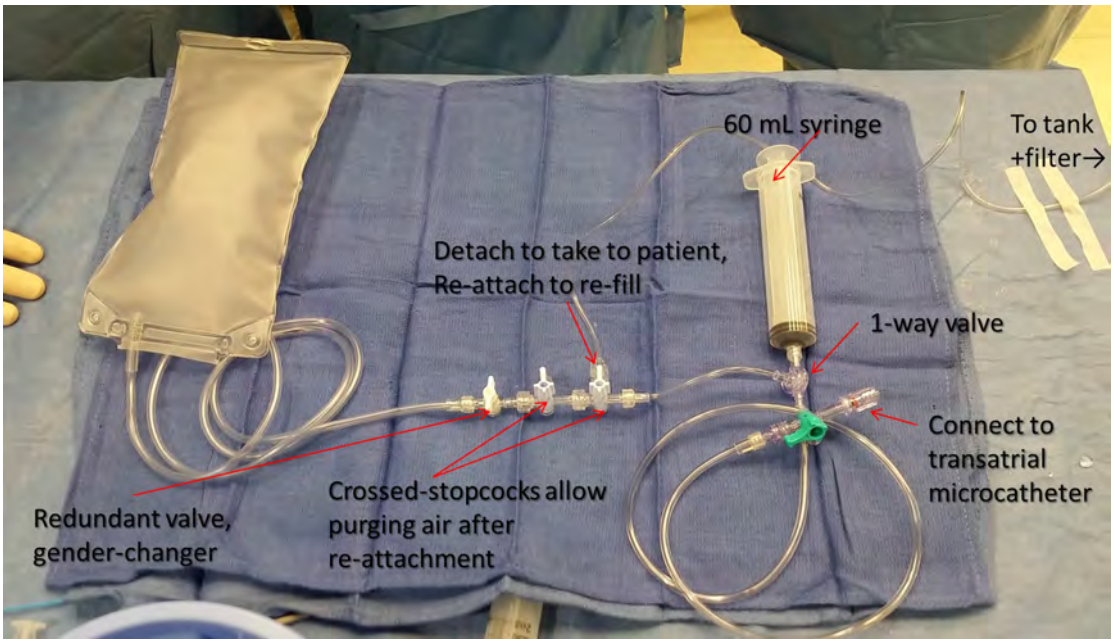

Figure 4-5: CO2 setup for transatrial pericardial insufflation

The connection to the CO2 tank should be detached before use in a patient; crossed stopcocks allow air to be purged after it the syringe is reattached for refilling. The system is filled and purged at least three times before use. The syringe has a one-way valve that allows it to fill with CO2 from the bag and to eject into a stopcock connected to the transatrial microcatheter.

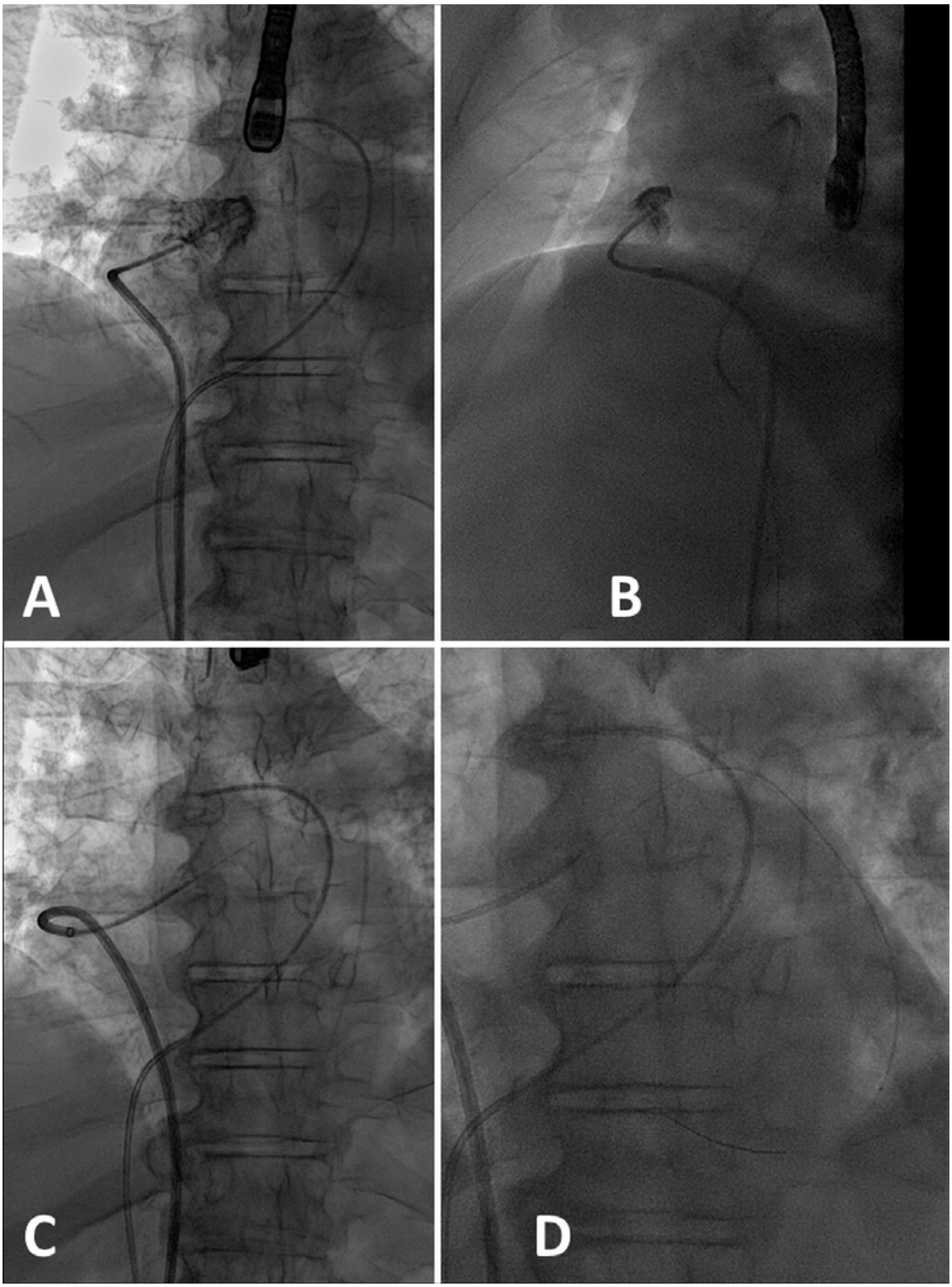

Figure 4-6: An example of transatrial guidewire exit

Antero-posterior (A) and lateral (B) contrast angiogram of the R atrial appendage from a catheter positioned at its crest. (C) The back-end of an 0.014" guidewire crosses the R atrial appendage. (D) A microcatheter is advanced over the guidewire into the pericardial space.

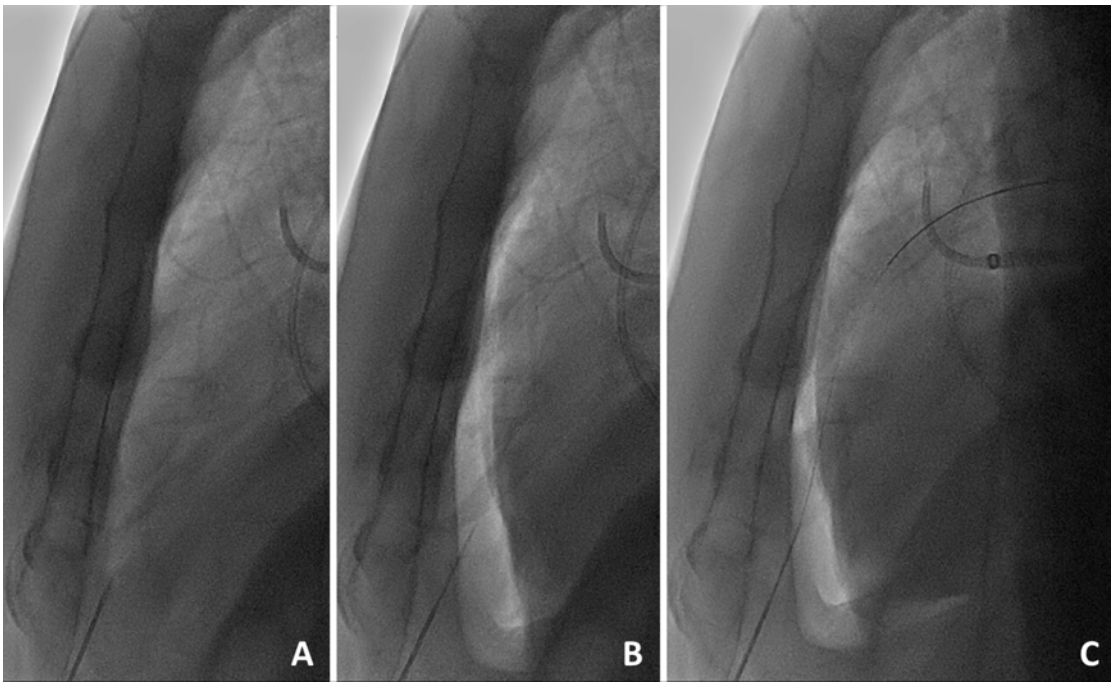

Figure 4-7: Subxiphoid access

After the transatrial pericardial microcatheter is placed, the subxiphoid needle is positioned outside the heart (A). In the lateral fluoroscopic projection, the pericardium is filled with 1.0-1.5mL/kg of CO2 to displace the heart posteriorly (B). The gas clearly visualizes the anterior wall of the heart to allow needle entry without cardiac contact. (C) The subxiphoid guidewire is then advanced through the needle and the procedure continues as usual.

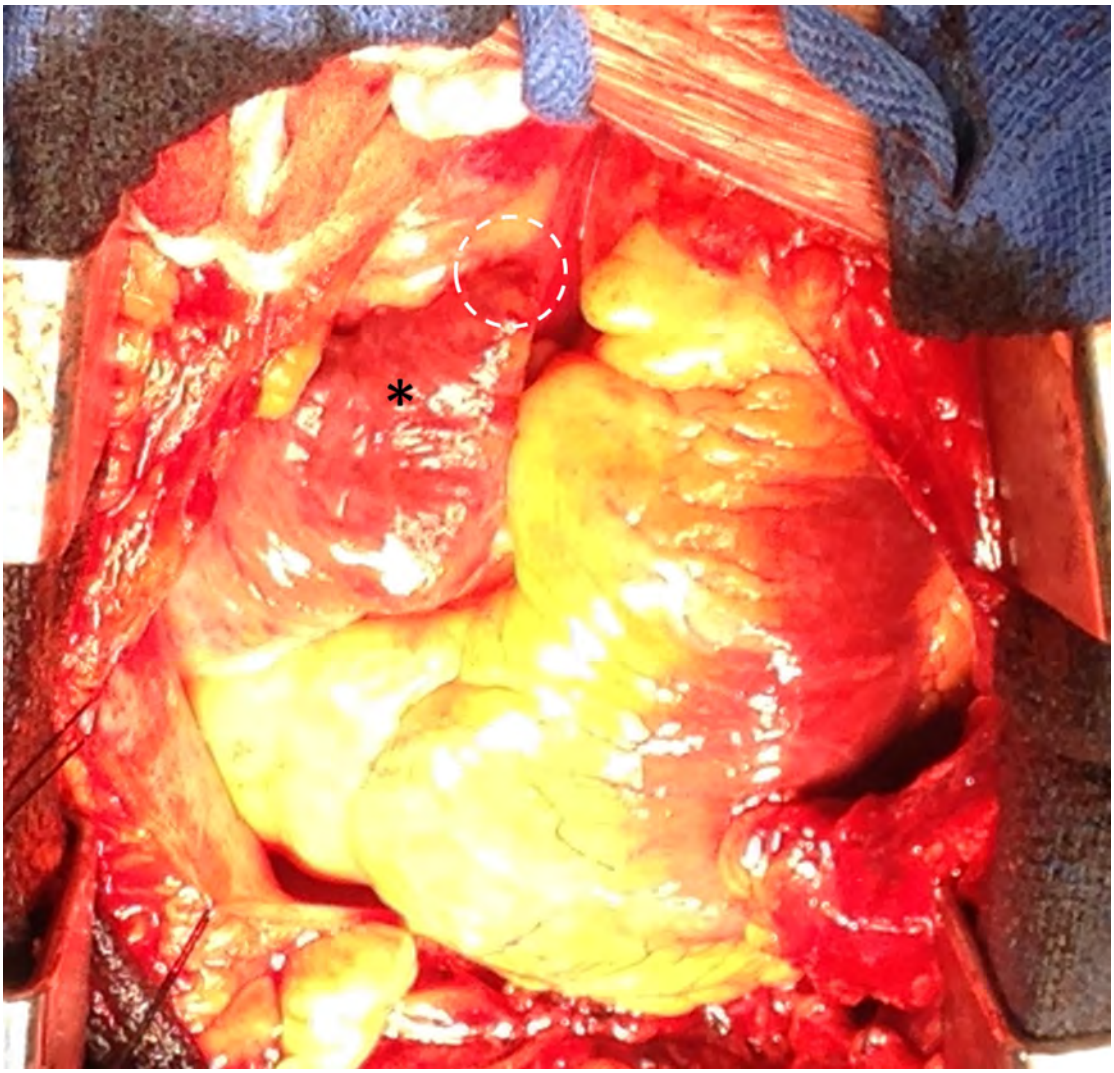

Figure 4-8: Operative inspection of a transatrial exit site

This patient required surgical repair of left ventricular abrasion attributed to the suture delivery sheath. Incidental inspection of the right atrial appendage (asterisk) showed plethora and inflammation but no bleeding or discrete hole at the site of right atrial exit from the crest of the right atrial appendage (dotted circle).

Figure 4-9: Exit angle and success

In this contrast pericardiogram from another patient, the right atrial appendage border (dotted red line) is depicted along with two theoretical wire exit trajectories. Trajectory 1 (orange) is aligned with the main axis of the right atrial appendage and oriented superiorly; failed right atrial exit along this trajectory may be related to the superior pericardial reflection. By contrast, trajectory 2 (green) is oriented more horizontally and leftwards.

Chapter 5. Fully percutaneous transthoracic left atrial access and closure as a potential access route for mitral valve interventions (*publication*)

5.1 Introduction

A number of transcatheter mitral valve prostheses have been tested in early human studies. However, because the mitral annulus is much larger than the aortic, and because these devices must incorporate fixation components to anchor them in the mitral annulus, they all require wide-bore access ports (≥10mm internal diameter). The obvious approach is transapical because it affords direct and coaxial access to the mitral. Achieving coaxiality with alternative approaches such as trans-septal is much more difficult. However, there is evidence from transcatheter aortic valve implantation studies that transapical access causes local scar formation, which can negatively impact LV function. LV morphology and function in patients with severe mitral regurgitation are very different and it likely that transapical access in these patients may affect LV function to a much greater degree.

Direct left atrial needle access through the right thoracic cavity was demonstrated in the 1950s, before the advent of cardiac catheterization. We explored whether this approach could be re-visited to deliver large transcatheter mitral valve devices.

5.2 The role of CMR

Direct left atrial access through the posterior chest wall and right thoracic cavity requires crossing a variety of anatomic boundaries and avoiding a number of critical structures. Visualization of each structure and determination of optimal trajectory is therefore important. For this reason, we developed the procedure using real-time CMR guidance. CMR allowed us to learn how single lung deflation affects the geometry of the heart and mediastinum and to correct the trajectory in real-time because all soft tissue structures are visible at all times. This would not be feasible using X-ray fluoroscopy and echocardiography. CMR also permits early identification and management of complications, such as pericardial or pleural bleeding. Once we gained a clear understanding of these dynamic anatomical parameters, we were able to replicate the technique using X-ray fluoroscopy and adjunctive rotational angiography imaging so that the intervention could be translated to clinic without needing a dedicated interventional CMR catheterization laboratory.

5.3 Candidate's contribution

I performed all the pre-clinical experiments (under MRI and X-ray imaging guidance). I collected the pre-clinical data and performed the statistical analysis. I also analysed the human CT studies. I drafted the manuscript and prepared the figures, tables and supplementary materials.

5.4 Fully percutaneous transthoracic left atrial access and closure as a potential access route for mitral valve interventions

An original manuscript published in the journal '*Circulations: Cardiovascular Interventions'* in 2015.

Fully Percutaneous Transthoracic Left Atrial Entry and Closure as a Potential Access Route for Transcatheter Mitral Valve Interventions

Toby Rogers, BM BCh, MRCP; Kanishka Ratnayaka, MD; William H. Schenke, BA; Merdim Sonmez, PhD; Ozgur Kocaturk, PhD; Jonathan R. Mazal, MS; Marcus Y. Chen, MD; Moshe Y. Flugelman, MD; James F. Troendle, PhD; Anthony Z. Faranesh, PhD; Robert J. Lederman, MD

Background—Percutaneous access for mitral interventions is currently limited to transapical and transseptal routes, both of which have shortcomings. We hypothesized that the left atrium could be accessed directly through the posterior chest wall under imaging guidance.

Methods and Results—We tested percutaneous transthoracic left atrial access in 12 animals (10 pigs and 2 sheep) under real-time magnetic resonance imaging or x-ray fluoroscopy plus C-arm computed tomographic guidance. The pleural space was insufflated with CO_2 to displace the lung, an 18F sheath was delivered to the left atrium, and the left atrial port was closed using an off-the-shelf nitinol cardiac occluder. Animals were survived for a minimum of 7 days. The left atrial was accessed, and the port was closed successfully in 12/12 animals. There was no procedural mortality and only 1 hemodynamically insignificant pericardial effusion was observed at follow-up. We also successfully performed the procedure on 3 human cadavers. A simulated trajectory to the left atrium was present in all of 10 human cardiac computed tomographic angiograms analyzed.

Conclusions—Percutaneous transthoracic left atrial access is feasible without instrumenting the left ventricular myocardium. In our experience, magnetic resonance imaging offers superb visualization of anatomic structures with the ability to monitor and address complications in real-time, although x-ray guidance seems feasible. Clinical translation seems realistic based on human cardiac computed tomographic analysis and cadaver testing. This technique could provide a direct nonsurgical access route for future transcatheter mitral implantation. **(*Circ Cardiovasc Interv*. 2015;8:e002538. DOI: 10.1161/CIRCINTERVENTIONS.114.002538.)**

Key Words: catheterization ■ endovascular procedures ■ heart valve prosthesis implantation ■ magnetic resonance imaging, interventional ■ mitral valve

Transcatheter mitral valve-in-valve or valve-in-ring implantation is feasible using prostheses designed for the aortic valve.[1,2] Implantation in the native mitral annulus presents distinct challenges: available aortic prostheses are too small, valve fixation is difficult because the annulus is elastic, and the subvalvular apparatus, which plays an important role in left ventricular function, should not be disrupted. At least 4 dedicated devices have undergone early human testing.[3–5] These are bulky and require large caliber access ports (up to 32F), mostly transapical.

Whether transapical access is associated with higher mortality than transfemoral remains unclear.[6–8] The higher mortality reported in some studies may reflect inclusion of higher risk patients or operator experience. Nonetheless, magnetic resonance imaging (MRI) and echocardiography detect apical wall motion abnormalities after transapical access, particularly in patients with increased left ventricle (LV) diameter, which can lead to long-term reduction in global LV function.[9–11] In the Placement of Aortic Transcatheter Valves (PARTNER) trial quality-of-life assessment, transcatheter aortic valve replacement via transapical approach demonstrated no benefit compared with conventional surgery.[12] Morbidity and mortality are likely even higher in patients with mitral valve disease because of preexisting LV dysfunction. Truly percutaneous transapical access using nitinol devices for closure is possible,[13] but complications do occur including pneumothorax, cardiac tamponade, LV pseudoaneurysm, and hemothorax related to coronary or intercostal vessel laceration or bleeding from the LV puncture site.[14]

Alternative approaches have been explored for mitral valve interventions: direct transatrial via minithoracotomy,[15]

Received November 21, 2014; accepted April 30, 2015.

From the Cardiovascular and Pulmonary Branch, Division of Intramural Research (T.R., K.R., W.H.S., M.S., O.K., J.R.M., M.Y.C., A.Z.F., R.J.L.) and Office of Biostatistics Research, Division of Cardiovascular Sciences (J.F.T.), National Heart Lung and Blood Institute, National Institutes of Health, Bethesda, MD; Department of Cardiology, Children's National Medical Center, Washington DC (K.R.); Institute of Biomedical Engineering, Bogazici University, Istanbul, Turkey (O.K.); and Department of Cardiology, Carmel Medical Center, Haifa, Israel (M.Y.F.).

The Data Supplement is available at http://circinterventions.ahajournals.org/lookup/suppl/doi:10.1161/CIRCINTERVENTIONS.114.002538/-/DC1.

Correspondence to Robert J. Lederman, MD, National Heart Lung and Blood Institute, National Institutes of Health, Bldg 10, Room 2c713, Bethesda, MD 20892. E-mail lederman@nih.gov

WHAT IS KNOWN

- Transcatheter mitral valve replacement requires a large caliber sheath and coaxiality between the delivery system and the mitral valve.
- Transapical access may not be an option in all patients, so alternative approaches are needed.

WHAT THE STUDY ADDS

- Fully percutaneous transthoracic left atrial access and closure is feasible in large animal models and affords superb coaxiality with the mitral valve.
- The procedure can be guided using x-ray fluoroscopy or real-time MRI.
- Cardiac computed tomographic analysis and human cadaver feasibility testing indicate that the left atrium can be accessed with a large caliber sheath through the posterior chest wall in humans.

transjugular transseptal,[16,17] and transfemoral transseptal.[18] However, a minithoracotomy still confers surgical morbidity. Transseptal delivery of large mitral implants has been demonstrated, but achieving coaxiality with the mitral valve can remain challenging. A straight shot to the mitral valve that permits large sheath access but does not violate the LV myocardium would be desirable and could reduce the engineering constraints of miniaturization, reduce procedural complexity, and improve patient outcomes.

Percutaneous left atrial (LA) access was first performed in the 1950s using long needles through the posterior chest wall to sample pressure.[19,20] At first glance, delivering large sheaths via this approach seems challenging because of interposed lung, but there is extensive surgical evidence that temporarily collapsing a lung to perform an intrathoracic intervention is safe.[21] In fact, diagnostic thoracoscopy with iatrogenic lung deflation is commonly performed in awake patients and confers extremely low morbidity and mortality.[22] Percutaneous transthoracic cardiac catheterization has also been performed in children with no alternative access, through the anterior chest into the pulmonary venous atrium and through the lower back into the inferior vena cava.[23,24]

We hypothesized that with imaging guidance and percutaneous techniques, it is possible to access the LA directly through the posterior chest wall by first displacing a lung with gas, then delivering a large sheath, and finally closing the LA port using off-the-shelf nitinol cardiac occluder devices. Compared with percutaneous transapical LV closure, we think that closing a port in the lower pressure LA may be preferable. Because of anatomic differences between large mammals and human, we tested this hypothesis in 2 different large animal models (porcine and ovine) and then explored feasibility of clinical translation with human cardiac computed tomographic (CT) analysis and human cadaver testing. We also explored different image guidance modalities, MRI and x-ray fluoroscopy, to simplify translation into patients.

Methods

Animal Experiments

The institutional animal care and use committee approved all procedures, which were performed according to contemporary National Institutes of Health guidelines. Animals were anesthetized with ketamine (25 mg/kg), midazolam (15 mg/kg), and glycopyrrolate (0.01 mg/kg) and maintained on sevoflurane (1%–4%) and mechanical ventilation. Femoral arterial and venous access was obtained with ultrasound guidance with animals supine.

The technique was developed in nonsurvival experiments on 10 naïve Yorkshire swine, not further described here. Subsequently, survival experiments were performed in 10 naïve Yorkshire swine with median bodyweight 51 kg (47–54 kg) and 2 naïve Dorset sheep (28 and 36 kg), all of which were survived for at least 7 days before euthanasia and necropsy.

Imaging

Experiments were performed first using MRI at 1.5T (Aera, Siemens) and later using biplane x-ray fluoroscopy enhanced by C-arm CT (Artis Zee and DynaCT, Siemens). Experiments are summarized in Figure 1. For MRI, trajectories were planned on isotropic 3-dimensional images, and the procedure was performed using custom MRI-antenna needles[25] and real-time MRI at frame rates ≤15 fps. MRI parameters and devices are provided in the Data Supplement.

Pericardial Autotransfusion Catheter Placement

An 8.3F multi-sidehole subxiphoid pericardial drain was placed after transatrial microcatheter CO_2 insufflation as described[26] and connected to the femoral vein to facilitate immediate autotransfusion for blood salvage. Unfractionated heparin (500–1000 IU) was infused into the pericardial space to prevent in situ thrombus.

Pleural CO_2 Insufflation to Displace Lung

A needle was advanced through the left lateral chest wall during small puffs of iodinated or gadolinium contrast (for x-ray or MRI visualization, respectively) until the pleural space was entered (Figure 2). This was exchanged for an 8.3F multi-sidehole pleural drain positioned in a dependent position to aspirate fluid but not CO_2. As with the pericardium, 500 to 1000 IU of unfractionated heparin was infused into the pleural space to prevent in situ thrombus formation and facilitate autotransfusion. The pleural space was insufflated with CO_2 titrated to displace lung sufficiently to allow a clear trajectory to the

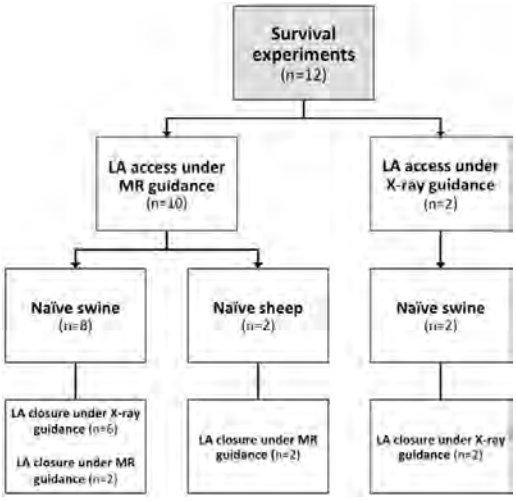

Figure 1. Experiment design. LA indicates left atrial.

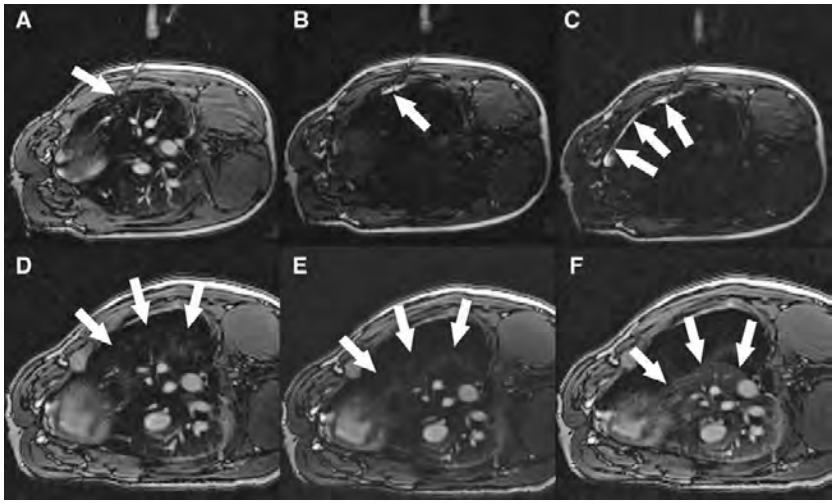

Figure 2. Magnetic resonance imaging (MRI)-guided pleural insufflation to displace lung. **A**, Needle (arrow) is advanced through the chest wall toward the pleura. **B**, Saturation mode MRI darkens tissue to enhance visibility of gadolinium contrast. Small aliquots of contrast injected through the needle (arrow) show that the tip is still within the chest wall. **C**, After advancing the needle further, contrast flows freely around the lung in the pleural space (arrows). Saturation mode MRI is then toggled off. **D–F**, After insertion of a drain, the pleural space is insufflated with CO_2 to deflate the lung despite positive pressure ventilation. Arrows indicate lung margin during progressive pleural insufflation.

LA. After insufflation, the ventilation rate was increased and tidal volumes reduced to keep airway pressure low.

Transthoracic LA Trajectory Planning and Access

Three-dimensional MRI or x-ray (C-arm CT and biplane fluoroscopy contrast angiograms) of the LA was acquired at baseline and after pleural insufflation. For x-ray guidance, we used a superimposed C-arm CT of LA and LV angiograms (syngo InSpace EP, Siemens). Swine and sheep were positioned respectively on the right side or prone to optimize working angles. A 20-cm needle was used to puncture through the posterior or lateral chest wall, pass through the empty pleural space, and enter the LA posteriorly (Figures 3 and 4). Needle tip position was confirmed by atrial pressure waveform and contrast injection. A stiff nitinol guidewire (Nitrex, Covidien) was introduced through the mitral valve to the LV apex, over which a 18F sheath (outer diameter, 7 mm; Large Check-Flo, Cook) and a custom-shortened dilator were advanced into the LA without predilatation. Sheath position and relation to the mitral valve were confirmed using MRI or biplane contrast angiography.

LA Closure

The LA port was closed with an off-the-shelf 5- or 6-mm nitinol atrial septal occluder (St Jude Medical, MN; Lepu Medical, Beijing, China). The distal disc was deployed within the LA, and the sheath and delivery catheter were withdrawn in tandem until the disc was in apposition with the LA wall. The proximal disc was deployed outside the heart within the pleural space, and the device was released.

Human Cadaver Study and Human CT Analysis

To explore feasibility for humans, we tested percutaneous transthoracic LA access and closure in 3 human cadavers (1 under MR and 2 under x-ray guidance). After femoral access, the cadavers were rolled prone and all procedural steps were identical to those previously described for animal procedures, using a larger sheath (Ascendra, Edwards Lifesciences, 26F/30F inner/outer diameter).

We also examined 10 random cardiac CT angiograms having full chest wall coverage among patients with mitral valve disease, dilated LA, or previous sternotomy in the *National Heart, Lung, and Blood Institute* anonymized and delinked database. This does not constitute human subjects research under US 45CFR§46.102(f). Each CT was examined for potential trajectories to the LA.

Statistical Analysis

Hemodynamic data are reported in the Table as median with first and third quartiles (Q1–Q3). Each hemodynamic parameter was analyzed in a linear mixed model with autoregressive–moving-average (1,1) correlation structure assumed within each animal. The model fit mean levels of each parameter at each of the 4 postbaseline follow-up measurements with baseline as the reference. Because there were 4 follow-up measures for each of 3 hemodynamic parameters, we used a Bonferroni correction factor of 12 to account for multiple comparisons. A multiplicity corrected P value ≤0.05 was considered statistically significant.

Results

Pericardial Access for Autotransfusion Catheter Placement

Transatrial pericardial access with a 2.8F microcatheter, insufflation of the pericardial space with CO2, placement of a subxiphoid 8.3F drain, and withdrawal of the transatrial microcatheter was uncomplicated in all 12 animals.

Pleural Insufflation

Pleural access and left lung deflation with CO_2 was uncomplicated in all 12 animals. 600 to 900 mL of CO_2 was required to displace the lung sufficiently to establish an unobstructed trajectory to the LA in both species. Pleural pressures remained low (8–10 mm Hg) and, despite lung displacement, ventilation was well tolerated with no increase in expired CO_2 or evidence of hemodynamic compromise (Table). Reductions in mean arterial pressure and heart rate were observed after pleural insufflation, which were likely caused by an increase in the inhaled anesthetic agent concentration required to allow for the reduction in ventilator tidal volumes. However, these changes were not statistically significant.

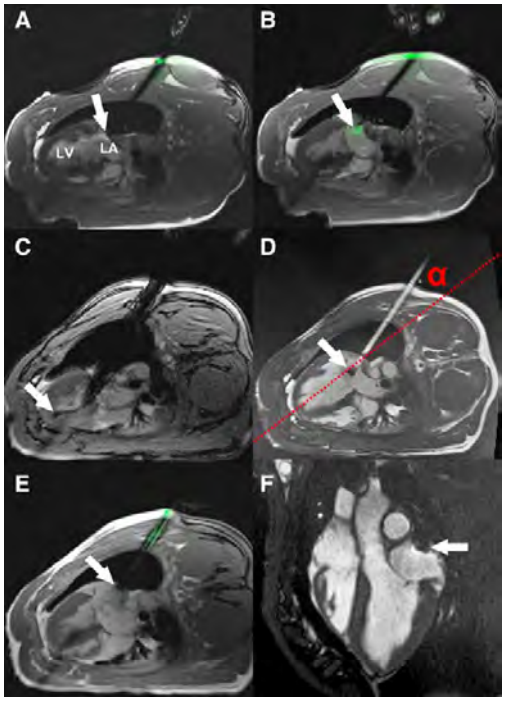

Figure 3. Real-time magnetic resonance imaging (MRI)–guided left atrial (LA) access and closure in swine. **A**, An active visualization MRI needle incorporating MRI electronics for enhanced visibility is introduced through the chest wall into the empty pleural space. The tip is positioned against the posterior LA wall (arrow). **B**, LA puncture: the active needle tip is clearly seen within the LA (arrow). **C**, Delivery of a large 18F sheath into the LA. The guidewire is visible in the apex of the left ventricle (LV; arrow). **D**, Filled with gadolinium contrast, the sheath trajectory to the LA is apparent. There is a passive marker at the tip of the sheath (arrow). The angle α represents the offset between the sheath trajectory and the long axis of the LV (dotted red line). **E**, A nitinol cardiac occluder device is loaded onto an active delivery cable, which incorporates MRI electronics for visualization. The distal disk is deployed within the LA and pulled back against the posterior wall (arrow). The proximal disk is deployed outside the heart. **F**, Seven days later, the nitinol cardiac occluder device remains in the intended position with no pericardial effusion.

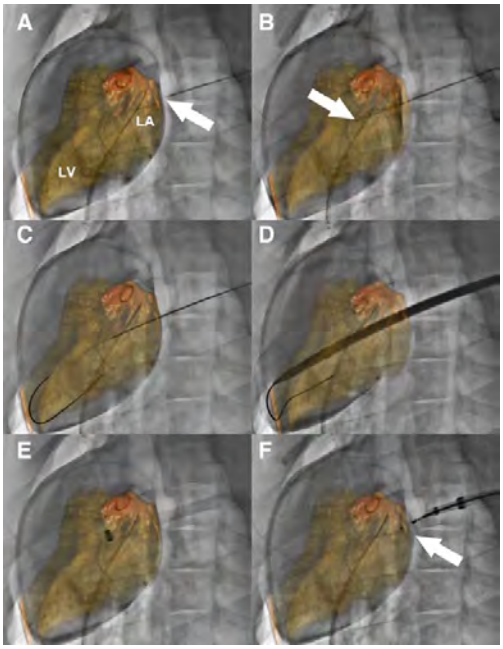

Figure 4. X-ray fluoroscopy and C-arm CT–guided left atrial (LA) access and closure in swine. **A**, A pigtail catheter is positioned in the LA via transseptal puncture. Contrast-enhanced cone-beam angiography is performed, and LA and left ventricle (LV) are segmented and overlaid on the fluoroscopic images. The needle tip (arrow) for LA puncture is positioned against the posterior wall of the LA. **B**, The needle (arrow) is advanced into the LA. **C**, A stiff wire is introduced through the mitral valve into the LV apex. **D**, A large sheath is advanced over the wire into the heart. **E**, After withdrawing the sheath dilator, the sheath tip is confirmed within the LA. **F**, The LA port is closed with a nitinol cardiac occluder device (arrow).

Trajectory Planning

In swine, pleural insufflation caused the heart to rotate, displacing the long axis of the LV by 7° (6°–14°) compared with baseline. A direct trajectory to the LA, avoiding important anatomic structures was achievable in all animals. Distance from skin to LA was 10 cm (9–11 cm) in swine and 11 cm in both sheep.

Transthoracic LA Access and Closure

The LA was successfully accessed in 10/10 swine, including 8 under MR guidance (Figure 3; Movie I in the Data Supplement) and 2 under x-ray guidance (Figure 4; Movie II in the Data Supplement). All succeeded in a single needle pass except in 1, wherein a custom needle that had become dull required a second pass. The stiff nitinol guidewire was positioned in the LV apex, over which the 18F sheath was advanced without predilation. Sheath advancement displaced the LA wall by 25 mm (20–30 mm; under x-ray guidance), but the wall recoiled as soon as the sheath tip entered the LA. No pericardial or pleural effusions developed during LA puncture or while the large sheath remained in place. Three-dimensional and cine MRI confirmed that the sheath trajectory was offset relative to the long axis of the LV by an angle α of ≤30° (Figure 3). The LA port was successfully closed with a single nitinol cardiac occluder device in all animals. During sheath withdrawal and LA port closure, accumulated blood was autotransfused intermittently using the prepositioned pericardial and pleural drains. Median pericardial and pleural autotransfusion volumes were 55 mL (40–73 mL) and 10 mL (10–75 mL), respectively. Animals were stable hemodynamically throughout, and no arrhythmias were observed (Table).

The LA was successfully accessed with a single pass and closed under MRI guidance in 2/2 sheep. One animal had minimal pericardial effusion (50 mL). The second required higher than expected intraprocedural autotransfusion (300 mL) without any hemodynamic compromise. Pleural effusion was negligible in both animals (10 and 20 mL).

There was no procedural mortality and all animals recovered uneventfully. At the end of the procedure, the pericardial and pleural spaces were aspirated to dryness, any remaining pleural CO_2 was aspirated, and the drains were withdrawn.

Table. Hemodynamics—MAP, HR, and Expired CO_2 in Swine (n=10) Undergoing Fully Percutaneous Transthoracic Left Atrial Access and Closure

Swine (n=10)	MAP, mm Hg	HR, bpm	Expired CO_2, mm Hg
Baseline	61 (53–74)	96 (77–102)	29 (27–32)
After lung deflation	57 (46–66)	88 (72–98)	28 (26–29)
After insertion of left atrial sheath	52 (45–64)	87 (69–97)	29 (27–31)
After closure	50 (47–59)	81 (67–91)	31 (29–33)
Follow-up	56 (48–72)	102 (84–113)	30 (30–33)

The 2 sheep were smaller animals with lower baseline blood pressure so were excluded from the analysis of hemodynamics. No differences retained statistical significance after correction for multiplicity. Data are presented as median (Q1–Q3). HR indicates heart rate; and MAP, mean arterial blood pressure.

Follow-Up

No complications were observed during the follow-up period of 7.5 days (7–8.5 days). Follow-up MRI confirmed stable position of the LA occluder device in all animals. Twelve of 12 animals had no pleural effusion. Eleven of 12 animals had no detectable or trace pericardial effusion 0 mL (0–6 mL). One pig, in which the LA was punctured twice, had a large but hemodynamically insignificant pericardial effusion (660 mL) at 7 days follow-up. No other complications were observed in any animal and all skin incisions healed well. On necropsy, the nitinol cardiac occluder device was well seated and fibrosed to the LA wall in all animals (data not shown).

Human CT Analysis

Cardiac CT angiograms from 10 patients (age 68years [59–73 years], 8/10 male) with full chest wall coverage were examined. A direct trajectory to the LA through the right posterior chest wall was achievable in all (Figure 5; Movie III in the Data Supplement). The right lung would need to be displaced by pleural insufflation, but the trajectory avoided important structures, including descending aorta and esophagus. The mean angle α between the achievable trajectory and the true long axis of the LV was 5° (4°–7°). Mean intercostal distance at the point of entry through the chest wall was 12 mm (11–15 mm).

We also tested whether there was a trajectory to the mitral valve from a right minithoracotomy incision, entering the right atrium, and passing through the interatrial septum. In all 10 patients this was achievable, but the offset angle between the trajectory and the true long axis of the LV was 56° (51°–58°).

Human Cadaver Study

In the prone position, right pleural insufflation and deflation of the right lung were straightforward whether under MR or x-ray guidance. This exposed a direct trajectory to the posterior wall of the LA avoiding other important structures, such as aorta and esophagus, in all 3 cadavers. The LA was successfully entered and a large 26F sheath was delivered. Pleural insufflation did not cause the heart to shift orientation within the thorax. As a result, the sheath trajectory remained well aligned with the long axis of the LV. The LA port was closed using a nitinol cardiac occluder device, and the right lung was reinflated by aspirating the pleural CO_2 (Figure 6; Movie IV in the Data Supplement).

Discussion

We describe a novel percutaneous technique to access the left heart to deliver interventional devices. The technique combines several innovations: (1) fully percutaneous transthoracic LA access with a needle followed by a large sheath; (2) pericardial autotransfusion catheter placement; (3) pleural

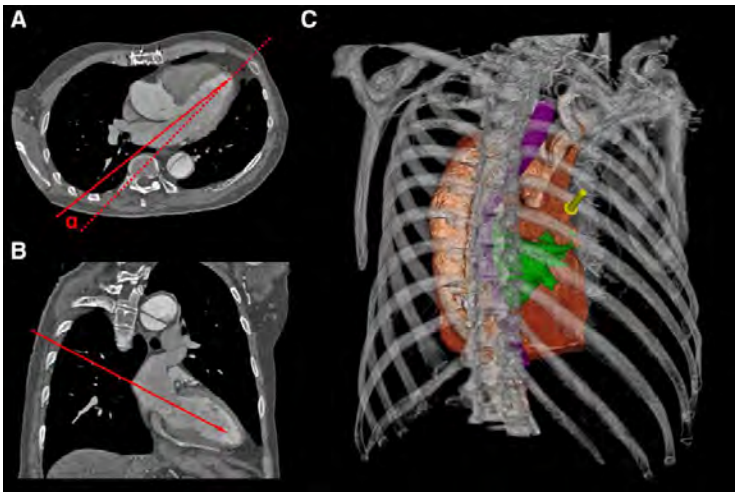

Figure 5. Human cardiac computed tomography (CT) angiography analysis. Axial (**A**) and sagittal (**B**) CT cross-sections showing simulated trajectory to the left atrium (LA; red line). The angle α represents the offset between the simulated trajectory and the true long axis of the left ventricle. **C**, Three-dimensional reconstruction showing skin entry point (yellow arrow). The LA is highlighted in green and the esophagus in purple.

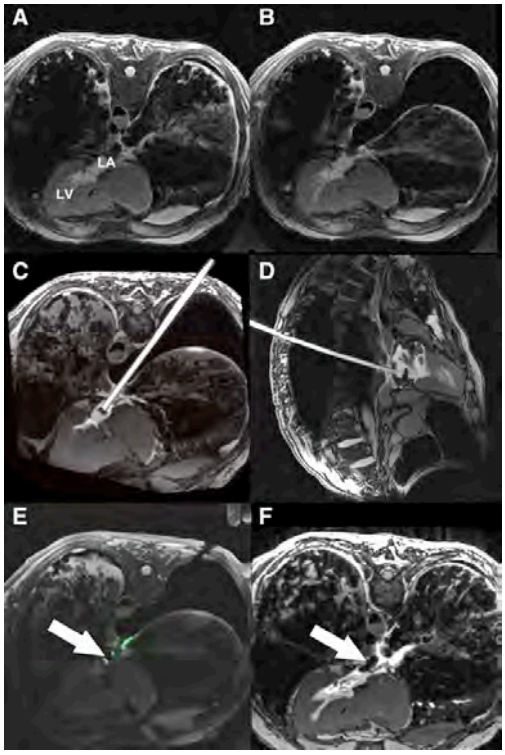

Figure 6. Real-time magnetic resonance imaging (MRI)–guided left atrial (LA) access and closure in a human cadaver. **A**, Axial MRI before lung deflation. **B**, MRI in the same plane after right lung deflation. An unobstructed trajectory to the LA is apparent. **C**, Axial MRI of large sheath filled with gadolinium contrast in the LA. **D**, Sagittal MRI of sheath in the LA. **E**, Deployment of a nitinol cardiac occluder device (arrow). The delivery cable incorporates MRI electronics to enhance device visualization. **F**, After lung reinflation, the device can be clearly seen across the posterior wall of the LA (arrow).

insufflation and lung displacement to create an unobstructed trajectory to the LA; and (4) closure of the LA port using off-the-shelf nitinol cardiac occluder devices. We demonstrated preclinical feasibility in 2 large animal models (porcine and ovine) and feasibility of clinical translation through performing the procedure in human cadavers and simulating on human cardiac CT images. Real-time MRI provided optimum usability, for example, continuous depiction of the deflated lung, but x-ray fluoroscopy assisted by C-arm CT provided adequate confirmation of lung displacement during sheath traversal of the pleural space for LA entry.

Pleural Insufflation to Create Unobstructed Trajectory to LA

Thoracoscopy to inspect the pleura, perform biopsy, or deliver therapy is an established technique usually performed under moderate sedation.[27] More advanced procedures, for example, lobectomy or management of spontaneous pneumothorax, are typically performed under general anesthesia with dual-lumen endotracheal tube to facilitate single lung ventilation and have excellent perioperative outcomes.[21,28,29] However, there is evidence that such interventions can be well tolerated in conscious nonintubated patients[30] even for long procedures and in older sicker patients.[31] Based on this extensive clinical experience, there is reason to expect that single lung deflation for the purpose of transthoracic LA access may be tolerated in patients.

Choice of Imaging Modality to Guide LA Access

The superior soft tissue visualization and multiplanar viewing capabilities of MRI are appealing to guide minimally invasive interventions, particularly interventions that violate vascular boundaries, in which every anatomic structure traversed must be visualized. MRI provides this capability. In this study, we demonstrated that LA access and closure could be safely performed using real-time MRI guidance. MRI also permitted easy access to the pleural space and titration of pleural insufflation to displace lung. Crucially, MRI afforded continuous monitoring for development of pericardial and pleural effusions during LA puncture and closure. Any accumulation of blood in the pericardial or pleural space was immediately identified and autotransfused.

Nonetheless, we explored whether the procedure could be performed using x-ray fluoroscopy. A transseptal pigtail catheter was positioned in the LA. Biplane contrast angiography and intrapericardial iodinated contrast delineated LA anatomy adequately. This enabled a trajectory to the LA to be planned in orthogonal x-ray projections. It was difficult to definitely establish adequate lung displacement using fluoroscopy only, but C-arm CT provided clear visualization of lung tissue and assurance of satisfactory lung displacement. In humans, where the preferred LA puncture site should be posterior and midway between left and right pulmonary vein ostia, dual transseptal guidewires in left and right pulmonary veins could offer a precise fluoroscopic target for LA puncture. Echocardiography could provide a substitute for real-time MRI to monitor for pericardial blood accumulation and guide autotransfusion.

We also explored using color overlays of the LA and LV, segmented from contrast-enhanced C-arm CT using software designed to guide electrophysiology procedures. The fusion images enhanced our ability to predict trajectories and determine optimal LA puncture location (Figure 4). In addition, the overlays aided in selecting optimal x-ray projection angles and may have reduced overall iodinated contrast usage.

Closure of LA Port

There is clinical precedent for the use of off-label nitinol cardiac occluder devices to seal large holes in vascular structures, including the LV apex or abdominal aorta.[13,32] Even in the high-pressure LV, hemostasis was rapidly achieved with reversal of anticoagulation. Hemostasis should be easier to achieve in the LA because the pressure is much lower than in the LV or systemic arteries, even in patients with mitral valve disease. In some animals, blood did accumulate in the pericardial or pleural space, but was easily managed by aspiration and autotransfusion, akin to standard surgical blood salvage technique. After aspirating to dryness, all drains were removed post procedure for animal comfort—although in humans they would be left in overnight. Only 1 large but hemodynamically insignificant pericardial effusion was observed at follow-up, in the 1 animal in which 2 LA punctures were made because a custom needle

had become dull. The animal recovered uneventfully and the effusion would not have accumulated had the pericardial drain remained in place post procedure.

Feasibility of Clinical Translation

We tested LA access and closure in 2 large animal models to determine whether the approach was feasible in different anatomies. The trajectories for unobstructed access to the LA were different in the 2 species but easily achievable by deflating the left lung. Importantly, all animals were hemodynamically stable with a large sheath in the LA. This approach could circumvent many of the risks associated with transapical access in patients with advanced mitral valve disease, in particular, acute hemodynamic instability and late LV pseudoaneurysm, ventricular arrhythmias, and decrement in LV function.

Human cardiac CT angiogram analysis confirmed that a theoretical trajectory exists in humans. In swine, pleural insufflation rotated the heart in the thorax, which resulted in an offset between the long axis of the heart and the achieved trajectory (Figure 3). Because the orientation of the heart in the human mediastinum is different, the trajectory is different from that in swine or sheep. In humans, the right lung would be deflated to puncture the LA posteriorly between the pulmonary veins (Figure 5). In this configuration, right lung deflation would deflect the right pulmonary veins away from the needle trajectory, exposing the posterior wall of the LA. This trajectory avoids other important structures, such as the aorta and esophagus. The mean intercostal distance at the point of entry through the chest wall was sufficient to accommodate a sheath 32F or larger.

To demonstrate that this trajectory was feasible, we accessed the LA in human cadavers and delivered a large sheath under either MRI or x-ray guidance (Figure 6). Pleural insufflation did not shift the orientation of the heart within the thorax in cadavers. We then closed the LA port with a nitinol cardiac occluder device and re-expanded the right lung.

Limitations

There are anatomic differences between humans and swine. For example, the descending aorta and esophagus vary in position within the thorax. Procedural tomography (such as C-arm CT and real-time MRI) is therefore recommended for trajectory planning. Pulmonary disease or chronic heart failure could increase the risk of single lung ventilation. Clotting disorders could increase bleeding. Off-label nitinol cardiac occluder devices may not assure hemostasis. Prior cardiothoracic surgery may cause pleural adhesions, which could impede lung displacement. Because our technique involves 2 points of fixation (chest wall and LA wall), sheath maneuverability is constrained. However, because excellent alignment with the LV long axis can be achieved by careful trajectory planning, we do not anticipate that excessive sheath manipulation would be required to achieve coaxial alignment to perform a mitral valve intervention.

Technical Considerations for Clinical Translation

To perform this procedure in patients under x-ray fluoroscopy guidance, we envision the following provisions: (1) The procedure would be performed under general anesthesia with a dual lumen endotracheal tube and bronchial blockers to facilitate intentional right lung collapse and single lung ventilation. (2) The patient would be positioned initially supine for standard percutaneous access and then rolled prone for transthoracic atrial access. (3) A temperature or transesophageal echocardiography probe would be used to identify the esophagus. (4) A pericardial drain may not be required in patients with prior sternotomy and pericardial adhesions. (5) Respiration would be suspended during LA puncture. (6) The guidewire would be advanced through the mitral valve into the LV over a balloon catheter to prevent chordal entrapment. (7) Anticoagulation would be reversed with protamine immediately before cardiac occluder device deployment. (8) A coaxial buddy wire would be used during LA port closure to allow LA access to be reestablished rapidly in case of inadvertent pull through of the nitinol cardiac occluder device. (9) Pleural and pericardial drains would be left in place for a short period after the procedure to drain any effusions.

Conclusions

Fully percutaneous transthoracic LA access is feasible to deliver large interventional devices to the mitral valve without violating the LV myocardium. The procedure can be guided by a variety of imaging modalities, although in our experience MRI guidance offers the greatest visualization of anatomic structures with the ability to monitor and address complications in real-time, for example, pericardial effusion. Clinical translation seems feasible based on human cardiac CT analysis and human cadaver testing. This technique could provide a direct and coaxial access route for transcatheter mitral valve interventions in the future.

Acknowledgments

We thank Katherine Lucas, Shawn Kozlov, and Joni Taylor for their help with animals, and Gaetano Paone and Adam Greenbaum of Henry Ford Hospital for their thoughtful comments.

Sources of Funding

This work was supported by the Division of Intramural Research, National Heart Lung and Blood Institute, National Institutes of Health (Z01-HL005062 and Z01-HL006040).

Disclosures

None.

References

1. Seiffert M, Conradi L, Baldus S, Schirmer J, Knap M, Blankenberg S, Reichenspurner H, Treede H. Transcatheter mitral valve-in-valve implantation in patients with degenerated bioprostheses. *JACC Cardiovasc Interv*. 2012;5:341–349. doi: 10.1016/j.jcin.2011.12.008.
2. Descoutures F, Himbert D, Maisano F, Casselman F, de Weger A, Bodea O, Van der Kley F, Colombo A, Giannini C, Rein KA, De Bruyne B, Petronio AS, Dahle G, Alfieri O, Vahanian A. Transcatheter valve-in-ring implantation after failure of surgical mitral repair. *Eur J Cardiothorac Surg*. 2013;44:e8–e15. doi: 10.1093/ejcts/ezt155.
3. De Backer O, Piazza N, Banai S, Lutter G, Maisano F, Herrmann HC, Franzen OW, Søndergaard L. Percutaneous transcatheter mitral valve replacement: an overview of devices in preclinical and early clinical evaluation. *Circ Cardiovasc Interv*. 2014;7:400–409. doi: 10.1161/CIRCINTERVENTIONS.114.001607.
4. Cheung A, Stub D, Moss R, Boone RH, Leipsic J, Verheye S, Banai S, Webb J. Transcatheter mitral valve implantation with Tiara

bioprosthesis. *EuroIntervention*. 2014;10(suppl U):U115–U119. doi: 10.4244/EIJV10SUA17.
5. Bapat V, Buellesfeld L, Peterson MD, Hancock J, Reineke D, Buller C, Carrel T, Praz F, Rajani R, Fam N, Kim H, Redwood S, Young C, Munns C, Windecker S, Thomas M. Transcatheter mitral valve implantation (TMVI) using the Edwards FORTIS device. *EuroIntervention*. 2014;10 (suppl U):U120–U128. doi: 10.4244/EIJV10SUA18.
6. Mack MJ, Brennan JM, Brindis R, Carroll J, Edwards F, Grover F, Shahian D, Tuzcu EM, Peterson ED, Rumsfeld JS, Hewitt K, Shewan C, Michaels J, Christensen B, Christian A, O'Brien S, Holmes D; STS/ACC TVT Registry. Outcomes following transcatheter aortic valve replacement in the United States. *JAMA*. 2013;310:2069–2077. doi: 10.1001/jama.2013.282043.
7. Schymik G, Würth A, Bramlage P, Herbinger T, Heimeshoff M, Pilz L, Schymik JS, Wondraschek R, Süselbeck T, Gerhardus J, Luik A, Gonska BD, Posival H, Schmitt C, Schröfel H. Long-term results of transapical versus transfemoral TAVI in a real world population of 1000 patients with severe symptomatic aortic stenosis. *Circ Cardiovasc Interv*. 2015;8: e000761. doi: 10.1161/CIRCINTERVENTIONS.113.000761.
8. Greason KL, Suri RM, Nkomo VT, Rihal CS, Holmes DR, Mathew V. Beyond the learning curve: transapical versus transfemoral transcatheter aortic valve replacement in the treatment of severe aortic valve stenosis. *J Card Surg*. 2014;29:303–307. doi: 10.1111/jocs.12323.
9. Meyer CG, Frick M, Lotfi S, Altiok E, Koos R, Kirschfink A, Lehrke M, Autschbach R, Hoffmann R. Regional left ventricular function after transapical vs. transfemoral transcatheter aortic valve implantation analysed by cardiac magnetic resonance feature tracking. *Eur Heart J Cardiovasc Imaging*. 2014;15:1168–1176. doi: 10.1093/ehjci/jeu103.
10. Forsberg LM, Tamás É, Vánky F, Engvall J, Nylander E. Differences in recovery of left and right ventricular function following aortic valve interventions: a longitudinal echocardiographic study in patients undergoing surgical, transapical or transfemoral aortic valve implantation. *Catheter Cardiovasc Interv*. 2013;82:1004–1014. doi: 10.1002/ccd.24812.
11. Barbash IM, Dvir D, Ben-Dor I, Corso PJ, Goldstein SA, Wang Z, Bond E, Okubagzi PG, Satler LF, Pichard AD, Waksman R. Impact of transapical aortic valve replacement on apical wall motion. *J Am Soc Echocardiogr*. 2013;26:255–260. doi: 10.1016/j.echo.2012.11.003.
12. Reynolds MR, Magnuson EA, Wang K, Thourani VH, Williams M, Zajarias A, Rihal CS, Brown DL, Smith CR, Leon MB, Cohen DJ; PARTNER Trial Investigators. Health-related quality of life after transcatheter or surgical aortic valve replacement in high-risk patients with severe aortic stenosis: results from the PARTNER (Placement of AoRTic TraNscathetER Valve) Trial (Cohort A). *J Am Coll Cardiol*. 2012;60:548–558. doi: 10.1016/j.jacc.2012.03.075.
13. Jelnin V, Dudiy Y, Einhorn BN, Kronzon I, Cohen HA, Ruiz CE. Clinical experience with percutaneous left ventricular transapical access for interventions in structural heart defects a safe access and secure exit. *JACC Cardiovasc Interv*. 2011;4:868–874. doi: 10.1016/j.jcin.2011.05.018.
14. Dudiy Y, Kliger C, Jelnin V, Elisabeth A, Kronzon I, Ruiz CE. Percutaneous transapical access: current status. *EuroIntervention*. 2014;10 (suppl U):U84–U89. doi: 10.4244/EIJV10SUA12.
15. Bruschi G, Barosi A, Colombo P, Botta L, Oreglia J, De Marco F, Paino R, Klugmann S, Martinelli L. Direct transatrial transcatheter SAPIEN valve implantation through right minithoracotomy in a degenerated mitral bioprosthetic valve. *Ann Thorac Surg*. 2012;93:1708–1710. doi: 10.1016/j.athoracsur.2011.08.084.
16. Schaefer U, Frerker C, Busse C, Kuck KH. Transjugular and transseptal treatment of a degenerated mitral valve prosthesis with a balloon-expandable biological valve. *Heart Lung Circ*. 2012;21:836–840. doi: 10.1016/j.hlc.2012.03.125.
17. Kaneko T, Swain JD, Loberman D, Welt FG, Davidson MJ, Eisenhauer AC. Transjugular approach in valve-in-valve transcatheter mitral valve replacement: direct route to the valve. *Ann Thorac Surg*. 2014;97:e161–e163. doi: 10.1016/j.athoracsur.2014.01.068.
18. Schaefer U, Frerker C, Schewel D, Thielsen T, Meincke F, Kreidel F, Kuck KH. Transfemoral and transseptal valve-in-valve implantation into a failing mitral xenograft with a balloon-expandable biological valve. *Ann Thorac Surg*. 2012;94:2115–2118. doi: 10.1016/j.athoracsur.2012.04.123.
19. Fisher DL. The use of pressure recordings obtained at transthoracic left heart catheterization in the diagnosis of valvular heart disease. *J Thorac Surg*. 1955;30:379–392.
20. Wood EH, Sutterer W, Swan HJ, Helmholz HF Jr. The technic and special instrumentation problems associated with catheterization of the left side of the heart. *Proc Staff Meet Mayo Clin*. 1956;31:108–115.
21. Naunheim KS, Mack MJ, Hazelrigg SR, Ferguson MK, Ferson PF, Boley TM, Landreneau RJ. Safety and efficacy of video-assisted thoracic surgical techniques for the treatment of spontaneous pneumothorax. *J Thorac Cardiovasc Surg*. 1995;109:1198–1203, discussion 1203.
22. Rahman NM, Ali NJ, Brown G, Chapman SJ, Davies RJ, Downer NJ, Gleeson FV, Howes TQ, Treasure T, Singh S, Phillips GD. Local anaesthetic thoracoscopy: British Thoracic Society Pleural Disease Guideline 2010. *Thorax*. 2010;65(suppl 2):ii54–ii60. doi: 10.1136/thx.2010.137018.
23. Maher KO, Murdison KA, Norwood WI Jr, Murphy JD. Transthoracic access for cardiac catheterization. *Catheter Cardiovasc Interv*. 2004;63:72–77. doi: 10.1002/ccd.20080.
24. Cheatham JP, McCowan TC, Fletcher SE. Percutaneous translumbar cardiac catheterization and central venous line insertion: an alternative approach in children with congenital heart disease. *Catheter Cardiovasc Interv*. 1999;46:187–192. doi: 10.1002/(SICI)1522-726X(199902)46:2<187::AID-CCD14>3.0.CO;2-S.
25. Saikus CE, Ratnayaka K, Barbash IM, Colyer JH, Kocaturk O, Faranesh AZ, Lederman RJ. MRI-guided vascular access with an active visualization needle. *J Magn Reson Imaging*. 2011;34:1159–1166. doi: 10.1002/jmri.22715.
26. Rogers T, Ratnayaka K, Schenke WH, Faranesh AZ, Mazal JR, O'Neill WW, Greenbaum AB, Lederman RJ. Intentional right atrial exit for microcatheter infusion of pericardial carbon dioxide or iodinated contrast to facilitate sub-xiphoid access [published online ahead of print October 28, 2014]. *Catheter Cardiovasc Interv*. doi: 10.1002/ccd.25698.
27. Rivera MP, Mehta AC, Wahidi MM. Establishing the diagnosis of lung cancer: Diagnosis and management of lung cancer, 3rd ed: American College of Chest Physicians evidence-based clinical practice guidelines. *Chest*. 2013;143(5 suppl):e142S–e165S. doi: 10.1378/chest.12-2353.
28. Sedrakyan A, van der Meulen J, Lewsey J, Treasure T. Video assisted thoracic surgery for treatment of pneumothorax and lung resections: systematic review of randomised clinical trials. *BMJ*. 2004;329:1008. doi: 10.1136/bmj.38243.440486.55.
29. Yan TD, Black D, Bannon PG, McCaughan BC. Systematic review and meta-analysis of randomized and nonrandomized trials on safety and efficacy of video-assisted thoracic surgery lobectomy for early-stage non-small-cell lung cancer. *J Clin Oncol*. 2009;27:2553–2562. doi: 10.1200/JCO.2008.18.2733.
30. Wu CY, Chen JS, Lin YS, Tsai TM, Hung MH, Chan KC, Cheng YJ. Feasibility and safety of nonintubated thoracoscopic lobectomy for geriatric lung cancer patients. *Ann Thorac Surg*. 2013;95:405–411. doi: 10.1016/j.athoracsur.2012.10.082.
31. Chen KC, Cheng YJ, Hung MH, Tseng YD, Chen JS. Nonintubated thoracoscopic lung resection: a 3-year experience with 285 cases in a single institution. *J Thorac Dis*. 2012;4:347–351. doi: 10.3978/j.issn.2072-1439.2012.08.07.
32. Greenbaum AB, O'Neill WW, Paone G, Guerrero ME, Wyman JF, Cooper RL, Lederman RJ. Caval-aortic access to allow transcatheter aortic valve replacement in otherwise ineligible patients: initial human experience. *J Am Coll Cardiol*. 2014;63(25 pt A):2795–2804. doi: 10.1016/j.jacc.2014.04.015.

5.5 Supplemental materials

5.5.1 MR imaging parameters

Steady-state free precession (SSFP) imaging followed usual parameters: repetition time (TR)/echo time (TE) 2.9/1.2ms; flip angle 57°; bandwidth 930Hz/pixel; field of view (FOV) 340x340mm; matrix 256x256pixels; slice thickness 6mm. Three-dimensional radial SSFP non-contrast whole heart parameters were TR/TE 3.1/1.56ms; flip angle 115°; bandwidth, 898Hz/pixel; FOV 220x220mm; voxel size 1.1x1.1x1.1mm; base resolution 192; radial views 12360. Real-time imaging used SSFP (TR/TE 2.9/1.4ms; flip angle 45°; bandwidth 1000Hz/pixel; matrix 192x108; FOV 300x300mm; GRAPPA Factor 2-4) or gradient echo (TR/TE 4.2/1.9ms; flip angle 15°; bandwidth 500Hz/pixel; matrix 192x144; FOV 300x300mm; GRAPPA Factor 2-4).

To assess for and quantify volume of pericardial effusion, contiguous true axial slices were acquired using a steady-state free precession (SSFP) sequence with breath hold and ECG gating. Slices were prescribed to include cardiac anatomy from base to apex to ensure coverage of the entirety of the pericardial space. Acquisition parameters were: repetition time (TR)/echo time (TE), 2.96/1.25msec; number of averages 2; acceleration factor (GRAPPA) 2; flip angle 80°; bandwidth 1157Hz/pixel; field of view 300x300mm; matrix 240x128 pixels; slice thickness 6mm; and slice distance 0mm. Pericardial and cardiac contours were drawn manually on each slice and the pericardial effusion volume was calculated by subtracting the total cardiac volume from the total pericardial volume using *Syngo Argus* MR analysis software (Siemens).

5.5.2 Interventional devices used in MR

We used a custom needle and closure device delivery cable, each incorporating a loop antenna for active visualization. This enables the devices to appear highlighted in colour in the real-time MR images. To visualize the 18Fr sheath in MR, a passive marker containing iron oxide particles was added to the tip, which appears as a dark artefact on the real-time MR images.

5.5.3 DynaCT imaging parameters

ECG triggered with breath hold, 4 sweeps with 5 second scan time/sweep, 90 kV, 0.80 degrees/frame, total of 4 sweeps.

Chapter 6. Transcatheter myocardial needle chemoablation under realtime MRI guidance

6.1 Introduction

Radiofrequency ablation for rhythm disorders is limited by the inability to instantaneously visualize and monitor ablation lesions, and by the mismatch between immediate injury and irreversible conduction block[151]. Magnetic resonance imaging (MRI) thermometry has shown potential for monitoring the effect of radiofrequency energy but only approximates the extent of irreversible lesions [152]. Late gadolinium enhancement MRI (LGE) correlates with histological lesion volume [153] but can only be performed once per procedure and is not a surrogate for real-time lesion monitoring during ablation. Furthermore, scar size by LGE several months post-ablation is up to 50% smaller than that measured acutely immediately post-ablation [154]. This could be explained by lesion contraction during fibrotic healing and by enhancement with LGE of both radiofrequency energy induced oedematous penumbra and the true necrotic core.

Radiofrequency ablation for ventricular tachycardia (VT) is further limited by the mismatch between thickness of left ventricular (LV) myocardium and shallowness of radiofrequency lesions[155]. Critical peri-infarct substrate can be deep within the myocardium and difficult to ablate via endocardial or epicardial approaches[156]. Failure to achieve permanent transmural tissue destruction is a common cause of therapeutic failure. MRI tissue characterization techniques can identify pathologic rhythm substrate tissues such as a critical re-entrant isthmus or a peri-infarct slow-conduction heterogeneous zone[157]. Areas of scar tissue by LGE have in animals shown close similarity to electroanatomic voltage maps[93]. Trans-catheter MRI guided radiofrequency ablation of atrial tissue has been reported in early human studies[123].

Chemoablation is already used for trans-coronary interventricular septal ablation in patients with hypertrophic cardiomyopathy [158], in the viscera for tumour ablation[159], and through the vein of Marshall for atrial fibrillation[160]. Caustic agents such as ethanol or acetic acid cause early coagulative necrosis, followed by late fibrosis and scarring [161]. These agents are considered safe, because if small quantities reach the blood pool they are immediately diluted down to a harmless concentration. Transarterial [162, 163] or retrograde transvenous [164] chemoablation may allow deeper endocardial lesion creation compared with radiofrequency

ablation, but are constrained by the myocardial territories incidentally subtended by the injected vessels and may lead to the destruction of excess tissue. Chemoablation for ventricular arrhythmias by direct endomyocardial injection may overcome these anatomic constraints and may allow more targeted tissue ablation. Pre-clinical feasibility of fluoroscopic or intracardiac echocardiography guided subendocardial ablation with ethanol has been demonstrated [165], although we are not aware of acetic acid chemoablation in the heart. These techniques remain limited because they do not allow differentiation of target tissues or real-time lesion monitoring.

We hypothesized that real-time MRI would enable substrate-guided myocardial chemoablation. We propose to use MRI to instantaneously visualize arrhythmia substrate and ablative agents doped with gadolinium-based contrast agents. In this report we demonstrate for the first time (1) feasibility of real-time MRI guided myocardial chemoablation in swine; (2) MRI characteristics, macroscopic appearance and histopathology of acute and chronic chemoablation lesions; (3) superior circumscription of myocardial acetic acid chemoablation lesions compared with ethanol lesions; and (4) anatomical and electrical interruption of a conductive isthmus in an animal model of ischemic cardiomyopathy.

6.2 Candidate's contribution

I created the animal model if ischaemic cardiomyopathy and performed all MRI-guided chemoablation experiments. Except for the first animal, I personally performed all subsequent endocardial and epicardial mapping experiments. I received assistance from St Jude Medical to analyse the electroanatomic maps but I collected all other data. I assisted with all necropsy, histological specimen collection and preparation, and participated in all histology review sessions. I drafted the manuscript and prepared the figures, tables and supplementary materials.

6.3 Methods

The institutional animal care and use committee approved all procedures, which were performed according to contemporary NIH guidelines. 18 Yorkshire swine with mean bodyweight 54(46-57)kg were anesthetized with mechanical ventilation. Chemoablation experiments were performed in a clinical MRI catheterization suite, equipped with sound-suppression communication headsets and with LCD projectors to display hemodynamics and real-time MRI images at the bedside (Figure 6-1)[15]. Electroanatomic mapping was performed

under X-ray guidance.

6.3.1 Evaluation of chemoablation agents

Gadolinium-based contrast agents can release free gadolinium (Gd^{3+}) in solutions with low pH. We therefore tested whether 50% acetic acid (pH 1.9) caused release of free gadolinium from three different commercially available gadolinium-based contrast agents (gadopentetate dimeglumine, Magnevist, *Bayer Healthcare*; gadofosveset trisodium, Ablavar, *Lantheus Medical Imaging*; and gadoterate meglumine, Dotarem, *Guerbet*).

The amount of Gd^{3+} was quantified using Arsenazo III, which binds to gadolinium ions to form a complex that can be quantified with a colorimetric assay[166]. The amount of free gadolinium was quantified by using Arsenazo III. Arsenazo III binds to gadolinium ions to form a complex, which can be quantified with a colorimetric assay. Standards at concentrations of 0 – 50 µg/ml Gd^{3+} were prepared with gadolinium (III) chloride hexahydrate (Alfa Aesar) prepared in 50% acetic acid (Mallinckrodt Baker). An ultraviolet-visible spectrophotometer (Shimadzu) was used to read absorbance values at 652 nm to form a linear calibration curve. Samples of MRI contrast agents (Magnevist 500mM Gd, Ablavar 250mM Gd, and Dotarem 500mM Gd) were prepared in 50% acetic acid (pH 1.9) at concentrations of 2% and 5% Gd^{3+}, and samples were incubated for 15 minutes before absorbance values at 652 nm were recorded. For Dotarem, values were also recorded after 30 minutes and 60 minutes of incubation time.

We characterized ethanol or acetic acid chemoablation lesions in experiments in 8 naïve swine. 4 animals were euthanized immediately and 4 were survived for at least 7 days. 70% ethanol and 50% acetic acid were doped with gadolinium-based contrast agent for MRI conspicuity (2% gadolinium by total volume). Pure ethanol was pre-diluted to 70% with sterile water because in higher concentrations gadopentetate can precipitate. 50% acetic acid is the optimal concentration for solid organ tumour ablation [167]. Small aliquots (0.1-0.6mL) of these two solutions were injected into the LV myocardium under real-time MRI guidance. Venous blood was collected before and immediately after chemoablation with acetic acid to assess for any effect on systemic pH and anion gap.

6.3.2 MRI guided chemoablation

Injections into the LV myocardium were delivered using a MRI-conditional deflectable sheath (*Imricor* and *Innotom*) with a passive marker tip and a custom injection needle catheter incorporating electronics for active visualization. The needle catheter appeared in

colour on real-time MRI. The sheath was introduced to the LV cavity via transarterial retrograde approach over a Nitinol guidewire (*Nitrex*) under interactive real-time MRI guidance[168]. The needle was navigated to the target myocardium, positioned orthogonally to the endocardial surface (Figure 6-2) and deployed to a depth of 4mm. The chemoablation agent was injected slowly in aliquots of 0.1-0.6mL and the needle was withdrawn after 30sec. Chemoablation lesions appeared bright in real-time inversion-recovery MRI as the chemoablation agent doped with gadolinium contrast was injected.

6.3.3 MRI scanning parameters

Steady-state free precession (SSFP) cine imaging: Repetition time (TR)/echo time (TE) 3.1/1.3ms; flip angle 57°; bandwidth 930Hz/pixel; field of view (FOV) 300mmx300mm; matrix 256x256pixels; slice thickness 8mm.

Three-dimensional radial SSFP non-contrast whole heart: TR/TE 3.1/1.5ms; flip angle 115°; bandwidth, 898Hz/pixel; FOV 220x220mm; voxel size 1.1x1.1x1.1mm; base resolution 192; radial views 12360.

Realtime MRI: TR/TE 2.9/1.4ms; flip angle 45°; bandwidth 1000Hz/pixel; matrix 192x108; FOV 300x300mm; GRAPPA Factor 2-4) or gradient echo (TR/TE 4.2/1.9ms; flip angle 15°; bandwidth 500Hz/pixel; matrix 192x144; FOV 300x300mm; GRAPPA Factor 2-4. A real-time inversion recovery sequence could be toggled on to highlight gadolinium enhancement of injection sites, relative to normal myocardium and areas of prior infarction. A non-selective inversion pre-pulse was performed before every bSSFP image acquisition with an interactive inversion time (TI). The next inversion pulse immediately followed the image acquisition, with no additional time for signal recovery. Typical imaging parameters were TI 417ms, TR/TE 2.54/1.27ms, flip angle 45°, FOV 300mm, slice thickness 6 mm, matrix 128x128, GRAPPA factor 2 and frame rate 2 frames/second. The real-time MRI user interface (Interactive Front End, *Siemens*) enabled control of slice plane and thickness, and toggling between rapid imaging for catheter navigation and high contrast real-time inversion-recovery MRI during injection.

Ex-Vivo 3D Hi-Res Isotropic T1-W SPGR: TR/TE 10/5.4ms; flip angle 20°; bandwidth 210Hz/pixel; matrix 320x320; FOV 180x180mm; voxel size 0.6x0.6x0.6mm; slab thickness 72mm; 120 slices per slab.

LGE PSIR segmented FLASH 724: TR/TE 8.2/3.2ms; flip angle 25°; bandwidth 140Hz/pixel; matrix 256x144; FOV 360x270mm; slice thickness 8mm.

MRI post-processing and image analysis: Images were analysed using QMass MR (*Medis*). Acutely, infarct and lesion could be differentiated by relative signal intensity on phase sensitive inversions recovery LGE (3 and 10 standard deviations above mean respectively). Chronically, lesion signal intensity was similar to infarct (3 standard deviations above mean).

6.3.4 Animal model of ischemic cardiomyopathy

10 pigs were pre-treated with amiodarone, aspirin and heparin, and underwent X-ray guided left coronary artery branch balloon occlusion. Obtuse marginal and diagonal arteries were selected for ethanol infarction ensuring that at least one interposed branch (e.g. first diagonal, first obtuse marginal or ramus intermedius) remained intact to provide a simulated VT isthmus. 1-2mL of 70% ethanol / 30% iopamidol contrast was infused through the balloon guidewire lumen to create infarcts. No sustained arrhythmias were observed and there was no mortality from this procedure. Animals were survived for 12(8-15) days before MRI guided isthmus chemoablation.

6.3.5 Real-time MRI guided isthmus chemoablation

0.2mmol/kg gadopentetate dimeglumine (*Bayer Healthcare*) was administered intravenously to the ischemic cardiomyopathy animals. Real-time inversion-recovery MRI identified areas of infarction containing gadolinium contrast. Firstly, to test feasibility of targeted isthmus chemoablation under MRI guidance, we ablated the normal myocardium interposed between the infarcted regions in 5 animals.

In the other 5 animals, we performed pre-and post-chemoablation electroanatomic mapping of the LV endocardium ± epicardium using a commercial system and catheters under X-ray guidance (NavX and EnSite Velocity; duo-decapolar Livewire and FlexAbility, *St Jude Medical*). Pericardial access for epicardial mapping was obtained via right atrial appendage exit[169]. Isthmus chemoablation was performed under real-time MRI guidance.

6.3.6 Ex-vivo MRI and histology

After euthanasia hearts were explanted and suspended in agar for ex-vivo high-resolution MRI. Specimens were fixed in 10% formalin, then sectioned and stained with hematoxylin and eosin (H&E) and Masson trichrome stains.

6.3.7 Statistics

Data were analysed using SPSS (v19.0, IBM) and are described as mean ± standard deviation

if normally distributed, otherwise as median (first and third quartile). Acute and chronic lesion volumes were tested for correlation using Pearson's correlation coefficient. Anion gap and pH pre-and post-chemoablation were compared using a paired *t*-test. A p value <0.05 was considered significant.

6.4 Results

6.4.1 Chemoablation lesion histology

In the 8 naïve animals, ethanol lesions exhibited stellate geometry with patchy areas of viable myocardium histologically, whereas acetic acid lesions, exhibited greater homogeneity and more circumscribed borders (Figure 6-3). Acetic acid lesions were 46% larger than ethanol lesions for the same injection volume. Based on these findings, we elected to perform chronic experiments with acetic acid. Acute lesions with either agent had a macroscopic area of discoloration with a haemorrhagic centre. H&E of acute lesion revealed hypereosinophilia of affected myocardial fibres with mild to moderately pyknotic nuclei and indistinct cross striations, consistent with cellular destruction (Figure 6-2).

H&E of chronic lesions revealed typical features of fibrosis and replacement of normal myocardial architecture. Masson trichrome stain revealed a zone of fibroplasia and fibrosis with collagen stained blue, normal myocardial fibres stained red and necrotic myocardial fibres stained purple (Figure 6-2). Chronic acetic acid lesions were well circumscribed with distinct margins between lesion and normal myocardium.

6.4.2 Chemoablation lesion appearances by MRI

As gadolinium-doped chemoablation agent was injected into the myocardium, the evolving lesion was visualized in real-time using real-time inversion-recovery MRI (Figure 6-2). 12(7-17)days after chemoablation, lesions enhanced using LGE after systemic gadolinium contrast administration (Figure 6-2). Volume of acute acetic acid chemoablation lesions correlated with volume of chronic lesions on LGE (0.78±0.39mL vs. 0.75±0.34mL, r=0.71, n=34, p<0.001).

6.4.3 Ischemic cardiomyopathy isthmus chemoablation

All 10 animals developed cardiomyopathy (left ventricular end-diastolic volume index 136±17mL/m^2; end-systolic volume index 83±13mL/m^2; ejection fraction 39±5%). After systemic gadolinium contrast administration, infarcts were distinguishable from normal

myocardium by LGE or real-time inversion-recovery MRI. Successful transcatheter chemoablation of the isthmus between infarcts was defined as presence of a confluent chemoablation lesion spanning the gap between infarcts and was achieved in all 10 animals with 2-5 injections (Figure 6-1). We mapped LV endocardial ± epicardial voltages before and after MRI guided chemoablation in 5 of these animals. Voltage maps confirmed that a functional ablation line through the isthmus of normal myocardium was successfully created in all 5 animals (Figure 6-1 and Figure 6-4). Voltages over infarcts were low (0.5-1.5mV), but voltages over chemoablation lesions were even lower (<0.5mV) with clearly defined borders (Figure 6-5). Local abnormal voltage activities with fragmented slow conduction were abolished with chemoablation (Figure 6-6).

6.4.4 Safety considerations

Chemoablation did not cause any conduction system disease or tachyarrhythmias in the early post-ablation period. No intramyocardial hematoma, myocardial perforation or rupture, pericardial effusion or tamponade occurred. Linear gadolinium-based contrast agents (Magnevist and Ablavar) released free gadolinium in 50% acetic acid solution (pH 1.9) within minutes, but did not in 70% ethanol (pH 7). A macrocyclic gadolinium-based contrast agent (gadoterate) did not release any free gadolinium after 60mins incubation in 50% acetic acid (Table 6-1). Chemoablation with acetic acid did not alter serum pH (pre- vs. post-procedure, 7.52 vs. 7.57, p=0.34) or anion gap (15.8 vs. 15.1, p=24; normal range in swine 10-25mEq/L).

6.5 Discussion

In this study, we demonstrate for the first time feasibility of real-time MRI guided transcatheter myocardial chemoablation. We show that gadolinium doping of chemoablative agents provides immediate visualization of lesion extent and continuity. Chemoablation lesions correlate with irreversible myocardial injury as evidenced by chronic LGE and histological tissue necrosis. Acetic acid creates homogeneous and well-circumscribed lesions compared with ethanol. In an animal model of ischemic cardiomyopathy we demonstrate successful substrate-guided chemoablation of a conductive isthmus between two infarcts, with functional ablation confirmed by endocardial and epicardial voltage mapping, and abolition of local abnormal voltage activities in areas of heterogeneous scar.

6.5.1 Substrate-guided ablation

Conventional electroanatomic mapping relies on surface voltage and activation maps to locate arrhythmia substrate, which can be challenging in the thick-walled LV. In contrast, LGE could afford direct visualization of culprit diseased myocardium for targeted anatomic substrate-guided ablation. Areas of LGE correspond with areas of low endocardial voltage in patients with ischemic cardiomyopathy[170]. Heterogeneous zones, which are a complex mixture of scar and viable myocardium, exhibit abnormal potentials more frequently than dense scar or normal myocardium[171], and commonly represent the arrhythmic substrate in patients with scar-related VT[157]. MRI-based computational simulation with identification of heterogeneous zones can accurately determine ablation targets[172] and may be used to predict the risk of VT for an individual patient[173]. These may enable entirely substrate-guided ablation in the future. MRI guided chemoablation could also be used to ablate different structures, for example the interventricular septum in patients with LV outflow tract obstruction.

6.5.2 Endocardial vs. epicardial ablation

Endocardial radiofrequency ablation fails to eliminate LV epicardial arrhythmia substrate in many patients [174]. Consequently, epicardial ablation is often required. Sub-xiphoid access to the naïve pericardium and epicardial ablation cause serious complications, including tamponade, abdominal haemorrhage and coronary artery occlusion in over 5% of patients [139]. Pericardial adhesions and epicardial fat can prevent effective ablation or mislead the operator to believe that effective ablation has been achieved [175]. In contrast, transcatheter needle chemoablation achieves full-thickness ablation from the endocardial surface, avoiding the need for epicardial access. Needle catheters have also been used to deliver radiofrequency energy deeper into the myocardium[176].

Chemoablation is not dependent on catheter tip contact force, and is not subject to steam pop and coagulum embolization, though these problems appear less common with modern irrigated radiofrequency ablation catheters. Chemoablation is unlikely to be subject to the phenomenon of reversible conduction block after radiofrequency ablation, because it does not appear to cause an oedematous penumbra.

6.5.3 Choice of chemoablation agent

Bioenzymatic myocardial ablation through topical epicardial application of a cellulose sponge soaked in collagenase to homogenize patchy scar tissue has been described, but the

result is not instantaneous and it is not clear whether transmural penetration of the enzyme is achievable[177]. We tested ethanol and acetic acid, the two most commonly used agents for tumour chemoablation in other organs. Based on our bench top and pre-clinical experiments, we favoured acetic acid for the following reasons: (1) it has been used safely in humans; (2) it achieved tissue necrosis with smaller injectate volumes compared with ethanol, reducing the risk of extravasation; (3) lesions within the myocardium were more homogenous, well-circumscribed and without patchy areas of viable tissue, an observation that corroborates prior reports using ethanol in the heart[165] and other organs [178]; and (4) we did not observe a change in serum pH or anion gap with acetic acid in swine. We confirmed in a bench top assay that a macrocyclic gadolinium-based contrast agent does not release free gadolinium after 60mins incubation in 50% acetic acid, whereas a linear agent does within minutes. Based on the dissociation half-lives ($T_{1/2}$) at low pH of the available macrocyclic contrast agents[179], we recommend gadoterate ($T_{1/2}$ 26.4hrs at pH 1) be the contrast of choice for chemoablation using acetic acid.

6.5.4 Realtime MRI guided catheter navigation

Co-registration of previously acquired computed tomography or MRI three-dimensional volumes and/or electroanatomic maps can be used to enhance catheter positioning. But co-registration is subject to errors from respiration and cardiac motion, does not permit real-time monitoring of lesions, and cannot accommodate for geometric changes imparted by catheters and guidewires.

For device visualization in MRI, we relied on passive markers on the deflectable sheath and active visualization of the needle catheter to navigate and target chemoablation. Using real-time MRI, needle position was confirmed on orthogonal short and long axis planes through the LV. Future integration of needle catheters with MRI-conditional electroanatomic mapping systems that track catheter position may simplify this task.

6.5.5 Chemoablation lesion imaging

Correlation between lesion volumes by MRI and macroscopic volumes of injury has been evaluated for radiofrequency catheter [153]. LGE best approximates macroscopic volumes of injury, but T2-weighted MRI overestimates and underestimates acute and chronic lesion volumes respectively. Although LGE may enable identification of radiofrequency lesions, it can only be performed once per procedure due to limitations in total gadolinium dose and cannot distinguish between true necrotic core and oedematous penumbra. Insufficient or

incomplete radiofrequency ablation likely explains current high recurrence rates after VT ablation.

Small volumes of solution containing gadolinium injected into the myocardium using needle catheters can be visualized in real-time. In this study, the volume of lesions immediately post-ablation correlated with the volume of LGE chronically. Extent of LGE correlates closely with volume of necrosis[180]. Chemoablation lesions that enhance on LGE imaging correspond to areas of myocardial necrosis and fibrosis histologically. Radiofrequency lesion size can shrink by up to 50% chronically compared to immediately post-ablation[154]. This phenomenon is likely caused by the reversible radiofrequency-induced oedematous penumbra around the true necrotic core. We did not observe this phenomenon with acetic acid lesions.

6.5.6 Isthmus ablation

Clinical usefulness of this technique depends on the ability to target specific tissues that can support VT. We demonstrate that real-time MRI permits precise targeting of chemoablation in an animal model of ischemic cardiomyopathy with an isthmus of normal myocardium between two areas of infarction. We demonstrate the ability to create chemoablation lesions confluent with the two infarcts, resulting in electroanatomic mapping confirmed disruption of the conductive isthmus.

6.5.7 Limitations

This was a preclinical feasibility study and we did not perform a head-to-head comparison of chemo versus radiofrequency ablation. However, the limitations of radiofrequency ablation in the thick-walled LV are well recognized. Despite the advent of irrigation-tip catheters to enable longer ablations, needle-tip electrodes to facilitate deeper delivery of radiofrequency energy[176] or contact force-sensing catheters to improve delivery of radiofrequency energy to the myocardium[181], procedural success rates remain low – almost certainly due to incomplete ablation. Porcine models of hemodynamically stable VT are difficult to create and for this reason we did not test ability of chemoablation to terminate arrhythmia. However, chemoablation did abolish late and fractionated electrograms within and around infarcted areas suggesting that critical substrate was eliminated. Recent data suggests that elimination of late potentials is at least as strong a predictor of freedom from VT in patients as non-inducibility [182, 183].

Equipping an MRI suite for interventional procedures require additional infrastructure,

including communication headsets, video projectors, and hemodynamic monitoring system[15]. Although there are no commercially available injection catheters for use in MRI, these are currently in development. Although we selected acetic acid, we recognize that alternative agents may be suitable for clinical use. We anticipate that if a small quantity of acetic acid reaches the blood pool (e.g. by tracking along the needle tract), it will be immediately diluted and metabolized.

Many patients with VT have implantable cardioverter defibrillators that usually would disqualify them from undergoing a MRI scan. MRI-conditional devices are increasingly common and patients with these newer devices would be eligible for MRI guided chemoablation. Nevertheless, implanted devices and leads can cause imaging artefacts, which could obscure target tissue and ablation lesions.

6.6 Conclusion

This is the first report of real-time MRI guided transcatheter myocardial chemoablation. MRI enables instantaneous visualization of arrhythmic substrate and real-time monitoring of irreversible ablation lesions. Acetic acid creates more homogenous and well-circumscribed ablation lesions compared with ethanol. Unlike radiofrequency energy, endocardial needle chemoablation achieves fully transmural and irreversible ablation lesions. We demonstrate feasibility of conductive isthmus ablation with abolition of local abnormal voltage activities in an animal model of ischemic cardiomyopathy. MRI guided chemoablation could improve procedural success of VT ablation.

6.7 Figures

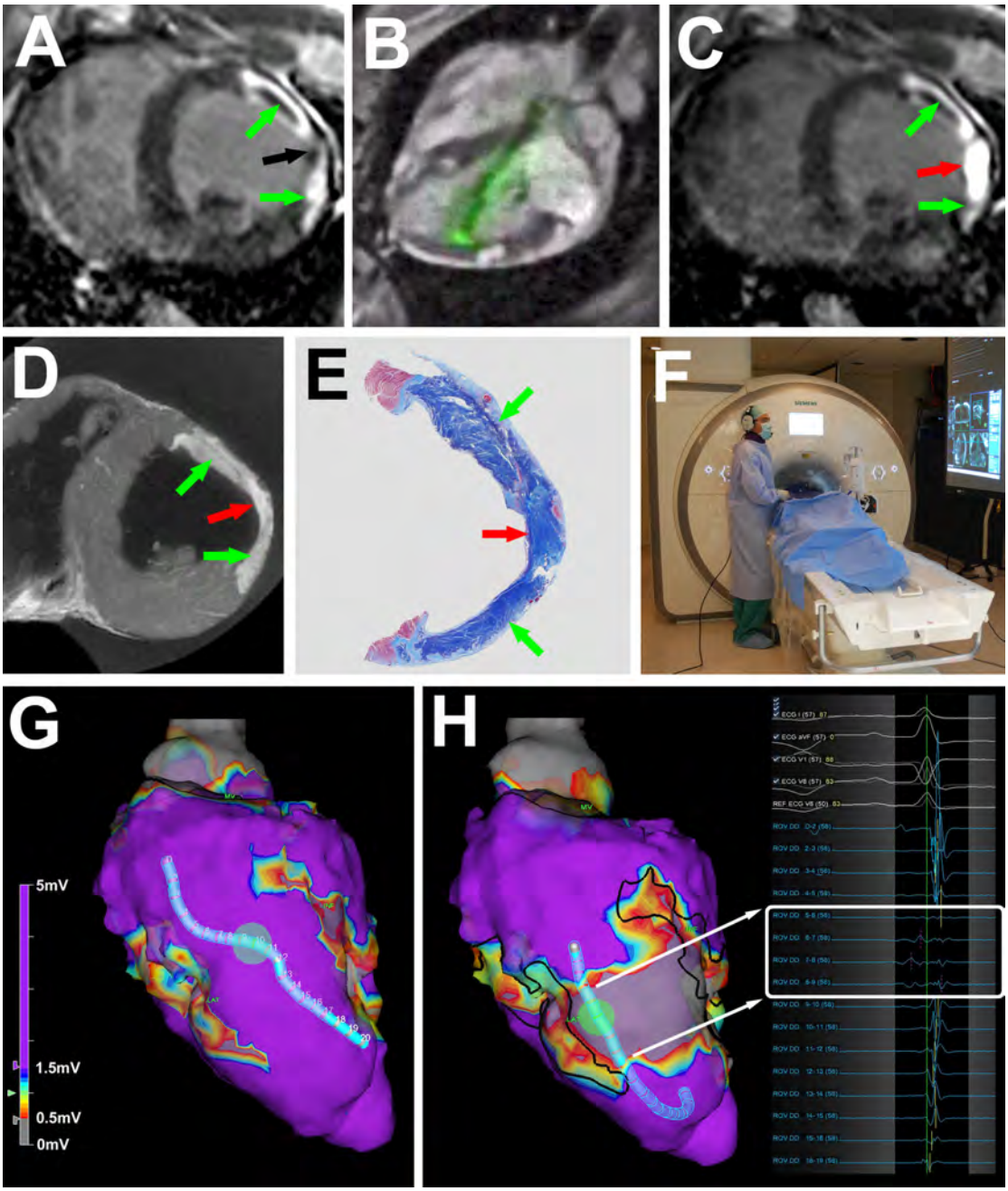

Figure 6-1: MRI guided chemoablation of a conductive isthmus

(A) Baseline LGE showing two infarcts (green arrows) with isthmus of normal myocardium (black arrow). (B) Real-time MRI guided chemoablation. The active visualization injection needle appears in green. (C) LGE after chemoablation showing infarcts (green arrows) and transmural chemoablation lesion (red arrow). (D) After 7 days, ex-vivo high-resolution MRI confirms transmural chemoablation lesion (red arrow) confluent with both infarcts (green arrows). (E) Wide-field Masson trichrome stain of a section through the heart in the same orientation as panels A, C and D. Normal myocardium appears pink, necrotic myocardium

appears purple and fibrotic tissue appears blue. (F) The operator wears a noise-cancelling headset for communication with staff in the control room. Real-time magnetic resonance images and hemodynamics are displayed in the room. (G) Endocardial voltage maps at baseline showing normal amplitude electrograms throughout the conductive isthmus. (H) Post-chemoablation, a band of very low (<0.5mV white box) voltages interrupts the isthmus. Black lines represent the margins of the original infarcts. LGE: late gadolinium enhancement; MRI: magnetic resonance imaging.

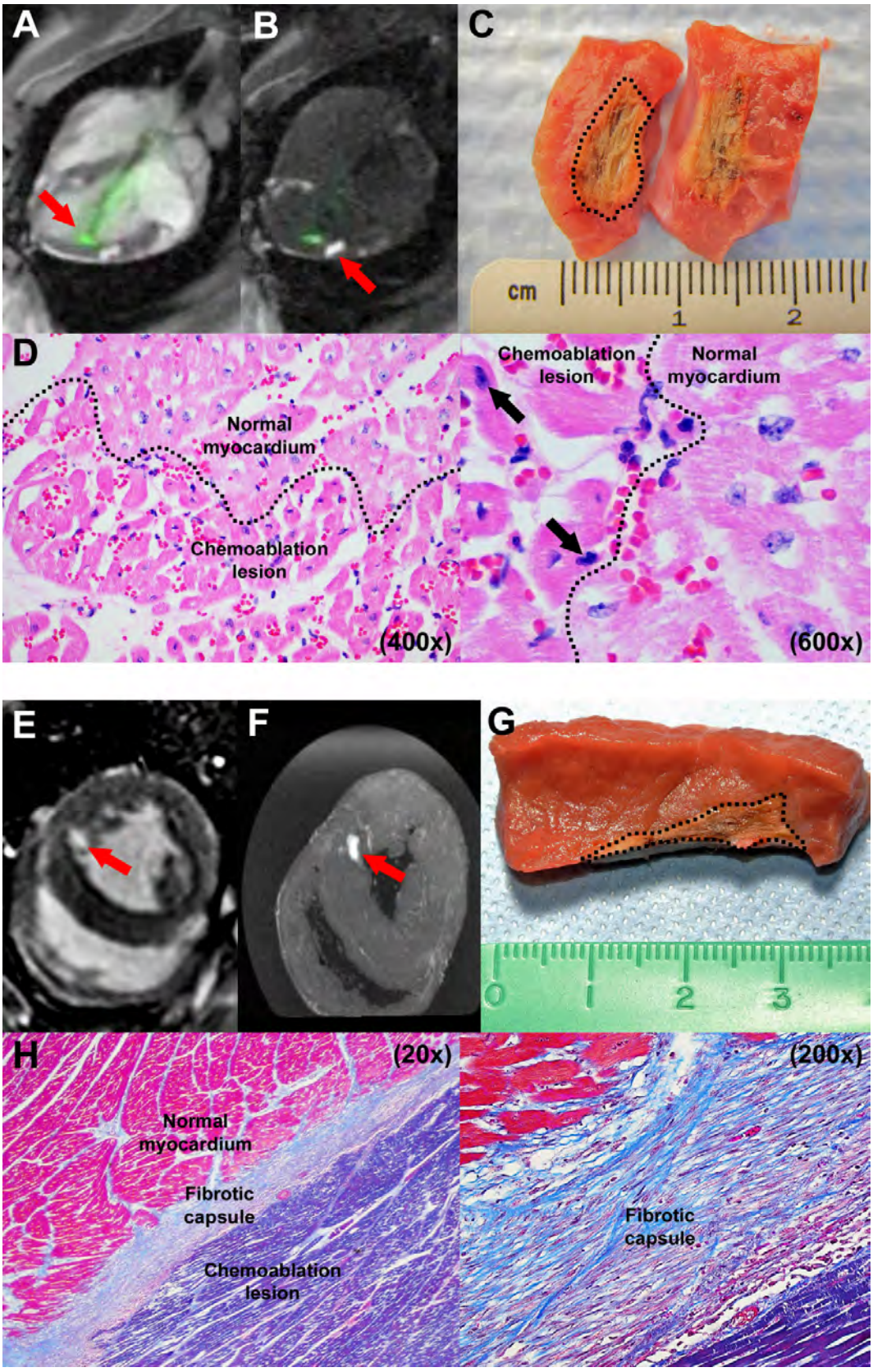

Figure 6-2: Ablation imaging and histology

(A) Real-time MRI during chemoablation. The active visualization injection needle appears green (arrow). (B) Real-time inversion-recovery MRI reduces signal from normal tissue,

highlighting chemoablation lesions containing gadolinium contrast (arrow). (C) Macroscopic appearance of an acute lesion, which has been butterflied open. The dotted line marks lesion margins. (D) Histology of acute lesion with H&E stains (400x and 600x magnification). Affected myocardial fibres are hypereosinophilic with mild to moderately pyknotic nuclei (black arrows). Dotted line marks border between chemoablation lesion and normal myocardium. (E) LGE and (F) ex vivo high resolution MRI of a chronic lesion after systemic gadolinium contrast administration. (G) Macroscopically, chronic lesions have well circumscribed margins (marked with dotted line). (H) Histology of a chronic lesion with trichrome stain (20x and 200x magnification). Collagen stains blue, normal myocardial fibres stain red and necrotic myocardial fibres stain purple. LGE: late gadolinium enhancement; MRI: magnetic resonance imaging.

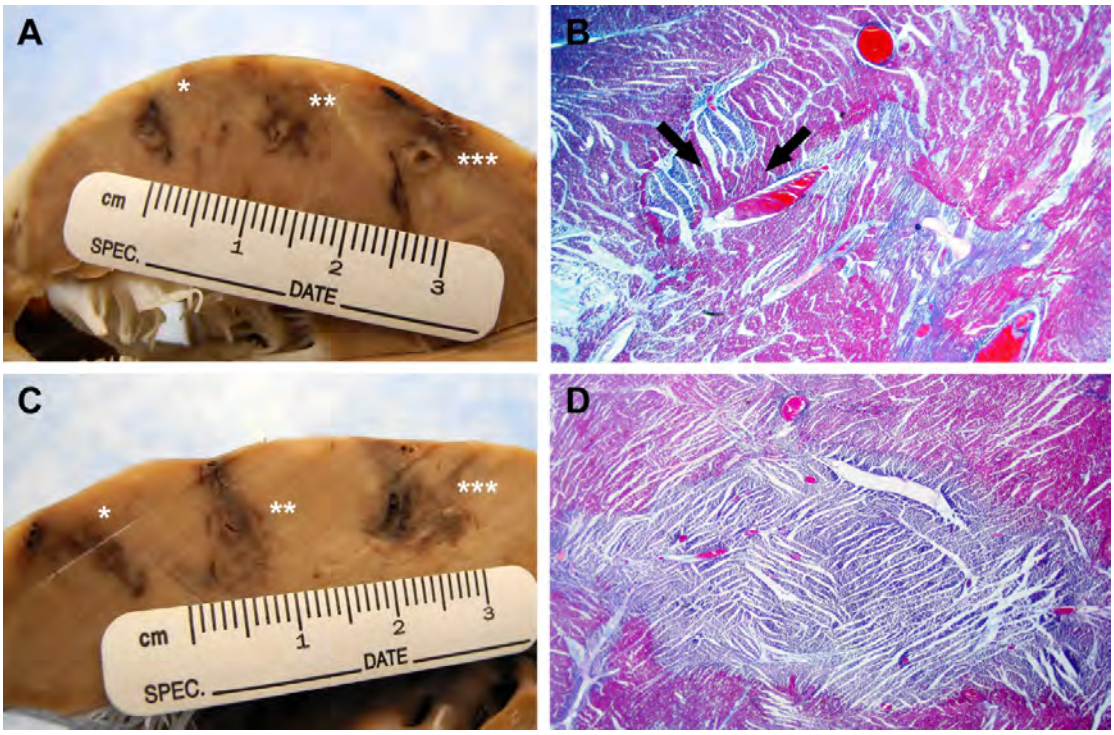

Figure 6-3: Ethanol vs. acetic acid

(A) Macroscopic appearance after fixing in formalin of 70% ethanol 0.2mL(*), 0.4mL(**) and 0.6mL(***) injections. (B) Trichrome stain of 0.6mL ethanol lesion (20x magnification). Lesion has stellate geometry with patchy areas of normal myocardium within the ablation field (black arrows). (C) Macroscopic appearance of 50% acetic acid 0.2mL(*), 0.4mL(**) and 0.6mL(***) injections. (D) Trichrome stain of 0.4mL acetic acid lesion (20x magnification). Lesion is homogeneous with well-circumscribed border and no patchy areas of normal myocardium are seen within the ablation field.

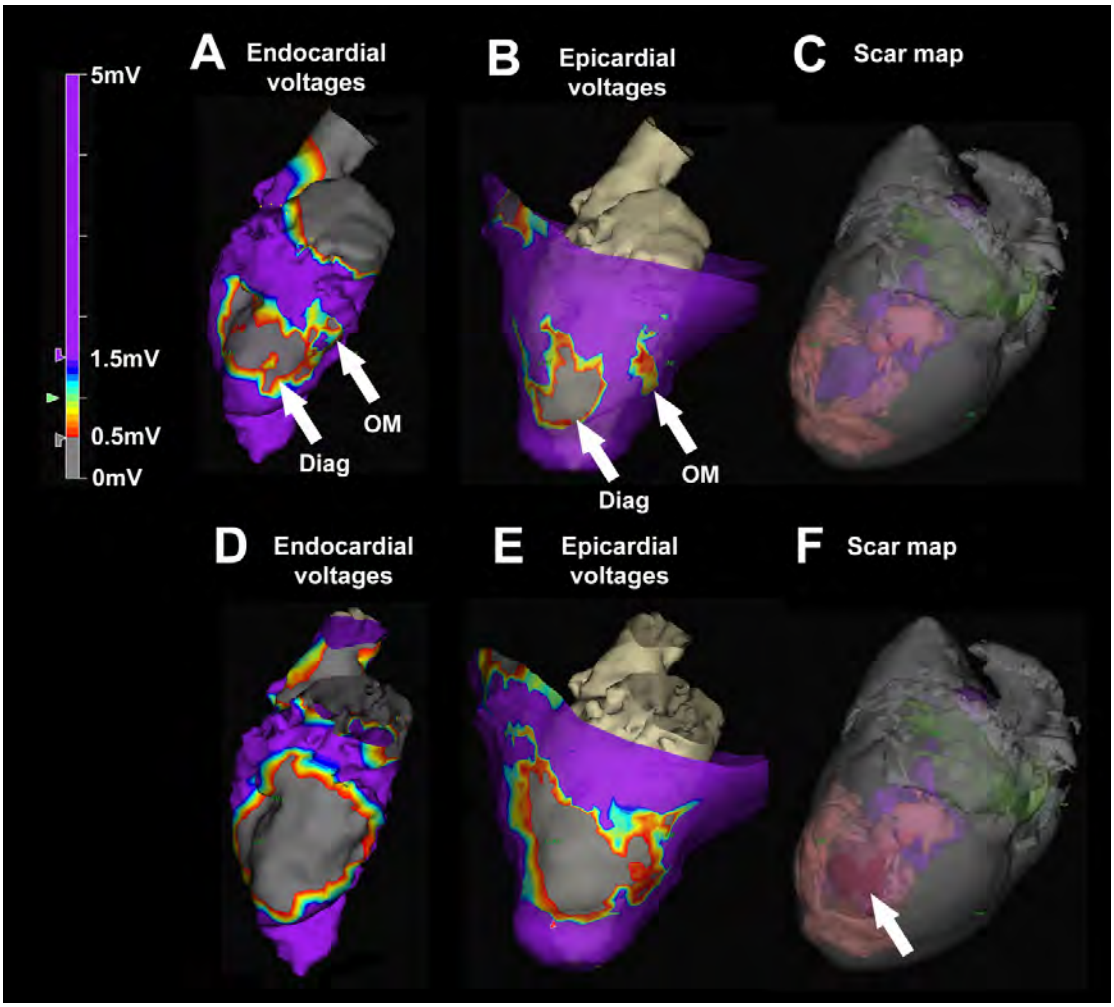

Figure 6-4: Left ventricular endocardial electroanatomic mapping before and after chemoablation in an animal model of ischemic cardiomyopathy

(A) Baseline endocardial voltage map demonstrates low voltages corresponding with the diagonal infarct (Diag) and an adjacent heterogeneous area corresponding with the obtuse marginal infarct (OM). Purple represents normal voltages (>1.5mV) and grey represents very low voltages (<0.5mV). (B) Baseline epicardial map demonstrates two distinct areas of low voltage separated by an isthmus of normal conduction. (C) Baseline three-dimensional scar map derived from high-resolution ex-vivo MRI shows infarct (pink). The LV cavity appears in purple and the left atrium in green. (D) Post-chemoablation endocardial voltage map demonstrates low voltages with abolition of the heterogeneous area between the two infarcts. (E) Post-chemoablation epicardial map confirmed interruption of the conductive isthmus. (F) The chemoablation lesion (arrow) appears in red and is confluent with the infarcts. LGE: late gadolinium enhancement; MRI: magnetic resonance imaging.

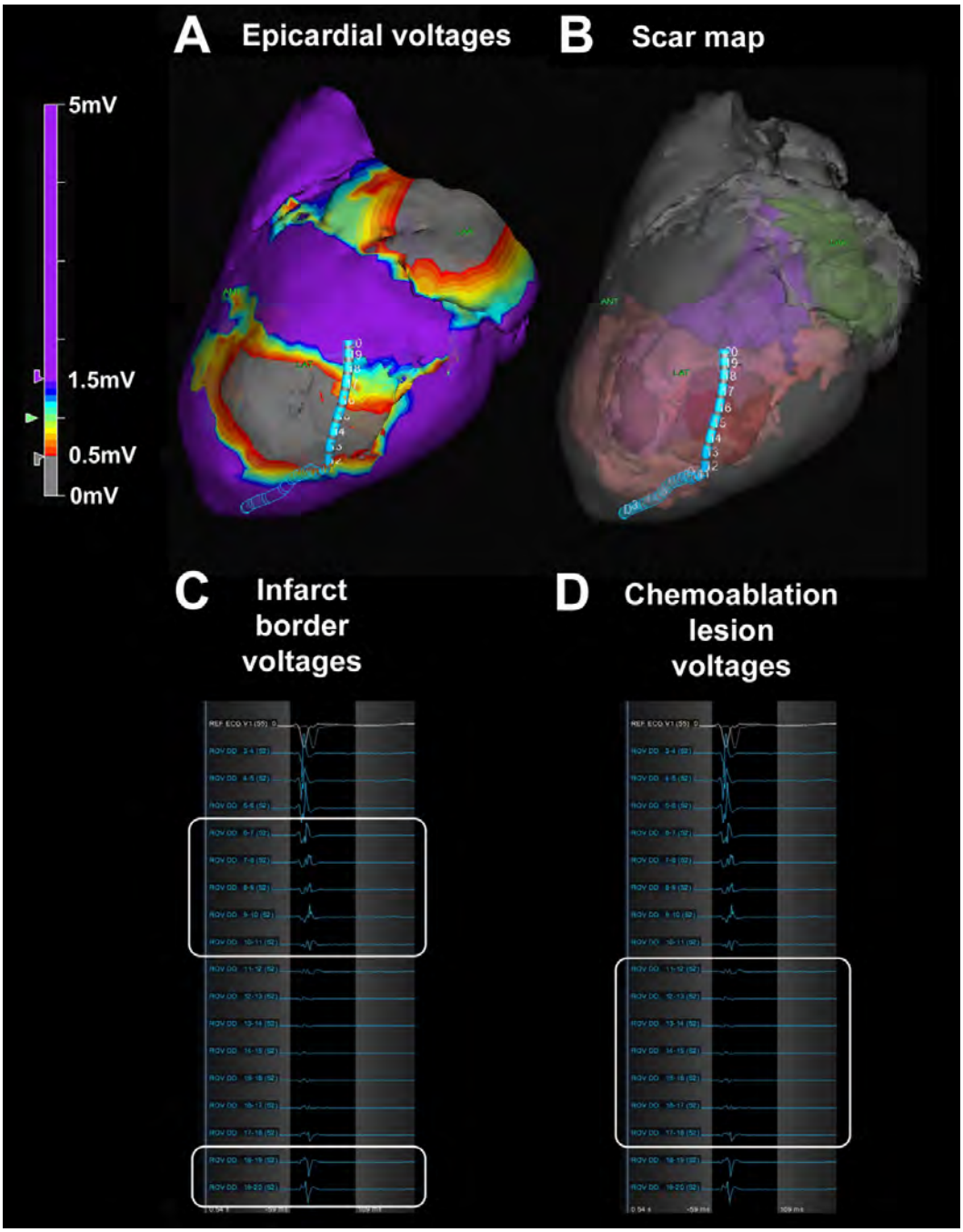

Figure 6-5: Scar border geometry

(A) Epicardial voltage map showing the duo-decapolar mapping catheter spanning the chemoablation lesion. (B) Three-dimensional scar map derived from high-resolution ex-vivo MRI showing catheter position relative to pre-existing infarct (pink) and chemoablation lesion (red). The left ventricular cavity appears in purple and the left atrium in green. (C) Electrograms from individual catheter electrodes demonstrate low voltages (0.5-1.5mV) over the pre-existing infarct borders (white boxes), and (D) extremely low voltages (<0.5mV) over the chemoablation lesion (white box). LGE: late gadolinium enhancement; MRI: magnetic resonance imaging.

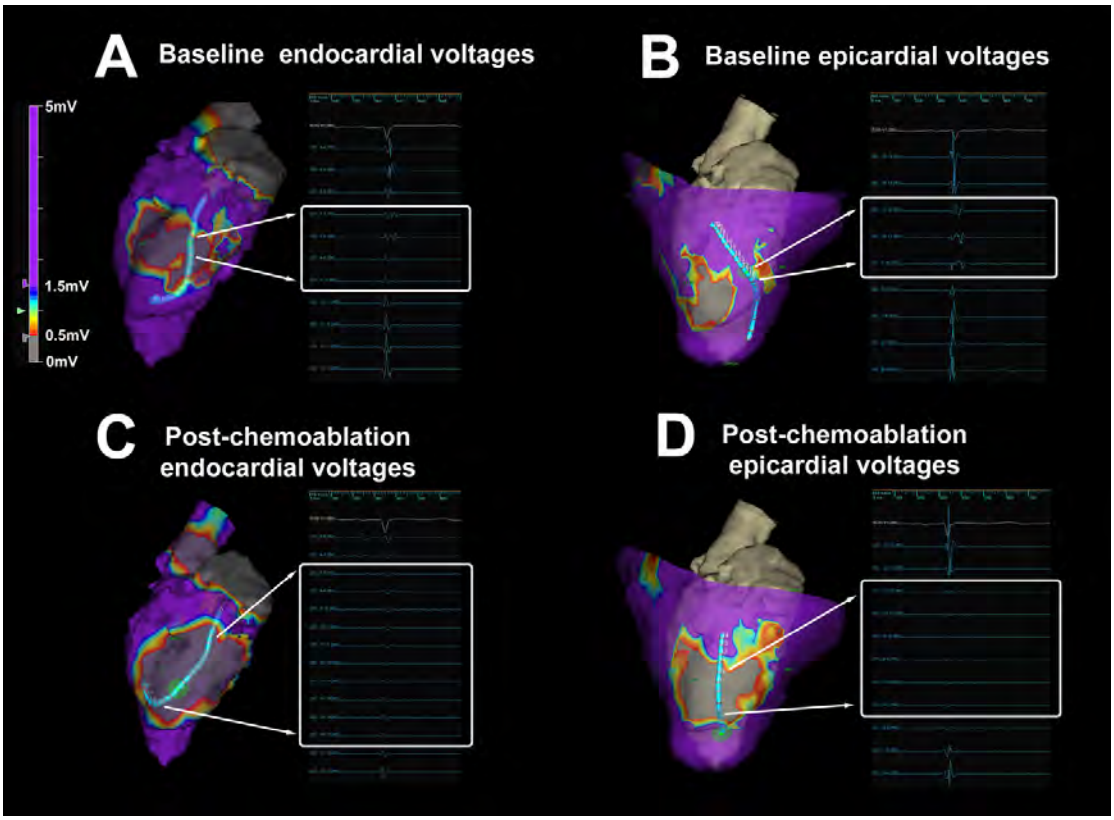

Figure 6-6: Abolition of abnormal electrocardiograms with chemoablation

(A-B) At baseline, endocardial and epicardial mapping demonstrates local abnormal voltage activities (LAVA) with fragmented slow conduction between the infarcts. (C-D) After chemoablation, LAVA are abolished. Very low amplitude and complete absence of far-field electrograms remain on endocardial and epicardial mapping respectively.

6.8 Table

Gadolinium-based contrast agent	Concentration in 50% acetic acid	Incubation time (minutes)	Free Gd^{3+} concentration (mg/ml)
Gadofosveset	2%	15	23
	5%	15	20
Gadopentatate	2%	15	40
	5%	15	42
Gadoterate	2%	15	<LOD
	5%	15	<LOD
	2%	30	<LOD
	5%	30	<LOD
	2%	60	<LOD
	5%	60	<LOD

Table 6-1: Concentration of free Gd^{3+} in 50% acetic acid solution with 2% or 5% gadolinium-based contrast agent

Chapter 7. Conclusions and future directions

7.1 Conclusions

Diagnostic cardiac catheterization using only CMR guidance is a clinical reality in a small but growing number of institutions. Now that good solutions for hemodynamic monitoring, communication between staff, and interactive manipulation of real-time images are available commercially, it is relatively straightforward to equip a standard MRI scanner for invasive procedures. A number of simple cardiovascular interventions have been demonstrated in early clinical trials over the last decade. The main limitation to widespread adoption remains paucity of available devices and in particular guidewires, without which interventions are not feasible. However, a number of MRI-conditional guidewires are in development or are already in early clinical trials in Europe. If they prove safe, MRI conspicuous and have the required mechanical properties, then cautious introduction of increasingly complex CMR guided cardiovascular interventions should be possible in the near future.

It would be wrong to suggest that CMR should replace all other imaging modalities for all applications. CMR guided coronary interventions for example, are not realistic because the spatial resolution of real-time CMR is insufficient and vastly inferior to fluoroscopy. Rather, the focus of interventional CMR research should be on two fronts: (1) improving safety and efficacy of existing interventions for which current imaging is inadequate; and (2) developing new interventions that are not feasible using X-ray or echocardiography. The novel interventions described in this thesis address both of these objectives. Intentional right atrial exit and CO_2 insufflation reduces complication from sub-xiphoid access to the naïve pericardium. Transthoracic direct left atrial access enables delivery of large mitral valve implants without injuring the left ventricular myocardium. Real-time CMR guided myocardial needle chemoablation is a completely new approach to arrhythmia substrate ablation in the ventricle and could be used to ablate other structures (e.g. the interventricular septum or intracardiac tumours causing obstruction to blood flow). Transatrial intrapericardial tricuspid annuloplasty is a much-needed therapy for a clinical problem for which there is currently no solution other than open chest surgery.

The value of CMR in the development process does not mean that CMR will necessarily be the preferred imaging guidance modality for clinical translation of these novel interventions.

X-ray fluoroscopy and echocardiography are widely available in most cardiac catheterization laboratories, whereas very few hospitals currently have interventional CMR capability. The investment to build interventional CMR cath labs is substantial and many of the simple tools we take for granted in the X-ray cath lab (e.g. commodity guidewires and catheters) are not yet commercially available. For this reason, we tested whether transatrial intrapericardial tricuspid annuloplasty (TRAIPTA), intentional right atrial exit and CO_2 insufflation, and transthoracic direct left atrial access could be performed using a combination of X-ray fluoroscopy, echocardiography, rotational angiography, or fusion imaging, and without the need for CMR. Indeed, whereas we used real-time MRI to titrate TRAIPTA implant tension in the animal experiments, in clinic we would expect tensioning to be performed under 3D echocardiography guidance and titrated to reduce tricuspid regurgitation. Measuring the volume of pericardial effusion with MRI after withdrawal of a right atrial appendage catheter would be unnecessary in clinic, as a sub-xiphoid drain would evacuate accumulating pericardial fluid. Rotational angiography could confirm lung displacement prior to direct left atrial needle entry and fusion imaging could provide sufficient anatomical landmarks to plan optimal trajectories.

Nonetheless, CMR played a critical role in the development process for these novel interventions. Assessing the dynamic impact of TRAIPTA tension on atrioventricular geometry would have been difficult – if not impossible – without the cross-sectional capability of real-time MRI. Accurately measuring pericardial effusion volume serially and non-invasively for intentional right atrial exit would have been equally challenging. Without the ability to characterize the geometric impact of single lung deflation and determine the optimal trajectories for transthoracic left atrial access, it would not have been possible to refine this procedure. More than any other, transthoracic direct left atrial access illustrates the value of CMR in the development process. The complexity of this procedure, with a needle trajectory that crosses and passes by a number of critical anatomic structures, required imaging in multiple planes with clear soft tissue depiction. Neither X-ray fluoroscopy nor echocardiography can provide this, and so there is no doubt in my mind that this intervention would not have been conceivable without CMR guidance. However, once we had tested and refined the procedural steps using CMR, it was then possible to replicate the intervention using X-ray with augmented imaging (e.g. rotational angiography). In a way, CMR served as the testing and training ground so that we could determine how to perform the procedure using more conventional and widely available imaging modalities. In contrast, MRI-guided myocardial chemoablation is a clear example where CMR is a truly disruptive

technology. It is not conceivable to perform this procedure using X-ray or echocardiography because neither affords the soft tissue characterization capability of MRI.

The interventions described in this thesis therefore illustrate how CMR can add value to different stages of the innovation process. While some of these novel interventions should be performed from start to finish using CMR guidance, others are better suited to clinical translation using more conventional imaging modalities. For these interventions, CMR served mainly to support device development, testing and technical refinement. An underutilized tool in interventional cardiology, I hope that this thesis will encourage others to embrace this powerful and enabling imaging tool to develop novel cardiovascular interventions in the future.

7.2 Future directions

Translating these novel cardiovascular interventions into humans requires a number of steps. Most importantly, clinical grade MRI-conditional or MRI-safe devices are needed. This requires engagement of industry and regulatory agencies. In the last decade, a number of medical device manufacturers specialising in interventional MRI applications have emerged and have built fruitful collaborations with academic institutions in Europe and the United States.

Transatrial intrapericardial tricuspid annuloplasty is currently the subject of a collaborative research and development contract between the National Institutes of Health and Cook Medical in the United States. The goal of this collaboration is to develop a clinical grade device for first-in-man testing.

Intentional right atrial exit and CO_2 insufflation has already been tested in humans undergoing left atrial appendage ligation. We are collaborating with several electrophysiologists in the United States to use this technique to facilitate pericardial access for ventricular tachycardia epicardial ablation.

Since publication of the manuscript, we have tested transthoracic left atrial access using X-ray fluoroscopy guidance in human cadavers in collaboration with the structural heart team at Henry Ford Hospital in Detroit, Michigan. The focus of these subsequent experiments was firstly to learn to perform the procedure using X-ray projection imaging, and secondly to determine the optimal approach for surgical bailout in case a complication occurs during the percutaneous intervention.

Real-time MRI guided myocardial chemoablation was developed in collaboration with St Jude Medical, who provided support for electroanatomic mapping. Two medical device manufacturers have been awarded contracts by the National Institutes of Health in the United States to build clinical needle injection catheters for first-in-man testing under an Investigational Device Exemption (IDE) clinical protocol.

Chapter 8. Appendices

8.1 Patent applications

8.1.1 Devices and methods for treating functional tricuspid regurgitation

International patent application published on 2nd October 2014.

Inventors: Robert J. Lederman, Kanishka Ratnayaka and Toby Rogers.

Describes devices and methods for treating functional tricuspid regurgitation through transcatheter delivery of circumferential devices that lie along the atrioventricular groove, imparting selective compression to the tricuspid annulus.

(12) INTERNATIONAL APPLICATION PUBLISHED UNDER THE PATENT COOPERATION TREATY (PCT)

(19) World Intellectual Property Organization
International Bureau

(43) International Publication Date
2 October 2014 (02.10.2014)

WIPO | PCT

(10) International Publication Number
WO 2014/159842 A1

(51) International Patent Classification:
A61F 2/24 (2006.01)

(21) International Application Number:
PCT/US2014/025300

(22) International Filing Date:
13 March 2014 (13.03.2014)

(25) Filing Language: English

(26) Publication Language: English

(30) Priority Data:
61/785,652 14 March 2013 (14.03.2013) US

(71) Applicant: **THE UNITED STATES OF AMERICA, AS REPRESENTED BY THE SECRETARY, DEPARTMENT OF HEALTH AND HUMAN SERVICES** [US/US]; National Institutes of Health, Office of Technology Transfer, 6011 Executive Boulevard, Suite 325, MSC 7660, Bethesda, MD 20852-7660 (US).

(72) Inventors: **LEDERMAN, Robert, J.**; 3916 Underwood Street, Chevy Chase, MD 20815 (US). **RATNAYAKA, Kanishki**; 811 14th St, NW, #1111, Washington, DC 20001 (US). **ROGERS, Toby**; Building 10, Room B1D219, 10 Center Drive, Bethesda, MD 20814 (US).

(74) Agent: **DUNCAN, Sandon, M.**; Klarquist Sparkman, LLP, One World Trade Center, Suite 1600, 121 SW Salmon Street, Portland, OR 97204 (US).

(81) Designated States *(unless otherwise indicated, for every kind of national protection available)*: AE, AG, AL, AM, AO, AT, AU, AZ, BA, BB, BG, BH, BN, BR, BW, BY, BZ, CA, CH, CL, CN, CO, CR, CU, CZ, DE, DK, DM, DO, DZ, EC, EE, EG, ES, FI, GB, GD, GE, GH, GM, GT, HN, HR, HU, ID, IL, IN, IR, IS, JP, KE, KG, KN, KP, KR, KZ, LA, LC, LK, LR, LS, LT, LU, LY, MA, MD, ME, MG, MK, MN, MW, MX, MY, MZ, NA, NG, NI, NO, NZ, OM, PA, PE, PG, PH, PL, PT, QA, RO, RS, RU, RW, SA, SC, SD, SE, SG, SK, SL, SM, ST, SV, SY, TH, TJ, TM, TN, TR, TT, TZ, UA, UG, US, UZ, VC, VN, ZA, ZM, ZW.

(84) Designated States *(unless otherwise indicated, for every kind of regional protection available)*: ARIPO (BW, GH, GM, KE, LR, LS, MW, MZ, NA, RW, SD, SL, SZ, TZ, UG, ZM, ZW), Eurasian (AM, AZ, BY, KG, KZ, RU, TJ, TM), European (AL, AT, BE, BG, CH, CY, CZ, DE, DK, EE, ES, FI, FR, GB, GR, HR, HU, IE, IS, IT, LT, LU, LV, MC, MK, MT, NL, NO, PL, PT, RO, RS, SE, SI, SK, SM, TR), OAPI (BF, BJ, CF, CG, CI, CM, GA, GN, GQ, GW, KM, ML, MR, NE, SN, TD, TG).

[Continued on next page]

(54) Title: DEVICES AND METHODS FOR TREATING FUNCTIONAL TRICUSPID VALVE REGURGITATION

FIG. 5A

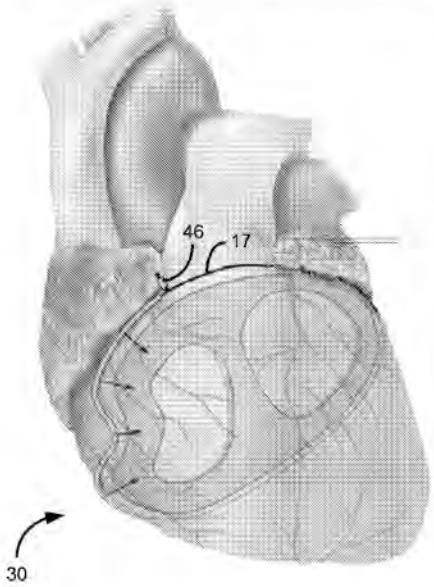

(57) Abstract: Disclosed here are devices and methods for treating functional tricuspid valve regurgitation and related conditions. Disclosed devices are adapted for applying force to an area of a patient's heart along or near the atrioventricular groove, and can include a tensioning element configured to be delivered by a flexible member guided through a catheter and positioned generally along or near the atrioventricular groove, and a compression member positionable along the tensioning element and over a desired segment of the atrioventricular groove to develop force to be applied to an adjacent area of the heart by selective tensioning of the tensioning element.

WO 2014/159842 A1

Declarations under Rule 4.17:

— *of inventorship (Rule 4.17(iv))*

Published:

— *with international search report (Art. 21(3))*

— *before the expiration of the time limit for amending the claims and to be republished in the event of receipt of amendments (Rule 48.2(h))*

DEVICES AND METHODS FOR TREATING FUNCTIONAL TRICUSPID VALVE REGURGITATION

CROSS-REFERENCE TO RELATED APPLICATIONS

This application claims the benefit of U.S. Provisional Patent Application No. 61/785,652, filed March 14, 2013, and entitled "DEVICES AND METHODS FOR TREATING FUNCTIONAL TRICUSPID VALVE REGURGITATION," which is incorporated by reference herein.

FIELD

This application is related to devices and methods for treating tricuspid valve regurgitation, including devices and methods for tricuspid valve annuloplasty.

BACKGROUND

Tricuspid valve regurgitation is a condition in which one of the valves of the heart "leaks" causing right ventricular blood to flow backwards into the right atrium. Commonly this occurs because the tricuspid valve annulus dilates beyond its ideal size. Addressing the condition is difficult because surgical tricuspid valve replacement is invasive and associated with significant morbidity and even mortality. Moreover, prosthetic tricuspid valves are prone to serious complications including thrombosis and infection, which makes the valve replacement approach less desirable.

It would be advantageous to develop approaches to addressing tricuspid valve regurgitation and other similar conditions of the heart that do not require replacement of organs or their components and minimize the risks presented by invasive surgery.

SUMMARY

Described below are new approaches to treating functional tricuspid valve regurgitation that address some of the limitations and risks of conventional approaches.

According to one implementation, a device for tricuspid valve annuloplasty or other procedure in the area of the heart's atrioventricular groove comprises a tensioning element and a compression member. The tensioning element can be configured to be delivered by a flexible member guided through a catheter and positioned along or near the heart's atrioventricular groove. The compression member is positionable along the tensioning element and over a desired segment

of the atrioventricular groove to develop force to be applied to an adjacent area of the heart by selective tensioning of the tensioning element.

The device can be deliverable through a catheter via the vasculature through the right atrium or right atrial appendage, or inserted along a trans-thoracic or subxiphoid or subcostal path. The compression member can be positionable along the tensioning element by using a capture device securable to the compression device to move the compression device relative to the tensioning element.

The compression member can be tubular and define a bore dimensioned to allow the tensioning element to pass through the compression member. In some implementations, the compression member has a groove dimensioned to receive the tensioning element and to assist in retaining contact between the tensioning element and the compression member.

The compression member can have at least one anti-slip feature configured to contact a surface to reduce slipping of the compression member relative to the heart when the compression member is in position over the desired segment with tension applied to the tensioning element. The anti-slip feature can comprise protruding barbs configured to an exterior surface of the heart.

The compression member can have a shaped profile along its length. The shaped profile can comprise at least two bends, at least one arch, an M-shaped portion and/or at least two inflection points between the segments of different curvatures.

The compression member can have a generally curved center segment, a generally straight center segment, and/or a center segment having a vertex.

The compression member can have end segments shaped to orient the compression member. The compression member can be self-orienting upon application of tension in a selected location for treatment. The compression element can be shaped such that the compression element is urged into a position normal to the treatment location as tension applied through the tensioning element is increased. The compression member can be comprised of multiple component parts separately deliverable through the catheter and configured to be assembled together near a treatment site.

The compression member can be resiliently deformable such that the compression member changes from a delivery shape suitable for delivery to a final shape after delivery to a treatment site is complete. The compression member can be at least partially defined by a first major radius of curvature and a second minor radius of curvature.

The device can comprise a protection member shaped to provide a protected space at least partially accommodating a blood vessel or other vital structure and to receive the tensioning element, wherein the protection member distributes force developed through increased tension in

the tensioning element to either side of the protected space. As just two examples, the protection member can be configured for positioning over a coronary artery, or over a pulmonary artery trunk.

According to another implementation, a method of using the device for tricuspid annuloplasty comprises positioning the tensioning element around the heart and generally along the heart's atrioventricular groove, positioning the compression member along the tensioning element an opposite a desired treatment location and applying force to the desired treatment location with the compression element by applying tension with the tensioning.

Imaging guidance can be used to ascertain positions of at least one of the catheter, the compression member, and the tensioning element.

The method can comprise positioning at least one compression member along the tensioning element along a desired segment of the atrioventricular groove, the compression member applying force to a desired area of the heart with increasing tension in the tensioning element. The method can comprise delivering the compression member through the catheter and through an opening in the right atrial appendage. The method can comprise delivering multiple compression member components to the treatment area and assembling the compression member components into the compression member.

The method can comprise delivering the compression member through the catheter and through the right atrium or an opening in the right atrial appendage.

The method can comprise positioning at least one protection member along a segment of the tensioning element, the at least one protection member being shaped to provide a protected space at least partially accommodating a blood vessel or other vital structure.

The foregoing and other features and advantages will become more apparent from the following detailed description of several embodiments which proceeds with reference to the accompanying figures.

BRIEF DESCRIPTION OF THE FIGURES

Fig. 1 is a schematic cross-sectional top plan view of a portion of a human heart, namely the tricuspid annulus, showing the annular dilation in dashed lines that causes functional tricuspid regurgitation.

Fig. 2 is a partial cross-sectional view of an anterior of a human heart showing a catheter extending from the right atrial appendage, a distal end of a flexible member extending from the catheter and around the heart and a capture loop for receiving the distal end of the flexible member.

Fig. 3A is an elevation view of the anterior of the heart of Fig. 2 showing that the flexible member has been guided through the capture loop.

Fig. 3B is an enlarged perspective of the catheter at the right atrial appendage showing that the distal end of the flexible member has been cinched around the heart and withdrawn into the catheter.

Fig. 4 is a schematic cross-section of the heart after the flexible member has been tensioned around the heart and over a compression member that applies force to the heart in predetermined areas.

Fig. 5A is another elevation view of the anterior of the heart showing the compression member of Fig. 4 in place over the tricuspid area of the heart and two protection devices in place over coronary artery segments.

Fig. 5B is an enlarged perspective view of one of the protection members of Fig. 5A in place over the corresponding coronary artery segment.

Fig. 6 is another view of the anterior of the heart showing another compression member in place to protect the right ventricle outflow tract (RVOT).

Fig. 7 is another view of the anterior of the heart showing another compression member in place on the pulmonary artery to provide resistance to flow.

Fig. 8A is a side elevation view of the compression member of Fig. 4.

Fig. 8B is a side elevation view of an alternative compression member having a relatively straight center segment.

Fig. 8C is a side elevation view of an alternative compression member having a center segment with a vertex.

DETAILED DESCRIPTION

I. Explanation of Terms

Unless otherwise noted, technical terms are used according to conventional usage. In order to facilitate review of the various embodiments of the disclosure, the following explanation of terms is provided:

The term "comprises" means "includes without limitation." Thus, "comprising a tensioning element" means "including a tensioning element," without excluding additional elements.

A "device for tricuspid valve annuloplasty" refers to a device that induces reshaping of an annulus of the heart's tricuspid valve to repair valvular insufficiency. Such devices include those that are placed in contact with the annulus of the tricuspid valve, and include those that exert their

action by compressive forces on the annulus, such as by placing a flexible annuloplasty member under tension, as in cerclage annuloplasty.

The term "flexible member" refers to an element that is sufficiently flexible to be introduced into the body, generally through a catheter, and manipulated along a desired path within the body, such as in and around the patient's heart. One example of such a flexible member is a "guide wire" of a conventional catheter, which can refer to a simple guide wire, a stiffened guide wire, or a steerable guide wire that is capable of puncturing and/or penetrating tissue, such as the right atrial appendage. The guide wire also can deliver energy to augment its ability to penetrate tissue, for example by puncturing it, delivering radiofrequency ablative energy or by delivering laser ablative energy.

As described below, the guide wire is used to position a separate "tensioning element" made of a suitable tensioning material generally along the heart's atrioventricular groove. Such a tensioning element is usually designed to remain deployed for the duration of the treatment. The tensioning element can be formed of any suitable tensioning material, including suture or ligature material or wire. The tensioning element may be comprised of segments made of different materials or having different properties, such as different elasticities. In some cases, the guide wire can also serve as the tensioning element.

A "capture device" is any suitable element or device that can be controlled, usually from outside the body, to engage the tensioning element (usually at a predetermined location along its length) to move and guide the tensioning element to a desired position and/or to manipulate it to increase its tension and the forces applied by it. For example, a capture device can be a conventional capture loop or a device having opposing members (like miniature forceps) that can pinch and hold the tensioning element.

The term "compression member" refers to an element that is designed to cooperate with the tensioning element to apply a desired force to an area along the path of the tensioning element. The compression member may be designed to provide a greater force to the area than would be applied by the tensioning element alone.

The term "protection member" refers to an element that is designed to cooperate with the tensioning element to provide a protected space to a blood vessel or other vital structure along the path of the tensioning element. In general, the protection member is designed so that the blood vessel or vital structure within the protection member experiences less force from the tensioning element than is exerted at adjacent areas at either end of the protection member.

In a "tricuspid valve annuloplasty" as described herein, a flexible member is placed around the annulus of the tricuspid valve, circumferential tension is developed in the flexible member or a tensioning element and resulting force is selectively applied around the tricuspid valve annulus. Examples of approaches to cerclage annuloplasty for a mitral valve are disclosed in U.S. Patent No. 8,211,171, which is incorporated herein by reference. The described approaches include a cerclage trajectory through a proximal coronary septal perforator vein and myocardium or annulus fibrosis interposing between that vein and the right ventricle or right atrium to create circumferential cerclage annuloplasty tension.

The compression and protection members disclosed herein can be made of an "MRI-compatible" material. Such materials are safe to use in the body during magnetic resonance imaging of the body, and do not substantially affect imaging quality of the MRI. An "MRI-safe" material is one that does not add substantial risk to a human or equipment by placing it in the magnetic field of an MR environment. Examples of MRI-compatible materials are non-ferrous materials, such as ceramics, plastics and non-magnetic composite materials. Austenitic stainless steels (of the 300 series) are neither ferromagnetic nor paramagnetic and therefore are MRI-compatible. Titanium and aluminum are MRI-compatible, even though they are not ideally paramagnetic. Particularly disclosed MRI-compatible materials of which the protective device may be made include nitinol, MP35N and cobalt-chromium alloys.

Unless otherwise explained, all technical and scientific terms used herein have the same meaning as commonly understood by one of ordinary skill in the art to which this disclosure belongs. The singular terms "a", "an", and "the" include plural referents unless context clearly indicates otherwise. The term "or" refers to a single element of stated alternative elements or a combination of two or more elements, unless context clearly indicates otherwise. For example, the phrase "rtMRI or echocardiography" refers to real-time MRI (rtMRI), echoradiography, or both rtMRI and echocardiography. Although methods and materials similar or equivalent to those described herein can be used in the practice or testing of the present disclosure, suitable methods and materials are described below. In case of a conflict, the present specification, including terms, will control. In addition, the materials, methods, and examples are illustrative only and not intended to be limiting.

II. Overview

One approach to tricuspid valve annuloplasty, or repair of the tricuspid valve, can be achieved by restricting dilation of the valve's free wall, which enhances coaptation or apposition of the tricuspid valve leaflets. According to the approaches described herein, functional tricuspid

valve regurgitation is treated by selectively introducing circumferential tension around the valve annulus to retard dilation. One goal is to augment the effective (forward) right ventricular stroke volume by reducing regurgitant (backward) right ventricular stroke volume. Specifically, the septal-lateral dimension of the tricuspid valve annulus is reduced by extracardiac force or pressure applied through a tensioning element (such as, e.g., a suture) usually in combination with a separate compression member. The tensioning element is positioned generally along the atrioventricular groove and tightened to increase force exerted through the compression member on a desired treatment area.

As mentioned above, the compression member is used in conjunction with the tensioning element to enhance the force applied at one or more selected areas. The compression member may be designed to preferentially deform as tension is increased in the tensioning element.

As also described above, another kind of member, called a protection member, may be introduced to protect certain vital structures, e.g., blood vessels, within the tensioning element from being deformed by the forces applied by the tensioning element. The functions of compression members and protection members may be combined in some applications.

In addition to tricuspid valve repair, related approaches are aimed at addressing congenital heart disease by providing an extracardiac force to compress the right ventricular outflow tract or pulmonary artery trunk in conjunction with or instead of surgical banding.

III. Embodiments

Fig. 1 is an anatomical schematic cross section of the heart viewed from above. As shown in Fig. 1 and described above, functional tricuspid valve regurgitation or "leakage" results when the free wall of the tricuspid valve dilates. Tricuspid valve annuloplasty, or repair of the heart valve, can be achieved by restricting the dilation of the free wall, which enhances coaptation of the tricuspid valve leaflets.

Fig. 2 depicts a catheter 12 that has been inserted from the femoral vein and directed to penetrate the right atrial appendage to exit the right atrial cavity and enter the pericardial or extracardiac space. A flexible member 16, sometimes referred to as a wire, is inserted through a sheath of the catheter, and is shown extending beyond a tip 14 of the catheter. A distal end 18 of the flexible member 16, which is the free end, is directed around the heart, such as in the "clockwise" direction as shown by the arrows. The path of the flexible member 16 as shown in Fig. 2 is generally along or near the atrioventricular groove on the exterior of the heart.

A capture loop 20 is provided, such as attached to the flexible member 16 and spaced from its distal end 18. Alternatively, the capture loop 20 can be provided on a dedicated flexible member that is separate from the flexible member 16.

As shown in Fig. 3A, the distal end 18 of the flexible member 16 can be routed around the heart and through the capture loop 20. Thereafter, the flexible member 16 can be withdrawn with the distal end 18 engaged with the capture loop 20 into and back through the catheter, as shown in Fig. 3B. The flexible member 16 can be replaced with a tensioning element 17 (see, e.g., Fig. 4), by attaching the tensioning element 17 to the flexible member 16 with the tensioning member 17 being pulled into place as the flexible member 16 is withdrawn. Tension is then increased in the tensioning member 17. A suitable capture device (the capture loop 20 being just one example) can be used to grasp the tensioning element 17 and to manipulate it as desired to effect the required tension. In this way, the circumferential tension around the heart exerted by the tensioning member causes the tricuspid valve annulus to shorten radially and enhances its coaptation. Thus, this approach can be described as providing extracardiac circumferential tension by a member or device delivered via a transatrial intrapericardial catheter.

Fig. 4 is a schematic view of a cross-section of the heart showing the location of the tensioning element 17 having been "pulled" into the location previously occupied by the flexible member 16, which has been withdrawn. As also shown in Fig. 4, there can be a knot or a locking mechanism, such as the lock 46 on the flexible member 16, set to "lock" or fix the tensioning element 17 in place once it has been cinched to a desired degree to provide the predetermined force.

In Fig. 4, a compression member 30 designed to work in conjunction with the tensioning element 17 is shown. Specifically, the compression member 30 is positioned between the heart and the tensioning element 17 such that it bears against the compression member 30 when it is tightened around the heart. In the case of the tensioning element 17 alone (or the flexible member 16 alone, as in some embodiments) and assuming a uniform construction thereof, the pressure exerted on the heart is fairly uniform throughout the closed loop encircling the heart. The compression member 30, however, is designed to cause greater force to be exerted on the heart as desired in areas where it is located.

The compression member 30 of Fig. 4 is also shown in Fig. 8A for greater clarity. As shown in Figs. 4 and 8A, the compression member 30 has a body 32, a first end 34 and a second end 36. The body 32 has a contoured shape to follow the outer periphery of the heart and to apply force to the heart at desired locations.

In the specific implementation shown, the body 32 can be described as having a shaped profile along its length. More specifically, the body has an "M"-shaped profile, with a first arch 38 adjacent the first end 34, and a second arch 40 adjacent the second end 36. Between the first arch 38 and the second arch 40 in the illustrated implementation, there is a bulge 42 that is positionable to apply greater force to a selected location, in this case to the tricuspid valve area.

Segments 43, 45, which extend from the first end 34 to the peak of the first arch 38 and from the second end 36 to the peak of the second arch 40, are shaped to follow the contours of areas of the heart against which they are designed to be positioned. These segments are referred to as lateral segments, and they tend to promote self-righting of the compression member 30 into a position parallel to the plane of the valve annulus as tension is applied through the tensioning element 17 to draw the compression member and segments 43, 45 into contact against the areas of the heart. Stated differently, these segments help the compression member adopt a position normal to the surface against which it is pressed when tension is applied. The compression member is generally self-orienting when tension is applied to it ends, which allows it to be pulled into position while maintaining a predictable position and then to exert force against the heart as desired.

The contoured shape or shaped profile of the body 32 may be described with one or more radii of curvature. Referring to Fig. 4, segments 43, 45 of each arch 38, 40 from its respective end 34, 36 to its peak can have a large radius of curvature r1. The remainder of each arch 38, 40, from its peak towards its inner end can have a smaller radius of curvature r2. The larger radius of curvature r1 conforms to the heart's surface, whereas the smaller radius of curvature r2 imparts a geometric reduction on a surface against which it bears.

By choice of materials or geometry, one or more segments of the compression member 30 may be designed to deform more easily or preferentially than other segments of the compression member 30.

Representative alternative compression members are shown in Figs. 8B and 8C. In contrast to the bulged center segment 42 of the compression member 30, a compression member 130 has a generally straight center segment 142. The straight section 142 allows force to be applied along a larger area of the heart than can be applied with the bulge 42. The compression member 130 has more pronounced changes in direction between the center section 142 and the adjoining arched sections 138, 140. Lateral segments 143, 145 (sometimes referred to as end segments because they extend inwardly from the ends 134, 136, respectively) tend to promote the self-righting of the compression member 130 when tension is applied.

Referring to Fig. 8C, a compression member 230 is more angled than the curved compression member 30. The compression member 230 can be described as having four or more bends. In the compression member 230, arched sections 238, 240 are mostly angled rather than fully curved. The compression member 230 has a center segment with a vertex 242 providing a pronounced point of focus for the application of force to the heart.

In the illustrated implementation, the various compression members have a grooved and/or tubular construction, or have eyelets, shaped to receive the tensioning element 16, thus coupling the compression member to the tensioning element 17 (or the flexible member 16). The various compression members described herein can be formed as a single piece, or it may comprise multiple segments that are assembled together in situ, (i.e., adjacent the treatment area within the body). Providing the compression member in multiple pieces may facilitate its introduction into the body through a catheter. Each compression member can have grooves or other patterning, such as on its inner surface, to enhance its "grip" in the treatment area.

Figs. 5A shows the compression member 30 in place and bearing against the tricuspid annulus after the flexible member has been cinched as desired. Specifically, the bulge 42 is oriented to apply greater force along the edge of the tricuspid annulus where dilation is greatest. The applied force to the anterior and posterior walls of the tricuspid annulus enhances leaflet coaptation.

As shown in Fig. 5A, and as best seen in Fig. 5B, a protection member 50 can be provided to protect certain structures from being deformed under the force applied by the flexible member 16. The protection member 50 can have a curved shape that defines a protected space 52 as shown in Fig. 5B. The protection member 50 can be positioned as shown with a left coronary artery (or other vital structure) received in the protected space 52. In this way, the coronary artery is protected from unintended deformation as the tensioning element is cinched tight to provide the appropriate force on the compression member. In the example of Fig. 5A, two such protection members are in use, but any number can be used.

As also shown in Fig. 5A, the compression member 30 can be provided with ant-slip features such as barbs 33 that tend to engage with the adjacent surface of the heart when the compression member 30 is forced against the heart by the tension in the tensioning element 17. The illustrated barbs 33 are exemplary, and they can be provided over more or less of the length of the compression member.

Fig. 6 shows an alternative implementation that is similar to Fig. 5A, but includes a compression member 60 instead of the compression member 30. The compression member 60 is

shaped to occupy a longer portion of the periphery of the heart than the compression member 30. By selecting the proper geometry and size, the compression member 60 can be positioned as shown to provide the desired force on the tricuspid annulus, and also to extend over and protect the right ventricle outflow tract and/or coronary arteries from undesirable compression.

Fig. 7 shows an alternative implementation that is similar in some aspects to Figs. 5A and 6, but instead includes a compression member 70 having a bulge designed to apply pressure to the right ventricular outflow tract or pulmonary artery trunk to create intended compression and thereby temporary resistance to blood flow as part of staged correction/palliation of congenital heart disease, in place of surgical "pulmonary artery banding." As can be seen in Fig. 7, the compression member 70 also has a greater length than the compression member 30 and includes long protection arches, e.g., 3-6 mm in length.

The various members 30, 130, 230, 50, 60 and 70 can be constructed of stainless steel, nitinol or any other suitable material. The members are preferably dimensioned for introduction to the treatment area via a catheter. Members that are resilient, elastic, or superelastic, it can be designed for delivery via a low-profile catheter. In addition, such members can be bound into a smaller size for easier delivery and then allowed to expand before deployment. Larger members may require delivery via a large-bore catheter. In addition, any of the members may be a provided as multiple-piece assemblies of components where the components are small enough for delivery via a catheter. The resulting member may be self-assembled in situ. In one example, the segments are beads having notches or other shapes that fit together to allow assembly into one member.

Members can be provided in different sizes based on the differences in typical tricuspid valve geometry. In addition, customized or bespoke members can be made based on measurements derived from cardiac imaging procedures such as angiography, ultrasound, computed tomography and/or magnetic resonance imaging.

Example 1

In an exemplary procedure, the following steps are performed:

1. From a transfemoral vein approach, position a catheter in the right atrial appendage.
2. Exit the right atrial appendage into the pericardial space using appropriate imaging guidance, and using a suitable catheter device, such as a Brockenbrough needle, an introducer sheath dilator, and/or a stiff guidewire (flexible member).
3. Introduce an access sheath from the femoral vein into the pericardial space.

4. Position a capture device (e.g., a snare or other type of capture device) in the pericardial space, or use a customized capture device integrated into the access sheath.

5. Navigate a distal end of a guidewire "clockwise" (viewed from below) around the base of the heart and into the capture device or snare.

6. Capture the guidewire and provide access to a free end of the guide wire.

7. Introduce one or more compression and protection devices over the guidewire.

8. Reposition the guidewire into the appropriate position with regard to the target structures (tricuspid valve, coronary arteries, RVOT, etc.) using imaging guidance and the access sheath.

9. Position the compression and protection devices using imaging guidance.

10. Withdraw guidewire to apply tension, or withdraw guidewire to position tensioning element and then apply tension.

11. Assess for reduction in tricuspid regurgitation, for freedom from coronary artery compression, and for freedom from MPA/RVOT compression, using any combination of ultrasound, MRI, and X-ray angiography.

12. Provide stimulation (pharmacologic or otherwise) to alter loading conditions and inotropic state as desired, under imaging guidance, to assure suitable application of therapeutic compression to the intended cardiac structure under "stressed" conditions.

13. Deliver and apply tension fixation device (e.g., a lock) or form a knot in tensioning element.

14. Deliver and apply atrial exit site closure, whether part of tension fixation device or a separate occluder which can be made of non-absorbable (e.g. Nitinol) or absorbable material device that provides for affixing patches on one or both sides of a heart surface to close an opening in the heart surface.

15. Assess for freedom from complications, address as needed.

16. Obtain vascular hemostasis.

In alternative procedures or methods, any one or more of these listed acts can be performed without performing others of these listed acts, and in such methods these acts can be performed alone or in combination with other acts, and the acts can be performed in the order given above or in other orders.

The described approaches provide for addressing functional tricuspid valve regurgitation and other similar heart conditions with minimally invasive surgery that does not require cardiopulmonary bypass or open heart surgery techniques.

In addition to the approaches described above, it is also possible to configure the devices and adapt the methods for transthoracic delivery of the tensioning element, as well as any compression member or protection member that may be used.

In view of the many possible embodiments to which the disclosed principles may be applied, it should be recognized that the illustrated embodiments are only preferred examples and should not be taken as limiting in scope. Rather, the scope of protection is defined by the following claims.

Claims:

1. A device for applying force to an area of a patient's heart along or near the atrioventricular groove, comprising:

a tensioning element configured to be delivered by a flexible member guided through a catheter and positioned generally along or near the atrioventricular groove; and

a compression member positionable along the tensioning element and over a desired segment of the atrioventricular groove to develop force to be applied to an adjacent area of the heart by selective tensioning of the tensioning element.

2. The device of claim 1, wherein the tensioning element or the compression member is deliverable through a catheter through the right atrium or right atrial appendage of the heart.

3. The device of claim 1 or claim 2, wherein the tensioning element or the compression member is deliverable through a catheter inserted along a trans-thoracic or subxiphoid path.

4. The device of any one of claims 1-3, wherein the compression member is positionable along the tensioning element by using a wire or cable securable to the compression device to move the compression device relative to the tensioning element.

5. The device of any one of claims 1-4, wherein the compression member is tubular and defines a bore dimensioned to allow the tensioning element to pass through the compression member.

6. The device of any one of claims 1-5, wherein the compression member has a groove dimensioned to receive the tensioning element and to assist in retaining contact between the tensioning element and the compression member.

7. The device of any one of claims 1-6, wherein the compression member has at least one anti-slip feature configured to contact a surface of the heart to reduce slipping of the compression member relative to the heart when the compression member is in position with tension applied to the tensioning element.

8. The device of claim 7, wherein the anti-slip feature comprises protruding barbs configured to grip an exterior surface of the heart.

9. The device of any one of claims 1-8, wherein the compression member has a shaped profile along its length.

10. The device of claim 9, wherein the shaped profile comprises at least two bends.

11. The device of claim 9 or claim 10, wherein the shaped profile comprises at least one arch.

12. The device of any one of claims 9-11, wherein the shaped profile comprises an M-shaped section.

13. The device of any one of claims 9-12, wherein the shaped profile comprises at least two inflection points between segments of different curvatures.

14. The device of any one of claims 9-13, wherein the shaped profile comprises a generally curved center segment.

15. The device of any one of claims 9-13, wherein the shaped profile comprises a generally straight center segment.

16. The device of any one of claims 9-13, wherein the shaped profile comprises a center segment having a vertex.

17. The device of any one of claims 1-16, wherein the compression member has end segments shaped to orient the compression member

18. The device of any one of claims 1-17, wherein the compression member is self-orienting upon application of tension in a selected location for treatment.

19. The device of any one of claims 1-18, wherein the compression member is comprised of multiple component parts separately deliverable through the catheter and configured to be assembled together at or near a treatment site.

20. The device of any one of claims 1-19, wherein the compression member is resiliently deformable such that the compression member changes from a delivery shape suitable for delivery through the catheter to a final shape after delivery to a treatment site.

21. The device of any one of claims 1-20, wherein a shape of the compression member is at least partially defined by a first major radius of curvature and a second minor radius of curvature.

22. The device of any one of claims 1-21, further comprising a protection member shaped to provide a protected space adapted to at least partially accommodate the pulmonary artery, the left atrium, an other blood vessel, or an other vital structure, and adapted to receive the tensioning element, wherein the protection member distributes force developed through increased tension in the tensioning element to either side of the protected space.

23. A method of applying force to an area of a patient's heart along or near the atrioventricular groove, comprising:

positioning a tensioning element around the heart and generally along the heart's atrioventricular groove;

positioning a compression member along the tensioning element and over a desired treatment location; and

applying force to the desired treatment location with the compression element by applying tension with the tensioning element.

24. The method of claim 23, further comprising using a catheter to deliver the compression member through the right atrium or right atrial appendage of the heart.

25. The method of claim 23 or claim 24, further comprising using imaging guidance to ascertain positions of at least one of the compression member, the tensioning element, and a catheter for delivering the compression member or the tensioning element.

26. The method of any one of claims 23-25, wherein the tensioning element interacts with the compression element to urge the compression element into a position normal to the treatment location as tension is increased.

27. The method of any one of claims 23-26, further comprising delivering the compression member through a catheter and through an opening in the right atrial appendage.

28. The method of any one of claims 23-27, further comprising delivering multiple compression member components to the treatment area and assembling the compression member components into the compression member.

29. The method of any one of claims 23-28, further comprising positioning at least one protection member along a segment of the tensioning element, the at least one protection member being shaped to provide a protected space at least partially accommodating a blood vessel or other vital structure.

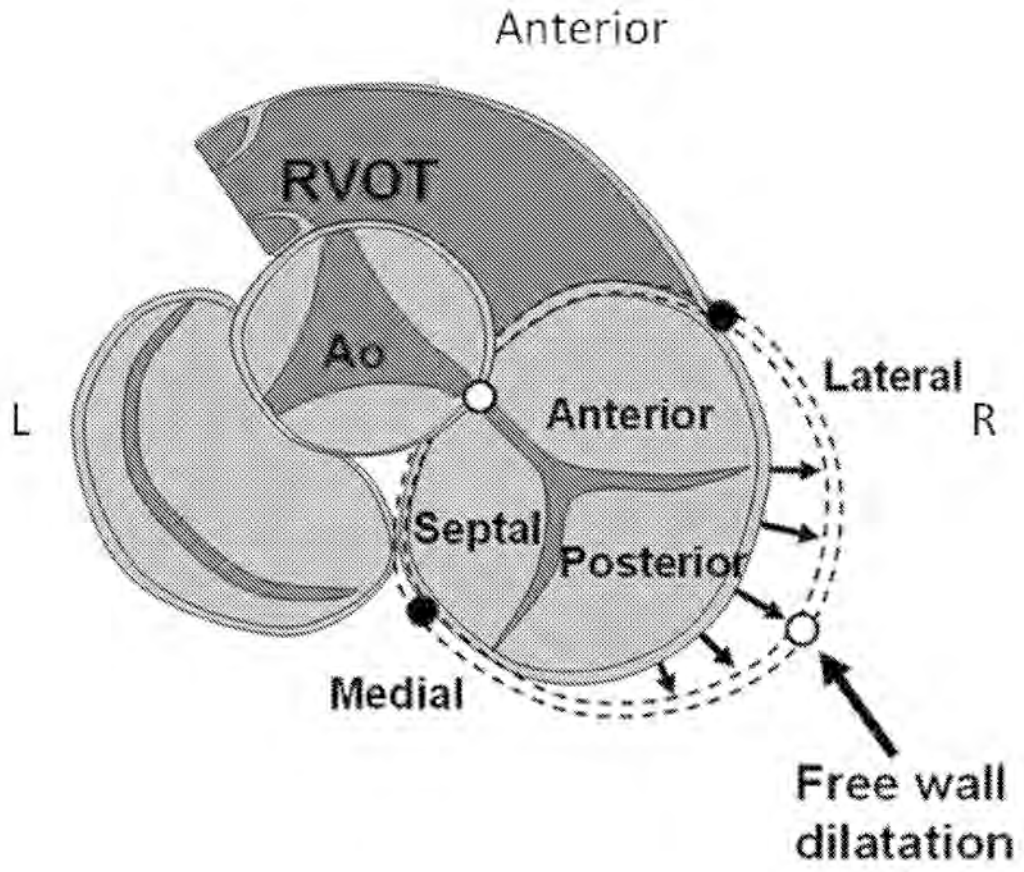
Anterior
RVOT
Ao
L
Lateral
R
Anterior
Septal
Posterior
Medial
Free wall
dilatation

FIG. 1

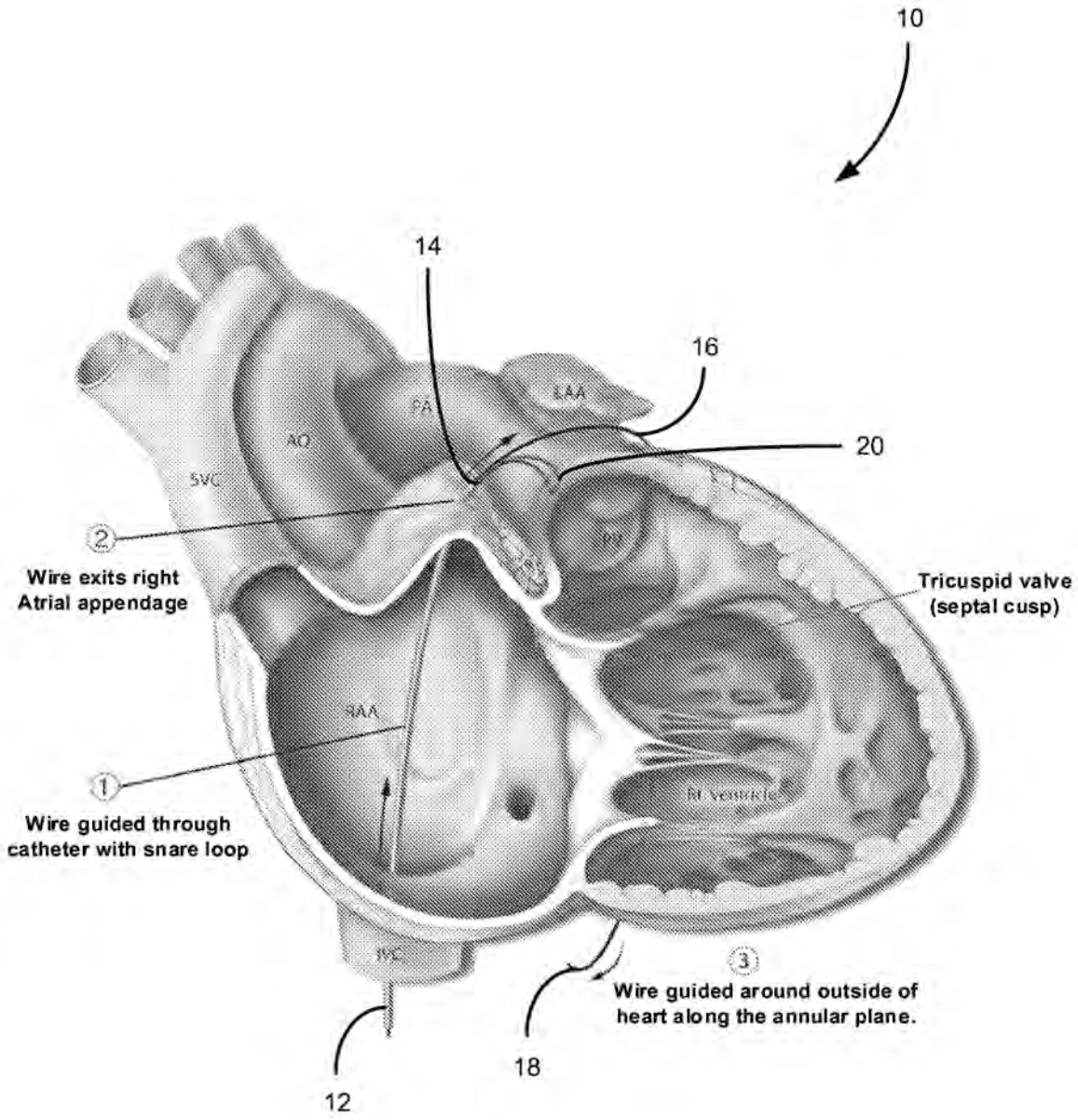
10
14
16
20
PA
LAA
AO
SVC
2
Wire exits right
Atrial appendage
Tricuspid valve
(septal cusp)
RAA
1
Wire guided through
catheter with snare loop
IVC
3
Wire guided around outside of
heart along the annular plane.
18
12

FIG. 2

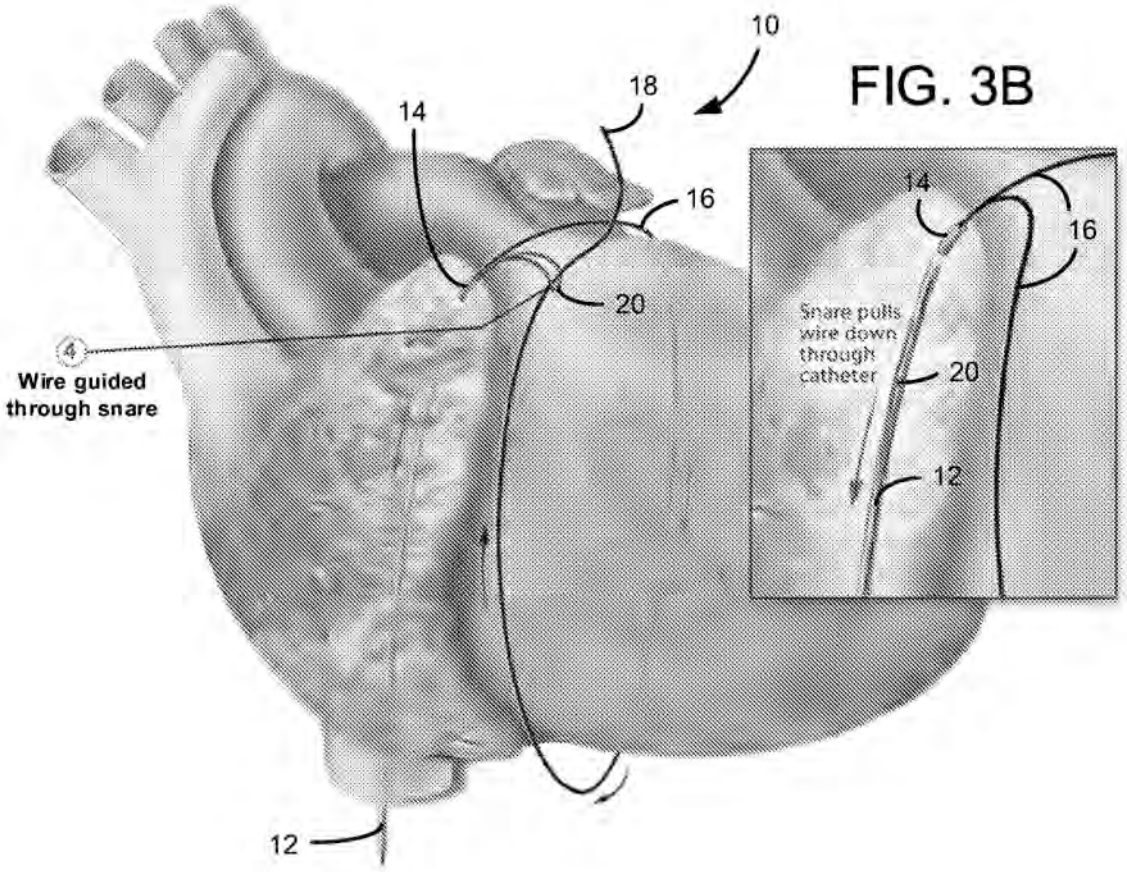
10
18
14
16
20
4
Wire guided
through snare
12
14
16
Snare pulls
wire down
through
catheter
20
12

FIG. 3B

FIG. 3A

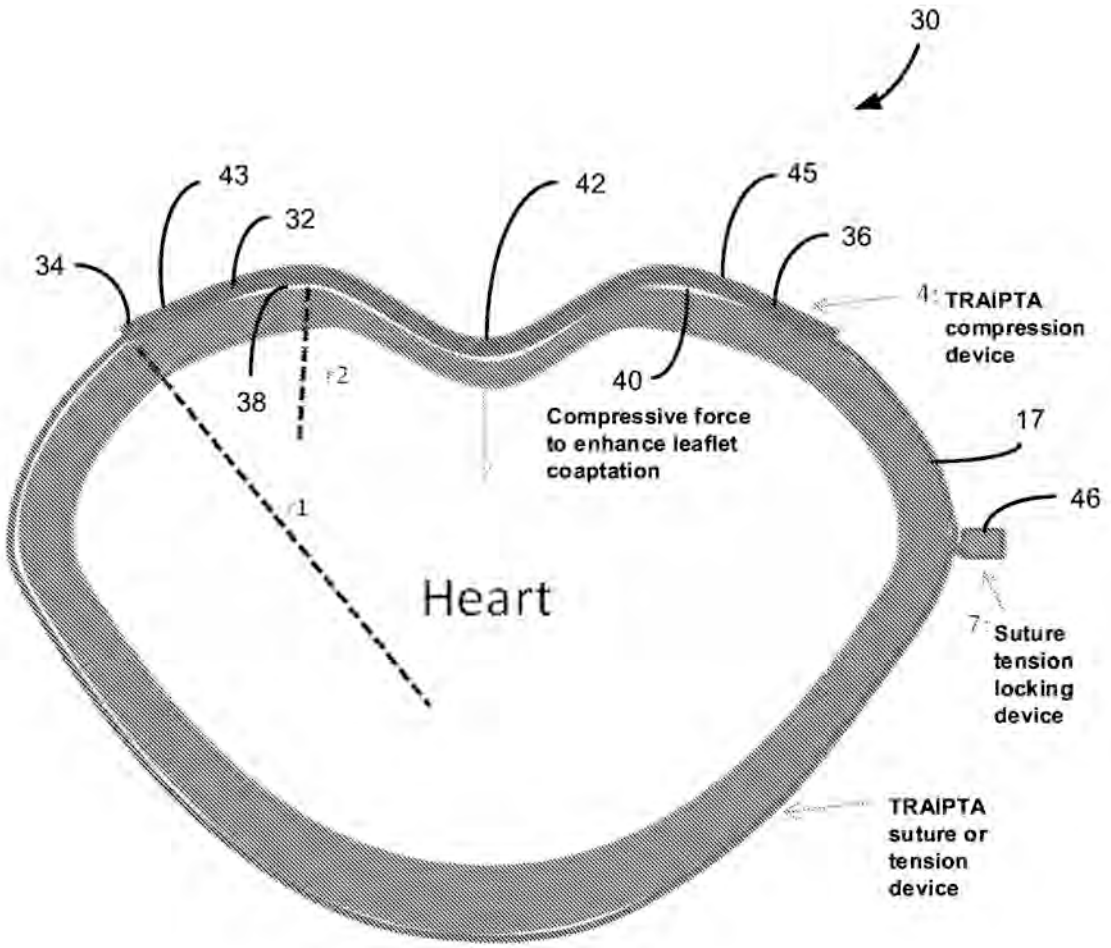
30
43
32
42
45
36
34
4: TRAIPTA compression device
38
r2
40
Compressive force to enhance leaflet coaptation
17
46
r1
Heart
7: Suture tension locking device
TRAIPTA suture or tension device

FIG. 4

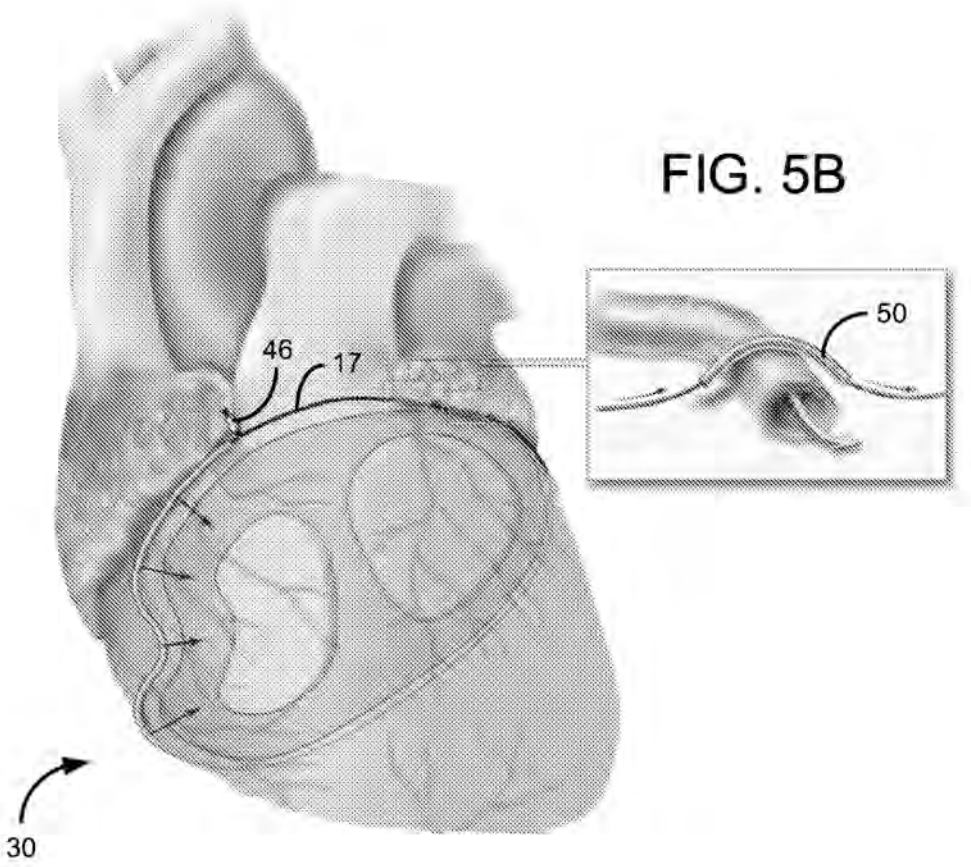

FIG. 5B

FIG. 5A

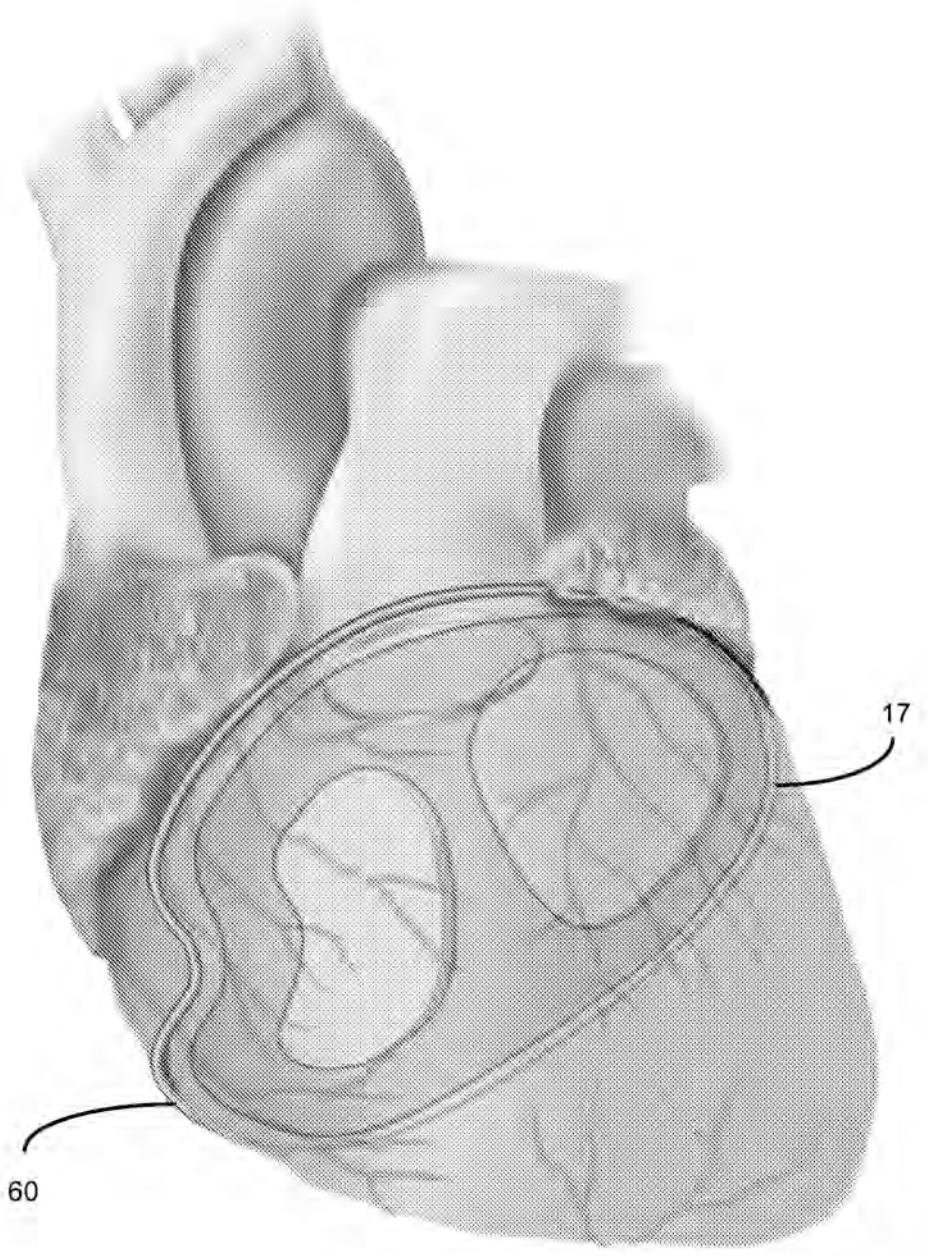

FIG. 6

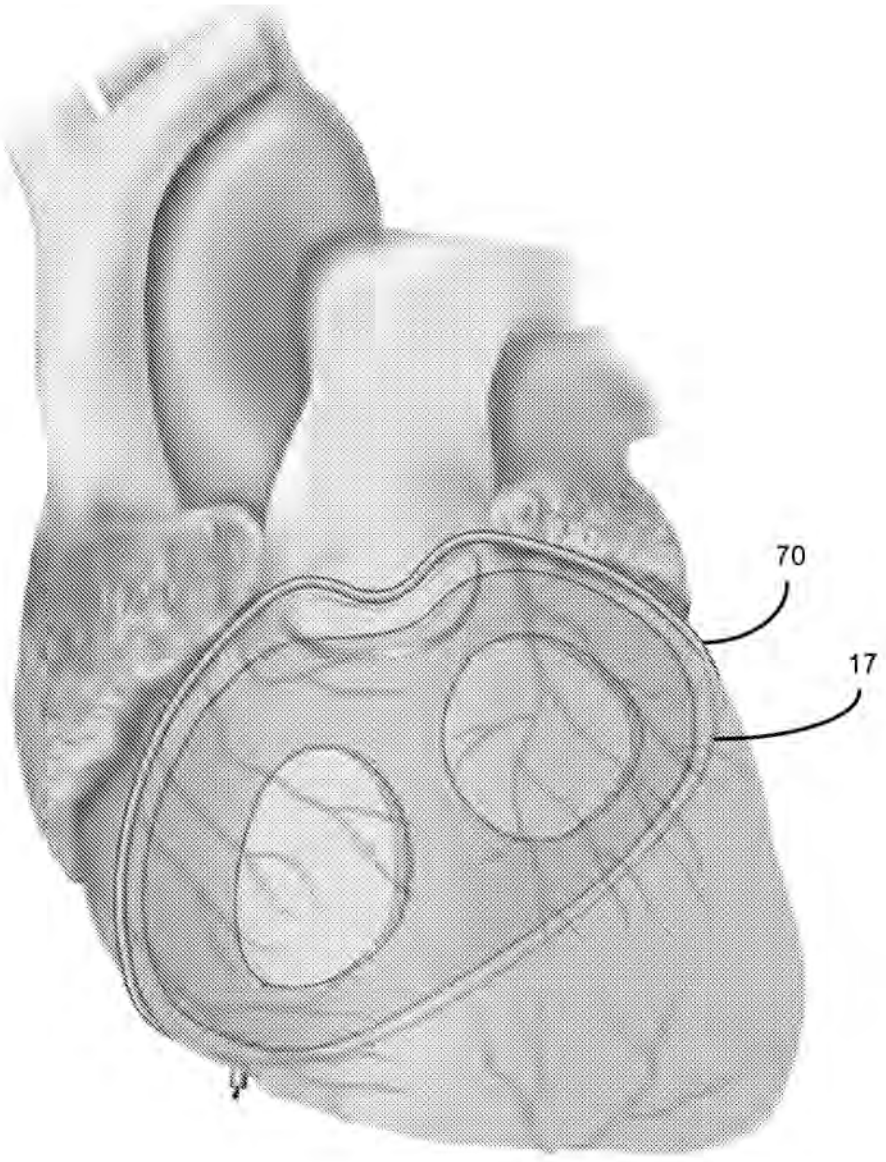

FIG. 7

7/8

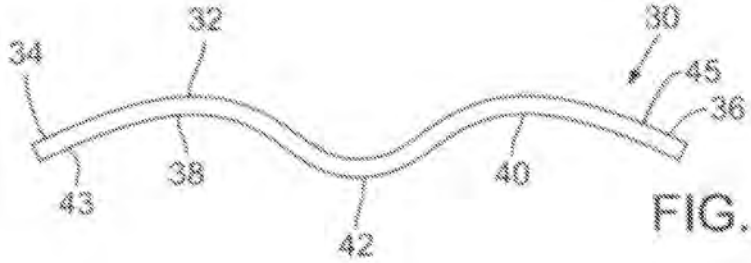

FIG. 8A

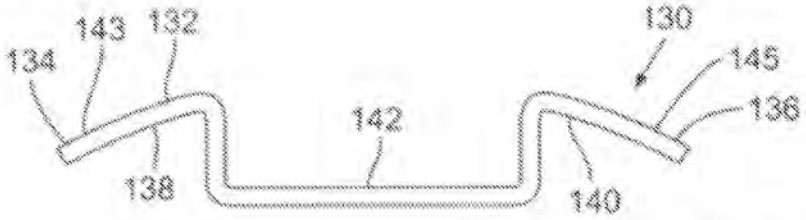

FIG. 8B

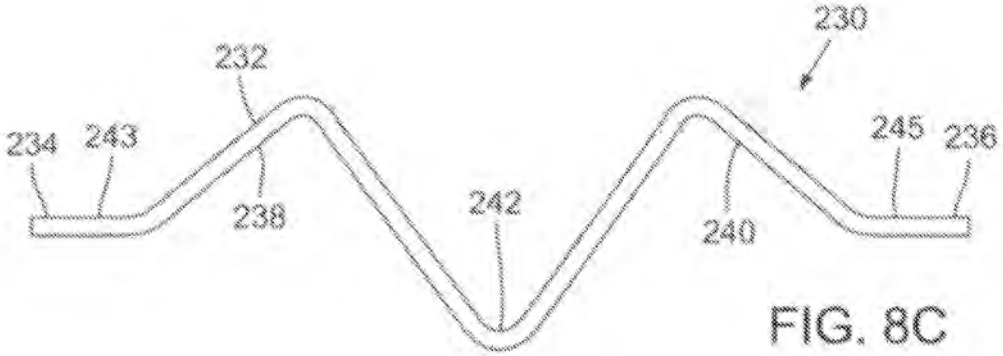

FIG. 8C

8.1.2 Encircling implant delivery systems and methods

International patent application published on the 18th December 2014.

Inventors: Toby Rogers, Robert J. Lederman, Merdim Sonmez, Dominique N. Franson and Ozgur Kocaturk.

Describes transcatheter devices and methods to encircle an anatomic structure (e.g. the heart) and deliver a circumferential device that can be tightened to impart compression to the anatomic structure resulting in geometric change.

(12) INTERNATIONAL APPLICATION PUBLISHED UNDER THE PATENT COOPERATION TREATY (PCT)

(19) World Intellectual Property Organization
International Bureau

(43) International Publication Date
18 December 2014 (18.12.2014)

WIPO | PCT

(10) International Publication Number
WO 2014/200764 A1

(51) International Patent Classification:
A61F 2/24 (2006.01)

(21) International Application Number:
PCT/US2014/040716

(22) International Filing Date:
3 June 2014 (03.06.2014)

(25) Filing Language: English

(26) Publication Language: English

(30) Priority Data:
61/834,357 12 June 2013 (12.06.2013) US

(71) Applicant: **THE UNITED STATES OF AMERICA, AS REPRESENTED BY THE SECRETARY, DEPARTMENT OF HEALTH & HUMAN SERVICES** [US/US]; National Institutes of Health, Office Of Technology Transfer, 6011 Executive Boulevard, Suite 325, Msc 7660, Bethesda, MD 20852-7660 (US).

(72) Inventors: **ROGERS, Toby**; Building 10, Room B1d219, 10 Center Drive, Bethesda, MD 20814 (US). **LEDERMAN, Robert, J.**; 3916 Underwood Street, Chevy Chase, MD 20815 (US). **SONMEZ, Merdim**; 4450 S Park Ave., Apt.1512, Chevy Chase, MD 20815 (US). **FRANSON, Dominique, N.**; Building 10, Room 2c713, 9000 Rockville Pike, Bethesda, MD 20892 (US). **KOCATURK, Ozgur**; 259 Congressional Lane, Apt. 312, Rockville, MD 20852 (US).

(74) Agent: **DUNCAN, Sandon, M.**; Klarquist Sparkman, LLP, One World Trade Center, Suite 1600, 121 Sw Salmon Street, Portland, OR 97204 (US).

(81) Designated States *(unless otherwise indicated, for every kind of national protection available)*: AE, AG, AL, AM, AO, AT, AU, AZ, BA, BB, BG, BH, BN, BR, BW, BY, BZ, CA, CH, CL, CN, CO, CR, CU, CZ, DE, DK, DM, DO, DZ, EC, EE, EG, ES, FI, GB, GD, GE, GH, GM, GT, HN, HR, HU, ID, IL, IN, IR, IS, JP, KE, KG, KN, KP, KR, KZ, LA, LC, LK, LR, LS, LT, LU, LY, MA, MD, ME, MG, MK, MN, MW, MX, MY, MZ, NA, NG, NI, NO, NZ, OM, PA, PE, PG, PH, PL, PT, QA, RO, RS, RU, RW, SA, SC, SD, SE, SG, SK, SL, SM, ST, SV, SY, TH, TJ, TM, TN, TR, TT, TZ, UA, UG, US, UZ, VC, VN, ZA, ZM, ZW.

(84) Designated States *(unless otherwise indicated, for every kind of regional protection available)*: ARIPO (BW, GH, GM, KE, LR, LS, MW, MZ, NA, RW, SD, SL, SZ, TZ, UG, ZM, ZW), Eurasian (AM, AZ, BY, KG, KZ, RU, TJ, TM), European (AL, AT, BE, BG, CH, CY, CZ, DE, DK, EE, ES, FI, FR, GB, GR, HR, HU, IE, IS, IT, LT, LU, LV, MC, MK, MT, NL, NO, PL, PT, RO, RS, SE, SI, SK, SM, TR), OAPI (BF, BJ, CF, CG, CI, CM, GA, GN, GQ, GW, KM, ML, MR, NE, SN, TD, TG).

[Continued on next page]

(54) Title: ENCIRCLING IMPLANT DELIVERY SYSTEMS AND METHODS

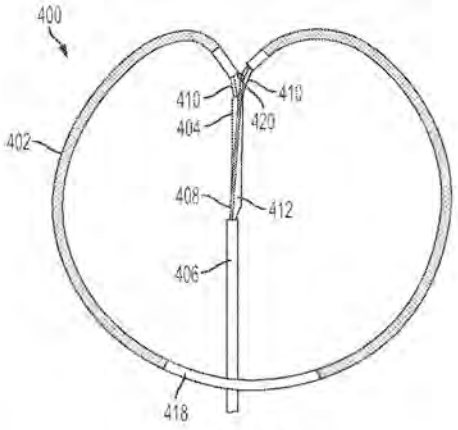

FIG. 14

(57) Abstract: Delivery devices for delivering encircling implants can include two separate limbs that are held together at a distal articulation by the implant being delivered. The implant can comprise a suture and/or a braided tube. The implant can extend through or over the limbs. The implant and at least a distal portion of the limbs can be compressible into a delivery shape that allows for advancement through the lumen of a delivery catheter. When the distal portion of the limbs move out of the delivery catheter, the limbs and implant can resiliently assume a loop shape that is complementary to a shape of a target around which the encircling implant is to be placed. The limbs are then retracted from along the implant to leave the implant in the desired delivery position. The delivery device can be used to place encircling implants around the heart or other targets, and the implant can be tightened to exert compressive force on the target.

WO 2014/200764 A1

Declarations under Rule 4.17:

— *of inventorship (Rule 4.17(iv))*

Published:

— *with international search report (Art. 21(3))*

ENCIRCLING IMPLANT DELIVERY SYSTEMS AND METHODS

RELATED APPLICATION

This application claims priority to U.S. Provisional Application No. 61/834,357, filed June 12, 2013, which is incorporated by reference in its entirety.

FIELD

This disclosure relates to devices and methods for delivering an encircling implant around an anatomic structure in the body.

BACKGROUND

Transcatheter procedures have enabled minimally invasive procedures that reduce morbidity, improve recovery time, and permit interventions to be performed on subjects who are not otherwise candidates for surgery. For example, transcatheter cardiovascular procedures have been widely used in recent years to perform angioplasty, place coronary artery stents, replace diseased or injured heart valves, and treat heart valve dysfunction by compressing the myocardial wall overlying the valve. However, advances in transcatheter procedures have been accompanied by challenges in developing technologies for remotely manipulating and modifying tissue and other objects within the body through the catheters.

One such challenge has been developing technology utilizing transcatheter procedures for encircling a target structure within the body with a continuous loop, such as a suture, such that the loop can be remotely tightened to compress the target structure around which the loop is positioned.

SUMMARY

Disclosed herein are delivery systems for delivering encircling implants through a catheter for placement around anatomical targets, such the heart or other organs. In some embodiments, the delivery systems can include two limbs that are held together at a distal articulation tip by the implant being delivered. The limbs can have separate proximal portions running through the catheter, or can be joined to form a single proximal portion running through the catheter. The implant can comprise a suture and/or a braided tube, for example, that is placed around the target structure for applying compressive force on the target structure. The implant can extend through or around the limbs of the delivery device during delivery. For example, in some embodiments an encircling suture implant runs through lumens of the limbs, while in other embodiments an

encircling tubular implant extends over the limbs. The implant and at least a distal portion of the limbs can be compressible into a delivery shape that allows for advancement through the lumen of a delivery catheter. When the distal portion of the limbs move out of the delivery catheter, the limbs can resiliently assume a predetermined loop shape that is complementary to a shape of a target around which the encircling implant is to be placed. The limbs can cause the implant to assume the similar loop shape. The limbs are then separately retracted from within or around the implant to leave the implant in the desired delivery position. In some embodiments, the implant can then be tightened to exert compressive force on the target. In embodiments having a tubular implant, a separate suture can run through the implant that can be tightened to apply compressive force to the implant and secure the implant around the target structure.

Some disclosed delivery devices for delivering a tubular implant include a guide having two resiliently deformable arms extending distally from a common proximal trunk and/or proximal portion that extends through the catheter and allows both arms to be retracted from within the tubular implant at the same time around opposite sides of the target structure. The tubular implant is folded in half during delivery with one half over one arm and the other half over the other arm, and with a fold or crease at a distal end bridging the gap between the distal ends of the two arms. The tubular implant can itself be resiliently deformable to help it unfold after being advanced out of the delivery catheter and assume the desired loop shape. The tubular implant can comprise a braided or woven material that allows the tubular implant to lengthen and shorten. The implant can comprise nitinol strands, for example, that form a braided tube that is resiliently deformable in the longitudinal shortening and lengthening directions, as well as in a manner that allows it to unfold and assume the desired loop shape. A suture or other cord can run through the braided tubular implant that can be tightened by pulling on a proximal end of the suture that extends through the delivery catheter. For example, the suture can include a slip knot or locking device adjacent to the two ends of the tubular implant that allows the looped portion of the suture passing through the implant to be adjusted in circumference. As the circumference of the suture loop is reduced, the tubular implant can tighten around the target and can reduce in length to prevent the implant from buckling or kinking. Further, the presence of the tubular material between the suture and the target tissue can prevent damage from the suture cutting into the tissue.

Some disclosed delivery devices for delivering an encircling suture implant include two separate hollow limbs that are held together at a distal articulation tip by the suture that is to be delivered. The suture extends through the hollow limbs which slide along the suture. At least a distal portion of the limbs is compressible into a delivery shape that allows the limbs to be

advanced through the lumen of a delivery catheter. As the distal portions of the limbs move out of the delivery catheter, the limbs cooperatively assume a loop shape that is complementary to the shape of a target around which the encircling suture is to be placed. The two limbs are then separately slid off opposite ends of the suture to leave only the suture in the desired delivery position while maintaining desired (for example constant) suture tension and position on the encircled structure. The delivery device can be used to place encircling sutures around an anatomic structure such as the heart or other organs, and the suture can be tightened to exert compressive force on the anatomic structure.

In some embodiments, a delivery device can include separate first and second delivery limbs linked at an articulation by a continuous flexible suture that is to be delivered and which extends through or around the first and second limbs to maintain the first and second delivery limbs together in an articulating relationship at an articulation tip. Each limb may include a proximal limb portion and a distal limb portion, and at least the distal limb portion of each limb is made of a material that is resiliently deformable into the delivery shape. When not deformed into the delivery shape the distal limb portions are configured to cooperatively form with a contralateral limb a loop that can be placed circumferentially around the portion of the target structure.

In some examples, the target structure is an anatomic or implanted structure in the body of a subject, for instance a target structure having a base portion connected to the body and a free portion over and around which the loop can be passed. In other examples, the target structure is a body organ, a portion of a body organ, or a surgically implanted device. Specific examples of target structures include a heart or atrial appendage, a cecal appendix, a gallbladder, a neoplasm, a uterus, a hemorrhoid, an uvula, an aneurysm, a transected blood vessel or other transected, folded or looped lumen, an intraocular crystalline lens or implanted intraocular lens or lens haptic, a urinary bladder, a kidney, a prostate or a foreign body. Targeted neoplasms particularly include examples such as polyploid or sessile neoplasms, for example colonic or nasal polyps.

The distal limb portions of the device can be cooperatively biased to assume a loop shape and size substantially complementary to the portion of the target structure around which the loop is to be circumferentially placed. The proximal limb portions of the first and second delivery limbs may be substantially parallel to one another in the delivery shape, and the distal limb portions may be substantially parallel to one another in the delivery shape. For example, the proximal and distal limb portions can be constrainable into the delivery shape by a lumen within a flexible delivery catheter though which the encircling suture is to be delivered to the target structure in the body. Delivery catheters can have a distal end for initial introduction into the body and an open proximal

end into which the delivery device is introduced and through which it may be controlled. The catheter may optionally have a tip that is capable of perforating tissue, or may be incorporated into or associated with a device (such as an endoscope) that has such capability. The catheter may be rigid or flexible or steerable (for example when incorporated into or otherwise associated with an endoscope).

In some embodiments, the limbs are flexible to conform to the shape of the lumen within the flexible delivery catheter, for example with the limbs parallel to one another within the confined space within the lumen. The proximal limb portions are able to maintain a substantially parallel relationship when only a distal portion of the proximal limb portions extend from the lumen, and the proximal limb portions may be connected together in at least one location to constrain their relative rotation and/or maintain them substantially parallel.

The suture has first and second terminal ends, and the suture may extend continuously through the delivery limbs within the percutaneous delivery device with the first and second terminal ends of the suture extending from an open proximal tip of the proximal limbs and/or the open proximal end of the delivery catheter. In another embodiment, the terminal ends of the suture emerge through an intermediate opening along each of the first and second delivery limbs (a "monorail" embodiment). The suture may be of any material that is sufficiently flexible and strong, such as fiber or wire, and can perform the intended function of the suture, such as tightening around and securing the target structure. In particular embodiments, the suture is capable of compressing the target structure, for example as a cerclage. The first and second delivery limbs are capable of being withdrawn from the suture, the catheter, and/or the body once the encircling suture is delivered around the target structure thereby leaving only the exposed suture encircling the target structure.

The loop is cooperatively formed by the distal limb portions when they are not deformed into the delivery shape, each distal limb portion forming substantially half of the loop, or each distal limb is symmetric or asymmetric with respect to its contralateral limb, or one or both distal limbs is semilunar, semi-ovoid, semi-circular, or substantially C-shaped, J-shaped, L-shaped, S-shaped, V-shaped or U-shaped. In some embodiments, the loop is substantially circular or cordiform and each distal limb portion forms a substantially semi-lunar or semi-cordiform shape joined at the articulation tip. The flexible distal limb portions cooperatively from geometric shapes, and the shape formed by each limb portion may be co-planar or not co-planar with the contralateral limb portion. The loop may extend at a predetermined angle with respect to a longitudinal axis of the proximal limb portion, for example by folding back toward the proximal limb portion.

Methods of use are also disclosed, such as methods of using the device to deliver an encircling suture around a target structure in a body through an elongated delivery catheter having a lumen, a proximal control end and a distal end. The delivery limbs are advanced through the catheter, articulated tip first, with the proximal and distal limb portions conforming to the delivery shape within the delivery catheter with the proximal and distal limb portions substantially conforming to the shape of the lumen of the delivery catheter. As the delivery limbs are further advanced the distal limb portions emerge from the lumen at the distal end of the delivery catheter, and the distal limb portions form the loop while at least a portion of the proximal limb portions are retained within the delivery catheter, for example in a substantially parallel relationship. The loop is then placed around the target structure to encircle it. The first and second delivery limbs may be individually or cooperatively moved to adjust the orientation of the loop with respect to the delivery catheter and the target structure to navigate or deliver the loop around the target. The first and second delivery limbs are then withdrawn over the suture and retracted into the delivery catheter to leave the now-exposed suture positioned and secured around the target structure. The suture can then be tightened around the target structure, for example to compress it. The delivery catheter can then be withdrawn from the suture delivery site or withdrawn entirely from the body.

The method can include introducing the catheter to the delivery site by a variety of methods. For example, the distal end of the delivery catheter can be introduced percutaneously or intraluminally into the body and the distal end of the delivery catheter then advanced to the target structure within the body. In some embodiments, the delivery catheter is inserted percutaneously through an introducer sheath into the body and advanced intravascularly through the inferior vena cava until the distal end of the delivery catheter penetrates the wall of the heart. The delivery limbs are then advanced out of the distal end of the delivery catheter until the distal delivery limbs form a loop that substantially conforms to the shape of a circumference of the heart. In a particular disclosed example, the loop assumes a pre-configured angle with respect to the proximal portions of the limbs, and the loop is advanced around the apex of the heart within the pericardial space, if the pericardium is intact, until the loop encircles the heart. The delivery limbs are then withdrawn proximally into the catheter to expose the suture which encircles the heart, and the suture is tightened by exerting tension on the terminal ends of the suture, for example to improve the function of a heart valve within the heart.

In some examples of the method, the distal end of the delivery catheter penetrates the heart through an atrial appendage, and the loop is configured to substantially conform to a circumference of a targeted atrial appendage of the heart. The loop is advanced around the atrial appendage within

the pericardial space, if present, until the loop encircles the targeted atrial appendage. Then the delivery limbs are withdrawn proximally into the catheter to expose the suture encircling the targeted atrial appendage and the suture is tightened by exerting tension on the terminal ends of the suture to exclude the targeted atrial appendage. Alternatively, the distal end of the delivery catheter approaches the heart by a trans-thoracic or sub-xiphoid path and the loop is advanced around the atrial appendage until the loop encircles the atrial appendage. Then the delivery limbs are withdrawn proximally into the catheter to expose the suture which encircles the atrial appendage and the suture is tightened by exerting tension on the terminal ends of the suture to tighten the suture and exclude the atrial appendage.

In alternative embodiments of the method, the distal end of the delivery catheter is inserted intraluminally into a body lumen or cavity and advanced to the target structure, for example through or otherwise in association with a laparoscope or bronchoscope. In some embodiments the body lumen is a gastrointestinal, genitourinary, vascular or respiratory lumen. Intraluminal embodiments may be introduced through an external body orifice (such as the mouth, nose or anus) instead of transcutaneously. However, a body cavity can also be entered through the skin, for example by insertion of a laparoscope though the abdominal wall into the peritoneum. Examples of other cavities into which the device may be introduced include the peritoneum, an anterior or posterior chamber of the eye, a gastrointestinal cavity, the pelvic cavity, a thoracic cavity, a uterine cavity, a urinary bladder, or a ventricle of the brain.

The device can be configured and used to perform a variety of transcatheter procedures such as the cardiovascular procedures discussed above. Other uses include grasping, retrieval, and/or repositioning of foreign bodies such as surgically implanted devices. The device can be used to introduce a protection or compression member to the target structure by advancing the compression member over the suture to a desired position with respect to the target structure. For example, when the target structure is the heart, and the compression device is advanced over the suture to a position on an external wall of the myocardium to exert pressure on its external wall to change a shape and function of a valve of the heart, such as a mitral or tricuspid valve. Alternatively, a protection device is advanced over the suture to a position on an external wall of the myocardium to bridge a coronary artery and avoid compression of the coronary artery when the suture is tightened around the heart. In yet other applications, the target structure is the right ventricular outflow tract or main pulmonary artery.

Methods are also disclosed for making a device for transcatheter delivery of a continuous flexible encircling suture around a circumference of a target structure within a body of a subject.

First and second delivery limbs are linked at an articulation by placing the suture through or around the first and second limbs to maintain the first and second delivery limbs together in an articulating relationship at an articulation tip. Each limb includes a proximal and distal limb portion. Each proximal limb portion has a delivery shape for advancement through a lumen, and each distal limb portion is resiliently deformable into the delivery shape. However the distal limb portion forms a portion of a loop when not deformed into the delivery shape, and the two distal limbs in the delivery position cooperatively form a loop that can be placed circumferentially around the target structure. The articulation tip may be introduced into a catheter lumen of a flexible catheter, and advanced distally within the catheter lumen until the proximal and distal limb portions are both compressed into a substantially linear delivery shape for advancement through the catheter to the target location.

The foregoing and other features and advantages of the invention will become more apparent from the following detailed description of a several embodiments which proceeds with reference to the accompanying figures. This summary of the description is intended as a summary of multiple specific embodiments of the device and method for the convenience of the reader, and are not to be construed as limitations of the claims or delineation of any essential elements.

BRIEF DESCRIPTION OF THE FIGURES

FIG. 1 is a view of the hollow limbs of the delivery device extending from the open distal tip of a delivery catheter, with the distal limbs assuming a preformed configuration that forms a loop for placement around a target structure.

FIG. 2 is an enlarged view of the articulation tip of the device of FIG. 1, with the arrow indicating the suture extending through the interior of the distal limbs and being exposed only at the articulation tip. The free terminal ends of the suture are shown emerging from the open proximal tip of the catheter; the catheter is shown schematically shorter than in actual use.

FIG. 3 is a view of the limbs retracted into the delivery catheter with only the articulation tip extending from the open distal tip of the delivery catheter, and illustrating how the assembly collapses for transcatheter delivery.

FIG. 4 is a view of an assembled embodiment of the delivery device in which the delivery catheter is a 7 French (F) introducer sheath having a hollow shaft through which the delivery limbs are advanced to deliver the suture loop, which is shown at the right margin of the figures.

FIG. 5 is an enlarged view of the atrial appendage illustrating the initial deployment of the limbs through the catheter that extends through the right atrial appendage into the pericardial space.

An introducer sheath passes from the right atrial appendage into the pericardial space. Through this introducer sheath the device is advanced in a folded or constrained state into the pericardial space for deployment. Both limbs and the suture-articulation are shown in the drawing.

FIG. 6 and 7 show a view of the heart and illustrate deployment of the limbs by further advancement of the articulation tip out of the catheter to allow both distal limbs to assume their preconfigured and unconstrained loop configuration, and advancement of the loop along the external wall of the heart and over the apex to encircle the heart. The preformed shape of the limbs allows it to surround the target structure (in this case the heart) and further be manipulated to its targeted position (in this case the atrioventricular groove).

FIG. 8 shows the partial retraction of the limbs over the suture to leave the exposed suture in the desired position around the heart along the path defined by the placement of the limbs around the heart. The suture is maintained at a desired (for example constant) tension as the limbs are retracted from the suture to maintain the suture in the desired position. This allows the suture to be positioned precisely in the target position. After the limbs are fully withdrawn, the desired tension can be fixed on this suture using a tension fixation mechanism such as a separate device or knot.

FIG. 9 schematically illustrates a top and side view of an embodiment of the delivery system in which the distal limbs are cooperatively configured to form a circular loop when the distal limbs are not compressed into a substantially parallel and linear delivery shape; the proximal limbs are shown secured together at a fixation point and with the proximal limbs substantially linear and parallel. The suture to be delivered extends through the delivery limbs, joins them at the articulation, and has free ends that extend from the open proximal tip of the limbs.

FIG. 10 is a view similar to FIG. 9, but with distal limbs that are cooperatively configured to form a non-circular loop in which the two halves of the loop formed by the distal limbs are mirror images of one another. The loop has both arcuate and relatively flattened portions.

FIG. 11 is a view similar to FIG. 10, but with distal limbs that are cooperatively configured to form an oblong loop in which the two limbs of the loop are asymmetric with respect to one another and generally extend perpendicular to the longitudinal axis of the proximal limbs.

FIG. 12 is an embodiment which is similar to the device of FIG. 9, but the sutures emerge from a limb opening in an intermediate portion of each limb instead of from the proximal tip of the limbs.

FIGS. 13 and 14 shows an alternative delivery system that includes an interrupted rigid loop having two arms, a suture, and a braided tubular implant positioned around the rigid loop and the suture.

FIG. 15 is an enlarged view of the atrial appendage illustrating the initial deployment of the delivery system of FIG. 14 through the right atrial appendage into the pericardial space.

FIGS. 16-18 show the heart and illustrate deployment of the rigid loop and implant from the delivery catheter such that they assume their preconfigured and unconstrained loop configuration, and advancement of the loop over the apex of the heart to encircle the heart. The preformed shape of the loop allows it to surround the target structure (in this case the heart) and further be manipulated to its targeted position (in this case the atrioventricular groove). FIG. 17 shows an enlarged portion of the loop, showing the rigid arms and suture within the tubular implant.

FIGS. 19 and 20 show retraction of the rigid arms from within the tubular implant to leave the implant and suture in the desired position around the heart.

FIG. 21 shows the implant and suture in place around the heart after the rigid arms have been withdrawn. A desired tension can be applied to the implant by the suture using a tension fixation mechanism such as a separate device or a slip knot. The implant can have a braided structure that allows it to shorten when tension is applied without buckling or "cheese wiring" of the heart tissue.

FIGS. 22A-F are MRI images showing views of the heart anatomy before and after an encircling implant is applied around the heart.

FIGS. 23A and 23B illustrates geometric changes in the heart resulting from placement of the encircling implant.

FIG. 24 is a chart showing tension vs. tricuspid annular geometry relationships in test pigs.

FIG. 25A-D shows coronary arteries and coronary sinus angiography following annuloplasty with an encircling suture. FIG. 25E shows an exemplary protective member that can be placed along an encircling implant to bridge over a vessel or other sensitive part of the target structure.

FIGS. 26-28 show examples of compressive members that can be placed along an encircling implant to apply local compressive forces on the target structure.

DETAILED DESCRIPTION

Explanation of Terms and Embodiments

Unless otherwise noted, technical terms are used according to conventional usage. In order to facilitate review of the various embodiments of the disclosure, the following explanation of terms is provided:

"Annuloplasty element" refers to a device that induces reshaping of an annulus of the heart to repair valvular insufficiency. Such devices include those that are placed in the atrioventricular

groove of the heart and exert their action by compressive forces on the annulus, for example by expansion of a resilient annuloplasty element, or placement of the annuloplasty element under tension, as in cerclage annuloplasty.

A "catheter" is a thin tube typically made of medical grade materials that can be inserted into the body to diagnose or treat disease or perform a medical/surgical procedure. Catheters can be modified to tailor them for cardiovascular, urological, gastrointestinal, neurovascular, ophthalmic and other applications. Catheters can be inserted into any body cavity or lumen, for example over a guide wire or through an introducer sheath. Some catheters may be made of a flexible material and/or have multiple lumens through which different instruments or therapeutic agents can be introduced. The catheter can function independently of or be incorporated into other instruments, such as a flexible endoscope. Endoscopic devices include endoscopes for introduction into the gastrointestinal tract (EGD, enteroscopy, colonoscopy, sigmoidoscopy), respiratory tract (rhinoscopy, bronchoscopy), ear (otoscopy), urinary tract, female reproductive system, abdominal or pelvic cavity (laparoscopy), interior of a joint (arthroscopy), organs of the chest (thoracoscopy and mediastinoscopy), the amnion (amnioscopy), fetus (fetoscopy), epidural space (epiduroscopy), and the eye (as in retinoscopy). The catheter may be inserted separately along with the endoscope, for example by being attached to the endoscope, or be incorporated into the endoscope as a separate lumen within the flexible tube that also contains the endoscope.

The term "compression member" refers to an element that is designed to cooperate with the tensioning element to apply a desired force to an area along the path of the tensioning element. The compression member may be designed to provide a greater force to the area than would be applied by the tensioning element alone.

The term "comprises" means "includes without limitation." Thus, "comprising A and B" means "including A and B" without excluding additional elements.

"Contralateral" refers to a corresponding part on an opposite side. In anatomy, the terms "ipsilateral" and "contralateral" typically refer to opposing portions of a corporeal lumen having symmetric right and left sides.

A "device for tricuspid valve annuloplasty" refers to a device that induces reshaping of an annulus of the heart's tricuspid valve to repair valvular insufficiency. Such devices include those that are placed in contact with the annulus of the triscuspid valve, and include those that exert their action by compressive forces on the annulus, such as by placing a flexible annuloplasty member under tension, as in cerclage annuloplasty.

The terms "distal" and "distally" refer to a location or direction that is, or a portion of a device that when implanted (for example placed within a blood vessel) is further downstream or farther away from the point of insertion. The terms "proximal" and "proximally" refer to a location or direction that is, or a portion of a device that when implanted, or placed within the blood vessel, is further upstream or closest to the point of insertion.

A "flexible member" refers to an element that is sufficiently flexible to be introduced into the body, generally as or through a catheter, and manipulated along a desired path within the body, such as in and around the patient's heart. One example of such a flexible member is a "guide wire" of a conventional catheter. The guide wire also can deliver energy to augment its ability to penetrate tissue, for example by puncturing it, delivering radiofrequency ablative energy or by delivering laser ablative energy.

"Guide wire" refers to a simple guide wire, a stiffened guide wire, or a steerable guide-wire catheter that is capable of puncturing and/or penetrating tissue. The guide-wire also can deliver energy to augment its ability to penetrate tissue, for example by puncturing it, delivering radiofrequency ablative energy or by delivering laser ablative energy. These are examples of a "penetrating device," which is a device capable of penetrating heart tissue, such as the myocardium.

A "mitral valve cerclage annuloplasty" refers to an annuloplasty procedure in which a tensioning element is placed around the heart, for example through or over at least a portion and preferably all of the coronary sinus, so that the circumferential tension is delivered around the mitral valve annulus and so that a tensioning element can be placed under selective degrees of tension to perform the annuloplasty. An example of cerclage annuloplasty is disclosed in U.S. Patent Publication No. 2005/0216039, which is incorporated herein by reference. However, mitral valve cerclage annuloplasty techniques also include other cerclage trajectories.

Components of the device disclosed herein can be made of an "MRI-compatible" material. Such materials are safe to use in the body during magnetic resonance imaging of the body, and do not substantially affect imaging quality of the MRI. An "MRI-safe" material is one that does not add substantial risk to a human or equipment by placing it in the magnetic field of an MR environment. Examples of MRI-compatible materials are non-ferrous materials, such as ceramics, plastics and non-magnetic composite materials. Austenitic stainless steels (of the 300 series) are neither ferromagnetic nor paramagnetic and therefore are MRI-compatible. Titanium and aluminum are MRI-compatible, even though they are not ideally paramagnetic. Particularly disclosed MRI-compatible materials of which the protective device may be made include nitinol, MP35N and cobalt-chromium alloys.

The term "protection member" refers to an element that is designed to cooperate with the tensioning element to provide a protected space to a blood vessel or other vital structure along the path of the tensioning element. In general, the protection member is designed so that the blood vessel or vital structure within the protection member experiences less force from the tensioning element than is exerted at adjacent areas at either end of the protection member.

A "shape memory" material has the ability to return from a deformed shape (temporary shape) to its original (permanent) shape in response to a trigger, such as a physical or thermal trigger, for example release of the material from physical constraint within a catheter lumen. Shape memory materials are typically made of alloys or polymers. In specific examples, the material is a superelastic nickel-titanium alloy such as nitinol or a nickel-chromium alloy such as inconel.

As used herein, the term "suture" or "ligature" is meant to encompass any suitable cord-like material and is not limited to only twisted strands, fibers of plastics. A suture is not used in the limited sense of a material that is moved through tissue on a surgical needle to penetrate tissue, but instead more broadly encompasses sutures that are used to encircle and/or compress an organ (as in cerclage of the uterus, ligation of a duct, or mitral or tricuspid annuloplasty of the heart). Both of the terms "suture" and "ligature" include metal and non-metal materials, wire or non-wire materials, natural and synthetic materials, absorbable and non-absorbable that are suitable for ligation or placement of tension or compression on a target structure within the body of a subject. In some embodiments, the suture is a thin and elongated cord. An example of a wire suture or ligature is an annuloplasty wire while examples of non-wire sutures are those made of catgut, silk, polyester, polyglycolic acid, polylactic acid, polydioxanone, nylon, and polypropylene. A variety of suture materials are supplied under names such as ETHILON, MONOCRYL, PROLENE, or VICRYL. Wire sutures are typically made of stainless steel, and can be similar to those used for orthopedic surgery or sternal closure.

"Target structure" includes both biological and non-biological materials. A biological target structure is made of biological tissue, for example an anatomic structure in the body of a subject. Such anatomic structures preferably have a base portion connected to the body and a free portion over and around which the loop can be placed. Examples of the target structures are a body organ, a portion of a body organ, or a surgically implanted device. Anatomic target structures include a heart or atrial appendage, a cecal appendix, a gallbladder, a neoplasm, a uterus, a hemorrhoid, an uvula, an aneurysm, a transected blood vessel or other transected, folded or looped lumen, an intraocular crystalline lens, a urinary bladder, a kidney, or a prostate gland. Targeted neoplasms particularly include examples such as a polyploid or sessile neoplasm. Examples of a non-

biological target structures are items that have been surgically or accidentally introduced into the body, such as a projectile or a displaced surgical implant.

"Tensioning material" is any material suitable to place compression on an object (such as an organ) around which it is looped. For example, the tensioning material may be suture that is wrapped around the uterus to perform a B-Lynch procedure to mechanically compress an atonic uterus and stop postpartum hemorrhage, or a mitral or tricuspid valve cerclage annuloplasty, in which an encircling material is placed under tension to remodel the mitral valve annulus.

Unless otherwise explained, all technical and scientific terms used herein have the same meaning as commonly understood by one of ordinary skill in the art to which this disclosure belongs. The singular terms "a", "an", and "the" include plural referents unless context clearly indicates otherwise. The term "comprising A or B" refers to a single element of stated alternative elements or a combination of two or more elements, unless context clearly indicates otherwise. For example, the phrase "rtMRI or echocardiography" refers to real-time MRI (rtMRI), echoradiography, or both rtMRI and echocardiography. Although methods and materials similar or equivalent to those described herein can be used in the practice or testing of the present disclosure, suitable methods and materials are described below. In case of conflict, the present specification, including terms, will control. In addition, the materials, methods, and examples are illustrative only and not intended to be limiting.

Exemplary Encircling Implant Delivery Systems and Methods

One exemplary embodiment of an encircling implant delivery device is shown in FIGS. 1-3, which depict a device 30 for delivering an encircling continuous flexible suture, wire, strip, cord, tube, line, or other encircling implant (referred to herein generally as suture 32) around a portion of a target structure (not shown) in a subject's body. The illustrated device 30 includes an elongated, flexible tubular delivery catheter 34 (FIG. 2) having a continuous lumen that begins at a proximal open tip 36 for controlling the catheter and terminates at an open distal delivery tip 38 that is suitable for introduction into the body. The catheter is made of a biocompatible material, and may for example be a flexible cardiovascular catheter that can be introduced over a guide wire and/or through a guide sheath. Within catheter 34 are separate first and second delivery limbs or arms 40, 42 maintained in an articulating relationship at an articulation tip 44 (FIGS. 1 and 2) by suture 32 that extends through first and second delivery limbs 40, 42. The terms "limb" and "arm" are used interchangeably herein. Since delivery limbs 40, 42 are not otherwise joined to one another by a coupling at the tip 44, limbs 40, 42 can slide freely along suture 32 toward or away from one

another. Hence limbs 40, 42 are capable of being folded together substantially parallel to one another while sliding through catheter 34, but are capable of articulating with respect to one another once they emerge from distal tip 38 of catheter 34. In other embodiments, the delivery limbs 40, 42 can have distal ends that join with a common trunk and/or proximal portion that extends through the catheter, these portions together comprising a guide for delivering the implant.

Although suture 32 can be made of any of the variety of materials previously discussed, the illustrated suture 32 is made of wire material, such as wire suture of the type used as a ligature in coronary sinus annuloplasty procedures. The suture 32 has first and second free terminal ends (FIG. 2) extending from proximal tip 36 of delivery catheter 34. Between the first and second free terminal ends, the suture 32 extends continuously in a loop through limbs 40, 42 and within delivery catheter 34.

Each limb 40, 42 includes a proximal limb portion 40a, 42a (FIG. 1) and a distal limb portion 40b, 42b. The proximal and distal limb portions can be made of the same or a different material, and in the illustrated embodiment are made of the same material, which in this example is a nitinol hypotube. However, other elastic or superelastic materials can be used. Proximal limb portions 40a, 42a have a longitudinal shape that can conform to the shape of the lumen of the delivery catheter. They are contained in substantially parallel relationship within the lumen as they move through the lumen and can continue to maintain that relationship even after the proximal limb portions 40a, 42a partially emerge from catheter 34, as shown in FIG. 1. Proximal limb portions 40a, 42a can be connected together in at least one location (for example by a collar, as discussed later in association with FIGS. 9-12) to constrain rotation of the first and second delivery limbs with respect to one another.

Flexible distal limb portions 40b, 42b are resiliently deformable into a substantially parallel delivery shape to extend along the longitudinal axis of the flexible delivery catheter (FIG. 3), but assume the shape of a loop (FIG. 1) cooperatively formed by the flexible distal limb portions 40b, 42b when they are not deformed into the delivery shape. For example, limbs 40, 42 (or at least distal limb portions 40b, 42b) can be made of a shape-memory material that is deformable into the parallel delivery shape that conforms to the path of the catheter, but when not constrained by the walls of the lumen distal limb portions 40b, 42b cooperatively form the loop. The loop shape can be preselected and preconfigured to assume a shape and size substantially complementary to a feature of the target structure. In the illustrated embodiment of FIGS. 1-2, the loop assumes the shape of a cross-section of the heart around the atrioventricular groove of the heart.

FIG. 4 illustrates another exemplary delivery device comprising a rigid metal tube or needle 54 extending distally from a proximal hub 46. The limbs of this delivery device have been independently retracted into and through the tube or needle 54, so that the remaining suture 32 forms loop 60. This delivery device can be used for surgical or percutaneous delivery methods, for example.

Returning to the embodiment of FIGS. 1-3, an exemplary method of delivery for a suture encirclement procedure can include the following steps, with reference to FIGS. 6-8. A guide wire can be introduced into a vein (such as the femoral vein) and advanced through the interior vena cava 18 to the right atrial appendage 12 of the heart 10, such as under fluoroscopic guidance. The wire can then pierce through the right atrial appendage 12 and into the pericardial space if the pericardium is present. An introducer sheath is advanced over the guide wire into the pericardial space, and contrast material can be injected into the pericardial space through a lumen of the catheter to visualize the cardiac contours. Catheter 34 is then advanced through the introducer sheath until distal tip 38 is also extending out of the right atrial appendage 12 and into the pericardial space.

FIG. 5 is an enlarged view of the atrial appendage 12. The catheter 34 has been advanced through the wall of the atrial appendage 12 to introduce the distal tip of the catheter into the pericardial space. The distal limbs 40b, 42b can then be deployed by withdrawing catheter 34 from the pericardial space to unsheathe distal limbs 40b, 42b. Alternatively, once the catheter is in place, the articulation tip 44 of the distal limbs 40b, 42b can be advanced out of the open catheter tip in the direction shown by the arrows in FIG. 5. As the distal limbs advance out of the catheter, they begin to move apart from their parallel delivery configuration toward their unconstrained configuration predetermined by the shape memory material of which they are made.

FIGS. 6 and 7 show the heart 10 with the apex 14 of the heart pointed toward the right. As the distal limbs 40b, 42b are further deployed from the catheter 34, they move farther apart to their unconstrained configuration predetermined by the shape memory material. As shown in FIG. 6, the two distal limbs articulate farther part at the articulation tip 44 where the ends of the distal limbs are held together by the continuous suture 32 that extends through the limbs. As the limbs articulate apart at the articulation tip, they also spread the suture contained within the limbs. Advancement of the distal limbs moves the articulation tip toward the apex 14 of the heart (FIG. 7) and over it.

As articulation tip 44 of the limbs is unsheathed by catheter 34, the shape memory material begins to spread distal limbs 40b, 42b apart (FIG. 6) to a maximum angle α (FIGS. 1 and 2), such

as approximately 50-55 degrees in one embodiment. In this particular embodiment, each distal limb 40b, 42b assumes an arcuate or semi-lunar shape, with each limb a mirror image of the other, as shown in FIG. 1. Each of the illustrated semi-lunar shapes can be planar, and the planes defined by each of distal limbs 40b, 42b may either be co-planar or at a non-coplanar angle to one another. The arcuate segment formed by each distal limb 40b, 42b begins at a junction between the proximal and distal limb portions and the arcuate segments end at or adjacent the articulation tip of the delivery limbs. The distal limb portions 40b, 42b are retained in the articulating relationship solely by the suture 32 to be delivered that extends through the limbs and spans a gap 44 between the distal limb portions.

As shown in FIGS. 7 and 8, the shape memory material is configured in its unconstrained configuration so that the plane of the loop defined by the distal limbs bends toward the catheter 34 and the proximal limbs to promote movement of the loop over the apex 14 of the heart and along the external wall of the heart contralateral to the wall along which the loop was advanced in FIG. 6.

Distal limbs 40b, 42b can comprise a resilient elastic or superelastic material that is configured to deflect back toward the delivery catheter 34 as the distal limbs emerge from the distal delivery end of the delivery catheter 34, as shown in FIGS. 6 and 7. During this deflection, distal limbs 40b, 42b move (within the pericardium if it is present) down toward the apex 14 of the heart and past it to then encircle a circumference of the heart 10 (FIG. 7). Distal limbs 40b, 42b can be positioned around the heart substantially in its atrioventricular groove 16 is some procedures, such as for an annuloplasty procedure.

Once the limbs 40b, 42b are in a desired target position, such that the limbs and the suture 32 that are contained therein encircle the heart, which can be confirmed by fluoroscopy, the limbs 40, 42 are withdrawn over the suture 32 through catheter 34 by sliding limb 40 towards one proximal terminal end of the suture and sliding limb 42 towards the other proximal terminal end of the suture (FIG. 8). The separate limbs are removed from opposite terminal ends of the suture to leave only cerclage suture 32 encircling the heart 10. The arrows in the FIG. 8 illustrate partial retraction of each limb over the suture back into the catheter 34. The limbs are retracted by manipulating their proximal ends which may be external to the introduction site of the catheter into the body. The limbs can be retracted separately or in tandem, but in the illustrated embodiment of FIG. 8 the two proximal limbs are tethered together so that they are retracted in unison by the operator pulling on them so they slide over the suture. As the distal limbs retract into the catheter, their distal ends move apart from the articulation tip 44 to incrementally expose the suture 32 that

they are delivering. As the limbs continue to be retracted, they completely expose the suture 32 such that the suture is left in the same position that the distal limbs occupied before their retraction. After the limbs have been retracted from the suture, the proximal free ends of the suture are then tied or otherwise joined together to retain the suture loop in the final delivery position.

The orientation of the loop with respect to catheter 34 can be controlled by moving one or both of limbs 42, 44. For embodiments in which limbs 42, 44 are secured together by a collar or other connector, limbs 42, 44 can be rotated within catheter 34 to change the plane(s) of deployment of the loop. If limbs 42, 44 are not connected together, they can be rotated independently of one another to selectively alter the angle between the plane of each half of the loop.

Once the limbs have been retracted to leave the suture 32 positioned around the target structure, tension can then applied to suture by pulling the free terminal ends of the suture, such as to compress the heart along the atrioventricular groove 16. In some embodiments, a slip knot can be used to tighten the suture loop by pulling on only one end of the suture. The suture 32 can be tied either by a locking mechanism (similar to a drawstring toggle) or a simple surgical knot. The free ends of the suture 32 proximal to the locking mechanism or knot can then be cut with a cutting device.

Although the disclosed encircling suture devices have been described in connection with the encirclement of the heart, the devices can be used to encircle a variety of target structures. The distal limb portions that form the loop can be pre-configured to assume a shape and size substantially complementary to a circumference or other feature of the target structure around which the loop is to be circumferentially or otherwise navigated or placed. Examples of the target structure are a body organ, neoplasm, or surgically implanted device. Even more particular examples are a heart or atrial appendage, cecal appendix, gallbladder, neoplasm such as a polyp, uterus, hemorrhoid, uvula, aneurysm, transected, folded or looped blood vessel or other lumen, intraocular crystalline lens or implanted intraocular lens or lens haptic, urinary bladder, kidney, prostate or foreign body.

Another exemplary encirclement suture delivery device 58 is shown in FIG.9, wherein delivery device 58 includes tubular proximal limbs 60a, 62a and tubular distal limbs 60b, 62b. Terminal ends 64, 66 of a continuous suture extend from the proximal open tips of limbs 60a, 62a. The suture extends across a gap between the open distal tips of limbs 60b, 62b to provide an articulation 68 around which limbs 60b, 62b articulate or pivot with respect to each other. This articulation can be in any direction and is not constrained by a hinge or other similar joint that

physically connects limbs 60b, 62b. In this specific example, limbs 60b, 62b each form a mirror image, symmetric half of loop 70 for delivering the suture that extends continuously through the tubular delivery device. The halves of the loop are generally symmetric with respect to articulation 68 and a fixation 72 that fixes limbs 60a, 62a together. As shown in the FIG. 9 side view, circular loop 70 is formed in a flat plane that extends at an angle β of about 120 degrees to the plane through limbs 60a, 62a. This arrangement permits the suture within the delivery device to be looped around the target structure in an orientation that is not an extension of the longitudinal axes of limbs 60a, 62a. Limbs 60a, 60b are joined at a fixation that joins the limbs together. The fixation 72 can be, for example, a weld, collar or adhesive that joins limbs together so they move together as they are being pulled off the suture that they are delivering. When the limbs are removed by pulling them off terminal ends 64, 66 of the suture, the suture remains around the target structure at the desired angular orientation.

FIG. 10 depicts yet another embodiment of the invention that is similar to that shown in FIG. 9, and in which corresponding parts have been given the same reference numbers as in FIG. 9 plus 100. This embodiment differs in that loop 170 is generally ovoid in shape instead of circular. Although limbs 160b, 162b still form mirror image, symmetric halves of loop 170, which extends at an angle β to the longitudinal axes of limbs 160a, 162a, loop 170 is not circular. It is instead ovoid or oblong, with each half of loop 170 being somewhat U-shaped or V-shaped. Although the halves of loop 170 are symmetric with respect to each-other, they are not themselves symmetric. In the depicted example, each half of the loop has a generally flat portion and an arcuate portion. The flat and arcuate portions meet at a vertex. In other embodiments, each half of the loop can be the shape of a form having a closed base and open arms, such as a C, J, L, or S-shape.

FIG. 11 shows yet another embodiment with an elongated or oblong loop, similar to FIG 10, and wherein like parts have been given like reference numbers plus 100. However, in this example limbs 260b, 262b do not forms halves of loop 270 that are symmetric mirror images of one another. Instead limb 260b forms a hemi-ovoid shape and limb 262b is generally straight or only slightly curved. This pre-configured shape, formed by the shape-memory materials of limbs 260b, 262b when not collapsed to the delivery shape in the lumen of the delivery device, provides a loop 270 that folds to one side of (to the right) of limbs 260a, 262a.

FIG. 12 depicts a monorail embodiment of the delivery device similar to FIG. 11, wherein like parts have been given like reference numbers plus 100. In this example, the suture to be delivered extends through limbs 360b, 362b and through only a portion of limbs 360a, 362a. The suture emerges through ports 380a, 380b that are respectively located in an intermediate portion of

limbs 360a, 362a that allow the suture to emerge more distally on the delivery device than in the embodiments of FIGS. 9-11 in which the suture emerges from the open proximal tip of each limb. As a result, the limbs ride like a monorail over the suture, and the total length of the suture can be reduced.

FIG. 14 shows another exemplary encircling implant delivery device 400, and FIG. 13 shows elements of the device 400 disassembled. The device 400 is configured to deliver a tubular implant 402 around the anatomical target. The device 400 also includes a resiliently deformable guide 404 (FIG. 13), a catheter 406, and a suture or other cord 408. The guide 404 includes two distal arms 410 extending from a common trunk 412 and a proximal portion 414 extending through the catheter 406. The arms 410 form a natural loop configuration (FIG. 13) when not deformed such that free ends of the two arms are adjacent each other but not attached, forming a break or gap 416 in the loop between the free ends of the arms. The tubular implant 402 is positioned over the arms 410 such that a central portion 418 of the tubular implant bridges the gap 416 and the two ends of the tubular implant are adjacent to the trunk 412 (FIG. 14). The suture 408 includes a loop that extends through the tubular implant 402 and a proximal strand that extends from the loop at joint 420, and extends through the catheter 406.

For delivery into a patient's vasculature, the implant 402, guide 404, and suture 408 are deformed and contained within the catheter 406 in a straightened configuration. While contained within the catheter 406, the arms 410 are resiliently deformed to extend distally in parallel in front of the trunk 410, with the gap 416 allowing the distal ends of the arms to be pointed distally side-by-side. The tubular implant is folded at the central portion 418 such that the central portion spans across the two distal ends of the arms 410 and the two ends of the tubular implant 402 extend proximally from the central portion 418 over the arms 410 in parallel within the catheter 406. The suture 408 extends through the folded tubular implant 402 in the same elongated configuration.

The tubular implant 402 can comprise any sufficiently strong, flexible, and biocompatible material to allow it to be implanted around a target structure and desirably tensioned. In some embodiments, the tubular implant 402 comprises a braided or woven material, while in other embodiments the tubular implant can comprise non-braided, non-woven continuous tube. In some braided or woven embodiments, tubular member 402 can be configured to be compressible and/or elongatable in the longitudinal direction of the implant, such as in order to accommodate reduction in the circumference around the target structure as the implant is tightened around the target structure. In some embodiments, the length of the tubular implant can be shortened by 50% or more relative to its length in a natural configuration. Such variability in length can allow the

tubular implant 402 to avoid buckling or kinking when it is tightened around the target structure. In some embodiments, as the length of the tubular implant 402 is shortened, the diameter of the tubular implant can increase in a corresponding manner, while in other embodiments, the diameter of the implant can remain substantially constant as the length changes. In some embodiments, the diameter of the tubular implant in its natural configuration can be about 2-5 mm, such as about 2-3 mm. In some embodiments, the tubular implant 402 can comprise a superelastic and/or shape memory material, such as braided nitinol, which can provide the implant with resilient deformability and help it to return to a natural shape (e.g., the shape shown in FIG. 14) when it is released from the delivery catheter 406, and can allow the implant to re-lengthen from a compressed state if tension around the target structure is released. The central portion 418 of the tubular implant can comprise a readily bendable and foldable tubular section that allows the central portion 418 to be folded 180 degrees while it is positioned within the delivery catheter.

The guide 404 can comprise any semi-rigid, resiliently deformable material, such as an elastic or superelastic metal, such nitinol. The arms 410 and other portions of the guide 404 can comprise solid rods, as they need not allow passage of another object within them. The suture 408 and the arms 410 can extend in parallel through the tubular implant 402. In other embodiments, the arms 410, trunk 412, and/or proximal portion 414 of the guide 404 can be tubular. In such embodiments, the suture 408 can extend through the tubular portions of the guide 404.

In the illustrated embodiment, the suture 408 extends alongside the arms 410 within the tubular implant 402 and joins at a knot or a sliding-locking device 420 near the juncture of the arms 410 and the trunk 412, with a proximal strand of the suture extending alongside the trunk and proximal portion 414 of the guide. The joint 420 can comprise a sliding Roeder's knot, or a slip knot, a device that allows for tightening and/or locking, or other adjustable feature that allows the circumference of the loop portion of the suture within the tubular implant 402 to be adjusted. For example, one end of the suture can include a knot or device at 420 and the suture can extend from the knot or device 420 around the circumference of the implant 402, through the knot or device 420, and extend proximally to a second end of the suture, similar to as shown in FIG. 14. In such embodiments, the single proximal end 408 of the suture can be pulled through the knot or device 420 to reduce the circumference of the loop portion of the suture, thereby tightening the implant around a target structure. In alternative embodiments, the suture can extend from one proximal end, with an intermediate loop portion extending through the tubular implant 402, and back to a second proximal end running parallel with the first proximal end. In such embodiments, both ends

of the suture can pass through a knot or device at 420 that allows for tightening of the intermediate loop portion by pulling on either or both of the proximal ends of the suture.

FIGS. 15-21 show an exemplary delivery method with the device 400, wherein the tubular implant 402 is implanted around the heart 10 at or near the atrioventricular groove 16 of the heart. FIG. 15 shows the catheter 406 extending through an aperture in the right atrial appendage 12 and into the intrapericardial space. The delivery device 400 can be introduced through any portion of the venous system, such as through the inferior vena cava 18, and then through the right atrial appendage 12. As shown in FIG. 15, the tubular implant 402 is advanced distally out of the catheter 406 in a folded configuration with the central portion 418 leading. The arms 410 of the guide 404 are positioned within each parallel half of the implant 402, though not visible in FIG. 15.

FIG. 16 shows the implant 402 being further deployed from the catheter 406 such that the implant and arms 410 within the implant begin to resiliently return to the configuration shown in FIG. 14. As shown, the distal end of the implant 420 recoils down and around the apex 14 of the heart as the implant expands apart to form a loop shape. The resilient nature of the arms 410 and/or the resilient nature of the tubular implant 402 (e.g., either or both can comprise nitinol or the like) can facilitate the motion of the implant shown in FIG. 16 and 18.

FIG. 17 is a partially broken-away view of the central portion 418 of the tubular implant 402, showing the distal ends of the two arms 410 positioned within the implant and spaced by 416, and showing the suture 408 running through the implant alongside the arms 410.

FIG. 18 shows the implant 402 resiliently articulating further toward the configuration shown in FIG. 14, with the central portion 418 of the implant moving toward the catheter 406. This resilient motion directs the implant 402 toward and around the atrioventricular groove 16 of the heart.

FIG. 19 illustrates the guide arms 410 being retracted out of the tubular implant 402 after the implant has been positioned at the desired implantation site adjacent to the atrioventricular groove 16. The proximal portion 414 and trunk 412 of the guide 404 are retracted proximally through the catheter 406, which pulls the two arms 410 out of the tubular implant 402 around either side of the heart. The break 416 between the arms 410 allows the arms to be retracted out of the implant 402 in opposite directions on either side of the heart. As the arms 410 are retracted, the implant 402 and suture 408 are left encircling the heart. FIG. 20 is a partially broken-away view of a section of the tubular implant 402, illustrating the motion of one of the arms 410 through the implant alongside the suture 408.

As shown in FIG. 21, after the arms 410 are fully retracted out of the tubular implant 402, the implant is fully deployed from the catheter 406 and the suture 408 remains extending through the implant and through the catheter. The proximal portion of the suture 408 can then be tensioned or pulled to tighten the implant 402 around the heart. The knot or device 420 allows the circumference of the looped portion of the suture to be reduced via tension in the proximal portion of the suture, and reduction in the circumference of the looped portion of the suture causes the implant 402 to also be tightened around the heart to a desired degree, as illustrated by the arrows in FIG. 21. Tightening the implant 402 around the heart brings the two ends of the implant towards each other to more fully encircle the heart. Once the desired degree of tightening of the implant 402 is achieved, the knot or device 420 can be secured or fastened to fix the circumference of the suture and implant around the heart. As described above, the implant 402 can foreshorten as the suture is tightened due to the braided or woven configuration of the implant, preventing the implant from kinking or buckling. The implant 402 also prevents the suture 408 from directly contacting the heart tissue (except for possibly a short segment near the knot or device 420), which prevents the suture from cutting into, or "cheese wiring" into, the myocardium and/or other heart tissue. The implant 402 instead provides a greater surface area in contact with the heart tissue to reduce pressure on the heart tissue and minimize local trauma to the tissue.

FIGS. 22A-F are MRI images showing views of the heart anatomy before and after an encircling implant 402 is applied around the heart. Significant changes in valve annulus dimensions and valve leaflet coaptation are observed as a result of the encircling implant. FIG. 22A is a 5 chamber view at baseline. The arrow denotes the tricuspid annulus. FIG. 22B is a 5-chamber view after annuloplasty, showing a reduced tricuspid valve annulus diameter. FIG. 22C is a 2-chamber view at baseline. FIG. 22D is a 2-chamber view after annuloplasty, showing a reduced tricuspid valve annulus diameter. FIG. 22E shows tricuspid leaflet coaptation at baseline, with the arrow denoting the length of coaptation. FIG. 22F shows increased tricuspid leaflet coaptation after annuloplasty.

FIG. 23 includes graphs and images illustrating geometric changes to the heart resulting from placement of the encircling implant 402. FIG. 23A shows mean tricuspid valve annular dimensions in 5 and 3-chamber MRI views. The left side of FIG. 23A shows septal-lateral dimensions, and the right side of FIG. 23A shows antero-posterior dimensions. FIG. 23B shows mean mitral valve annular dimensions in 4 and 2-chamber MRI views. The left side of FIG. 23B shows septal-lateral dimensions, and the right side of FIG. 23A shows antero-posterior dimensions. Annular dimension measurements are performed in mid-systole. In both the tricuspid valve and

the mitral valve, annular dimensions are significantly decreased from the baseline measurements (left column in graphs) to the post-implantation (middle column) and follow-up measurements (right column). "*" indicates $p < 0.05$ and "**" indicates $p < 0.001$.

FIG. 24 is a chart showing the amount of tension applied to the encircling implant compared to tricuspid annulus septal-lateral dimensions, in two test pigs. Tensioning the encircling implant was measured using a force meter attached to the suture, and was performed three times at each different level of tension, for each test pig. The suture was released back to a relaxed state in between each cycle. "*" indicates $p < 0.001$. The chart of FIG. 24 clearly illustrates that the annulus dimensions decreased as tension in the implant increased.

As with other embodiments described herein, the device 400 can optionally include compressive elements and/or bridge elements positioned around, within, and/or embedding in the tubular implant 402. Such elements, as described in U.S. Patent No. 8,211,171, , which is incorporated by reference herein, can be positioned various locations around the heart and used to exert compressive remodeling forces at desired locations on the heart and/or used to provide a bridge over sensitive areas, such as a coronary artery, where application of pressure is not desired.

An exemplary bridge element is shown in FIG. 25E. FIGS. 25A-D show coronary arteries and coronary sinus angiography following annuloplasty with an encircling implant, such as the tubular implant 402. FIG. 25A is a left coronary artery angiogram showing the tensioned encircling implant (arrow). FIG. 25B is a right coronary artery angiogram showing the tensioned encircling implant (arrow). FIG. 25C is a coronary sinus angiogram showing the tensioned encircling implant (arrow). FIG. 25D is a left coronary angiogram with the rigid bridge element of FIG. 25E mounted within the encircling implant (arrow) to prevent left anterior descending coronary artery compression.

FIGS. 26-28 show exemplary compression members 500, 520, and 540 can be included with the tubular implant 402. The compression member 500 can have an "M" shape with a central projection 502 that presses into the tissue to impart increased pressure, two raised portions 504, and two end portions 506. The raised portions 504 and end portions 506 can generally follow the curvature of the tissue. The compression member 520 can have a similar shape but with a flattened central portion 522 that presses into the tissue to impart increased pressure more evenly over its length. Member 520 also include two raised portions 504 at the ends of the central portion 522, and two end portions 526. The raised portions 524 and end portions 526 can generally follow the curvature of the tissue. The compression member 540 can have a similar shape to member 500 but

with a more sharply pointed central portion 542 that presses into the tissue to impart increased pressure, and with more pronounced raised portions 544 and flattened end portions 546.

Exemplary Procedures Using the Disclosed Devices

The disclosed delivery devices and encircling implants can be used in a variety of procedures, such as cardiovascular and non-cardiovascular procedures, where placement of an encircling implant in the body is desired. In addition to other procedures disclosed herein, the disclosed encircling implant delivery devices can be introduced via a delivery catheter through any path through the venous system to the right atrial appendage and through a puncture in the right atrial appendage to access the intrapericardial space, or the devices can be delivered through any portion of the arterial system and into or toward the heart and then delivered through a puncture in the heart wall to access the intrapericardial space, or the devices can be delivered percutaneously directly into the intrapericardial space, or from any other access route into the intrapericardial space. In addition, the disclosed encircling implant delivery devices, or variations thereof, can be used to place encircling implants around any of various other target organs or structures in the body via transvascular or percutaneous delivery routes. In any procedure wherein a puncture or other aperture is formed in the native anatomy, such aperture can be sealed after the implantation of the encircling implant by placement of cardiac closure device, such as nitinol atrial-septal occluder device, or other sealing mechanism.

The methods disclosed herein relative to annuloplasty and other encirclement of portions of the heart can be performed while the heart is still beating, and titrated in real-time to regurgitation under varying loading conditions imposed by hemodynamic provocations such as exercise and volume. This provides a significant advantage over prosthetic valve implantation or other intra-cameral surgical procedures wherein the heart must be at least partially stopped and/or extra-corporeal assistance devices must be used to pump and oxygenate the blood. In addition, methods disclosed herein can avoid long term anticoagulation treatments because the implant is extra-vascular.

The following are several exemplary procedures using the disclosed encirclement implant delivery devices.

A. Transcatheter Mitral Valve Annuloplasty

The delivery devices disclosed herein may be used in methods of improving the function of a mitral valve in a subject in which an annuloplasty implant, for example an encircling implant that

exerts compressive remodeling forces on the mitral valve is introduced at least partially around the mitral valve, for example at least partially over the coronary sinus and/or over a coronary artery. The delivery devices can also be used to deploy compressive elements (such as those shown in FIGS. 26-28) around the heart and/or to place protective devices (such as that shown in FIG. 25E) between the encircling implant and the coronary artery, with the encircling implant separated from the underlying coronary artery by the bridge of the device. Compressive remodeling forces can be exerted by the annuloplasty device (for example by applying tension on a tensioning element to alter the shape or configuration of the mitral valve annulus to reduce its circumference) while supporting the annuloplasty element via the bridge to inhibit application of pressure to the coronary artery. The function of the mitral valve in the patient is thereby improved without impairing coronary blood flow.

Briefly described, the encircling implant is introduced at least partially around the mitral valve by advancing the encircling implant in or on the resilient limbs/arms of the delivery device, with the limbs/arms folded against one another in an endovascular delivery catheter. The endovascular catheter is advanced through the vascular system of the subject to the heart, and the distal limbs/arms are deployed from the catheter until they assume the desired shape for guiding the encircling implant around the heart. The encircling implant may include a tensioning element such as a ligature, suture, or tubular body. The tensioning element can extend through or over any protective device that are placed over the coronary artery so that the tensioning element is supported by the protective device. The protective device can optionally also be integrated directly into the tensioning element.

Tension is transmitted through the tensioning element material. Tension can be applied by pulling one or both ends of a suture/cord passing through the encircling implant, or by pulling ends of the encircling implant itself, such as in the case where a tensioning suture passes proximally and is externalized at the point of vascular access. Tension is applied under imaging guidance until the desired degree of mitral annular circumferential reduction is accomplished, or until the mitral valve regurgitation is reduced, or until other endpoints are achieved such as mitral valve inflow obstruction. Tension is secured using a tension fixation device applied to both ends of the tensioning device, such as at the right atrium or right ventricle where the two cerclage trajectories cross, or at the point of vascular access, or in between the two. Tension can be delivered by counter pressure against the fixation device, for example, applied through a delivery catheter. Before fixation, tension can be released or reduced, for example, to reposition the protection device or to achieve a lower degree of mitral annular circumferential reduction.

B. Transcatheter Tricuspid Valve Annuloplasty

The disclosed delivery devices can also be used in Transcatheter Tricuspid Valve Annuloplasty procedures, such as that disclosed in International Patent Application No. PCT/US2014/025300, filed March 13, 2014, which is incorporated by reference herein.

In one such procedure, a delivery device delivers an encircling implant including a tensioning element and at least one compression member along the atrioventricular groove of the heart. The tensioning element can comprise a tubular body or a suture/cord delivered through the delivery catheter by deployment of the resilient limbs/arms to position the encircling implant in a desired orientation along or near the heart's atrioventricular groove, and subsequent withdrawal of the limbs/arms to leave the encircling implant around the heart. In embodiments wherein the encircling implant comprises an encircling suture, the compression member can be advanced along the suture and over a desired target position of the atrioventricular groove to apply force to the underlying wall of the heart by selective tensioning of the suture. In embodiments wherein the encircling implant comprises a tubular implant, the compression member can be delivered over or within the tubular implant, or the tubular implant can be pre-configured to include the compression member along its length, such as within, over, or in the wall of the tubular body. The delivery device and encircling implant can alternatively be delivered through a catheter inserted along a trans-thoracic or subxiphoid or subcostal path.

In some embodiments a compression member can be tubular and define a bore dimensioned to allow the encircling implant to pass through the compression member. In some implementations, the compression member has a groove dimensioned to receive the encircling implant and to assist in retaining contact between the tensioning portion of the encircling implant and the compression member. A compression member can incorporate an anti-slip feature configured to contact a surface to reduce slipping of the compression member relative to the heart tissue when the compression member is in position over/under the desired segment with tension applied to the encircling implant. The anti-slip feature can comprise protruding barbs configured to an exterior surface of the heart.

The compression member can have a shaped profile along its length. As illustrated in FIGS. 26-28, the shaped profile can comprise at least two bends, at least one arch, an M-shaped portion and/or at least two inflection points between the segments of different curvatures. The compression member can have a generally curved center segment, a generally straight center segment, and/or a center segment having a vertex. The compression member can have end segments shaped to orient the compression member, and can be self-orienting upon application of tension in a selected

location for treatment. The compression element can be resiliently deformable such that the compression member changes from a delivery shape suitable for delivery to a final shape after delivery to a treatment site is complete. The compression member can be at least partially defined by a first major radius of curvature and a second minor radius of curvature.

This procedure can also include the use of a protection member, such as that shown in FIG. 25E, shaped to provide a protected space at least partially accommodating a blood vessel or other vital structure and to receive the tensioning suture or be incorporated into, over, or within, a tubular implant, so that the protection member distributes force developed through increased tension in the tensioning suture to either side of the protected space. As just two examples, the protection member can be configured for positioning over a coronary artery, or over a pulmonary artery trunk.

C. Left Atrial Appendage Ligation

In subjects with atrial fibrillation a thrombus can form in the appendage of the left atrium, and the thrombus can embolize to distant organs. If the embolism travels to the brain, a stroke can occur and result in death or long term disability. Although such patients can be treated with anti-coagulants to help prevent the formation of the thrombus, the use of anti-coagulants can themselves lead to unwanted bleeding, hemorrhagic strokes and death. Surgical methods have been developed to isolate the atrial appendage, for example by suturing or stapling along its base or ostial neck to prevent the flow of blood into the appendage. However, it is desirable to isolate the atrial appendage using minimally invasive or intravascular techniques.

The delivery devices disclosed herein can be used to deliver a tension suture or other encircling implant around the base of the atrial appendage. Once the encircling implant is tightened to compress the base of the appendage, blood cannot flow into the lumen of the appendage and formation of a thrombus is avoided. The encircling implant can be placed around the atrial appendage using a variety of approaches, for example by introducing the delivery catheter through the right atrial appendage. The limbs/arms of the device can then deployed from the tip of the delivery catheter under fluoroscopic guidance, and the distal portions of the limbs/arms (and optionally also the implant itself) can be pre-formed to assume a shape that folds over and loops around the left atrial appendage. The limbs/arms can then be withdraw through the catheter and the encircling implant tightened to close the neck of the appendage and prevent blood pooling in it.

In view of the many possible embodiments to which the principles of the disclosed technology may be applied, it should be recognized that illustrated embodiments are only examples

and should not be considered a limitation on the scope of the disclosure. Rather, the scope of the disclosure is defined by the following claims. We therefore claim all that comes within the scope and spirit of these claims.

Claims:

1. A device for delivering through a catheter an encircling implant around a portion of a target structure in a body, the device comprising:

first and second delivery limbs linked at an articulation region between distal ends of the first and second limbs by a continuous flexible encircling implant that is to be delivered and which extends through or over the first and second limbs to maintain the distal ends of the first and second limbs together in an articulating relationship at a distal articulation tip,

wherein at least a distal limb portion of each limb is resiliently deformable into the delivery shape but when not deformed into the delivery shape is configured to cooperatively form with the contralateral limb a loop that can be placed circumferentially around the portion of the target structure in order to locate the encircling implant around the portion of the target structure.

2. The device of claim 1, wherein the encircling implant is tubular and the first and second delivery limbs extend within a lumen of the tubular implant during delivery.

3. The device of claim 1, wherein the encircling implant is a suture, wire, cable, or cord that extends through the first and second delivery limbs during delivery.

4. The device of any one of claims 1-3, wherein the distal limb portions are cooperatively biased to assume a loop shape and sized substantially complementary to the portion of the target structure around which the loop is to be circumferentially placed.

5. The device of any one of claims 1-4, wherein the target structure comprises a base portion connected to the body and a free portion over and around which the loop can be passed.

6. The device of any one of claims 1-5, wherein the target structure comprises a heart or atrial appendage, a cecal appendix, a gallbladder, a neoplasm, a uterus, a hemorrhoid, an uvula, an aneurysm, a transected blood vessel or other transected, folded or looped lumen, an intraocular crystalline lens or implanted intraocular lens or lens haptic, a urinary bladder, a kidney, a prostate or a foreign body.

7. The device of any one of claims 1-2 or 4-6, wherein the first and second delivery limbs extend alongside a looped portion of a suture within a lumen of the encircling implant during delivery of the encircling implant around the target structure, and with the first and second delivery limbs retracted from the lumen of the encircling implant the looped portion of the suture can be reduced in circumference to tighten the encircling implant around the target structure.

8. The device of claim 1, wherein the first and second limbs are separate and proximal limb portions of the first and second delivery limbs are substantially parallel to one another in the delivery shape, and the distal limb portions are substantially parallel to one another in the delivery shape.

9. The device of claim 8, wherein the proximal and distal limb portions are constrainable into the delivery shape by a lumen within a flexible delivery catheter though which the encircling implant is to be delivered to the target structure in the body, wherein the delivery catheter comprises a distal end for initial introduction into the body and a proximal end for controlling the delivery catheter.

10. The device of claim 9, wherein the proximal limb portions are flexible to conform to the shape of the lumen within the flexible delivery catheter with the proximal limb portions parallel to one another, and the proximal limb portions are sufficiently rigid to maintain a substantially parallel relationship when only a distal portion of the proximal limb portions extends from the lumen, and the proximal limb portions are connected together in at least one location to rotationally constrain the proximal limb portions with respect to each other.

11. The device of claim 10, further comprising the delivery catheter, wherein the suture comprises first and second terminal ends, and the suture extends continuously through the delivery limbs within the percutaneous delivery device with the first and second terminal ends of the suture extending from the proximal tip of the delivery catheter or an intermediate opening along each of the first and second delivery limbs.

12. The device of claim 11, wherein the delivery catheter comprises a distal penetrating tip capable of penetrating body tissue.

13. The device of any one of claims 1-12, wherein the first and second delivery limbs are capable of being withdrawn from the encircling implant and from the body once the encircling implant is delivered around the target structure.

14. The device of any one of claims 1-13, wherein the loop is cooperatively formed by the distal limb portions when they are not deformed into the delivery shape, each distal limb portion forming substantially half of the loop, or each distal limb is symmetric or asymmetric with respect to its contralateral limb, or one or both distal limbs is semilunar, semi-ovoid, semi-circular, or substantially C-shaped, J-shaped, L-shaped, S-shaped, V-shaped or U-shaped.

15. The device of any one of claims 1-14, wherein the loop is substantially circular or cordiform and each distal limb portion forms a substantially semi-lunar or semi-cordiform shape joined at the articulation tip.

16. The device of any one of claims 1-15, wherein the loop extends at a predetermined angle with respect to a longitudinal axis of the catheter.

17. The device of any one of claims 1-16, wherein the loop folds back toward the proximal limb portion.

18. The device of any one of claims 1-17, wherein the flexible distal limb portions of the first and second delivery limbs cooperatively form geometric shapes, such as asymmetric nested semilunar arcs, that are substantially co-planar or not-coplanar when the flexible distal limb portions form the loop.

19. The device of claim 1, wherein the delivery limbs are removable from their positions around or within the continuous encircling implant to leave the encircling implant in place around the target structure after the delivery limbs are removed from the encircling implant, and the encircling implant can be tightened after placement around the target structure to circumferentially compress the target structure.

20. A device for delivering a continuous flexible encircling implant around a portion of a target structure in a subject's body, the device comprising:

a flexible delivery catheter having a lumen, a proximal end for controlling the catheter and a distal delivery end for introduction into the body;

a guide comprising first and second delivery limbs maintained in an articulating relationship at a distal articulation tip by the continuous flexible encircling implant, wherein the encircling implant extends through or over the first and second delivery limbs and bridges a gap between distal ends of the first and second delivery limbs to form the articulation tip,

wherein at least distal portions of the first and second delivery limbs are resiliently deformable into a delivery shape to extend along the longitudinal axis of the delivery catheter, but resiliently assume a loop shape cooperatively formed by the two distal limb portions when not deformed into the delivery shape, and the loop shape is a size and shaped substantially complementary to a feature of the target structure such that the distal limb portions cause the encircling implant to assume a loop shape for placement of the encircling implant around the target structure.

21. The device of claim 20, wherein at least the distal limb portions comprise a superelastic or shape-memory material.

22. The device of either of claims 20 or 21, wherein the distal limb portions in the delivery shape deflect toward the delivery catheter as the distal limb portions emerge from the distal delivery end of the delivery catheter.

23. The device of any one of claims 20-22, wherein the encircling implant comprise a tubular implant and the distal limb portions extend through a lumen of the tubular implant.

24. The device of any one of claims 20-22, wherein the encircling implant is non-tubular and extends through lumens in the first and second delivery limbs.

25. The device of any one of claims 20-24, wherein an orientation of the loop with respect to the delivery catheter is controllable by moving one or both of the first and second delivery limbs.

26. The device of any one of claims 20-25, wherein the distal limb portions are configured to assume a shape and size substantially complementary to a circumference of the target

structure around which the loop is to be circumferentially navigated or placed, and the target structure comprises a body organ, neoplasm, or surgically implanted device.

27. The device of any one of claims 20-26, wherein the target structure comprises a heart or atrial appendage, cecal appendix, gallbladder, neoplasm such as a polyp, uterus, hemorrhoid, uvula, aneurysm, transected, folded or looped blood vessel or other lumen, intraocular crystalline lens or implanted intraocular lens or lens haptic, urinary bladder, kidney, prostate or foreign body.

28. The device of claim 27, wherein the target structure comprises a heart, and the distal limb portions are configured to deflect the loop toward the delivery catheter and around the apex of the heart.

29. A method of using the device of any one of claims 1-28 to deliver an encircling implant around a target structure in a body through an elongated delivery catheter having a lumen, a proximal control end and a distal end, the method comprising:

advancing the delivery limbs through the catheter, articulated tip first, with the limbs substantially conforming to the shape of the lumen of the delivery catheter;

further advancing the delivery limbs until the distal limb portions emerge from the lumen at the distal end of the delivery catheter, and the distal limb portions form the loop while at least a portion of the limbs or a proximal guide member attached to the limbs is retained within the delivery catheter.

30. The method of claim 29, further comprising placing the loop around the target structure to encircle the target structure.

31. The method of claim 30, further comprising individually or cooperatively moving the first and second delivery limbs to adjust an orientation of the loop with respect to the delivery catheter and the target structure.

32. The method of any one of claims 30-31, further comprising withdrawing the first and second delivery limbs from the encircling implant into the delivery catheter to leave the encircling implant positioned and secured around the target structure, wherein a desired tension is

applied to the encircling implant while the limbs are withdrawn to maintain the encircling implant in a desired position until the two free ends of the suture are subsequently secured together.

33. The method of claim 32, further comprising tightening the encircling implant around the target structure.

34. The method of either claim 32 or 33, further comprising withdrawing the delivery catheter from the body.

35. The method of claim 29, comprising inserting the distal end of the delivery catheter percutaneously, for example through an introducer sheath, or intraluminally, for example through an endoscope, into the body and advancing the distal end of the delivery catheter to the target structure within the body.

36. The method of claim 35 wherein the delivery catheter is inserted percutaneously through an introducer sheath into the body and advanced intravascularly through the inferior vena cava until the distal end of the delivery catheter penetrates the wall of the heart, then advancing the delivery limbs out of the distal end of the delivery catheter until the distal delivery limbs form the loop.

37. The method of claim 36, wherein the loop substantially conforms to a shape substantially conforming to a circumference of the heart, and the loop assumes a pre-configured angle with respect to the proximal portions of the limbs, and the loop is advanced around the apex of the heart within the pericardial space, if the pericardium is intact, until the loop encircles the heart, then the delivery limbs are withdrawn proximally into the catheter to leave the encircling implant which encircles the heart, and the encircling implant is tightened by exerting tension on the terminal ends of the encircling implant or by tightening a suture passing through the implant, to improve a function of a heart valve within the heart.

38. The method of claim 37, wherein

(a) the distal end of the delivery catheter penetrates the heart through an atrial appendage, and the loop substantially conforms to a circumference of a targeted atrial appendage of the heart, and the loop is advanced around the atrial appendage within the pericardial space, if

present, until the loop encircles the targeted atrial appendage, then the delivery limbs are withdrawn proximally into the catheter to expose the suture which encircles the targeted atrial appendage and the suture is tightened by exerting tension on the terminal ends of the suture to exclude the targeted atrial appendage; or

(b) The distal end of the delivery catheter approaches the heart by a trans-thoracic or sub-xiphoid path and the loop is advanced around the atrial appendage until the loop encircles the atrial appendage, then the delivery limb are withdrawn proximally into the catheter to expose the suture which encircles the atrial appendage and the suture is tightened by exerting tension on the terminal ends of the suture to tighten the suture and exclude the atrial appendage.

39. The method of claim 36 wherein the distal end of the delivery catheter is inserted intraluminally into a body lumen and advanced to the target structure, for example through a laparoscope or bronchoscope.

40. The method of claim 39, wherein the body lumen is a gastrointestinal, genitourinary, vascular or respiratory lumen.

41. The method of claim 36 wherein the distal end of the delivery catheter is inserted percutaneously into the body and advanced to the target structure.

42. The method of claim 41, wherein the distal end of the delivery catheter is inserted percutaneously into a body cavity.

43. The method of claim 42 wherein the body cavity is a peritoneum, an anterior or posterior chamber of the eye, a gastrointestinal cavity, a thoracic cavity, a uterine cavity, a urinary bladder, or a ventricle of the brain.

44. The method of claim 39 wherein the target structure is a foreign body that is to be repositioned within or retrieved from the body.

45. The method of any one of claims 34-44 wherein a protection device or a compression device is advanced over the implant into a desired position with respect to the target

structure, or a compression device is included as part of the encircling implant during delivery of the implant.

46. The method of claim 45, wherein the target structure is the heart, and the compression device is advanced over the implant to a position on an external wall of the myocardium to exert pressure on the external wall and change a shape and function of a valve of the heart.

47. The method of claim 46, wherein the valve is the mitral or tricuspid valve.

48. The method of claim 45, wherein the target structure is the heart, and a protection device is advanced over or within the implant to a position on an external wall of the myocardium to bridge a coronary artery and avoid compression of the coronary artery when the suture is tightened around the heart.

49. The method of any one of claims 29-36, wherein the target structure is the right ventricular outflow tract or main pulmonary artery.

50. A method of making a device for transcatheter delivery of a continuous flexible encircling suture around a circumference of a target structure within a body of a subject, the method comprising:

providing separate first and second delivery limbs;

linking the first and second delivery limbs at an articulation by placing the suture through or around the first and second limbs to maintain the first and second delivery limbs together in an articulating relationship at an articulation tip,

wherein each limb comprises a proximal limb portion having a longitudinal axis, and a flexible distal limb portion,

wherein each proximal limb portion has a delivery shape for advancement through a lumen, and each distal limb portion comprises a material that is resiliently deformable into the delivery shape but forms a portion of a loop when not deformed into the delivery shape such that the distal limbs in the delivery position cooperatively form a loop that can be placed circumferentially around the portion of the target structure.

51. The method of claim 50, further comprising inserting the articulation tip of the first and second delivery limbs into a catheter lumen of a flexible delivery catheter, and advancing the articulation tip distally within the catheter lumen until the proximal and distal limb portions are maintained in the delivery shape in a substantially linear shape.

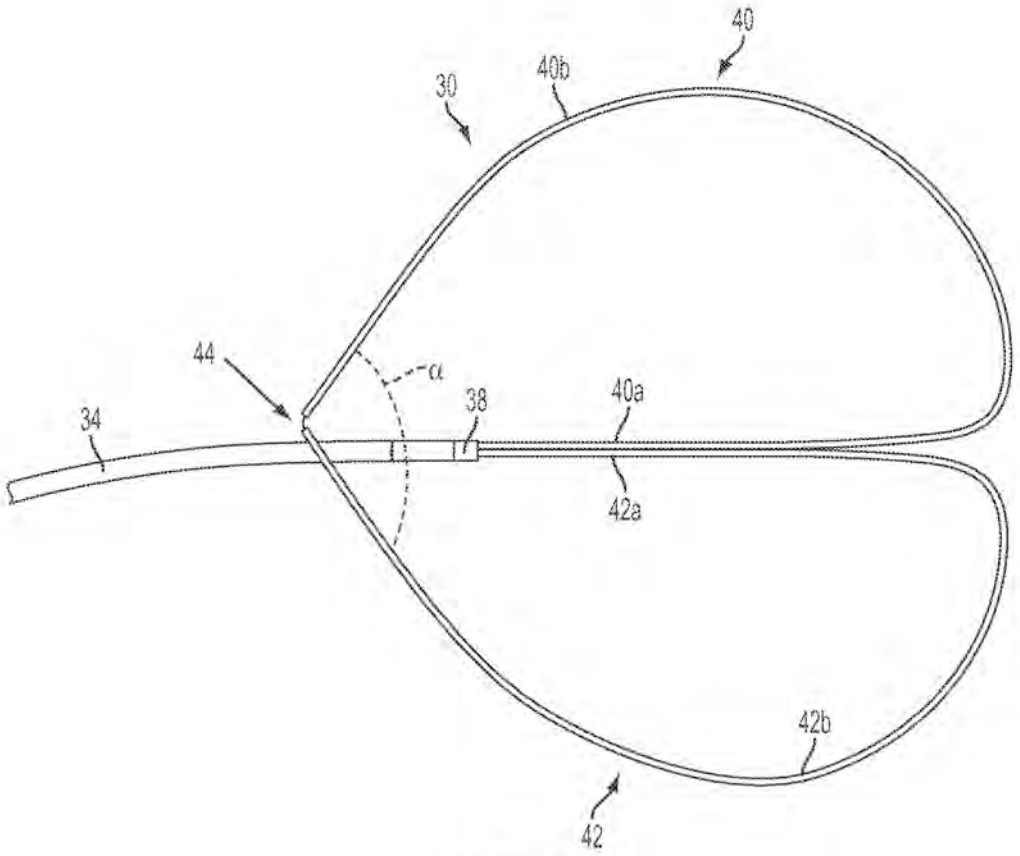

FIG. 1

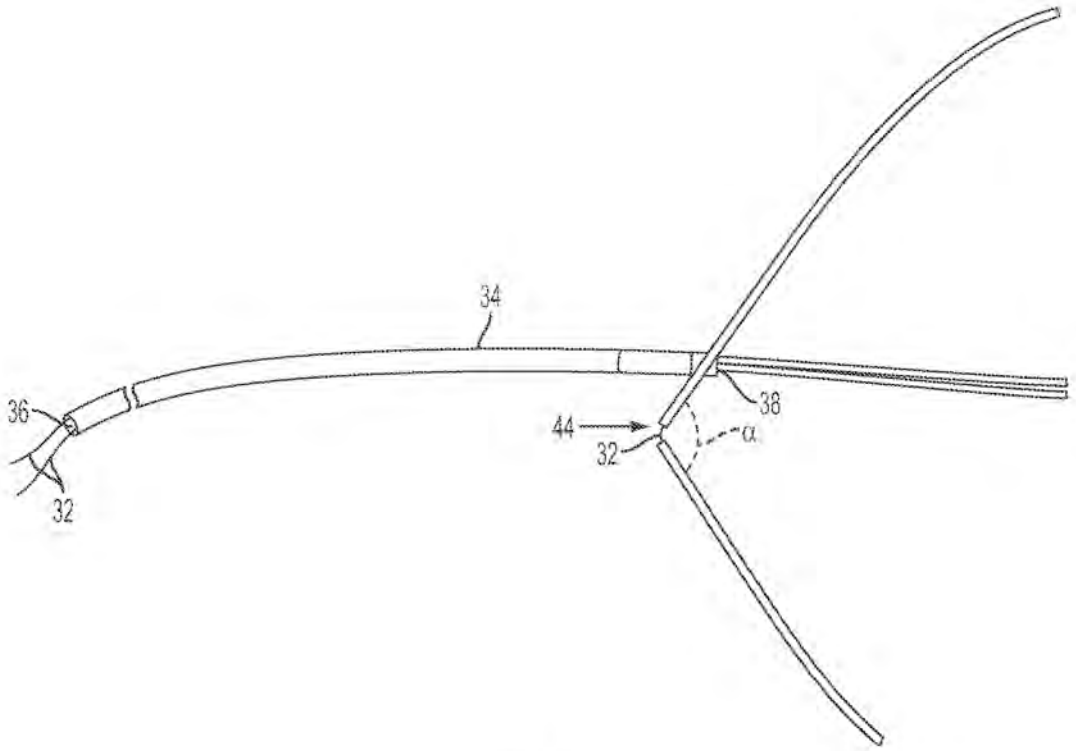

FIG. 2

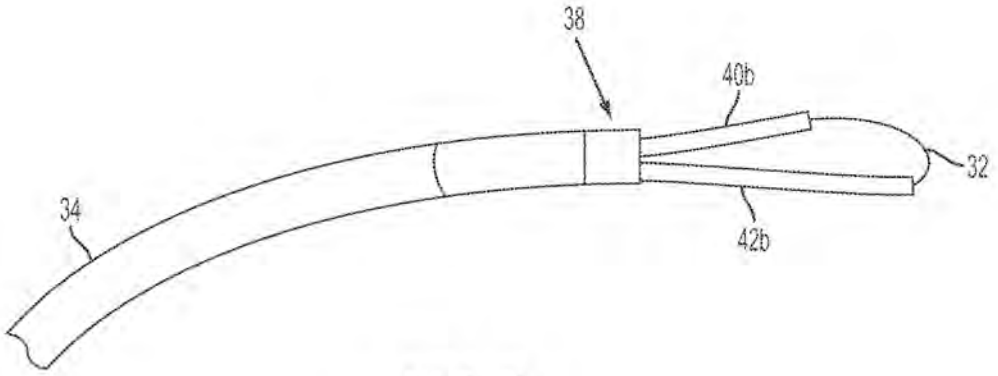

FIG. 3

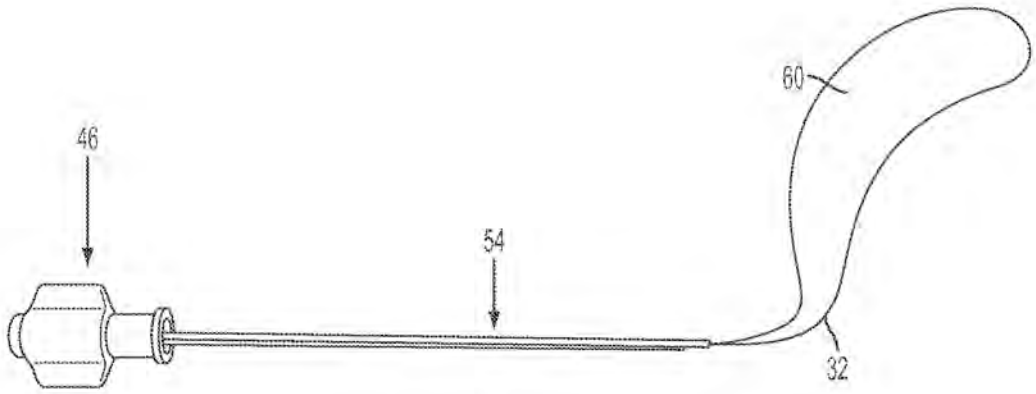

FIG. 4

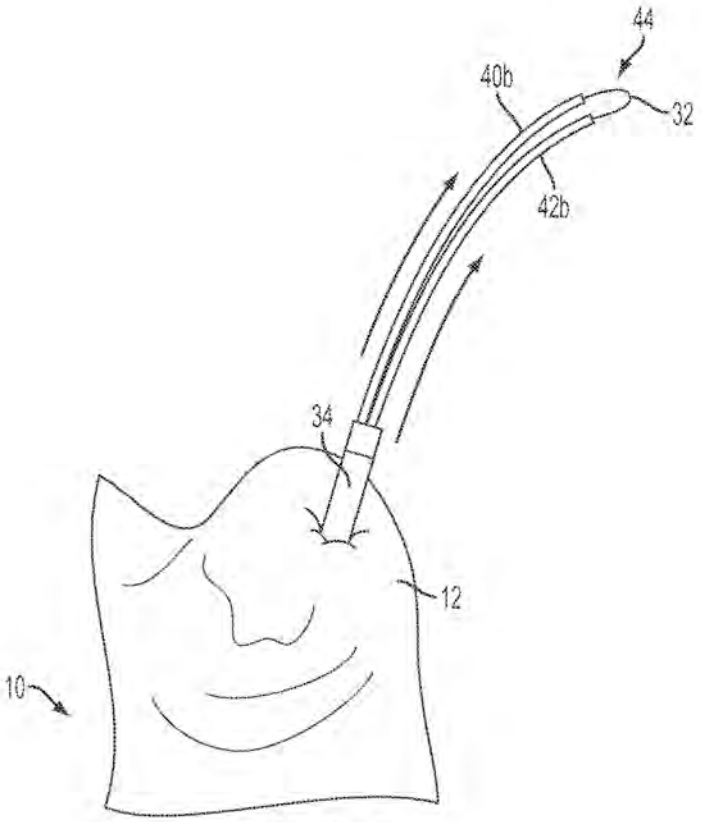

FIG. 5

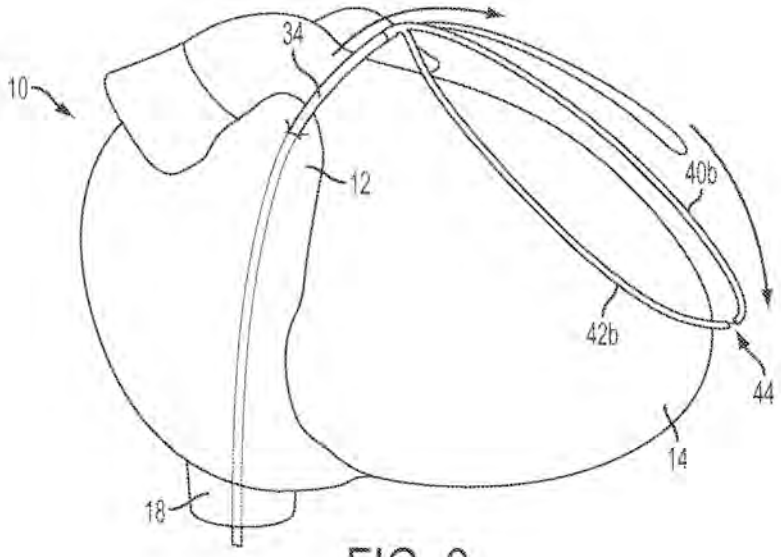

FIG. 6

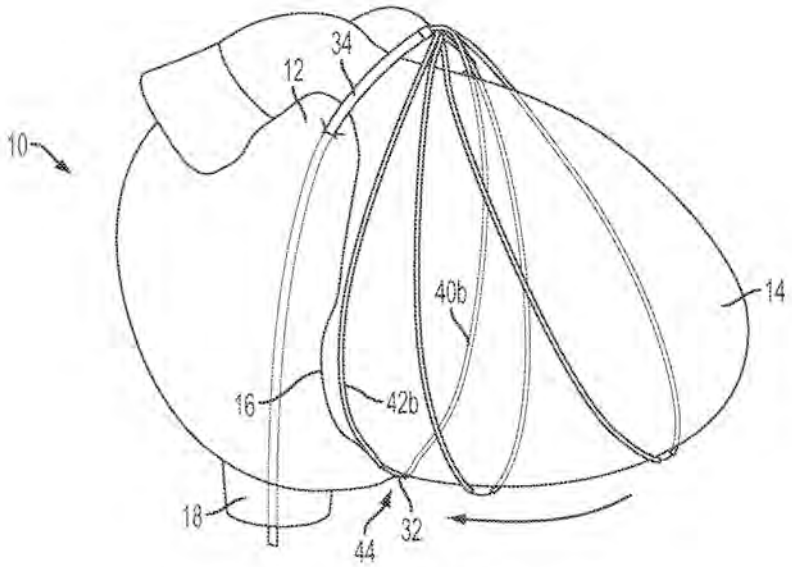

FIG. 7

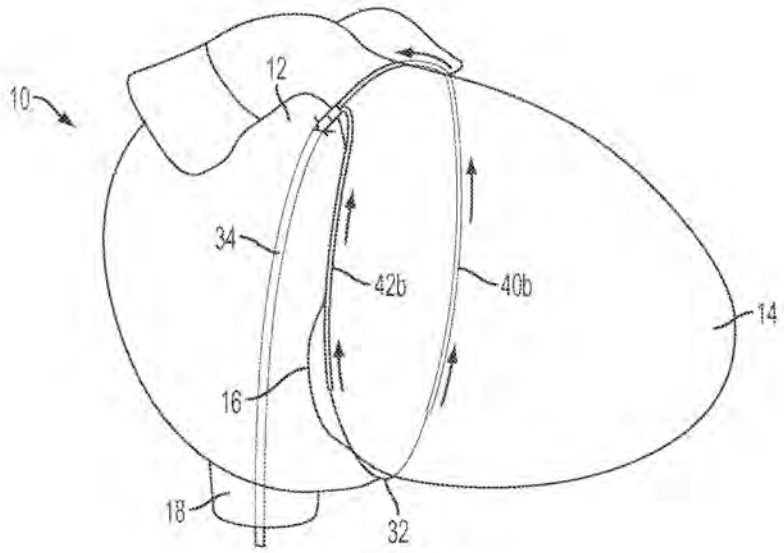

FIG. 8

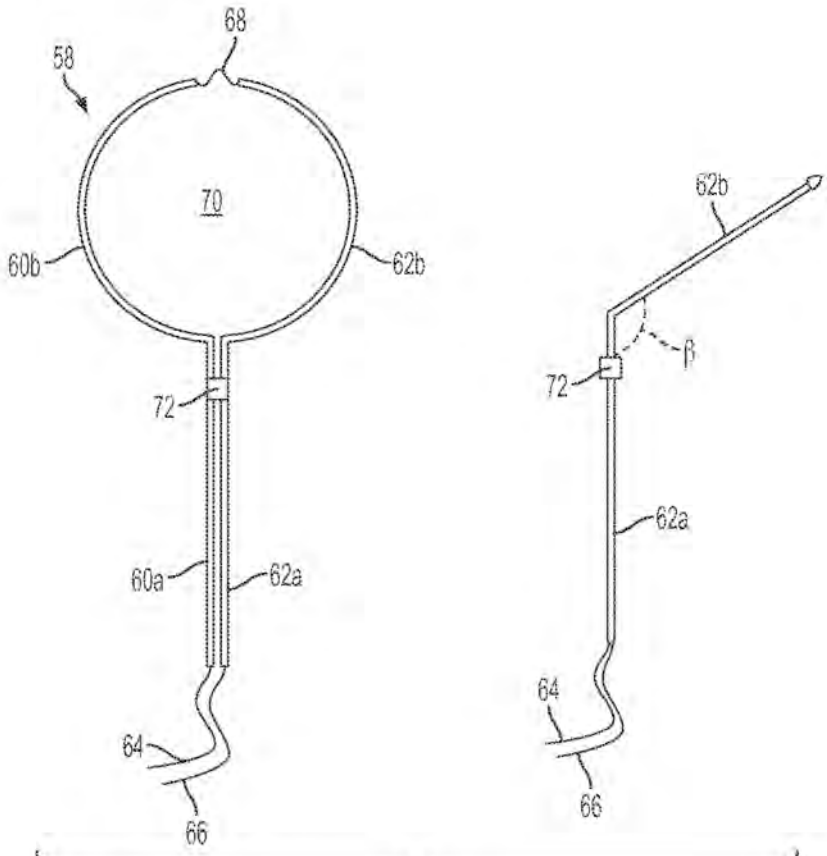

FIG. 9

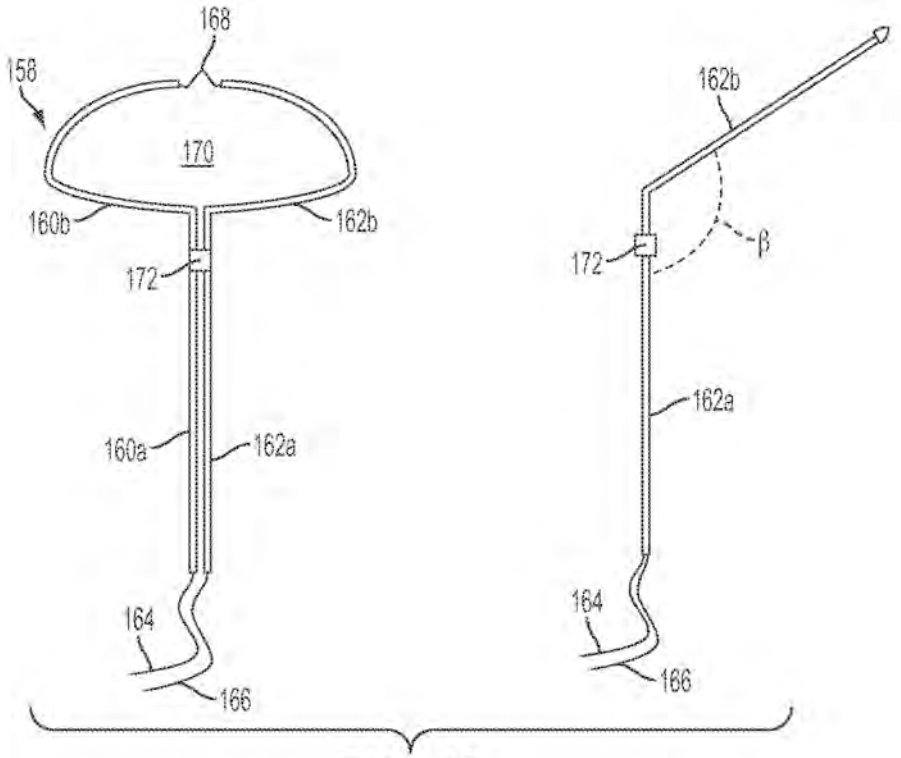
168
158
170
160b
162b
172
160a
162a
164
166
162b
β
172
162a
164
166

FIG. 10

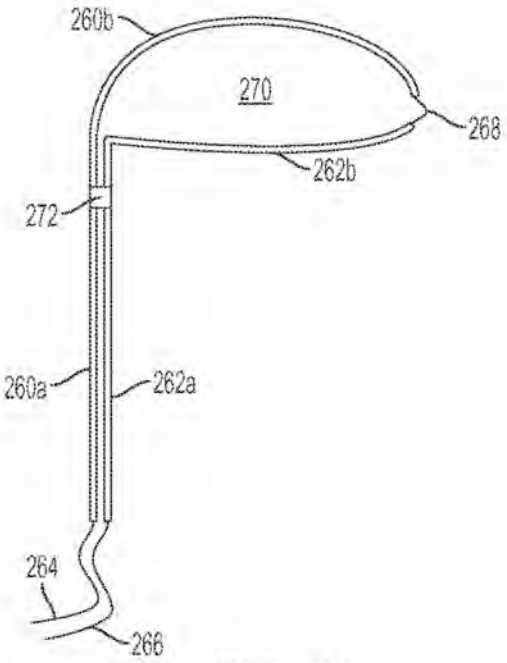
260b
270
268
262b
272
260a
262a
264
266

FIG. 11

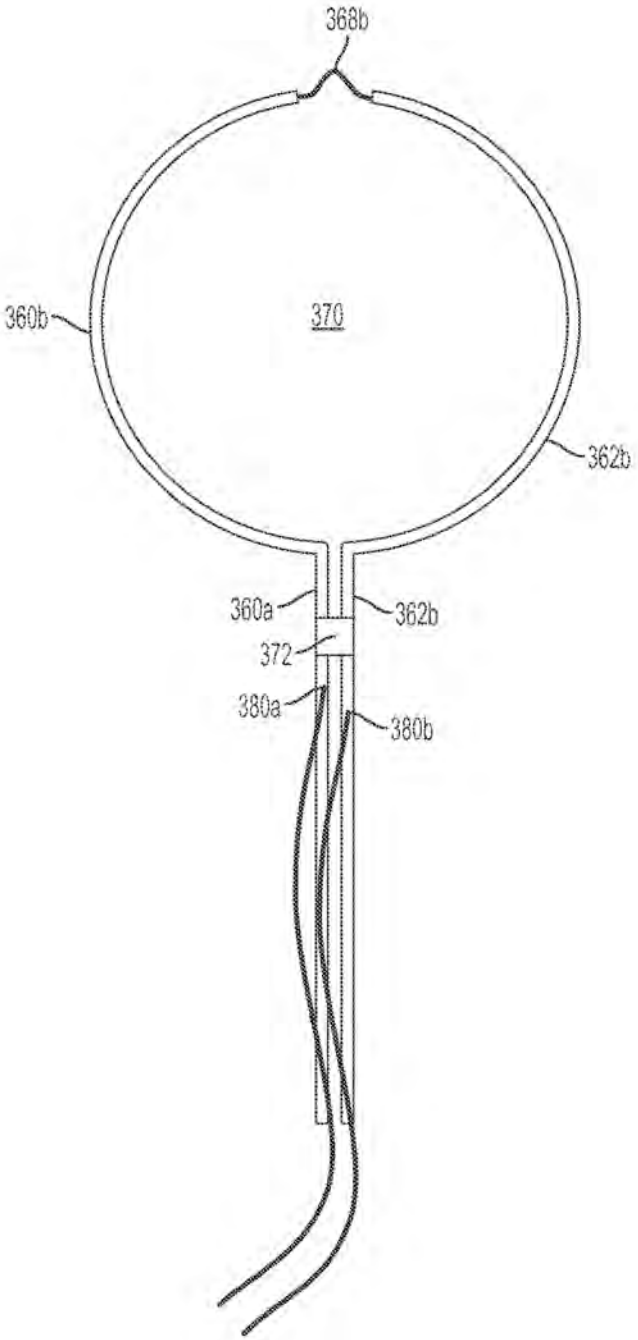

FIG. 12

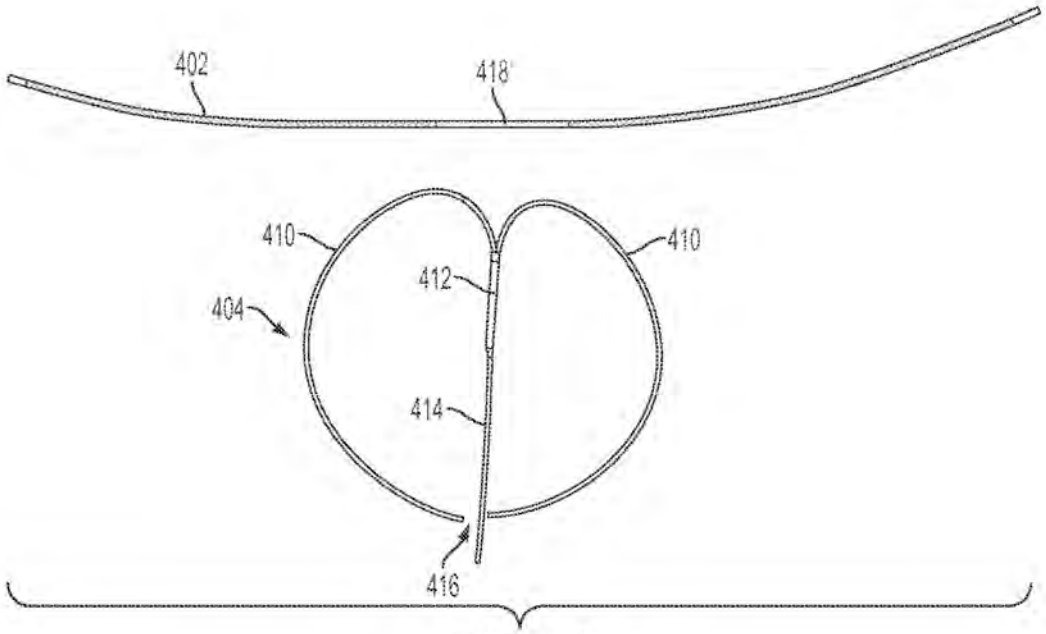
402
418
410
410
412
404
414
416

FIG. 13

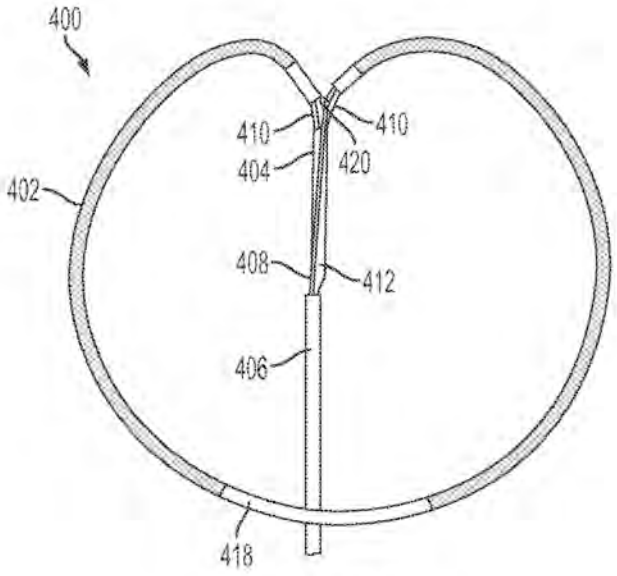
400
410
410
404
420
402
408
412
406
418

FIG. 14

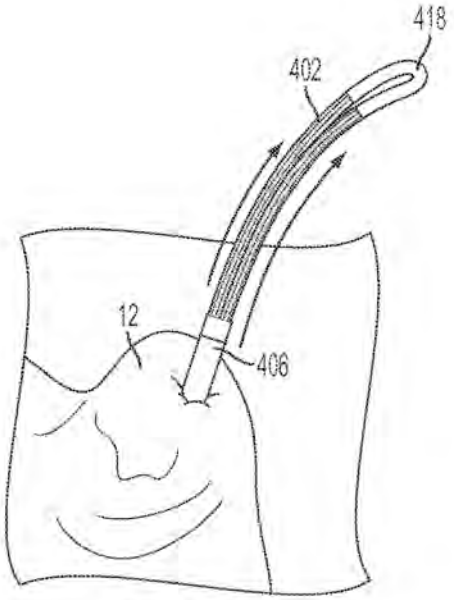

FIG. 15

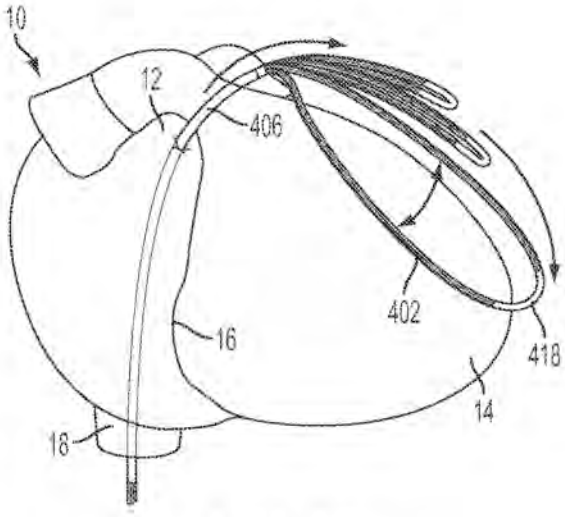

FIG. 16

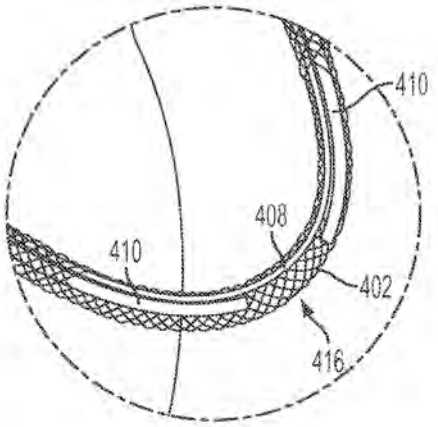

FIG. 17

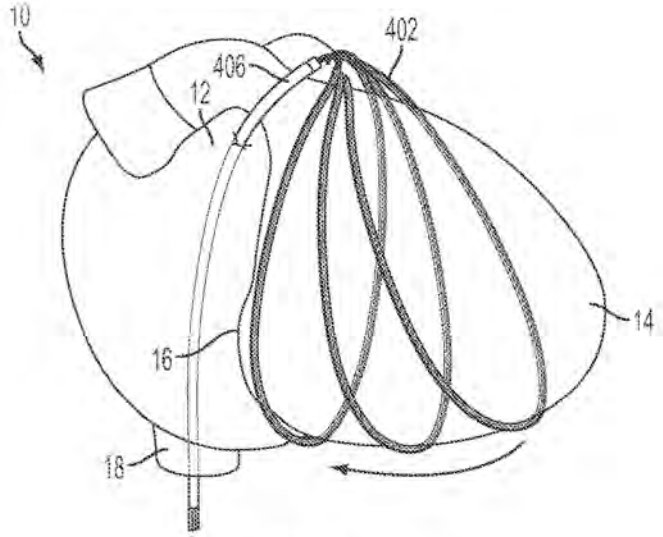

FIG. 18

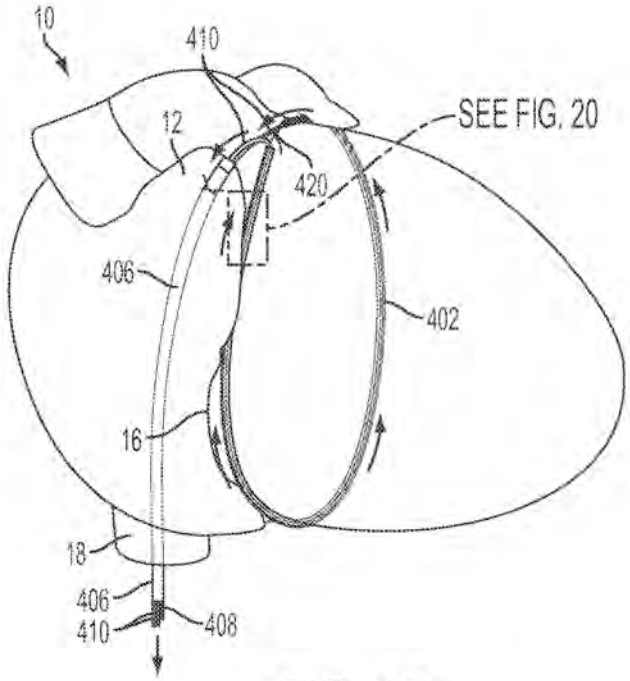

FIG. 19

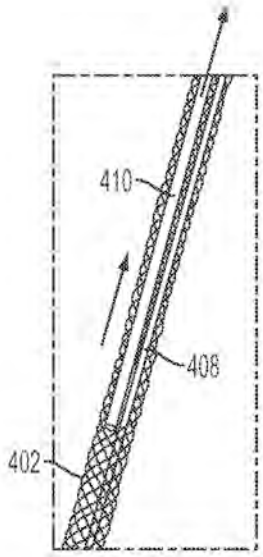

FIG. 20

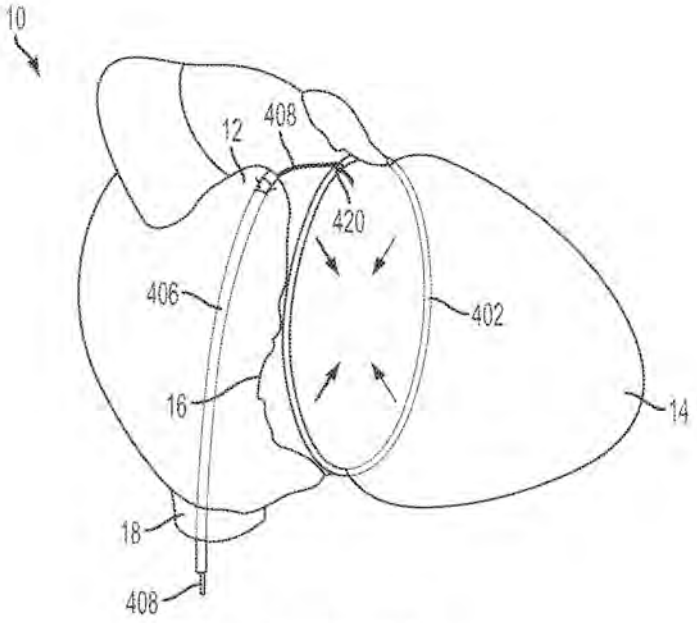

FIG. 21

FIG. 22A

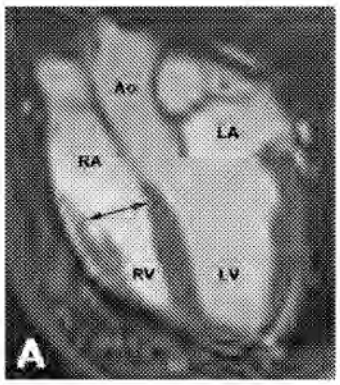

FIG. 22B

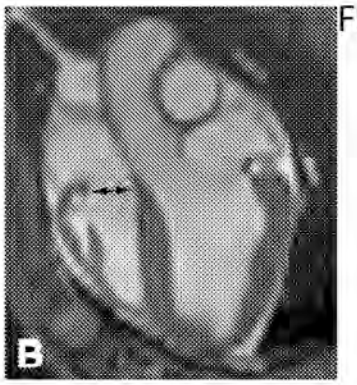

FIG. 22C

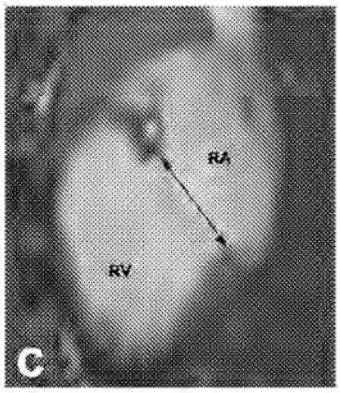

FIG. 22D

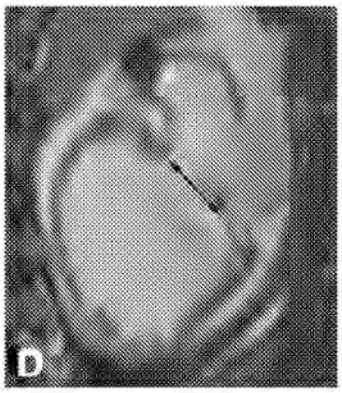

FIG. 22E

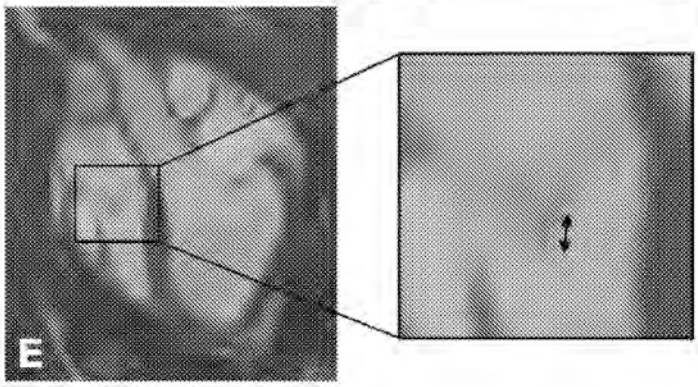

FIG. 22F

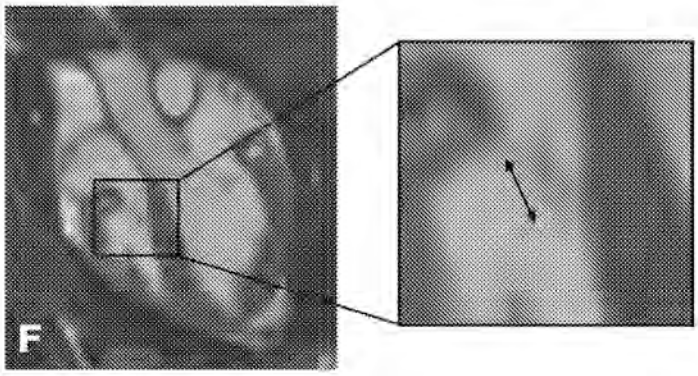

FIG. 23A

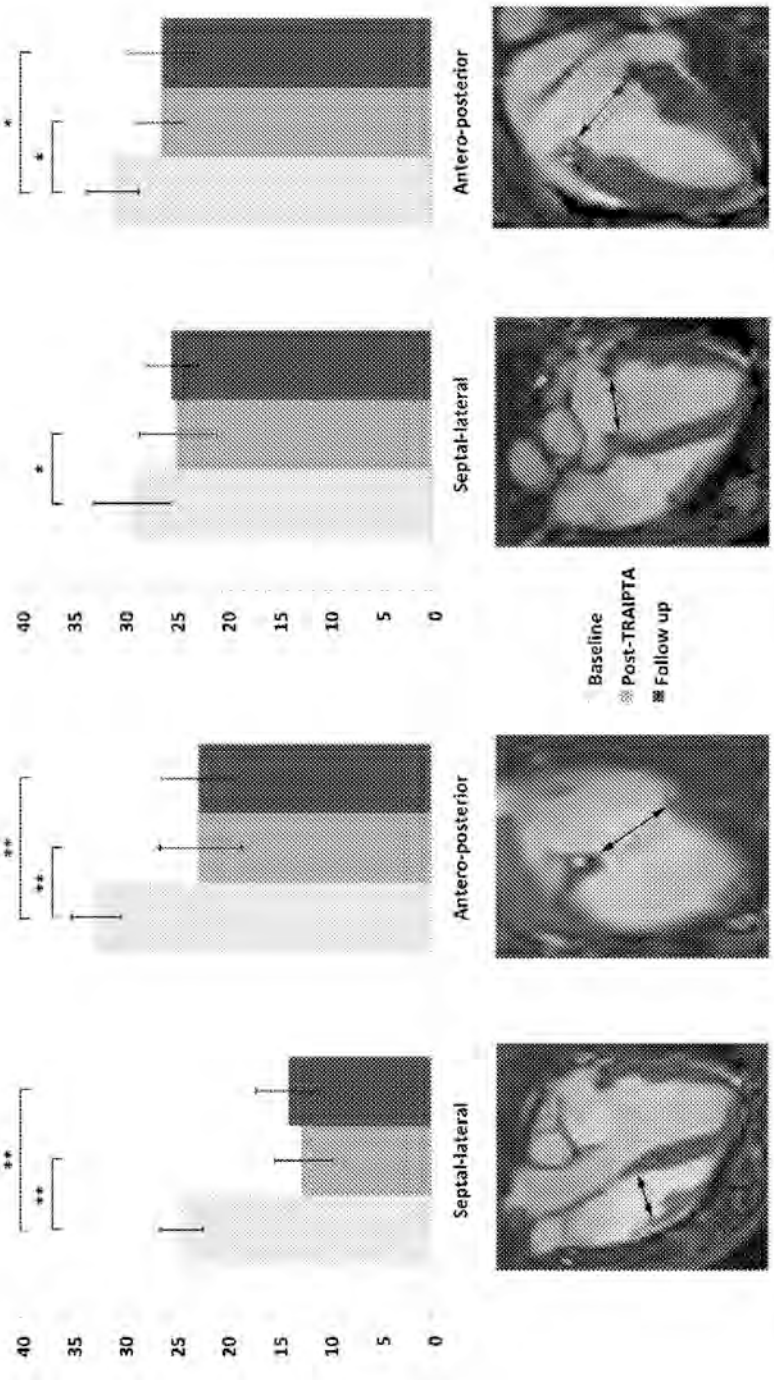

FIG. 23B

FIG. 24

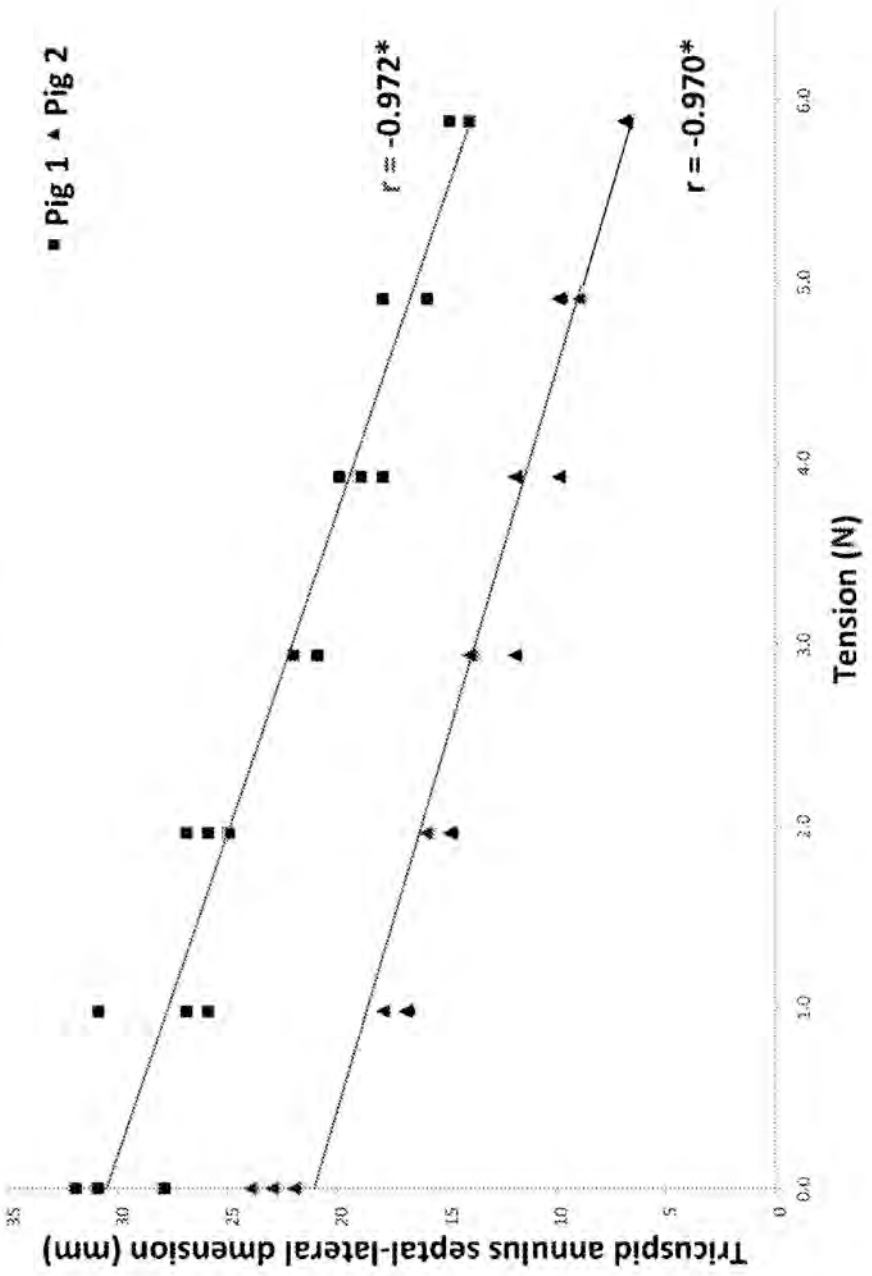
Pig 1 Pig 2
r = -0.972*
r = -0.970*
Tricuspid annulus septal-lateral dimension (mm)
Tension (N)
0
5
10
15
20
25
30
35
0.0
1.0
2.0
3.0
4.0
5.0
6.0

FIG. 25A

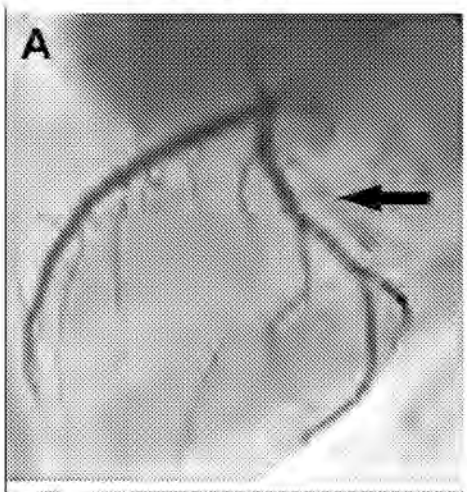

FIG. 25B

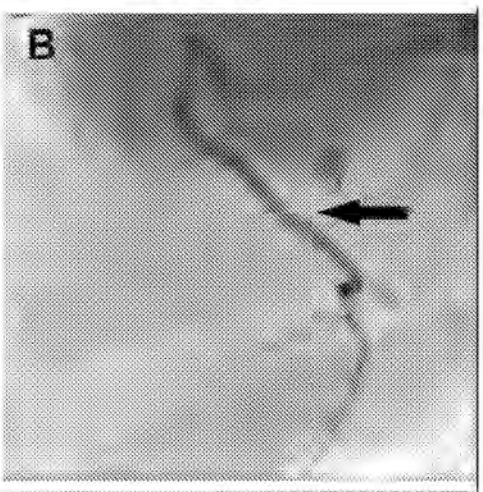

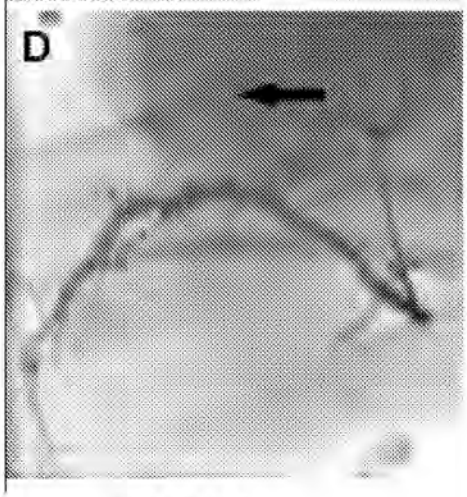

FIG. 25C

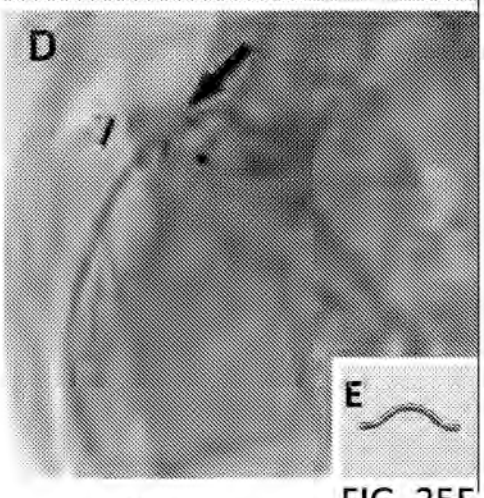

FIG. 25D

FIG. 25E

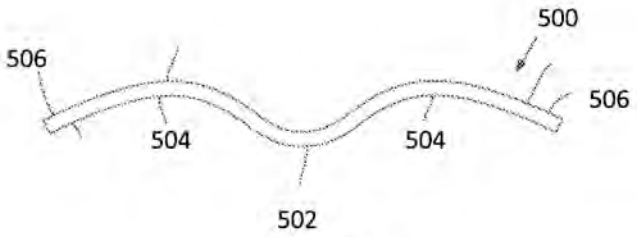

FIG. 26

FIG. 27

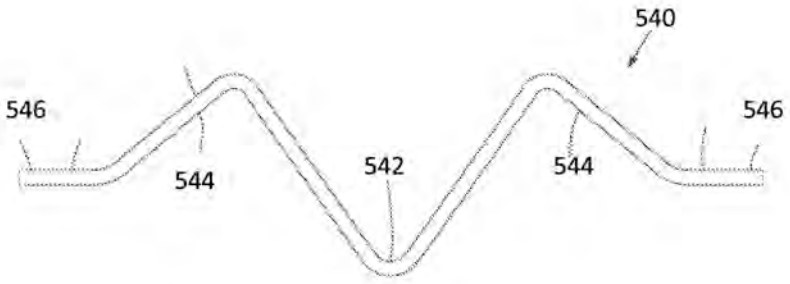

FIG. 28

17/17

8.2 Transatrial intrapericardial tricuspid annuloplasty risk analysis

Category	Event	Probability	Severity	Risk (probability × severity)	Risk mitigation strategy
General	Death	1	5	5	• There is a risk of death with all invasive cardiac procedures • Mitigate risk with informed consent
	Cardiopulmonary arrest	1	5	5	• There is a risk of cardiopulmonary arrest from arrhythmia, pericardial tamponade or hypovolemic shock • These individual risks are described in more detail below • Close monitoring of the patient during the procedure shall mitigate risk
	Radiation	4	1	4	• Fluoroscopy is necessary to guide this procedure • The dose is comparable to that received from many diagnostic medical x-ray and nuclear medicine procedures • There is a possibility of risk to an unborn child. Women of childbearing age will be asked whether they could be pregnant or perform a pregnancy test
	Medications (known risks of commonly used medications – e.g. narcotics, anxiolytics, anticoagulants)	2	4	8	• No new or experiment medications are required for this procedure • All medications are commonly used in cardiac catheterization laboratories and potential complications are well known
	Allergic reaction or anaphylaxis to medication or iodinated contrast agent	1	5	5	• This risk is no greater than other invasive cardiac procedures or diagnostic X-ray investigations • Patients sensitive to iodinated contrast shall be pre-medicated with antihistamines and steroids
	Iodinated contrast-induced nephropathy	2	3	6	• Minimize total volume of contrast used during procedure • Monitor renal function pre- and post-procedure • Pre-hydrate with intravenous fluids
	Thrombosis and thromboembolism	2	3	6	• Small thrombi forming on catheters in the venous system can embolize to the lungs but are unlikely to cause any significant harm • Small emboli could theoretically cross a patent foramen ovale into the systemic circulation but this risk is no greater than right heart catheterization

Score	1	2	3	4	5
Probability	Rare	Uncommon	Common	Normal	
Severity	Easy to correct, no anticipated harm to patient	Difficult to correct, no anticipated harm to patient	Potentially harmful to patient	Likely harmful, even with immediate correction	Life threatening
Risk (probability × severity)	1-4	5-9	10-20	>20	
Interpretation	Negligible	Tolerable	Tolerable but undesirable	Intolerable	

Category	Event	Probability	Severity	Risk (probability × severity)	Risk mitigation strategy
					• Pulmonary emboli large enough to cause hemodynamic compromise are extremely unlikely from this procedure • Administration of intravenous heparin shall mitigate this risk
	Pain	3	3	6	• Pain is common with all invasive procedures • This risk shall be mitigated with careful use of analgesics, well before vascular access is obtained
Femoral access	Superficial hematoma/bruising	3	1	3	• Superficial hematoma/bruising can be easily managed with simple pressure • Patients shall be warned of this common risk in informed consent
	Femoral vascular injury (e.g. pseudoaneurysm, arteriovenous fistula, dissection)	1	2	2	• Injury to femoral vessels shall be avoided by careful technique including fluoroscopic landmarks and/or ultrasound guidance • Monitoring of activated clotting time (ACT) to ensure reversal of anticoagulation before • Careful hemostasis including use of arterial access closure devices (e.g. Angioseal)
	Retroperitoneal bleeding/hematoma	2	3	6	• High punctures shall be avoided by careful technique including fluoroscopic landmarks and/or ultrasound guidance • Retroperitoneal bleeding shall be suspected and ruled out early in the event of unexplained hypotension
	Infection	2	4	8	• Sterile technique shall be used • This risk is no greater than other invasive cardiac procedures
	Significant bleeding (requiring surgery or transfusion)	2	3	6	• There is a risk of hemorrhage from vascular access and from bleeding into the pericardial via the right atrial appendage puncture • Patients will be crossmatched pre-procedure
Trans-auricular pericardial access	Right atrial tear/perforation requiring urgent surgical repair	2	5	10	• Initial puncture shall be made with small guidewire, which is then upsized to stiff guidewire

Score	1	2	3	4	5
Probability	Rare	Uncommon	Common	Normal	
Severity	Easy to correct, no anticipated harm to patient	Difficult to correct, no anticipated harm to patient	Potentially harmful to patient	Likely harmful, even with immediate correction	Life threatening
Risk (probability × severity)	1-4	5-9	10-20	>20	
Interpretation	Negligible	Tolerable	Tolerable but undesirable	Intolerable	

Category	Event	Probability	Severity	Risk (probability × severity)	Risk mitigation strategy
					• Large sheaths shall be delivered over stiff guidewire to minimize risk of tearing the right atrium • Once inside the pericardial space, sheath manipulation shall be minimized to prevent trauma to pericardial access port through the right atrial appendage
	Pericardial effusion	3	1	3	• Most hemorrhagic effusions can be drained through the pericardial sheath • Pericardial washout shall be performed to minimize risk of pericarditis and/or adhesion formation
	Pericardial tamponade	2	5	10	• Tamponade shall be detected early from hemodynamics and/or procedural imaging (e.g. echocardiography, MRI) • Most effusions can be drained through trans-auricular pericardial sheath or by subxiphoid drain insertion • If tamponade results from trauma/tear to the right atrium then emergency surgery may be required
	Arrhythmia	3	1	3	• Most likely arrhythmias are atrial rather than ventricular • Continuous ECG monitoring shall ensure swift recognition and treatment to mitigate risk
Annuloplasty (early)	Coronary artery compression	3	3	9	• Protection elements shall be positioned along the implant to deflect compressive force away from important underlying structures • Coronary angiography shall be performed with implant under tension but prior to final locking to ensure patency of coronary arteries
	Coronary sinus compression	3	3	9	• Protection elements shall be positioned along the implant to deflect compressive force away from important underlying structures
	Implant infection	1	5	5	• Sterile technique shall be used • Prophylactic antibiotics shall be given pre- and post-procedure
	Failure to deliver implant to atrioventricular groove	2	3	6	• Whole system is retrievable up to point of final locking and release

Score	**1**	**2**	**3**	**4**	**5**
Probability	Rare	Uncommon	Common	Normal	
Severity	Easy to correct, no anticipated harm to patient	Difficult to correct, no anticipated harm to patient	Potentially harmful to patient	Likely harmful, even with immediate correction	Life threatening
Risk (probability × severity)	1-4	5-9	10-20	>20	
Interpretation	Negligible	Tolerable	Tolerable but undesirable	Intolerable	

Category	Event	Probability	Severity	Risk (probability × severity)	Risk mitigation strategy
	Pericarditis	3	4	12	• Pericarditis can be very painful for the patient and can lead to accumulation of pericardial effusion • Pericardial washout with saline shall be performed after implant deployment • Intra-pericardial steroid (e.g. Triamcinolone) shall be given prior to pericardial port closure • Oral non-steroidal anti-inflammatory drugs (NSAID) shall be given post-procedure
Annuloplasty (late)	Tissue erosion from implant	1	4	4	• Implant is designed to be non-traumatic • Tensioning element is not in direct contact with myocardium • Implant should become rapidly fibrosed to the myocardium minimizing risk of long-term erosion
	Coronary artery compression caused by displacement of a protection element	2	4	8	• Displacement of a protection element and subsequent coronary artery compression could lead to ischemia and/or infarction • As the implant becomes fibrosed to the myocardium, the risk of displacement becomes lesser and lesser
	Failure of tensioning element (e.g. gradual loosening or sudden rupture)	1	3	3	• If the tensioning element fails, the implant will loosen resulting in a loss of annuloplasty effect • Besides recurrence of tricuspid regurgitation, the risk to the patient from this should be minimal
	Implant infection	1	5	5	• Early suspicion if spiking fevers and/or persistently raised inflammatory markers
	Pericardial adhesions	3	4	12	• Severe adhesions could render future cardiac surgery more difficult • Intra-pericardial steroid (e.g. Triamcinolone) given prior to pericardial port closure shall mitigate the risk of chronic pericardial adhesion formation
Pericardial port closure	Failure to deploy closure device	2	4	8	• Use safety wire to maintain access in case of accidental pull-through of closure device

Score	**1**	**2**	**3**	**4**	**5**
Probability	Rare	Uncommon	Common	Normal	
Severity	Easy to correct, no anticipated harm to patient	Difficult to correct, no anticipated harm to patient	Potentially harmful to patient	Likely harmful, even with immediate correction	Life threatening
Risk (probability × severity)	1-4	5-9	10-20	>20	
Interpretation	Negligible	Tolerable	Tolerable but undesirable	Intolerable	

Category	Event	Probability	Severity	Risk (probability × severity)	Risk mitigation strategy
	Failure to achieve hemostasis	2	4	8	• Anticoagulation shall be reversed prior to pericardial port closure • Sub-xiphoid pericardial access can be obtained for drain insertion • Safety wire ensure trans-auricular pericardial access can be re-established, pericardial drainage and washout can be performed – before closure is re-attempted
	Tissue erosion from closure device	1	4	8	• This is a recognized risk of Nitinol occluder devices but is rare • Device should endothelialize rapidly after deployment so risk of erosion is extremely low

Score	1	2	3	4	5
Probability	Rare	Uncommon	Common	Normal	
Severity	Easy to correct, no anticipated harm to patient	Difficult to correct, no anticipated harm to patient	Potentially harmful to patient	Likely harmful, even with immediate correction	Life threatening
Risk (probability × severity)	1-4	5-9	10-20	>20	
Interpretation	Negligible	Tolerable	Tolerable but undesirable	Intolerable	

REFERENCES

1. Johnson JN, Hornik CP, Li JS, Benjamin DK, Jr., Yoshizumi TT, Reiman RE, Frush DP and Hill KD. Cumulative radiation exposure and cancer risk estimation in children with heart disease. *Circulation*. 2014;130:161-7.

2. Venneri L, Rossi F, Botto N, Andreassi MG, Salcone N, Emad A, Lazzeri M, Gori C, Vano E and Picano E. Cancer risk from professional exposure in staff working in cardiac catheterization laboratory: insights from the National Research Council's Biological Effects of Ionizing Radiation VII Report. *Am Heart J*. 2009;157:118-24.

3. Duerk JL, Butts K, Hwang KP and Lewin JS. Pulse sequences for interventional magnetic resonance imaging. *Top Magn Reson Imaging*. 2000;11:147-62.

4. Dana C. Peters FRKTMGWFBJEHKKVCAM. Undersampled projection reconstruction applied to MR angiography. *Magn Reson Med*. 2000;43:91-101.

5. Elgort DR, Wong EY, Hillenbrand CM, Wacker FK, Lewin JS and Duerk JL. Real-time catheter tracking and adaptive imaging. *J Magn Reson Imaging*. 2003;18:621-6.

6. Dick AJ, Raman VK, Raval AN, Guttman MA, Thompson RB, Ozturk C, Peters DC, Stine AM, Wright VJ, Schenke WH and Lederman RJ. Invasive human magnetic resonance imaging during angioplasty: feasibility in a combined XMR suite. *Catheter Cardiovasc Interv*. 2005;64:265-74.

7. White MJ, Thornton JS, Hawkes DJ, Hill DL, Kitchen N, Mancini L, McEvoy AW, Razavi R, Wilson S, Yousry T and Keevil SF. Design, Operation, and Safety of Single-Room Interventional MRI Suites: Practical Experience From Two Centers. *J Magn Reson Imaging*. 2014.

8. Bakker CJ, Hoogeveen RM, Weber J, van Vaals JJ, Viergever MA and Mali WP. Visualization of dedicated catheters using fast scanning techniques with potential for MR-guided vascular interventions. *Magn Reson Med*. 1996;36:816-20.

9. Bakker CJ, Bos C and Weinmann HJ. Passive tracking of catheters and guidewires by contrast-enhanced MR fluoroscopy. *Magn Reson Med*. 2001;45:17-23.

10. Buecker A, Spuentrup E, Schmitz-Rode T, Kinzel S, Pfeffer J, Hohl C, van Vaals JJ and Gunther RW. Use of a nonmetallic guide wire for magnetic resonance-guided coronary artery catheterization. *Invest Radiol*. 2004;39:656-60.

11. Tzifa A, Krombach GA, Kramer N, Kruger S, Schutte A, von Walter M, Schaeffter T, Qureshi S, Krasemann T, Rosenthal E, Schwartz CA, Varma G, Buhl A, Kohlmeier A, Bucker A, Gunther RW and Razavi R. Magnetic resonance-guided cardiac interventions using magnetic resonance-compatible devices: a preclinical study and first-in-man congenital interventions. *Circ Cardiovasc Interv*. 2010;3:585-92.

12. Miquel ME, Hegde S, Muthurangu V, Corcoran BJ, Keevil SF, Hill DL and Razavi RS. Visualization and tracking of an inflatable balloon catheter using SSFP in a flow phantom and in the heart and great vessels of patients. *Magn Reson Med*. 2004;51:988-95.

13. Razavi R, Hill DL, Keevil SF, Miquel ME, Muthurangu V, Hegde S, Rhode K, Barnett M, van Vaals J, Hawkes DJ and Baker E. Cardiac catheterisation guided by MRI in children and adults with congenital heart disease. *Lancet*. 2003;362:1877-82.

14. Kuehne T, Yilmaz S, Schulze-Neick I, Wellnhofer E, Ewert P, Nagel E and Lange P. Magnetic resonance imaging guided catheterisation for assessment of pulmonary vascular resistance: in vivo validation and clinical application in patients with pulmonary hypertension. *Heart*. 2005;91:1064-9.

15. Ratnayaka K, Faranesh AZ, Hansen MS, Stine AM, Halabi M, Barbash IM, Schenke WH, Wright VJ, Grant LP, Kellman P, Kocaturk O and Lederman RJ. Real-time MRI-guided right heart catheterization in adults using passive catheters. *Eur Heart J*. 2013;34:380-9.

16. Kantor HL, Briggs RW and Balaban RS. In vivo 31P nuclear magnetic resonance measurements in canine heart using a catheter-coil. *Circ Res*. 1984;55:261-6.

17. Martin AJ, Plewes DB and Henkelman RM. MR imaging of blood vessels with an intravascular coil. *J Magn Reson Imaging*. 1992;2:421-9.

18. Hurst GC, Hua J, Duerk JL and Cohen AM. Intravascular (catheter) NMR receiver probe: preliminary design analysis and application to canine iliofemoral imaging. *Magn Reson Med*. 1992;24:343-57.

19. Kandarpa K, Jakab P, Patz S, Schoen FJ and Jolesz FA. Prototype miniature endoluminal MR imaging catheter. *J Vasc Interv Radiol*. 1993;4:419-27.

20. Atalar E, Bottomley PA, Ocali O, Correia LC, Kelemen MD, Lima JA and Zerhouni EA. High resolution intravascular MRI and MRS by using a catheter receiver coil. *Magn Reson Med*. 1996;36:596-605.

21. Hillenbrand CM, Elgort DR, Wong EY, Reykowski A, Wacker FK, Lewin JS and Duerk JL. Active device tracking and high-resolution intravascular MRI using a novel catheter-based, opposed-solenoid phased array coil. *Magn Reson Med*. 2004;51:668-75.

22. Worthley SG, Helft G, Fuster V, Fayad ZA, Shinnar M, Minkoff LA, Schechter C, Fallon JT and Badimon JJ. A novel nonobstructive intravascular MRI coil: in vivo imaging of experimental atherosclerosis. *Arterioscler Thromb Vasc Biol*. 2003;23:346-50.

23. Ladd ME, Erhart P, Debatin JF, Hofmann E, Boesiger P, von Schulthess GK and McKinnon GC. Guidewire antennas for MR fluoroscopy. *Magn Reson Med*. 1997;37:891-7.

24. Ocali O and Atalar E. Intravascular magnetic resonance imaging using a loopless catheter antenna. *Magn Reson Med*. 1997;37:112-8.

25. Atalar E, Kraitchman DL, Carkhuff B, Lesho J, Ocali O, Solaiyappan M, Guttman MA and Charles HK, Jr. Catheter-tracking FOV MR fluoroscopy. *Magn Reson Med*. 1998;40:865-72.

26. Burl M, Coutts GA, Herlihy DJ, Hill-Cottingham R, Eastham JF, Hajnal JV and Young IR. Twisted-pair RF coil suitable for locating the track of a catheter. *Magn Reson Med*. 1999;41:636-8.

27. Rivas PA, Nayak KS, Scott GC, McConnell MV, Kerr AB, Nishimura DG, Pauly JM and Hu BS. In vivo real-time intravascular MRI. *J Cardiovasc Magn Reson*. 2002;4:223-32.

28. Susil RC, Yeung CJ and Atalar E. Intravascular extended sensitivity (IVES) MRI antennas. *Magn Reson Med*. 2003;50:383-90.

29. Sonmez M, Saikus CE, Bell JA, Franson DN, Halabi M, Faranesh AZ, Ozturk C, Lederman RJ and Kocaturk O. MRI active guidewire with an embedded temperature probe and providing a distinct tip signal to enhance clinical safety. *J Cardiovasc Magn Reson*. 2012;14:38.

30. Guttman MA, Ozturk C, Raval AN, Raman VK, Dick AJ, DeSilva R, Karmarkar P, Lederman RJ and McVeigh ER. Interventional cardiovascular procedures guided by real-time MR imaging: an interactive interface using multiple slices, adaptive projection modes and live 3D renderings. *J Magn Reson Imaging*. 2007;26:1429-35.

31. Dumoulin CL, Souza SP and Darrow RD. Real-time position monitoring of invasive devices using magnetic resonance. *Magn Reson Med*. 1993;29:411-5.

32. Leung DA, Debatin JF, Wildermuth S, McKinnon GC, Holtz D, Dumoulin CL, Darrow RD, Hofmann E and von Schulthess GK. Intravascular MR tracking catheter: preliminary experimental evaluation. *AJR Am J Roentgenol*. 1995;164:1265-70.

33. Ladd ME, Zimmermann GG, McKinnon GC, von Schulthess GK, Dumoulin CL, Darrow RD, Hofmann E and Debatin JF. Visualization of vascular guidewires using MR tracking. *J Magn Reson Imaging*. 1998;8:251-3.

34. Campbell-Washburn A, Rogers T, Xue H, Hansen MS, Lederman RJ and Faranesh AZ. Dual echo positive contrast bSSFP for real-time visualization of passive devices during MRI-guided cardiovascular catheterization. *J Cardiovasc Magn Reson*. 2014;In press.

35. Srinivasan S and Ennis DB. Variable flip angle balanced steady-state free precession for lower SAR or higher contrast cardiac cine imaging. *Magn Reson Med*. 2013.

36. Wu X, Akgun C, Vaughan JT, Andersen P, Strupp J, Ugurbil K and Van de Moortele PF. Adapted RF pulse design for SAR reduction in parallel excitation with experimental verification at 9.4 T. *J Magn Reson*. 2010;205:161-70.

37. Ladd ME and Quick HH. Reduction of resonant RF heating in intravascular catheters using coaxial chokes. *Magn Reson Med*. 2000;43:615-9.

38. Lee C, McNamara C and Viohl I. Connector and guidewire connectable thereto. *United States Patent*. 2004.

39. Yeung CJ, Susil RC and Atalar E. RF safety of wires in interventional MRI: using a safety index. *Magn Reson Med*. 2002;47:187-93.

40. Serfaty JM, Yang X, Foo TK, Kumar A, Derbyshire A and Atalar E. MRI-guided coronary catheterization and PTCA: A feasibility study on a dog model. *Magn Reson Med*. 2003;49:258-63.

41. Weiss S, Vernickel P, Schaeffter T, Schultz V and Gleich B. A safe transmission line for interventional devices. *5th International MRI Symposium*. 2004.

42. Wong EY, Zhang Q, Duerk JL, Lewin JS and Wendt M. An optical system for wireless detuning of parallel resonant circuits. *J Magn Reson Imaging*. 2000;12:632-8.

43. Konings MK, Bartels LW, van Swol CF and Bakker CJ. Development of an MR-safe tracking catheter with a laser-driven tip coil. *J Magn Reson Imaging*. 2001;13:131-5.

44. Eggers H, Weiss S, Boernert P and Boesiger P. Image-based tracking of optically detunable parallel resonant circuits. *Magn Reson Med*. 2003;49:1163-74.

45. Weiss S, Schaeffter T, Brinkert F, Kuhne T and Bücker A. [An approach for safe visualization and localization of catheter during MR-guided intravascular procedures]. *Z Med Phys*. 2003;13:172-6.

46. Bell JA, Saikus CE, Ratnayaka K, Barbash IM, Faranesh AZ, Franson DN, Sonmez M, Slack MC, Lederman RJ and Kocaturk O. Active delivery cable tuned to device deployment state: enhanced visibility of nitinol occluders during preclinical interventional MRI. *J Magn Reson Imaging*. 2012;36:972-8.

47. Hofmann LV, Liddell RP, Eng J, Wasserman BA, Arepally A, Lee DS and Bluemke DA. Human Peripheral Arteries: Feasibility of Transvenous Intravascular MR Imaging of the Arterial Wall. *Radiology*. 2005;235:617-22.

48. Larose E, Yeghiazarians Y, Libby P, Yucel EK, Aikawa M, Kacher DF, Aikawa E, Kinlay S, Schoen FJ, Selwyn AP and Ganz P. Characterization of Human Atherosclerotic Plaques by Intravascular Magnetic Resonance Imaging. *Circulation*. 2005;112:2324-2331.

49. Kocaturk O, Kim AH, Saikus CE, Guttman MA, Faranesh AZ, Ozturk C and Lederman RJ. Active two-channel 0.035'' guidewire for interventional cardiovascular MRI. *J Magn Reson Imaging*. 2009;30:461-5.

50. Quick HH, Kuehl H, Kaiser G, Bosk S, Debatin JF and Ladd ME. Inductively coupled stent antennas in MRI. *Magn Reson Med*. 2002;48:781-90.

51. Kivelitz D, Wagner S, Schnorr J, Wetzler R, Busch M, Melzer A, Taupitz M and Hamm B. A vascular stent as an active component for locally enhanced magnetic resonance

imaging: initial in vivo imaging results after catheter-guided placement in rabbits. *Invest Radiol*. 2003;38:147-52.

52. Kuehne T, Fahrig R and Butts K. Pair of resonant fiducial markers for localization of endovascular catheters at all catheter orientations. *J Magn Reson Imaging*. 2003;17:620-4.

53. Quick HH, Zenge MO, Kuehl H, Kaiser G, Aker S, Massing S, Bosk S and Ladd ME. Interventional magnetic resonance angiography with no strings attached: wireless active catheter visualization. *Magn Reson Med*. 2005;53:446-55.

54. Spuentrup E, Ruebben A, Schaeffter T, Manning WJ, Gunther RW and Buecker A. Magnetic resonance--guided coronary artery stent placement in a swine model. *Circulation*. 2002;105:874-9.

55. Wildermuth S, Dumoulin CL, Pfammatter T, Maier SE, Hofmann E and Debatin JF. MR-guided percutaneous angioplasty: assessment of tracking safety, catheter handling and functionality. *Cardiovasc Intervent Radiol*. 1998;21:404-10.

56. Yang X, Bolster BD, Jr., Kraitchman DL and Atalar E. Intravascular MR-monitored balloon angioplasty: an in vivo feasibility study. *J Vasc Interv Radiol*. 1998;9:953-9.

57. Buecker A, Adam GB, Neuerburg JM, Kinzel S, Glowinski A, Schaeffter T, Rasche V, van Vaals JJ and Guenther RW. Simultaneous real-time visualization of the catheter tip and vascular anatomy for MR-guided PTA of iliac arteries in an animal model. *J Magn Reson Imaging*. 2002;16:201-8.

58. Godart F, Beregi JP, Nicol L, Occelli B, Vincentelli A, Daanen V, Rey C and Rousseau J. MR-guided balloon angioplasty of stenosed aorta: in vivo evaluation using near-standard instruments and a passive tracking technique. *J Magn Reson Imaging*. 2000;12:639-44.

59. Omary RA, Frayne R, Unal O, Warner T, Korosec FR, Mistretta CA, Strother CM and Grist TM. MR-guided angioplasty of renal artery stenosis in a pig model: a feasibility study. *J Vasc Interv Radiol*. 2000;11:373-81.

60. Buecker A, Neuerburg JM, Adam GB, Glowinski A, Schaeffter T, Rasche V, van Vaals JJ, Molgaard-Nielsen A and Guenther RW. Real-time MR fluoroscopy for MR-guided iliac artery stent placement. *J Magn Reson Imaging*. 2000;12:616-22.

61. Dion YM, Ben El Kadi H, Boudoux C, Gourdon J, Chakfe N, Traore A and Moisan C. Endovascular procedures under near-real-time magnetic resonance imaging guidance: an experimental feasibility study. *J Vasc Surg*. 2000;32:1006-14.

62. Feng L, Dumoulin CL, Dashnaw S, Darrow RD, Delapaz RL, Bishop PL and Pile-Spellman J. Feasibility of stent placement in carotid arteries with real-time MR imaging guidance in pigs. *Radiology*. 2005;234:558-62.

63. Kuehne T, Saeed M, Higgins CB, Gleason K, Krombach GA, Weber OM, Martin AJ, Turner D, Teitel D and Moore P. Endovascular stents in pulmonary valve and artery in swine: feasibility study of MR imaging-guided deployment and postinterventional assessment. *Radiology*. 2003;226:475-81.

64. Wacker FK, Hillenbrand C, Elgort DR, Zhang S, Duerk JL and Lewin JS. MR imaging-guided percutaneous angioplasty and stent placement in a swine model: Comparison of open- and closed-bore scanners. *Academic Radiology*. 2005;12:1085.

65. Raval AN, Telep JD, Guttman MA, Ozturk C, Jones M, Thompson RB, Wright VJ, Schenke WH, DeSilva R, Aviles RJ, Raman VK, Slack MC and Lederman RJ. Real-time magnetic resonance imaging-guided stenting of aortic coarctation with commercially available catheter devices in Swine. *Circulation*. 2005;112:699-706.

66. Bartels LW, Bos C, van Der Weide R, Smits HF, Bakker CJ and Viergever MA. Placement of an inferior vena cava filter in a pig guided by high-resolution MR fluoroscopy at 1.5 T. *J Magn Reson Imaging*. 2000;12:599-605.

67. Bücker A, Neuerburg JM, Adam GB, Glowinski A, Schaeffter T, Rasche V, van Vaals JJ and Gunther RW. Real-time MR Guidance for inferior vena cava filter placement in an animal model. *J Vasc Interv Radiol*. 2001;12:753-6.

68. Frahm C, Gehl HB, Lorch H, Zwaan M, Drobnitzky M, Laub GA and Weiss HD. MR-guided placement of a temporary vena cava filter: technique and feasibility. *J Magn Reson Imaging*. 1998;8:105-9.

69. Bücker A, Neuerburg JM, Adam G, Glowinski A, van Vaals JJ and Gunther RW. [MR-guided coil embolisation of renal arteries in an animal model]. *Rofo*. 2003;175:271-4.

70. Fink C, Bock M, Umathum R, Volz S, Zuehlsdorff S, Grobholz R, Kauczor HU and Hallscheidt P. Renal embolization: feasibility of magnetic resonance-guidance using active catheter tracking and intraarterial magnetic resonance angiography. *Invest Radiol*. 2004;39:111-9.

71. Seppenwoolde JH, Bartels LW, van der Weide R, Nijsen JF, van het Schip AD and Bakker CJ. Fully MR-guided hepatic artery catheterization for selective drug delivery: a feasibility study in pigs. *J Magn Reson Imaging*. 2006;23:123-9.

72. Raval AN, Karmarkar PV, Guttman MA, Ozturk C, Sampath S, DeSilva R, Aviles RJ, Xu M, Wright VJ, Schenke WH, Kocaturk O, Dick AJ, Raman VK, Atalar E, McVeigh ER and Lederman RJ. Real-Time MRI-Guided Endovascular Recanalization of Chronic Total Arterial Occlusion in a Swine Model [In Press]. *Circulation*. 2005.

73. Raman VK, Karmarkar PV, Guttman MA, Dick AJ, Peters DC, Ozturk C, Pessanha BS, Thompson RB, Raval AN, DeSilva R, Aviles RJ, Atalar E, McVeigh ER and Lederman RJ. Real-time magnetic resonance-guided endovascular repair of experimental abdominal aortic aneurysm in swine. *J Am Coll Cardiol*. 2005;45:2069-77.

74. Eggebrecht H and Quick HH. [Personal Communication]. 2005.

75. Schalla S, Saeed M, Higgins CB, Martin A, Weber O and Moore P. Magnetic resonance--guided cardiac catheterization in a swine model of atrial septal defect. *Circulation*. 2003;108:1865-70.

76. Feng L, Dumoulin CL, Dashnaw S, Darrow RD, Guhde R, Delapaz RL, Bishop PL and Pile-Spellman J. Transfemoral catheterization of carotid arteries with real-time MR imaging guidance in pigs. *Radiology*. 2005;234:551-7.

77. Omary RA, Green JD, Schirf BE, Li Y, Finn JP and Li D. Real-time magnetic resonance imaging-guided coronary catheterization in swine. *Circulation*. 2003;107:2656-9.

78. Quick HH, Kuehl H, Kaiser G, Hornscheidt D, Mikolajczyk KP, Aker S, Debatin JF and Ladd ME. Interventional MRA using actively visualized catheters, TrueFISP, and real-time image fusion. *Magn Reson Med*. 2003;49:129-37.

79. Buecker A, Spuentrup E, Grabitz R, Freudenthal F, Muehler EG, Schaeffter T, van Vaals JJ and Gunther RW. Magnetic resonance-guided placement of atrial septal closure device in animal model of patent foramen ovale. *Circulation*. 2002;106:511-5.

80. Rickers C, Jerosch-Herold M, Hu X, Murthy N, Wang X, Kong H, Seethamraju RT, Weil J and Wilke NM. Magnetic resonance image-guided transcatheter closure of atrial septal defects. *Circulation*. 2003;107:132-8.

81. Schalla S, Saeed M, Higgins CB, Weber O, Martin A and Moore P. Balloon sizing and transcatheter closure of acute atrial septal defects guided by magnetic resonance fluoroscopy: assessment and validation in a large animal model. *J Magn Reson Imaging*. 2005;21:204-11.

82. Kuehne T, Yilmaz S, Meinus C, Moore P, Saeed M, Weber O, Higgins CB, Blank T, Elsaesser E and Schnackenburg B. Magnetic resonance imaging-guided transcatheter implantation of a prosthetic valve in aortic valve position: Feasibility study in swine. *J Am Coll Cardiol*. 2004;44:2247-2249.

83. Dick AJ, Guttman MA, Raman VK, Peters DC, Pessanha BS, Hill JM, Smith S, Scott G, McVeigh ER and Lederman RJ. Magnetic resonance fluoroscopy allows targeted delivery of mesenchymal stem cells to infarct borders in Swine. *Circulation*. 2003;108:2899-904.

84. Lederman RJ, Guttman MA, Peters DC, Thompson RB, Sorger JM, Dick AJ, Raman VK and McVeigh ER. Catheter-based endomyocardial injection with real-time magnetic resonance imaging. *Circulation*. 2002;105:1282-4.

85. Corti R, Badimon J, Mizsei G, Macaluso F, Lee M, Licato P, Viles-Gonzalez JF, Fuster V and Sherman W. Real time magnetic resonance guided endomyocardial local delivery. *Heart*. 2005;91:348-53.

86. Karmarkar PV, Kraitchman DL, Izbudak I, Hofmann LV, Amado LC, Fritzges D, Young R, Pittenger M, Bulte JW and Atalar E. MR-trackable intramyocardial injection catheter. *Magn Reson Med*. 2004;51:1163-72.

87. Krombach GA, Pfeffer JG, Kinzel S, Katoh M, Gunther RW and Buecker A. MR-guided percutaneous intramyocardial injection with an MR-compatible catheter: feasibility and changes in T1 values after injection of extracellular contrast medium in pigs. *Radiology*. 2005;235:487-94.

88. Saeed M, Lee R, Martin A, Weber O, Krombach GA, Schalla S, Lee M, Saloner D and Higgins CB. Transendocardial delivery of extracellular myocardial markers by using combination X-ray/MR fluoroscopic guidance: feasibility study in dogs. *Radiology*. 2004;231:689-96.

89. Hazel SJ, Paterson HS, Edwards JR and Maddern GJ. Surgical treatment of atrial fibrillation via energy ablation. *Circulation*. 2005;111:e103-6.

90. Susil RC, Yeung CJ, Halperin HR, Lardo AC and Atalar E. Multifunctional interventional devices for MRI: a combined electrophysiology/MRI catheter. *Magn Reson Med*. 2002;47:594-600.

91. Lardo AC, McVeigh ER, Jumrussirikul P, Berger RD, Calkins H, Lima J and Halperin HR. Visualization and temporal/spatial characterization of cardiac radiofrequency ablation lesions using magnetic resonance imaging. *Circulation*. 2000;102:698-705.

92. Reddy V, Malchano Z, Dukkipati S, Holmvang G, Schmidt E, Dumoulin C, Mallozzi R and Ruskin J. Interventional MRI: Electroanatomical Mapping Using Real-time MR Tracking of a Deflectable Catheter [Abstract]. *Heart Rhythm*. 2005;2:S279-S280.

93. Dukkipati SR, Mallozzi R, Schmidt EJ, Holmvang G, d'Avila A, Guhde R, Darrow RD, Slavin G, Fung M, Malchano Z, Kampa G, Dando JD, McPherson C, Foo TK, Ruskin JN, Dumoulin CL and Reddy VY. Electroanatomic mapping of the left ventricle in a porcine model of chronic myocardial infarction with magnetic resonance-based catheter tracking. *Circulation*. 2008;118:853-62.

94. Hoffmann BA, Koops A, Rostock T, Mullerleile K, Steven D, Karst R, Steinke MU, Drewitz I, Lund G, Koops S, Adam G and Willems S. Interactive real-time mapping and catheter ablation of the cavotricuspid isthmus guided by magnetic resonance imaging in a porcine model. *Eur Heart J*. 2010;31:450-6.

95. Vergara GR, Vijayakumar S, Kholmovski EG, Blauer JJ, Guttman MA, Gloschat C, Payne G, Vij K, Akoum NW, Daccarett M, McGann CJ, Macleod RS and Marrouche NF. Real-time magnetic resonance imaging-guided radiofrequency atrial ablation and visualization of lesion formation at 3 Tesla. *Heart Rhythm*. 2011;8:295-303.

96. Ganesan AN, Selvanayagam JB, Mahajan R, Grover S, Nayyar S, Brooks AG, Finnie J, Sunnarborg D, Lloyd T, Chakrabarty A, Abed HS and Sanders P. Mapping and ablation of the

pulmonary veins and cavo-tricuspid isthmus with a magnetic resonance imaging-compatible externally irrigated ablation catheter and integrated electrophysiology system. *Circ Arrhythm Electrophysiol*. 2012;5:1136-42.

97. Arepally A, Karmarkar PV, Weiss C, Rodriguez ER, Lederman RJ and Atalar E. Magnetic resonance image-guided trans-septal puncture in a swine heart. *J Magn Reson Imaging*. 2005;21:463-7.

98. Raval AN, Karmarkar PV, Guttman MA, Ozturk C, DeSilva R, Wright VJ, Schenke WH, Atalar E, McVeigh ER and Lederman RJ. Real-Time MRI Guided Atrial Septal Puncture and Balloon Septostomy in Swine [In Press]. *Catheter Cardiovasc Interv*. 2005.

99. Barbash IM, Saikus CE, Faranesh AZ, Ratnayaka K, Kocaturk O, Chen MY, Bell JA, Virmani R, Schenke WH, Hansen MS, Slack MC and Lederman RJ. Direct percutaneous left ventricular access and port closure: pre-clinical feasibility. *JACC Cardiovasc Interv*. 2011;4:1318-25.

100. Halabi M, Ratnayaka K, Faranesh AZ, Hansen MS, Barbash IM, Eckhaus MA, Wilson JR, Chen MY, Slack MC, Kocaturk O, Schenke WH, Wright VJ and Lederman RJ. Transthoracic delivery of large devices into the left ventricle through the right ventricle and interventricular septum: preclinical feasibility. *J Cardiovasc Magn Reson*. 2013;15:10.

101. Ratnayaka K, Saikus CE, Faranesh AZ, Bell JA, Barbash IM, Kocaturk O, Reyes CA, Sonmez M, Schenke WH, Wright VJ, Hansen MS, Slack MC and Lederman RJ. Closed-chest transthoracic magnetic resonance imaging-guided ventricular septal defect closure in swine. *JACC Cardiovasc Interv*. 2011;4:1326-34.

102. Halabi M, Faranesh A, Schenke W, Wright V, Hansen M, Saikus C, Kocaturk O, Lederman R and Ratnayaka K. Real-time cardiovascular magnetic resonance subxiphoid pericardial access and pericardiocentesis using off-the-shelf devices in swine. *J Cardiovasc Magn Reson*. 2013;15:61.

103. Kee ST, Rhee JS, Butts K, Daniel B, Pauly J, Kerr A, O'Sullivan GJ, Sze DY, Razavi MK, Semba CP, Herfkens RJ and Dake MD. 1999 Gary J. Becker Young Investigator Award. MR-guided transjugular portosystemic shunt placement in a swine model. *J Vasc Interv Radiol*. 1999;10:529-35.

104. Kee ST, Ganguly A, Daniel BL, Wen Z, Butts K, Shimikawa A, Pelc NJ, Fahrig R and Dake MD. MR-guided transjugular intrahepatic portosystemic shunt creation with use of a hybrid radiography/MR system. *J Vasc Interv Radiol*. 2005;16:227-34.

105. Arepally A, Kamarkar P, Weiss C and Atalar E. Percutaneous MR-Guided Transvascular Access of the Mesenteric Venous System-Study in a Swine Model [In Press]. *Radiology*. 2005.

106. Paetzel C, Zorger N, Seitz J, Volk M, Nitz WR, Herold T, Feuerbach S and Lenhart M. Intraarterial contrast material-enhanced magnetic resonance angiography of the aortoiliac system. *J Vasc Interv Radiol*. 2004;15:981-4.

107. Manke C, Nitz WR, Djavidani B, Strotzer M, Lenhart M, Volk M, Feuerbach S and Link J. MR imaging-guided stent placement in iliac arterial stenoses: a feasibility study. *Radiology*. 2001;219:527-34.

108. Paetzel C, Zorger N, Bachthaler M, Hamer OW, Stehr A, Feuerbach S, Lenhart M, Volk M, Herold T, Kasprzak P and Nitz WR. Magnetic resonance-guided percutaneous angioplasty of femoral and popliteal artery stenoses using real-time imaging and intra-arterial contrast-enhanced magnetic resonance angiography. *Invest Radiol*. 2005;40:257-62.

109. Rogers T, Ratnayaka K and Lederman RJ. MRI catheterization in cardiopulmonary disease. *Chest*. 2014;145:30-6.

110. Di Salvo TG, Mathier M, Semigran MJ and Dec GW. Preserved right ventricular ejection fraction predicts exercise capacity and survival in advanced heart failure. *J Am Coll Cardiol*. 1995;25:1143-53.

111. Ghio S, Gavazzi A, Campana C, Inserra C, Klersy C, Sebastiani R, Arbustini E, Recusani F and Tavazzi L. Independent and additive prognostic value of right ventricular systolic function and pulmonary artery pressure in patients with chronic heart failure. *J Am Coll Cardiol*. 2001;37:183-8.

112. Muthurangu V, Taylor A, Andriantsimiavona R, Hegde S, Miquel ME, Tulloh R, Baker E, Hill DLG and Razavi RS. Novel Method of Quantifying Pulmonary Vascular Resistance by Use of Simultaneous Invasive Pressure Monitoring and Phase-Contrast Magnetic Resonance Flow. *Circulation*. 2004;110:826-834.

113. Muthurangu V, Atkinson D, Sermesant M, Miquel ME, Hegde S, Johnson R, Andriantsimiavona R, Taylor AM, Baker E, Tulloh R, Hill D and Razavi RS. Measurement of total pulmonary arterial compliance using invasive pressure monitoring and MR flow quantification during MR-guided cardiac catheterization. *Am J Physiol Heart Circ Physiol*. 2005;289:H1301-6.

114. Ohno Y, Hatabu H, Murase K, Higashino T, Nogami M, Yoshikawa T and Sugimura K. Primary pulmonary hypertension: 3D dynamic perfusion MRI for quantitative analysis of regional pulmonary perfusion. *AJR Am J Roentgenol*. 2007;188:48-56.

115. Ugander M, Oki AJ, Hsu LY, Kellman P, Greiser A, Aletras AH, Sibley CT, Chen MY, Bandettini WP and Arai AE. Extracellular volume imaging by magnetic resonance imaging provides insights into overt and sub-clinical myocardial pathology. *Eur Heart J*. 2012;33:1268-78.

116. Nishimura RA and Carabello BA. Hemodynamics in the cardiac catheterization laboratory of the 21st century. *Circulation*. 2012;125:2138-50.

117. Fujimoto N, Borlaug BA, Lewis GD, Hastings JL, Shafer KM, Bhella PS, Carrick-Ranson G and Levine BD. Hemodynamic responses to rapid saline loading: the impact of age, sex, and heart failure. *Circulation*. 2013;127:55-62.

118. Blumberg FC, Arzt M, Lange T, Schroll S, Pfeifer M and Wensel R. Impact of right ventricular reserve on exercise capacity and survival in patients with pulmonary hypertension. *Eur J Heart Fail*. 2013;15:771-5.

119. Xue H, Kellman P, Larocca G, Arai AE and Hansen MS. High spatial and temporal resolution retrospective cine cardiovascular magnetic resonance from shortened free breathing real-time acquisitions. *J Cardiovasc Magn Reson*. 2013;15:102.

120. Xue H, Inati S, Sorensen TS, Kellman P and Hansen MS. Distributed MRI reconstruction using gadgetron-based cloud computing. *Magn Reson Med*. 2014.

121. Krueger JJ, Ewert P, Yilmaz S, Gelernter D, Peters B, Pietzner K, Bornstedt A, Schnackenburg B, Abdul-Khaliq H, Fleck E, Nagel E, Berger F and Kuehne T. Magnetic resonance imaging-guided balloon angioplasty of coarctation of the aorta: a pilot study. *Circulation*. 2006;113:1093-100.

122. Eitel C, Piorkowski C, Hindricks G and Gutberlet M. Electrophysiology study guided by real-time magnetic resonance imaging. *Eur Heart J*. 2012;33:1975.

123. Grothoff M, Piorkowski C, Eitel C, Gaspar T, Lehmkuhl L, Lucke C, Hoffmann J, Hildebrand L, Wedan S, Lloyd T, Sunnarborg D, Schnackenburg B, Hindricks G, Sommer P and Gutberlet M. MR Imaging-guided Electrophysiological Ablation Studies in Humans with Passive Catheter Tracking: Initial Results. *Radiology*. 2014:122671.

124. Dickfeld T, Kato R, Zviman M, Lai S, Meininger G, Lardo AC, Roguin A, Blumke D, Berger R, Calkins H and Halperin H. Characterization of radiofrequency ablation lesions with gadolinium-enhanced cardiovascular magnetic resonance imaging. *J Am Coll Cardiol*. 2006;47:370-8.

125. Arujuna A, Karim R, Caulfield D, Knowles B, Rhode K, Schaeffter T, Kato B, Rinaldi CA, Cooklin M, Razavi R, O'Neill MD and Gill J. Acute Pulmonary Vein Isolation Is Achieved by a Combination of Reversible and Irreversible Atrial Injury After Catheter Ablation: Evidence From Magnetic Resonance Imaging. *Circulation: Arrhythmia and Electrophysiology*. 2012;5:691-700.

126. Harrison JL, Jensen HK, Peel SA, Chiribiri A, Grøndal AK, Bloch LØ, Pedersen SF, Bentzon JF, Kolbitsch C, Karim R, Williams SE, Linton NW, Rhode KS, Gill J, Cooklin M, Rinaldi CA, Wright M, Kim WY, Schaeffter T, Razavi RS and O'Neill MD. Cardiac magnetic resonance and electroanatomical mapping of acute and chronic atrial ablation injury: a histological validation study. *Eur Heart J*. 2014.

127. Celik H, Ramanan V, Barry J, Ghate S, Leber V, Oduneye S, Gu Y, Jamali M, Ghugre N, Stainsby JA, Shurrab M, Crystal E and Wright GA. Intrinsic Contrast for Characterization of Acute Radiofrequency Ablation Lesions. *Circ Arrhythm Electrophysiol*. 2014.

128. Ranjan R, Kato R, Zviman MM, Dickfeld TM, Roguin A, Berger RD, Tomaselli GF and Halperin HR. Gaps in the ablation line as a potential cause of recovery from electrical isolation and their visualization using MRI. *Circ Arrhythm Electrophysiol*. 2011;4:279-86.

129. Ranjan R, Kholmovski EG, Blauer J, Vijayakumar S, Volland NA, Salama ME, Parker DL, MacLeod R and Marrouche NF. Identification and acute targeting of gaps in atrial ablation lesion sets using a real-time magnetic resonance imaging system. *Circ Arrhythm Electrophysiol*. 2012;5:1130-5.

130. Peters DC, Wylie JV, Hauser TH, Nezafat R, Han Y, Woo JJ, Taclas J, Kissinger KV, Goddu B, Josephson ME and Manning WJ. Recurrence of atrial fibrillation correlates with the extent of post-procedural late gadolinium enhancement: a pilot study. *JACC Cardiovasc Imaging*. 2009;2:308-16.

131. Lederman RJ. Cardiovascular interventional magnetic resonance imaging. *Circulation*. 2005;112:3009-17.

132. Paetzel C, Zorger N, Bachthaler M, Volk M, Seitz J, Herold T, Feuerbach S, Lenhart M and Nitz WR. Feasibility of MR-guided Angioplasty of Femoral Artery Stenoses Using Real-time Imaging and Intraarterial Contrast-enhanced MR Angiography. *Rofo*. 2004;176:1232-6.

133. Otaki M and Lust RM. Modification of De Vega's tricuspid annuloplasty for experimental tricuspid regurgitation. *J Card Surg*. 1994;9:399-404.

134. Walter EMD, Delmo Walter E, Vasilyev N, Sill B, Padala M, Jimenez J, Yoganathan A, Hetzer R and del Nido P. Creation of a tricuspid valve regurgitation model from tricuspid annular dilatation using the cardioport video-assisted imaging system. *J Heart Valve Dis*. 2011;20:184-188.

135. Bai Y, Chen H-Y, Zong G-J, Jiang H-B, Li W-P, Wu H, Zhao X-X and Qin Y-W. Percutaneous establishment of tricuspid regurgitation: an experimental model for transcatheter tricuspid valve replacement. *Chin Med J*. 2010;123:806-809.

136. Bartus K, Bednarek J, Myc J, Kapelak B, Sadowski J, Lelakowski J, Yakubov SJ and Lee RJ. Feasibility of closed-chest ligation of the left atrial appendage in humans. *Heart Rhythm*. 2011;8:188-93.

137. Price MJ, Gibson DN, Yakubov SJ, Schultz JC, Di Biase L, Natale A, Burkhardt JD, Pershad A, Byrne TJ, Gidney B, Aragon JR, Goldstein J, Moulton K, Patel T, Knight B, Lin AC and Valderrábano M. Early Safety and Efficacy of Percutaneous Left Atrial Appendage Suture Ligation: Results From the U.S. Transcatheter LAA Ligation Consortium. *J Am Coll Cardiol*. 2014;64:565-572.

138. Sosa E, Scanavacca M, d'Avila A and Pilleggi F. A new technique to perform epicardial mapping in the electrophysiology laboratory. *J Cardiovasc Electrophysiol*. 1996;7:531-6.

139. Sacher F, Roberts-Thomson K, Maury P, Tedrow U, Nault I, Steven D, Hocini M, Koplan B, Leroux L, Derval N, Seiler J, Wright MJ, Epstein L, Haissaguerre M, Jais P and Stevenson WG. Epicardial ventricular tachycardia ablation a multicenter safety study. *J Am Coll Cardiol*. 2010;55:2366-72.

140. Koruth JS, Aryana A, Dukkipati SR, Pak HN, Kim YH, Sosa EA, Scanavacca M, Mahapatra S, Ailawadi G, Reddy VY and d'Avila A. Unusual complications of percutaneous epicardial access and epicardial mapping and ablation of cardiac arrhythmias. *Circ Arrhythm Electrophysiol*. 2011;4:882-8.

141. Boyle NG and Shivkumar K. Epicardial interventions in electrophysiology. *Circulation*. 2012;126:1752-69.

142. Lim HS, Sacher F, Cochet H, Berte B, Yamashita S, Mahida S, Zellerhoff S, Komatsu Y, Denis A, Derval N, Hocini M, Haissaguerre M and Jais P. Safety and prevention of complications during percutaneous epicardial access for the ablation of cardiac arrhythmias. *Heart Rhythm*. 2014;11:1658-65.

143. Maisch B, Ristić AD, Seferović PM, Tsang TSM, Pankuweit S, Maksimović R, Rupp H, Oh JK, Seward JB, Nassef JM, Tajik AJ and Watson TJ. *Interventional Pericardiology*. Heidelberg: Springer Medizin Verlag; 2011.

144. Verrier RL, Waxman S, Lovett EG and Moreno R. Transatrial access to the normal pericardial space: a novel approach for diagnostic sampling, pericardiocentesis, and therapeutic interventions. *Circulation*. 1998;98:2331-3.

145. Cohn WE, Winkler JA, Tuzun E, Hjelle A, Bassett K, Ahmad A and Frazier OH. Contrast pericardiography facilitates intrapericardial navigation under fluoroscopy. *Ann Thorac Surg*. 2010;90:1537-40.

146. Rogers T, Ratnayaka K, Schenke WH, Faranesh AZ, Mazal JR, O'Neill WW, Greenbaum AB and Lederman RJ. Intentional right atrial exit for microcatheter infusion of pericardial carbon dioxide or iodinated contrast to facilitate sub-xiphoid access. *Catheter Cardiovasc Interv*. 2014.

147. Cho KJ and Hawkins IF. *Carbon Dioxide Angiography: Principles, Techniques, and Practices*: CRC Press; 2007.

148. Harris PA, Taylor R, Thielke R, Payne J, Gonzalez N and Conde JG. Research electronic data capture (REDCap)--a metadata-driven methodology and workflow process for providing translational research informatics support. *Journal of biomedical informatics*. 2009;42:377-81.

149. Yamada T, McElderry HT, Platonov M, Doppalapudi H and Kay GN. Aspirated air in the pericardial space during epicardial catheterization may elevate the defibrillation threshold. *Int J Cardiol*. 2009;135:e34-5.

150. Rogers T, Ratnayaka K, Sonmez M, Franson DN, Schenke WH, Mazal JR, Kocaturk O, Chen MY, Faranesh AZ and Lederman RJ. Transatrial intrapericardial tricuspid annuloplasty. *JACC Cardiovasc Interv*. 2015;8:483-91.

151. Kowalski M, Grimes MM, Perez FJ, Kenigsberg DN, Koneru J, Kasirajan V, Wood MA and Ellenbogen KA. Histopathologic characterization of chronic radiofrequency ablation lesions for pulmonary vein isolation. *J Am Coll Cardiol*. 2012;59:930-8.

152. Kolandaivelu A, Zviman MM, Castro V, Lardo AC, Berger RD and Halperin HR. Noninvasive assessment of tissue heating during cardiac radiofrequency ablation using MRI thermography. *Circulation Arrhythmia and electrophysiology*. 2010;3:521-9.

153. Harrison JL, Jensen HK, Peel SA, Chiribiri A, Grondal AK, Bloch LO, Pedersen SF, Bentzon JF, Kolbitsch C, Karim R, Williams SE, Linton NW, Rhode KS, Gill J, Cooklin M, Rinaldi CA, Wright M, Kim WY, Schaeffter T, Razavi RS and O'Neill MD. Cardiac magnetic resonance and electroanatomical mapping of acute and chronic atrial ablation injury: a histological validation study. *Eur Heart J*. 2014;35:1486-95.

154. McGann C, Kholmovski E, Blauer J, Vijayakumar S, Haslam T, Cates J, DiBella E, Burgon N, Wilson B, Alexander A, Prastawa M, Daccarett M, Vergara G, Akoum N, Parker D, MacLeod R and Marrouche N. Dark regions of no-reflow on late gadolinium enhancement magnetic resonance imaging result in scar formation after atrial fibrillation ablation. *J Am Coll Cardiol*. 2011;58:177-85.

155. Bartlett TG, Mitchell R, Friedman PL and Stevenson WG. Histologic evolution of radiofrequency lesions in an old human myocardial infarct causing ventricular tachycardia. *J Cardiovasc Electrophysiol*. 1995;6:625-9.

156. Kramer JB, Saffitz JE, Witkowski FX and Corr PB. Intramural reentry as a mechanism of ventricular tachycardia during evolving canine myocardial infarction. *Circ Res*. 1985;56:736-54.

157. Estner HL, Zviman MM, Herzka D, Miller F, Castro V, Nazarian S, Ashikaga H, Dori Y, Berger RD, Calkins H, Lardo AC and Halperin HR. The critical isthmus sites of ischemic ventricular tachycardia are in zones of tissue heterogeneity, visualized by magnetic resonance imaging. *Heart Rhythm*. 2011;8:1942-9.

158. Sigwart U. Non-surgical myocardial reduction for hypertrophic obstructive cardiomyopathy. *Lancet*. 1995;346:211-4.

159. Ellman BA, Parkhill BJ, Marcus PB, Curry TS and Peters PC. Renal ablation with absolute ethanol. Mechanism of action. *Invest Radiol*. 1984;19:416-23.

160. Baez-Escudero JL, Keida T, Dave AS, Okishige K and Valderrabano M. Ethanol infusion in the vein of Marshall leads to parasympathetic denervation of the human left atrium: implications for atrial fibrillation. *Journal of the American College of Cardiology*. 2014;63:1892-901.

161. Baggish AL, Smith RN, Palacios I, Vlahakes GJ, Yoerger DM, Picard MH, Lowry PA, Jang IK and Fifer MA. Pathological effects of alcohol septal ablation for hypertrophic obstructive cardiomyopathy. *Heart*. 2006;92:1773-8.

162. Brugada P, de Swart H, Smeets JL and Wellens HJ. Transcoronary chemical ablation of ventricular tachycardia. *Circulation*. 1989;79:475-82.

163. Tholakanahalli VN, Bertog S, Roukoz H and Shivkumar K. Catheter ablation of ventricular tachycardia using intracoronary wire mapping and coil embolization: description of a new technique. *Heart Rhythm*. 2013;10:292-6.

164. Wright KN, Morley T, Bicknell J, Bishop SP, Walcott GP and Kay GN. Retrograde coronary venous infusion of ethanol for ablation of canine ventricular myocardium. *J Cardiovasc Electrophysiol*. 1998;9:976-84.

165. Weismuller P, Mayer U, Richter P, Heieck F, Kochs M and Hombach V. Chemical ablation by subendocardial injection of ethanol via catheter--preliminary results in the pig heart. *Eur Heart J*. 1991;12:1234-9.

166. Clogston JD and Patri AK. Detecting and measuring free gadolinium in nanoparticles for MRI imaging. *Methods Mol Biol*. 2011;697:101-8.

167. Ohnishi K, Yoshioka H, Ito S and Fujiwara K. Prospective randomized controlled trial comparing percutaneous acetic acid injection and percutaneous ethanol injection for small hepatocellular carcinoma. *Hepatology*. 1998;27:67-72.

168. Ratnayaka K, Faranesh AZ, Hansen MS, Stine AM, Halabi M, Barbash IM, Schenke WH, Wright VJ, Grant LP, Kellman P, Kocaturk O and Lederman RJ. Real-time MRI-guided right heart catheterization in adults using passive catheters. *Eur Heart J*. 2013;34:380-9.

169. Greenbaum AB, Rogers T, Paone G, Flynn S, Borgi J, Guerrero M, O'Neill WW and Lederman RJ. Intentional right atrial exit and CO2 insufflation allows safe subxiphoid needle entry into the empty pericardial space: first human experience. *JACC Clinical Electrophysiology*. 2015;In Press.

170. Cochet H, Komatsu Y, Sacher F, Jadidi AS, Scherr D, Riffaud M, Derval N, Shah A, Roten L, Pascale P, Relan J, Sermesant M, Ayache N, Montaudon M, Laurent F, Hocini M, Haissaguerre M and Jais P. Integration of merged delayed-enhanced magnetic resonance imaging and multidetector computed tomography for the guidance of ventricular tachycardia ablation: a pilot study. *J Cardiovasc Electrophysiol*. 2013;24:419-26.

171. Oduneye SO, Pop M, Shurrab M, Biswas L, Ramanan V, Barry J, Crystal E and Wright GA. Distribution of abnormal potentials in chronic myocardial infarction using a real time magnetic resonance guided electrophysiology system. *J Cardiovasc Magn Reson*. 2015;17:27.

172. Ashikaga H, Arevalo H, Vadakkumpadan F, Blake RC, 3rd, Bayer JD, Nazarian S, Muz Zviman M, Tandri H, Berger RD, Calkins H, Herzka DA, Trayanova NA and Halperin HR. Feasibility of image-based simulation to estimate ablation target in human ventricular arrhythmia. *Heart Rhythm*. 2013;10:1109-16.

173. Relan J, Chinchapatnam P, Sermesant M, Rhode K, Ginks M, Delingette H, Rinaldi CA, Razavi R and Ayache N. Coupled personalization of cardiac electrophysiology models for prediction of ischaemic ventricular tachycardia. *Interface Focus*. 2011;1:396-407.

174. Komatsu Y, Daly M, Sacher F, Cochet H, Denis A, Derval N, Jesel L, Zellerhoff S, Lim HS, Jadidi A, Nault I, Shah A, Roten L, Pascale P, Scherr D, Aurillac-Lavignolle V, Hocini M,

Haissaguerre M and Jais P. Endocardial ablation to eliminate epicardial arrhythmia substrate in scar-related ventricular tachycardia. *J Am Coll Cardiol*. 2014;63:1416-26.

175. van Huls van Taxis CF, Wijnmaalen AP, Piers SR, van der Geest RJ, Schalij MJ and Zeppenfeld K. Real-time integration of MDCT-derived coronary anatomy and epicardial fat: impact on epicardial electroanatomic mapping and ablation for ventricular arrhythmias. *JACC Cardiovasc Imaging*. 2013;6:42-52.

176. Sapp JL, Beeckler C, Pike R, Parkash R, Gray CJ, Zeppenfeld K, Kuriachan V and Stevenson WG. Initial human feasibility of infusion needle catheter ablation for refractory ventricular tachycardia. *Circulation*. 2013;128:2289-95.

177. Yagishita D, Ajijola OA, Vaseghi M, Nsair A, Zhou W, Yamakawa K, Tung R, Mahajan A and Shivkumar K. Electrical homogenization of ventricular scar by application of collagenase: a novel strategy for arrhythmia therapy. *Circ Arrhythm Electrophysiol*. 2013;6:776-83.

178. Ohnishi K, Ohyama N, Ito S and Fujiwara K. Small hepatocellular carcinoma: treatment with US-guided intratumoral injection of acetic acid. *Radiology*. 1994;193:747-52.

179. Frenzel T, Lengsfeld P, Schirmer H, Hutter J and Weinmann HJ. Stability of gadolinium-based magnetic resonance imaging contrast agents in human serum at 37 degrees C. *Invest Radiol*. 2008;43:817-28.

180. Kim RJ, Fieno DS, Parrish TB, Harris K, Chen EL, Simonetti O, Bundy J, Finn JP, Klocke FJ and Judd RM. Relationship of MRI delayed contrast enhancement to irreversible injury, infarct age, and contractile function. *Circulation*. 1999;100:1992-2002.

181. Sohns C, Karim R, Harrison J, Arujuna A, Linton N, Sennett R, Lambert H, Leo G, Williams S, Razavi R, Wright M, Schaeffter T, O'Neill M and Rhode K. Quantitative Magnetic Resonance Imaging Analysis of the Relationship between Contact Force and Left Atrial Scar Formation after Catheter Ablation of Atrial Fibrillation. *J Cardiovasc Electrophysiol*. 2013.

182. Vergara P, Trevisi N, Ricco A, Petracca F, Baratto F, Cireddu M, Bisceglia C, Maccabelli G and Della Bella P. Late potentials abolition as an additional technique for reduction of arrhythmia recurrence in scar related ventricular tachycardia ablation. *Journal of cardiovascular electrophysiology*. 2012;23:621-7.

183. Jais P, Maury P, Khairy P, Sacher F, Nault I, Komatsu Y, Hocini M, Forclaz A, Jadidi AS, Weerasooryia R, Shah A, Derval N, Cochet H, Knecht S, Miyazaki S, Linton N, Rivard L, Wright M, Wilton SB, Scherr D, Pascale P, Roten L, Pederson M, Bordachar P, Laurent F, Kim SJ, Ritter P, Clementy J and Haissaguerre M. Elimination of local abnormal ventricular activities: a new end point for substrate modification in patients with scar-related ventricular tachycardia. *Circulation*. 2012;125:2184-96.